

KIM KUNTZE

Strategies for Red-Light Photoswitching

KIM KUNTZE

Strategies for Red-Light Photoswitching

ACADEMIC DISSERTATION

To be presented, with the permission of
the Faculty of Engineering and Natural Sciences
of Tampere University,
for public discussion in the auditorium K1702
of the Konetalo building, Korkeakoulunkatu 6, Tampere,
on 1st of September 2023, at 13 o'clock.

ACADEMIC DISSERTATION

Tampere University, Faculty of Engineering and Natural Sciences
Finland

<i>Responsible supervisor and Custos</i>	Professor Arri Priimägi Tampere University Finland	
<i>Supervisor</i>	Assistant Professor Stefano Crespi University of Uppsala Sweden	
<i>Pre-examiners</i>	Associate Professor Jonathon Beves University of New South Wales Australia	Professor Stephen Fletcher University of Oxford United Kingdom
<i>Opponent</i>	Privatdozent Zbigniew L. Pianowski Karlsruhe Institute of Technology Germany	

The originality of this thesis has been checked using the Turnitin OriginalityCheck service.

Copyright © 2023 Kim Kuntze

Cover design: Roihu Inc.

ISBN 978-952-03-2999-0 (print)
ISBN 978-952-03-3000-2 (pdf)
ISSN 2489-9860 (print)
ISSN 2490-0028 (pdf)
<http://urn.fi/URN:ISBN:978-952-03-3000-2>



Carbon dioxide emissions from printing Tampere University dissertations have been compensated.

PunaMusta Oy – Yliopistopaino
Joensuu 2023

ACKNOWLEDGEMENTS

The work for this thesis was carried out in the Smart Photonic Materials group at the Faculty of Engineering and Natural Sciences of Tampere University, under the supervision of **Prof. Arri Priimägi**. The Academy of Finland (Flagship Programme PREIN, No. 320165, and Centre of Excellence LIBER, No. 346147), the European Research Council (Starting Grant PHOTOTUNE, No. 679646), the Tampere University graduate school, the Finnish Cultural Foundation, and the City of Tampere Science Fund are gratefully acknowledged for funding the work. I would also like to express my gratitude to the preliminary examiners, **Prof. Jonathon Beves** from the University of New South Wales and **Prof. Stephen Fletcher** from the University of Oxford, for their extremely kind words regarding my work, as well as to my opponent-to-be, **Priv.-doz. Zbigniew L. Pianowski** from Karlsruhe Institute of Technology.

First of all, this was not supposed to happen. I joined the SPM group in June 2016 and wrote my BSc and MSc theses for Arri. I was then set on leaving Tampere behind, searching for new topics to learn and perhaps even returning to my beautiful hometown of Turku. However, one does not simply leave the SPM group – in August 2019 I found myself returning to the synthesis of very familiar molecular structures. I admit that I have had regrets for my decision; it is difficult to be the sole person interested in the fundamentals of pure organic chemistry in a group and university focusing mostly on materials. I am still unsure whether I have learned enough during my PhD to make me a capable postdoctoral researcher. On the other hand, I could not imagine a better supervisor and role model for a young scientist than you are, Arri. It is a unique combination for a professor to strive for top-notch publications while genuinely caring for every single individual's well-being, personal growth and career possibilities. If all supervisors understood work-life balance as well as you do, the academia would certainly be a better place. It has been a privilege to work for you, and for this reason I conclude that I will rather bless than curse the day I first knocked on your door to ask for a summer job.

I am also glad to have been introduced to so many fantastic scientists over the years, the highlight being my research visit to the group of **Prof. Ben Feringa** at the

University of Groningen in 2022. Those months were more educative and inspiring than I could have wished for, and I thank you for your hospitality. I am equally grateful for the fruitful collaborations with **Profs. Stefano Crespi, Dennis Chung-Yang Huang, Stefan Hecht, Timo Laaksonen, Peter Saalfrank, Wybren-Jan Buma** and **Mariangela Di Donato, Drs. Zafar Ahmed, Nikita Durandin, Evgenii Titov, Michiel Hilbers** and **Elina Kalenius**, and **Antti Siiskonen**. Stefano, I would especially like to thank you for becoming my second supervisor even when you were already buried under a mountain of commitments – in addition to being a co-founder and driving force of the wonderful motor project I got to embark upon. It has been a pleasure to work with such a talented, knowledgeable and positively crazy scientist. Your duck stickers always make my day. Please try to take care of yourself. Zafar and Antti, thank you for all the support during my MSc studies and first months of my PhD, and for starting the research lines on *ortho*-fluoroaminoazobenzenes and iodine catalysis that I was able to build on later.

Experimental research would not be possible without excellent support staff. **Dr. Suvi Lehtimäki** and **Anna Railanmaa**, you have been outstanding in keeping the RedLabs functional. However, I am even more grateful for all the lunches and coffee breaks, especially since for a long time you were some of the very few people who understood that a proper time for lunch is at 11. And Suvi, thank you for introducing me to Xordle and Symble. I would also like to give my thanks to **Dr. Alexandre Efimov** for maintaining our analytical instruments in top shape, to **Dr. Renze Sneep** for helping with the LC-MS and SFC in Groningen, to **Eija Sappinen** for maintaining our labs, and to **Kirsi Viitanen** for all her help with financial matters.

Teaching has been one of my greatest delights during these four years. I would like to thank **Prof. Nonappa** and **Drs. Terttu Hukka, Markus Lahikainen** and **Riikka Lahtinen**, as well as the wonderful students of this university, for the opportunities in developing my pedagogical skills – and Arri for not being too strict about keeping my teaching hours below the limit. I enjoyed every single lecture and exercise session I was offered. Terttu, special thanks for the six-year collaboration on Organic Chemistry 1. Not every teacher would trust a PhD student with as much responsibility as you have, and I am deeply indebted by that. Markus, I don't know how many working days I've spent talking with you about teaching, science and life since I got to know you during my first summer in the group, but maybe more than Arri would've liked. Since you got your well-deserved teacher position, it has been nice to hear the most recent Festia gossip through you, in addition to the ever-important therapy sessions when things haven't gone like planned for one of us and

the valuable discussions on how to develop teaching. I hope you will pop into my office in the future as well.

We have only just made the transition from official collaborators to workmates, and I have already written more than two pages. I'm afraid this will only get more long-winded from now on. I have been fortunate to work in a group of great people and a wonderful atmosphere – the SPM spirit truly exists. Not only that, we have shared the labs with a nice bunch of people from other groups. I would like to call you all my friends. I have seen most of you almost daily for years, shared my excitements and disappointments, and probably told more about birds than anybody would have liked to hear. In fact, I have met many of you more times in a week than I see my non-workmate friends in a year! It has been my pleasure to work alongside you all.

We didn't have other synthesisists in our group when I began my PhD, so my time was mostly spent with the students of **Prof. Nuno Candeias**. Those were the days when our fume hoods got to witness Wittig reactions, cycloadditions, rearrangements, mechanistic studies... I really enjoyed this time. **Tatu Rimpiläinen**, thanks for introducing me to the lecture videos of **Prof. David Van Vranken** and in general the beauty of understanding molecular orbital interactions to explain reaction mechanisms. The lectures have largely determined the way I want to teach organic chemistry. I also remember fondly your dry humour and all the funny little incidents that occurred, the highlight being the hole your heat gun made to the pristine two-week-old fume hood. **Drs. Rafael Vale** and **Jagadish Salunke**, in addition to being great chemists, you made the lab a little bit more pleasant through your presence. Rafael, I will always remember the sound of glassware hitting the lab wall after a disappointing TLC, and will always be amazed at how fast your brain works both related to chemistry and when clever remarks are needed. Jagadish, you are a legend in our labs, not only due to the window thing, but also because you are probably the friendliest person to ever have worked here.

Dr. Suvi Holmstedt, you were the last remnant of the synthesis group, the only true organic chemist in our labs. I can't put to words how important your friendship was during the first two years of my PhD, and how difficult it felt when you left. You were the person to put on some music, to stir up a discussion, to invent a bad joke. "Mitä voi tehdä sekä kastike että eräs juures?" is still one of my all-time favourite riddles. In general, the lab or the coffee room was always a bit more lively when you were around. You never ran out of words but also listened to what others had to say, and this combination made discussing anything with you easy. In addition to being an extremely nice person, you are also inspirational as a chemist, showing

incredible lab skills and coming up with more ideas for new projects every week than I foresee myself inventing in the next decade. This university would definitely need you in the future.

Delightedly, at one point I got to welcome a couple of new synthesists to our group. **Dr. Rakesh Puttreddy**, your project was a pain, and I think we spent most of our time complaining about either that or the university. Still, I enjoyed all the chats we had in the lab and in the coffee room. We did also talk about other things such as MasterChef Australia or the ethical aspects of publishing, and running home from work with you was always a pleasure. I'm glad to see that your projects paid off in the end and that you don't have to work with oligothiophenes anymore. **Jani Viljakka**, you were the best student I ever supervised – well, also the only one, but that's beside the point. You were pedantic and accurate on a level I could never achieve, and a tremendous help to me with two of my doctoral publications, as well as a couple of other projects that we will hopefully finalise in the future. On top of that, you were always very good company despite working too hard and having too short coffee breaks. May your discs fly far!

At some point I began to notice that physicists can be pretty nice people as well. **Dr. Matti Virkki**, you were in the group already in 2016 and only now when I'm writing this preface are you slowly drifting away from Tampere. I might have mentioned you already among the collaborators, as you have been an invaluable help in all the optical studies over the years. More than that, I will cherish the kilometre competitions we had on the coffee room whiteboard, and the many discussions we often had in the afternoon, typically starting with an innocent work-related question and ending one hour later when we realised it's already time to call it a day. Kireitä ketjuja ja liukkaita latuja Ouluun tai minne ikinä päädytkin! **Alex Berdin**, you are also among the longest-standing group members, and perhaps represent best the aforementioned SPM spirit with your everlasting curiosity and openness to new adventures. I admire the way you find almost every aspect of science intriguing and constantly dive into new topics – unlike me, as you may have noticed in the infamous remote group meeting when I accidentally told my honest opinion about some optics paper while having my microphone open. I still find this incident equally embarrassing and hilarious, and hope that you don't hold grudges. Among the oldest co-workers is also **Dr. Chiara Fedele**. Thank you for all the discussions (especially about the imposter syndrome), your Italian accent, all the SPM group meeting reminders, the morning runs at the LIBER events, all the times you organised a farewell gift for somebody in the group, and for successfully solving my Finnish

riddles, often before any native speakers! And **Dr.** (soon Prof.) **Hao Zeng**, thank you for all the weird questions in the corridors as well as the badminton matches.

Over the years, the group has grown with quite a few friendly faces. **Zixuan Deng**, thank you for all the deep (sometimes perhaps too deep) discussions; I particularly remember the one we had when driving to Kuusamo in January 2021. I'm also glad that you made me play badminton despite my apprehensions. Speaking of Kuusamo, thanks to **Drs. Semyon Chervinsky, Klaudia Dradrach** and **Hongshuang Guo** for the trip – it was one of the highlights of that year for me, and I was happy to see many of you ski and see reindeer for the first time in your lives. Special thanks to Klaudia for being the only person ever to join me for a stroll to the city centre on more than one occasion. Shame on everybody else – you have legs, use them. **Yasaman Nemati**, thank you for teaching me the secrets of drinking hot water. **Matias Paatelainen**, your attitude towards presentations, science and life in general is pure gold and has saved many boring meetings. It's funny to always find you in the coffee room. This said, I would also like to tell that I admire your systematic way to tackle problems in your research, which typically leads to you eventually solving every single one of them. And we shouldn't forget your incredible warm-up dance skills. **Sami Vesamäki**, thanks for the climbing lectures and stories about warming up your house. You are the best boxelier I have ever met. **Mari Isomäki**, thank you for hosting the ESC semi-final evening and all the nice discussions we've had (I seem to like talking to people). **Roshan Nasare**, getting another synthetic chemist to the group was a delight – I hope your crosslinker project will get a happy ending and I'll try to help with that more in the future. I'm sorry for not being too excited about the stock market. **Artem Boichuk**, it was a pleasure to notice that even though you work mainly on photonics, you are also interested in organic synthesis. In addition, thanks for joining the owl trip! **Dr. Kevin Chevrier**, despite your short stay, we managed to do quite a bit, ranging from after-work runs to the Pedantle sessions that you introduced. **Jianfeng Yang**, thank you for the badminton plays. **Jenna Hakola, Simo Rantamäki** and other summer students, thanks for livening up the atmosphere.

From outside the SPM group, I would particularly like to thank **Dr. Jussi Isokuorti** for collaborations on multiple photochemical projects, but even more so for all the talks and laughs over the years. I was always astonished by how excited you were about triplet states and by your determination to advance your scientific career, while still always having time for helping others. I'm also glad to have shared my office with **Anastasiia Matiukhina**. Our discussion about mould growing on hapankorppu still puts a smile on my face. And Profs. **Nikolai Tkatchenko** and

Nonappa, **Drs. Murthy Grandhi** and **Ajayakumar Murugan Rathamony**, and **Matias Häyrynen**, thank you for the CAM badminton plays.

As mentioned, my visit to Groningen, the hidden pearl of The Netherlands, was perhaps the highlight of my PhD. In addition to the country being among the best on this planet and the city being perhaps even more beautiful and cosy than Turku (which is saying a lot), I attribute this to the unbelievably warm welcome I received from everybody working in the Feringa group. **Dr. Daisy Pooler**, from the moment I met you outside Nijenborgh 4, I felt part of the lab community. Whenever I listen to ABBA or Vengaboys (not Wankerboys like I thought), I will remember the angry lady at the door, the correct way to pronounce wa'er, absurdly many kapsalon lunches, our discussions on hyphenation (thanks for proofreading the motor chapter, by the way!) and the karaoke nights, and feel triumphant for knowing the word pious. Lemons and oil droplets will always remind me of our XRD experiment and the most interesting molecular structure I have ever made. The moment when the correct and very unexpected crystal structure formed on your computer screen is perhaps the coolest individual thing in my chemistry career. Thank you for all of these memories, and many others. You are vocal in the best possible way, a very capable chemist, and always happy to help others – overall, a great human being.

Other members of the group were equally important in creating the perfect working atmosphere. **Dr. Cosima Stähler**, you struck me as a very friendly person on the first day, and that proved to be true. The coffee room Wordle sessions were one of the important routines of each day. I always admired the way you could speak so fluently and with the exactly right words, both in the coffee room conversations and more formal occasions. **Kathy Liu**, thanks for being the best fume hood neighbour and for introducing me to the wonders of Strava and slang words ("lit"). Already as a master's student, you were working with complex synthesis and materials applications, and I'm sure your PhD back in the U.S. will be more than successful. **Adrien Combe**, I've missed the "Hyvää huomenta" wishes from you, as well as your helpfulness and positively French stand on cheese-filled croissants. **Carlijn van Beek**, thanks for the tea breaks and for helping me out with tax officials. And of course, thanks to all of you for the Mamma Mia! evening. **Dr. George Alachouzos**, **John de Boer**, **Daniel Döllerer**, **Max Fellert**, **Robert Kluifhooft**, **Bianka Sieredzinska**, **Lotte Stindt**, **Roza Weber** and others – thank you for everything! It was a memorable spring. Take good care of my forks. (Postscript: I heard that you have already lost all of them – I take back all these nice words.)

I must say that I felt empty when I returned to Finland. Groningen had already become my home, and I missed its bicycle-filled streets, parks, birds, food, and most

of all people. It was the weirdest feeling to return home and not feel at home. I guess that's how Frodo felt after returning to the Shire. Anyway, among all of this it was delightful to discover that in addition to reuniting with the old group members, I got to meet a new chemist who had started during my absence: **Henning Meteling**. I'm happy that such a talented chemist and pleasant person is part of our group. Thanks for blasting music in the lab, the chess puzzles, the Lord of the Rings memes, the afternoon runs, and for promoting a vegan diet in our group. And of course for proofreading my thesis – I didn't change all the “colloquial” phrasings, though. This said, I must express my disapproval on your working hours: it is not acceptable to work over nine hours a day and frequently also in the weekends. On the positive side, although you didn't drink any hot beverages at first, I have been able to teach you the oldest and noblest of PhD traditions – no matter what the situation in your research, there is always time for a cup of tea.

Speaking of breaks, I have yet to name our official fika expert, **Dr. Tero-Petri Ruoko**. T-P, especially during the last couple of years you have become an integral part of our coffee breaks and lunches. Thanks for every cup, all the Rings of Power rants, the Friday chocolates, and the times we've been able to tweak Arri's nose. I've particularly enjoyed our discussions regarding the future of chemistry in our university and how the teaching could be developed. I hope you get the chance to pursue these goals, either here or in another city located about two hours southwest from here where perhaps we could both work one day.

Outside work, I want to express my gratitude to my family and friends. **Mum** and **Dad**, thank you for all the support you have given over the years, the times in Houtskär and the suppers. **Visa** and **Iida**, I have enjoyed our sports activities, huutopussi games, your Tampere visits and all the correspondence in between. And we shouldn't forget the infamous doughnuts. The entire **Posse**, thank you for all the memorable get-togethers, runs, Sequence matches and pleasant chats. **Sebastian** and the whole youngish birder gang, our transect line trips and other activities have balanced the lab challenges nicely. **Peter** and **Päivi**, your encouraging words about research and our discussions on bird censuses have been valuable. And **Meri**, I could not hope for a better person to share my life with. Thank you for being there for me every day and even coming to Groningen with me, listening to my complaints and excitements and putting up with my forgetfulness – not to mention all the rocky roads. I can just hope and try to make you as happy as you have made me.

Tampere, August 1st 2023

Kim Kuntze

ABSTRACT

Responsive, adaptive and even intelligent molecular systems have been identified as the key to next-generation pharmaceuticals and functional materials. Photoswitches, compounds that isomerise reversibly between two distinct ground-state species upon excitation with light and consequently give rise to a macroscopic effect, are an integral part of this future. Their potential application areas range from photopharmacology to optoelectronics and soft robotics. However, most conventional photoswitch structures such as azobenzenes absorb ultraviolet light, high-energy photons that are detrimental to many artificial materials and especially to living systems. To harness their full potential, photoswitches should function efficiently with visible light that is benign to the environment. Red or near-infrared light would be the ideal stimulus for switches utilised in biological context, as these wavelengths are least absorbed by living tissue. The same applies to light-driven molecular motors, compounds that exhibit unidirectional rotation upon photoexcitation. In addition to absorption in the red part of the visible spectrum, both switches and motors should exhibit efficient and fast photoisomerisation, favourable thermal isomerisation kinetics and tolerance towards different environments in order to be useful in real-life applications. In this light, it is crucial to understand the underlying fundamental mechanisms that govern these attributes.

In this thesis, we explore three different approaches to realise photoswitching with red light: (i) synthetic modifications of azobenzenes, (ii) utilisation of new photoswitch cores that inherently absorb low-energy photons, and (iii) indirect isomerisation with red-light photocatalysts. We study each strategy from a theoretical viewpoint and demonstrate that they all provide means to induce isomerisation with red light, each with unique advantages and challenges in terms of promoting efficient, fast and robust switching. As a result, a single optimal photoswitch system cannot be designed; instead, the challenge lies in identifying the best design for each application. The same principles can also be applied to molecular motors, giving rise to visible-light-powered unidirectional rotary motion on a molecular level. We show that drawing inspiration from red-light-absorbing photoswitches has repercussions not only on the visible-light absorption but also on enhanced rotation dynamics.

TIIVISTELMÄ

Vuorovaikutteiset, muotoutuvat ja jopa älykkäät molekyyliarakenteet ovat avain uuden sukupolven lääkeaineisiin ja toiminnallisiin materiaaleihin. Valokytkimet eli yhdisteet, jotka isomeroituvat reversiibelisti valon vaikutuksesta johtaen makroskooppisten ominaisuuksien muutoksiin, ovat erottamaton osa tätä tulevaisuutta. Mahdolliset sovelluskohteet ulottuvat lääketieteestä elektroniikkaan ja robotiikkaan. Valitettavasti useimmat valokytkinrakenteet, esimerkiksi laajalti käytetyt atsobentseenit, absorboivat ultraviolettivaloa, joka on vahingollista monille materiaaleille ja erityisesti eläville soluille. Jotta valokytkinten koko potentiaali voidaan hyödyntää, tarvitaan harmittomalla näkyvällä valolla toimivia yhdisteitä. Puna- tai infrapunavallo olisi ihanteellinen ärsyke biologian alalla käytettäville kytkimille. Sama pätee myös molekyylimoottoreihin eli yhdisteisiin, jotka pyöriivät valon vaikutuksesta yksisuuntaisesti. Lisäksi sekä kytkinten että moottorien tulisi isomerisoida valon vaikutuksesta tehokkaasti ja nopeasti, termisten isomerisaatioreaktioiden tulisi olla sovelluskohteesta riippuen hitaita tai nopeita ja yhdisteiden tulisi toimia hyvin erilaisissa ympäristöissä. Näiden ominaisuuksien hallitsemiseksi on tärkeää ymmärtää niiden taustalla olevat mekanismit.

Tässä väitöskirjassa tutkimme kolmea keinoa toteuttaa valokytkentä punaisella valolla: (i) atsobentseenien absorptiospektrin siirtäminen rakennetta muokkaamalla, (ii) uusien, valmiiksi punaista valoa absorboivien rakenteiden hyödyntäminen ja (iii) epäsuora valokytkentä punavalolla aktivoitavia katalyyttejä hyödyntäen. Tarkastelemme strategioita teoreettiselta kannalta ja osoitamme, että niistä jokainen mahdollistaa valokytkennän punaista valoa käyttäen. Kullakin strategialla on etunsa ja haasteensa tehokkaan, nopean ja kestävä valokytkennän toteuttamiseksi. Tästä johtuen yksi ihanteellinen valokytkinmalli ei voi saavuttaa kaikkia eri sovelluksille asetettuja tavoitteita, vaan tulevaisuuden haaste on löytää kuhunkin käyttöön paras ratkaisu. Samoja periaatteita voidaan soveltaa myös molekyylimoottoreihin, jolloin molekulaarisen tason yksisuuntainen kiertoliike voidaan saada aikaan näkyvällä valolla. Lisäksi punaisella valolla toimivien valokytkinten rakenteita hyödyntämällä moottorien rotaatiota saadaan tehostettua.

CONTENTS

1	Introduction.....	1
1.1	Aim and scope of this work.....	2
1.2	Outline	4
2	Photoswitching.....	5
2.1	Photoswitches based on <i>E</i> – <i>Z</i> isomerisation	5
2.2	Photoswitches based on cyclisation reactions	11
2.3	Characterisation of photoswitches	14
3	Spectral tuning of azobenzenes	19
3.1	Red-shifting the π – π^* absorption band: electron-donating substituents, push-pull systems and protonated azobenzenes	19
3.2	Utilising the n – π^* absorption band: <i>ortho</i> -substitution	22
3.3	Fluoroaminoazobenzenes	26
4	Inherently blue: indigoid photoswitches	35
4.1	Hemiindigos and hemithioindigos.....	36
4.2	Indigos and thioindigos.....	39
4.3	Indigo photoswitching in the solid.....	43
5	Indirect isomerisation of azobenzenes	51
5.1	Catalytic isomerisation mechanisms	52
5.2	Isomerisation catalysed by iodine and molecular oxygen	58
6	Beyond switches: molecular motors driven by visible light	65
6.1	Molecular motors based on rotation around a double bond.....	65
6.2	Molecular motors based on barbituric acid.....	73
7	Conclusions and outlook.....	83

SYMBOLS AND ABBREVIATIONS

ε	molar absorption coefficient at a given wavelength
φ	photoisomerisation quantum yield
λ	wavelength
χ	molar fraction
τ	thermal isomerisation lifetime
Abs	absorbance at a given wavelength
Abs_0	absorbance at $t = 0$, i.e. at the start of a thermal isomerisation experiment
Abs_∞	absorbance at $t \rightarrow \infty$, i.e. when a thermal equilibrium has been reached
b	stretch factor in a stretched exponential fit
I_{exc}	excitation light intensity
k_{ISC}	intersystem crossing rate constant
k_T	thermal isomerisation rate constant
l	optical path
S_0	singlet ground state
S_n	n^{th} excited singlet state
T_1	first excited triplet state
T_g	glass transition temperature
t	time
$t_{1/2}$	thermal isomerisation half-life
AB	azobenzene
Cat	catalyst
DASA	donor-acceptor Stenhouse adduct
DCM	dichloromethane
DFT	density functional theory
dma	dimethylamine
DIPEA	<i>N,N</i> -diisopropylethylamine

DMSO	dimethylsulfoxide
EWG	electron-withdrawing group
FMO	frontier molecular orbital
ISC	intersystem crossing
HPLC	high-performance liquid chromatography
MB	methylene blue
MeCN	acetonitrile
NIR	near-infrared
NMR	nuclear magnetic resonance
P4VP	poly(4-vinylpyridine)
PBMA	poly(<i>n</i> -butyl methacrylate)
PdPc	palladium phthalocyanine
PET	photoinduced electron transfer
PEZI	photochemical <i>E</i> – <i>Z</i> isomerisation
PHMA	poly(<i>n</i> -hexyl methacrylate)
PMMA	poly(methyl methacrylate)
PhMe	toluene
pip	piperidine
pram	proline amide
pres	proline methyl ester
prol	prolinol
PS	polystyrene
PSD	photostationary state distribution
PSS	photostationary state
pyr	pyrrolidine
TD-DFT	time-dependent density functional theory
TET	triplet energy transfer
THF	tetrahydrofuran
THI	thermal helix inversion
UV	ultraviolet

ORIGINAL PUBLICATIONS

- Publication I Kuntze, K., Viljakka, J., Titov, E., Ahmed, Z., Kalenius, E., Saalfrank, P. & Priimägi, A. Towards low-energy-light-driven bistable photoswitches: *ortho*-fluoroaminoazobenzenes. *Photochemical & Photobiological Sciences* **2022**, 21, 2, 159–173.
- Publication II Kuntze, K., Viljakka, J., Virkki, M., Huang, C.-Y., Hecht, S. & Priimägi, A. Red-light photoswitching of indigos in polymer thin films. *Chemical Science* **2023**, 14, 10, 2482–2488.
- Publication III Kuntze, K., Isokuortti, J., Siiskonen, A., Durandin, N. A., Laaksonen, T. & Priimägi, A. Azobenzene photoswitching with near-infrared light mediated by molecular oxygen. *Journal of Physical Chemistry B* **2021**, 125, 45, 12568–12573.
- Publication IV Kuntze, K.,[†] Pooler, D. R. S.,[†] Di Donato, M., Hilbers, M. F., van der Meulen, P., Buma, W. J., Priimägi, A., Feringa, B. L. & Crespi, S. A visible-light-driven molecular motor based on barbituric acid. *Chemical Science* **2023**.

[†] Equal contribution

AUTHOR'S CONTRIBUTIONS

- Publication I The author actively participated in planning the molecular designs and performed all synthetic work, photochemical measurements and data analysis with the help of J. Viljakka, except for some experiments carried out earlier by Z. Ahmed and mass spectrometry carried out by E. Kalenius. The author wrote the first draft of the manuscript, with input from E. Titov in the computational part. The final manuscript was written together with all the coauthors.
- Publication II The author actively participated in planning the experiments and performed all experimental work and data analysis with the help of J. Viljakka. The author wrote the first draft of the manuscript. The final manuscript was written together with all the coauthors.
- Publication III The author actively participated in planning the experiments and performed all experimental work and data analysis with the help of J. Isokuortti and N. A. Durandin except for the initial studies made by A. Siiskonen. The author wrote the first draft of the manuscript. The final manuscript was written together with all the coauthors.
- Publication IV The author actively participated in planning the synthetic studies, performed all synthetic work and participated in performing the photochemical studies and data analysis, most of which were carried out by D. R. S. Pooler and S. Crespi. The author wrote the first draft together with D. R. S. Pooler and S. Crespi. The final manuscript was written together with all the coauthors.

1 INTRODUCTION

Organic chemistry is one of the very foundations on which our modern civilisation is built. Through deep knowledge of the reactivity of molecules we can investigate biochemical processes, cure diseases, and ultimately understand life. By establishing structure-property relationships on the molecular level we are able to tailor materials for a wide array of vital everyday applications. Few structures and functions are outside the reach of a capable organic chemist. So few, in fact, that one is left wondering whether the field is already complete. This illusion is quickly shattered by a quick comparison of a living organism and a synthetic piece of plastic, demonstrating how far we still are from truly mastering chemistry. In contrast to the adaptive, interactive and even intelligent character of biomolecular assemblies and living organisms, most human-made molecular structures are static by nature. A pharmaceutical can be engineered to attack predominantly cancerous cells or certain pathogens, but its activity does not change after it is synthesised. Similarly, the mechanical properties of a polymer coating are fixed at the time of its fabrication. In order to realise the next generation of medicine and materials, we must find a way to bring life-like features to the realm of synthetic systems.^{1,2}

In search of such materials, scientists have explored ways to control phenomena such as self-assembly and phase transitions with, for example, electrostatic and magnetic forces, temperature fluctuations or light, bringing systems out of equilibrium.³⁻⁶ One of the persisting approaches is based on the use of molecular switches, compounds that interchange reversibly between two or more distinct states in response to an external stimulus.⁷ This nanoscopic event alters the physicochemical properties of the compound, and if the switch is integrated into a larger structure, may even lead to function at the macroscopic level.⁸⁻¹⁰ On the other hand, so-called molecular motors capable of unidirectional rotation¹¹ open up new pathways for converting nanoscale phenomena into macroscopic response.¹²⁻¹⁵

While switches fuelled by chemical reactions,¹⁶⁻¹⁸ electric currents¹⁹⁻²¹ and other stimuli are also actively studied, in this thesis the focus will be on *photoswitches*, molecules that isomerise upon exposure to light. They are particularly attractive motifs as the wavelength, intensity and polarisation of light can be controlled precisely in space and time, a light stimulus can be induced remotely, and no waste

is accumulated in the system.^{22,23} Thus, it is no wonder that photoisomerisable molecules such as azobenzenes, diarylethenes and spiropyrans, as well as light-driven molecular motors, are increasingly applied for potential use in medicine,^{24–28} biosciences,^{29–32} catalysis,^{33–37} soft robotics,^{38–40} energy storage,^{41–47} electronics^{48–52} and optics,^{53–55} and fabrication of both nanoscopic and macroscopic structures.^{56,57}

Each application inflicts different demands on the photoinduced molecular-level changes needed for the desired function. For this reason, a single photoswitch structure capable of meeting the requirements of all applications cannot be designed. Instead, various photoswitch families have been developed, each with unique behaviour upon isomerisation: some photoswitches exhibit large changes in geometry and dipole moment, for others it is simply the changes in conjugation or absorption that give rise to photoinduced function. In addition, the structural and photochemical properties of the photoswitches need to be compatible with the application environment. For instance, water solubility and resistance towards cellular redox reactions are crucial in photopharmacology. Within a photoswitch family, these features can be tuned through synthetic modifications^{58,59} or by incorporating the switches into supramolecular assemblies that change their microenvironment.^{60–66}

Most photoswitches suffer from one critical incompatibility: one of the isomers is only accessible through excitation with ultraviolet light. This high-energy irradiation has a degrading effect on many materials and is particularly detrimental to living systems. To tackle this problem, photoswitches that can be isomerised with lower-energy red or near-infrared light, while maintaining the favourable properties of the parent molecule, are needed.^{58,67,68} Three approaches toward this goal can be identified: (i) tuning the spectral qualities of conventional photoswitches, (ii) developing new photoswitch families that inherently operate with low-energy light, and (iii) utilising red-light photocatalysts to isomerise conventional switches. To this date, none of these strategies have been perfected to the point of being practically useful for the aforementioned applications. Thus, more research is needed on all three fronts to truly harness the potential of photoswitches.

1.1 Aim and scope of this work

The objective of this thesis is to introduce, investigate and optimise strategies for inducing *E–Z* photoisomerisation with low-energy light. In particular, we strive towards systems that can be switched with visible or even near-infrared light in both

directions while exhibiting good thermal stability. Before zooming into this topic, the reader is provided with general knowledge of the molecular structures, isomerisation pathways and characterisation of known photoswitch families, as well as the theoretical principles of photoisomerisation. After this, the aim is to provide guidelines for shifting the switching wavelengths towards the red end of the visible spectrum and beyond. The aforementioned three strategies for accomplishing red-light photoswitching are then presented, providing both theoretical and practical considerations for each (Figure 1). Finally, it is shown how the same methods can also be utilised in red-shifting the excitation wavelengths of light-driven molecular motors.

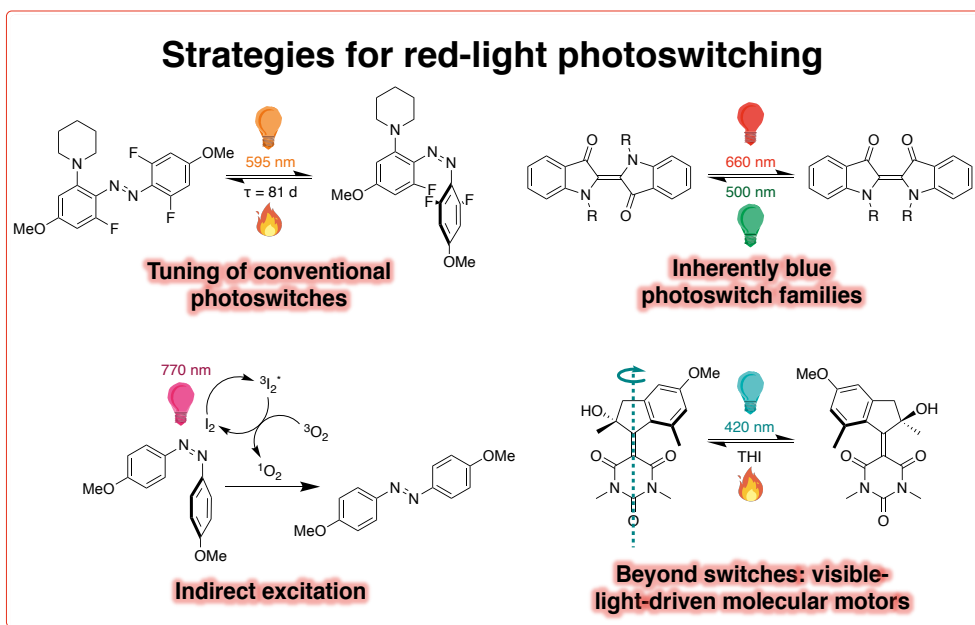


Figure 1. The focal areas of this thesis, with examples from the original publications of this thesis.

Extensive literature reviews are presented for each focal area of this thesis. They are exemplified by the four original publications. **Publication I** explores ways to modify the spectral properties of azobenzenes, the most widely used photoswitches, through combined *ortho*-amination and -fluorination. Through a systematic study of different substitution patterns and amino substituents, the structural features leading to the best compromise between highly red-shifted absorption bands and desired photoswitching dynamics are revealed. **Publication II** investigates an emerging class of photoswitches, *N,N*-difunctionalised indigo derivatives, demonstrating that with

a suitable synthetic design this inherently red-light-absorbing photoswitch family can be utilised efficiently both in a solution and in a polymeric environment. **Publication III** presents molecular iodine as a new near-infrared-light photocatalyst capable of isomerising suitably substituted azobenzenes from *Z* to *E*. Most interestingly, it is shown that the reaction is mediated by molecular oxygen. **Publication IV** focuses on the design of a synthetically simple visible-light-driven molecular motor and comprehensive studies of its photochemical behaviour. Originating from unexpected reactivity in a Knoevenagel condensation, the motor has a quaternary stereocentre featuring a hydroxy group, which promotes unidirectional rotation by stabilising the thermal step leading to progressive motion and by enhancing its excited-state rotation through a hydrogen-bond lasso effect that improves the photoisomerisation quantum yield.

While the publications represent different approaches to accomplishing red-light photoswitching, they are similar in their nature. None of the works present entirely new concepts or state-of-the-art solutions for accomplishing photoswitching with red light, although especially Publications II and IV mark distinct advances on the respective fronts. Instead, our studies aim at understanding different phenomena crucial for this ultimate goal, paving the way for further research. In addition to systematic studies made in Publications I and II, unexpected discoveries are investigated in Publications III and IV. All of these add to our understanding of photoswitch systems responsive to low-energy light.

1.2 Outline

This thesis comprises seven chapters. After familiarising the reader with the background and motivation for the study in Chapter 1, the theoretical framework of photoswitching is presented in Chapter 2, which also discusses the related experimental and computational methods. Chapter 3 showcases the structural modifications that have been implemented to red-shift the absorption bands of azobenzenes. In Chapter 4, less known photoisomerisable compounds operating with visible or near-infrared light are introduced. A third approach for red-light photoswitching, based on indirect photocatalytic pathways, is discussed in Chapter 5. In Chapter 6, it is shown how the principles explored in Chapters 3–5 can be applied for designing visible-light-driven molecular motors. Finally, the conclusions of this thesis are presented in Chapter 7 along with some perspectives on the potential next steps in this line of research.

2 PHOTOSWITCHING

When azobenzene crystals are irradiated with near-ultraviolet light, their colour changes from yellow to orange.⁶⁹ A distortion in the geometry of the crystals may also be observed. When purple or blue light is shone on the crystals, their original colour and shape are restored. This, of course, is a classic example of photoswitching arising from the fact that azobenzene molecules can exist as two isomers with different spectral properties and geometry.⁷⁰ But what are these isomers and how is it possible to convert from one to the other with specific wavelengths of electromagnetic radiation? In this chapter we will take a closer look into the chemistry behind this phenomenon: What structural features allow for a compound to function as a photoswitch? What are the photochemical and thermal mechanisms involved in the isomerisation? How can the various parameters of photoswitching be studied? An understanding of these fundamentals is crucial for the tailoring of photoswitching dynamics. Photoswitching is addressed in two sections based on whether it is purely based on *E*–*Z* (or *trans*–*cis*) isomerisation about a double bond (Chapter 2.1), or (also) involves the closing or opening of a ring (Chapter 2.2). *E*–*Z* switches are emphasised, as they are the focus of the next chapters. It should be stressed that even though all prominent photoswitch families and their properties are presented, this chapter is only meant to provide essential background information for the following chapters. For a proper introduction to the myriad of photoswitch families reported up to date, the reader is directed to excellent recent reviews.^{7,58,59} Finally, in Chapter 2.3, we shall go through the experimental methods of studying the photochemistry of these molecules.

2.1 Photoswitches based on *E*–*Z* isomerisation

The aforementioned azobenzene is a prime example of a molecule that can be switched with light between two states, the *E* and *Z* isomers (Figure 2a). The azo bridge provides the isomerisable unit, while the phenyl substituents account for the extended π -system required for absorption in the near-UV and visible light regime.⁷¹ In addition to azobenzene derivatives and their heteroarene equivalents built around

a N=N bond,^{72,73} *E*–*Z* photoswitches can also be made with other π -systems. Photoswitches such as (stiff-)stilbenes,⁷⁴ indigoids,⁷⁵ hemipiperazines,⁷⁶ and retinal that our eyesight is based on,⁷⁷ are based on the isomerisation of a C=C double bond, while hydrazone⁷⁸ and iminothioindoxyl⁷⁹ photoswitches rely on a C=N unit. These photoswitch families are exemplified in Figure 2b. Although the photochemical considerations in this section are given for azobenzene, they apply for other *E*–*Z* photoswitches as well, with some exceptions that are mentioned when necessary.

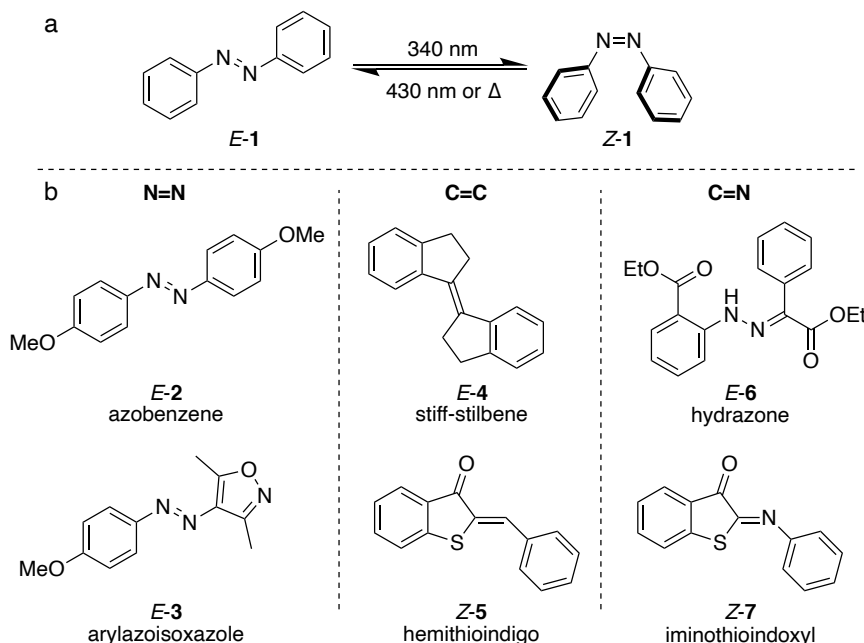


Figure 2. (a) *E*–*Z* isomerisation of azobenzene. (b) Selected examples of *E*–*Z* photoswitches based on N=N, C=C and C=N motifs. The isomer with lowest ground-state energy is depicted.

The *E* isomer of azobenzene is planar and its phenyl rings point in opposite directions, hence minimising steric effects. In the case of the *Z* isomer, however, the close proximity of the phenyl rings forces the molecule into a twisted conformation (Figure 2a).⁷⁰ As a result of increased steric interactions and reduced conjugation, the ground state energy of the *Z* isomer is ca. 12 kcal mol⁻¹ higher in energy compared to the *E* isomer.⁷¹ Thus, in the absence of light, azobenzene exists solely as the *E* isomer and the metastable *Z* isomer is only reached via photochemical pathways (*vide infra*). This is generally true for most photoswitches. However, in some cases, the energy difference between the isomers is so small that under equilibrating conditions a substantial fraction of the molecules exists as the metastable isomer. For example,

for certain indigoids the energy difference is only ca. 1 kcal mol⁻¹ or less, leading to dark equilibria where the isomer distribution is close to equal.^{80–82} It should also be noted that for some switches such as **5** and **7**, the stable isomer is actually assigned the *Z* notation. When generalised *E*–*Z* switching is described in this chapter, the *Z* isomer is denoted the metastable isomer.

The absorption spectrum of *E*-**1** in the ultraviolet-visible wavelength range is governed by an intense ($\epsilon = 23,000 \text{ M}^{-1} \text{ cm}^{-1}$) band at 316 nm (*n*-hexane).⁷¹ This arises from the symmetry-allowed transition from π to π^* , leading to the S_2 state. Another, significantly weaker ($\epsilon = 405 \text{ M}^{-1} \text{ cm}^{-1}$) band is located at 449 nm,⁷¹ corresponding to the $n\text{--}\pi^*$ transition that leads to the lower-energy S_1 state. This transition is symmetry-forbidden due to the orthogonality of the n and π^* orbitals, and it is only allowed to this extent because of planarity-breaking molecular vibrations coupled to the electronic transitions. The situation changes for *Z*-**1**. Due to the twisting of the molecule, the π -system is shortened, lowering the energy of the highest occupied π orbital and raising the energy of the lowest unoccupied π^* orbital. As a result, the energy of the $\pi\text{--}\pi^*$ transition increases, which is observed as a hypsochromic shift of the related peak in the absorption spectrum.⁷¹ Simultaneously, the probabilities of the $n\text{--}\pi^*$ and $\pi\text{--}\pi^*$ transitions increase and decrease, respectively, visible in the peak intensities. These factors together explain the observed spectral differences between the isomers (Figure 3).

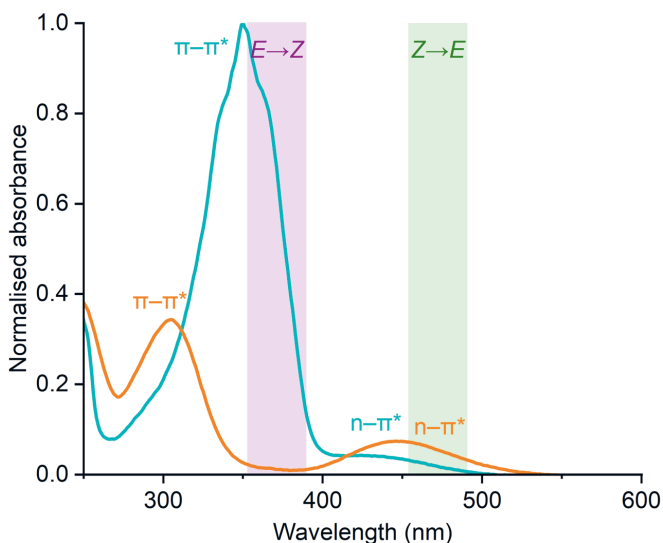


Figure 3. The absorption spectra of *E*-**2** and *Z*-**2** in *n*-hexane, visualising the $\pi\text{--}\pi^*$ and $n\text{--}\pi^*$ absorption bands of each isomer and typical isomerisation wavelengths.

The distinct absorption spectra allow for isomer-specific excitation to either S_1 or S_2 state, which is the key to photoisomerisation between the two species.⁷² In Figure 4, a schematic potential energy landscape of **1** is presented. Upon excitation at the $n-\pi^*$ band at ca. 450 nm, *E*-**1** is brought to the Frank-Condon geometry on S_1 . It then follows a barrierless pathway to a conical intersection leading to the ground-state *Z* isomer^{83–87} with an overall quantum yield of 0.25 in *n*-hexane.⁸⁸ When excitation at the $\pi-\pi^*$ band is applied, vibrational cooling from S_2 to S_1 takes place before the aforementioned pathway to *Z*-**1**.^{83–87} The quantum yield of photoisomerisation is lower when the $\pi-\pi^*$ band is used, only 0.11 in *n*-hexane,⁸⁸ which indicates the existence of an additional, non-productive relaxation mechanism, possibly through crossing to an S_3 state.⁸⁶ Due to deficiencies in the experimental and computational tools used to probe the reaction, no consensus has been reached on the nature of these pathways, although an out-of-plane rotation is widely supported for the $S_1 \rightarrow S_0$ deactivation and an in-plane inversion (with perhaps a torsional component) for the $S_2 \rightarrow S_1 \rightarrow S_0$ route.⁷² The matter is further complicated by the fact that the potential energy surfaces are solvent-dependent.^{72,89} In any case, excitation at both the $n-\pi^*$ and $\pi-\pi^*$ absorption bands leads to isomerisation from *E* to *Z*. Through similar pathways, excitation at the respective absorption bands of *Z*-**1** leads to isomerisation back to *E*.^{72,87,90} Because of the spectral shapes of the isomers, $\pi-\pi^*$ is typically used for *E* \rightarrow *Z* isomerisation and $n-\pi^*$ for the reverse reaction (Figure 3). Thermal back-isomerisation to *Z*-**1** has a barrier of ca. 22 kcal mol⁻¹ and occurs with a half-life of some 2 days at 25 °C.⁷² This reaction has traditionally been considered to proceed via inversion,^{72,91} but the arguably most convincing experimental and computational studies have instead suggested a rotational mechanism involving crossing to the first excited triplet state T_1 .^{83,92}

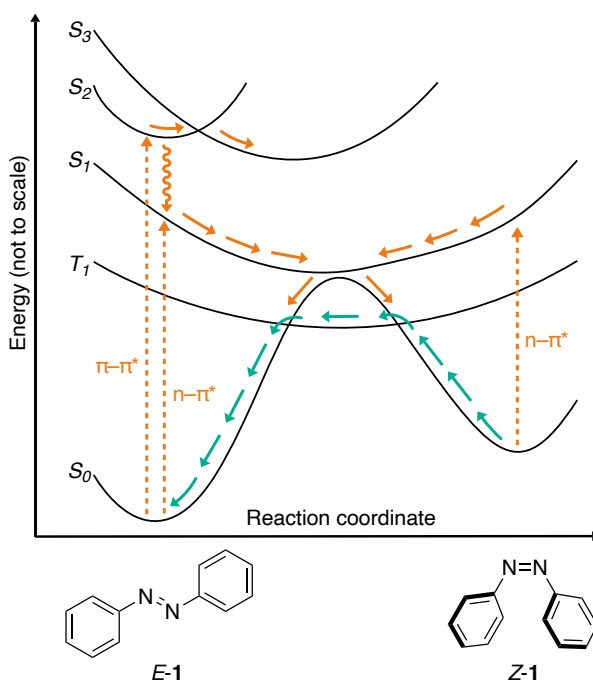


Figure 4. A schematic depiction of the photochemical (orange) and thermal (turquoise) isomerisation pathways of azobenzene. Dashed lines represent the absorption of a photon, solid lines traversing on the potential energy surfaces, and wavy lines vibrational cooling.

Similar mechanisms exist for other *E*–*Z* switches as well, but the exact photochemical and thermal pathways need to be determined individually for each photoswitch, as the energy landscapes can differ significantly.⁷² For instance, the substitution pattern of azobenzenes and azoheteroarenes dictates whether thermal isomerisation proceeds via rotation, inversion, rotation-assisted inversion or yet another pathway, e.g., a hydrazone intermediate possible for tautomerisable azoarenes.^{93,94} Also the absorption spectra are notably different for different photoswitch families: as an obvious example, the *n*– π^* absorption band does not exist for switches that isomerise about a C=C bond. The spectral characteristics of different molecular structures are discussed in more detail in Chapters 3 and 4.

We shall now revisit the concept of isomer-specific excitation leading to exclusive reaction from *E* to *Z* or vice versa. For most photoswitches, quantitative switching is not possible due to spectral overlap of the isomers. Instead, a photostationary state (PSS) is reached with wavelength-specific isomer distribution (PSD). If thermal isomerisation is slow enough (half-life of seconds or more), PSD is determined by the molar absorptivity coefficients $\epsilon_{E/Z}$ and isomerisation quantum yields $\phi_{E/Z \rightarrow Z/E}$.

At PSS, the isomer concentrations are constant, and thus, the rates of the reverse photoisomerisation reactions are equal:

$$\varphi_{E \rightarrow Z} I_{exc} (1 - 10^{-\varepsilon_E l [E]}) = \varphi_{Z \rightarrow E} I_{exc} (1 - 10^{-\varepsilon_Z l [Z]}) \quad (1)$$

Here, I_{exc} is the volumetric photon flux in photon moles per solvent volume over time (later called the excitation intensity) and l the light path in the medium. Evident from Equation 1, the excitation intensity does not have an effect on the PSD. If ground-state isomerisation is fast, also a thermal component needs to be accounted for. In dilute solutions (and sometimes in other environments as well) thermal isomerisation follows simple first-order kinetics with a temperature-dependent rate constant k . In this case, also the excitation intensity affects the PSD:

$$\varphi_{E \rightarrow Z} I_{exc} (1 - 10^{-\varepsilon_E l [E]}) = \varphi_{Z \rightarrow E} I_{exc} (1 - 10^{-\varepsilon_Z l [Z]}) + k_T [Z] \quad (2)$$

For most applications, a good PSD is required for the $E \rightarrow Z$ reaction, i.e. the $Z:E$ ratio in the PSS should be high. Thus, the metastable state should be stable enough or the excitation intense enough for the second term in Equation 2 not to affect the equilibrium. Apart from this, the optimal thermal stability of the metastable isomer is application-specific: in some cases, fast thermal back-isomerisation is favourable,^{54,95,96} in which case $Z \rightarrow E$ photoisomerisation is not needed. On the other hand, many applications rely upon efficient photoswitching between two stable states. On this basis, photoswitches are sometimes classified as T-type switches that isomerise back to the stable state thermally, and P-type switches for which only photochemical back-isomerisation is viable. In practice, no such division can always be made: thermal half-lives of azobenzenes vary from microseconds⁹⁷ (sub-picoseconds for certain azoheteroarene salts⁹⁸) to years⁹⁹ and are often highly environment-dependent,^{100,101} and the whole concept of a “stable” metastable isomer is linked to the time scale on which the photoswitching-induced function takes place.

Speaking of function, it is time to look at the photoinduced changes upon isomerisation. In the case of $E-Z$ switches, geometry is the dominating difference between the isomers. For azobenzenes, $E \rightarrow Z$ isomerisation reduces the distance between the *para* carbons from 10 to 5.9 Å, while the molecular shape changes from rod-like to bent.⁷¹ This can be used to control their self-assembly processes^{102–107} and to activate or deactivate catalytic^{34,35} or biologically active sites^{26–29} through steric interactions or preorganisation. When blended with a self-assembled system, for

example a liquid crystalline material, the shape change can be used to disturb the order, leading to phase transition^{108–110} and subsequently even macroscopic-level deformation.^{8,111,112} Also mechanical forces can be induced when the photoswitch is covalently bound to a polymer or elastomer network.^{112,113} Apart from geometry, also other properties change upon isomerisation. The dipole moment of *E*-**1** (and other symmetrical switches) is zero, but that of *Z*-**1** is 3.0 Debye, which is often a complementary factor in driving photoinduced function. The isomerisation can also be utilised as a memory element for an intelligent material,¹¹⁴ or for energy storage due to the energy difference between the isomers. Most of these demonstrations have been carried out with azobenzene derivatives,^{52,115} but the same principles apply to all *E*–*Z* switches. However, there are differences in the extent to which shape and other associated properties change and in how well the switch can be utilised in the application-specific environment. For instance, large geometrical changes are challenging to induce in confined environments typical for materials science applications,^{116,117} whereas in biological context factors such as water solubility^{59,118} and resistance to reduction (e.g., by glutathione)²⁹ are crucial.

2.2 Photoswitches based on cyclisation reactions

Compared to the simple isomerisation of *E*–*Z* switches, the pathways of photocyclisation are diverse: all the examples depicted in Figure 5 proceed via different isomerisation mechanisms, not to mention the photoswitch families such as fulgides,¹¹⁹ dihydroazulenes,^{120,121} chromenes^{122,123} and arene-bridged imidazole dimers^{124–128} that are omitted. Also the photoinduced physicochemical response varies greatly. We shall first focus on the most straightforward reaction, the electrocyclisation of diarylethenes.^{129,130} Exemplified by **8-o**, the open-ring isomer of a diarylethene features two aromatic sides that are linked by a C=C bridge. This aromaticity lowers their energy in contrast to the closed-ring isomer.¹³¹ Contrary to stilbenes, the double bond is constrained inside a cyclic structure, preventing *E*–*Z* isomerisation. The π -systems of the molecule are cross-conjugated and as a result, the transition to the lowest-lying excited state typically requires the use of UV light. Following excitation, a conrotatory six-electron electrocyclic ring-closure takes place,¹³² typically with relatively high quantum yields (mostly 0.3–0.6).¹³⁰ This reaction leads to an extended π -system, evident as the appearance of colour (Figure 6). Ground-state isomerisation via a disrotatory mechanism is allowed,¹³² but the energy barriers are typically large, especially so for dithianes for which the energy

difference between the isomers is small.¹³¹ Thus, for well-designed derivatives, thermal isomerisation takes place on a timescale of years at room temperature.¹³⁰ Quantitative isomerisation in the reverse direction is, however, easily achieved via visible-light excitation at the absorption band of the closed-ring isomer. The switching is highly robust, some structures enduring more than 10,000 switching cycles.^{130,133} Because of their outstanding thermal stability and negligible photodegradation as well as the distinct spectral and electronic differences between the isomers, diarylethenes are good candidates for memory components.^{51,130,134} The change in conjugation can also be utilised in photoswitchable organic field-effect transistors^{49,51} and catalysts.³⁶ Geometry changes are small compared to *E-Z* switches, which makes solid-state switching easy;^{116,117} yet, even this small shape change has been exploited in bringing about macroscopic deformations in crystalline and polymeric materials.^{135–137}

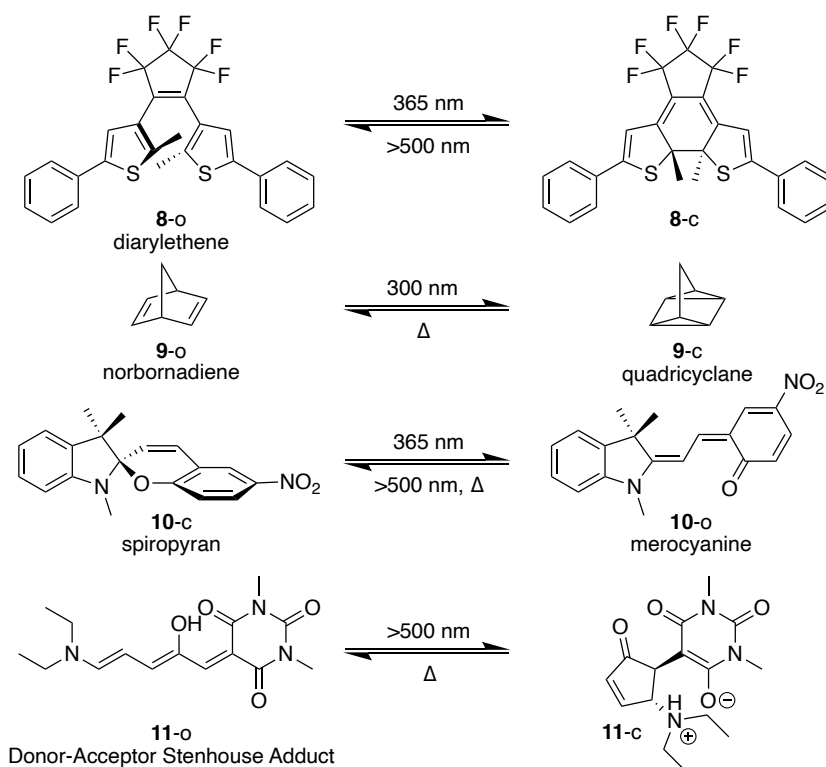


Figure 5. Selected photoswitch families based on photocyclisation reactions.

Another class of photoswitches that undergo photocyclisation in one elementary step are norbornadienes, derivatives of **9-o**. The mechanism is distinctly different, a [2+2] cycloaddition that can be induced via direct photoexcitation or indirectly using triplet sensitisers.¹³⁸ Because the π -system is lost during cyclisation, no low-energy transitions exist for quadricyclane and thanks to this negative photochromism (Figure 6), the system does not suffer from competing photoisomerisation to the reverse direction. Only thermal back-isomerisation with a substantial barrier is possible. Isomerisation does not induce changes in geometry or conjugation, but owing to the ring strain of the two formed three-membered rings, the energy of the metastable isomer **9-c** is ca. 21 kcal mol⁻¹ higher than that of **9-o**, and for some derivatives, the difference is even greater.¹³⁹ Although **9** only absorbs very energetic UV light (<300 nm), structural modifications lower the excitation energy, allowing visible-light photoisomerisation while retaining good thermal stability of the quadricyclane.¹⁴⁰ These red-shifted norbornadiene derivatives can be utilised in the storage of solar energy (the so-called MOST systems);^{41,43} it can be released as heat by catalysing the quadricyclane \rightarrow norbornadiene reaction with homogeneous or heterogeneous transition metal catalysts.^{141,142}

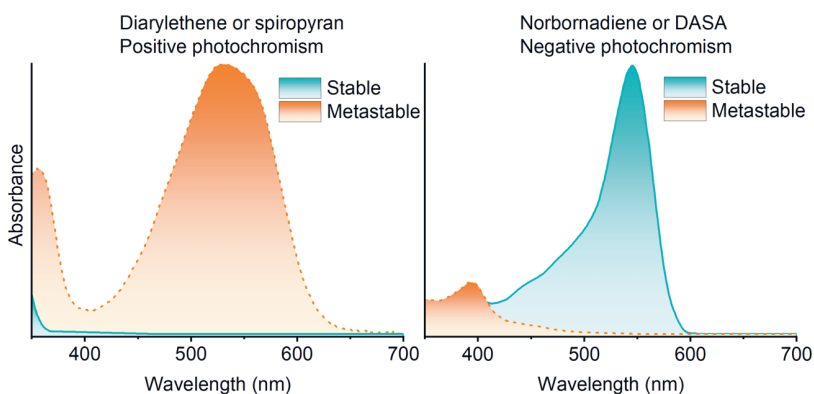


Figure 6. Schematic depictions of the absorption spectra of the stable and metastable isomers of a diarylethene or a spiropyran and norbornadiene or a DASA, demonstrating the difference between positive and negative photochromism.

The isomerisation mechanisms of the two remaining photoswitches are similar. The thermodynamically stable ring-closed form of spiropyran can be excited with UV light to bring about a six-electron electrocyclic ring opening.^{143,144} The resulting open-ring *Z*-merocyanine form will then isomerise thermally to the thermodynamically favoured *E* isomer. Merocyanines are highly conjugated and thus

absorb in the visible light regime. They exhibit strong solvatochromism, showing zwitterionic character in polar solvents and a neutral quinoidal structure in non-polar media.¹⁴⁵ Thermal back-isomerisation takes place on a timescale of minutes and can also be induced photochemically through excitation at the visible-light absorption band.¹⁴⁴ Moreover, also other stimuli such as changes in temperature, pH or temperature can be utilised to isomerise the molecule between the spiropyran and merocyanine forms.¹⁴⁶ Drastic differences in the geometry (and subsequently in, e.g., aggregation tendency),¹⁴⁶ dipole moment (4–6 to 14–18 D),¹⁴⁷ acidity¹⁴⁸ and fluorescence properties¹⁴⁹ exist between the neutral closed-ring and zwitterionic open-ring structures, which makes spiropyrans particularly interesting for stimuli-responsive dynamic materials.¹⁴⁶

Donor-Acceptor Stenhouse Adducts (DASAs) isomerise in a reversed fashion. The highly conjugated linear isomer has strong electron-donating and -withdrawing units across the π -system, lowering the energy of its π – π^* transition considerably: excitation wavelengths lie in the red end of the visible spectrum.^{150,151} After initial $E \rightarrow Z$ isomerisation, a thermal conrotatory four-electron electrocyclic ring-closure takes place.^{152–154} Conjugation is lost upon cyclisation so that the closed-ring isomer does not absorb visible light. This negative photochromism allows quantitative photoisomerisation to the closed-ring isomer. Concurrently, no excitation bands exist to induce the reverse reaction photochemically, limiting the application areas of DASAs.¹⁵⁵ Furthermore, the optimal structures for highly red-shifted absorption of the linear form (so-called second-generation DASAs) come with a price: the energy of the linear form is raised, even over that of the closed form, resulting in compromised thermodynamic equilibria with 2–83% of the coloured isomer; the equilibria are both solvent- and temperature-dependent.^{151,156} This issue can be countered by modifying the acceptor unit, allowing quantitative photoisomerisation in one direction and near-quantitative thermal isomerisation in the other.¹⁵⁷ The rate of the thermal ring-opening is highly solvent-dependent, isomerisation half-lives ranging from minutes to several hours even for the same molecular structure.¹⁵⁶

2.3 Characterisation of photoswitches

Regardless of the photoswitch family, the essential switching parameters include the spectral properties and wavelength-specific PSDs for both photoisomers as well as the thermal stability of the metastable species. The PSDs, in turn, are dictated by the molar absorption coefficients and isomerisation quantum yields of the isomers. The

experimental methodology used to determine these parameters is introduced in this section. Computational tools are also crucial for verifying experimental findings and understanding the pertinent photochemical mechanisms, but their detailed description falls outside the scope of this thesis. Herein, it is sufficient to know that conventional density functional theory (DFT) and time-dependent DFT (TD-DFT) methods are typically used to model the geometry, electronic transitions and isomerisation mechanisms of photoswitches, often accompanied by *ab initio* simulations.^{80,83,93,94,99,158,159}

Molar absorptivity (or extinction) **coefficients** ϵ (typically in $\text{dm}^3 \text{mol}^{-1} \text{cm}^{-1}$) for a specific wavelength are derived from the measured absorbance *Abs* (unitless) at that wavelength using the Beer-Lambert law. The value can be determined from a single spectrum or more accurately from a concentration series. In addition to the generally reported peak maxima (e.g., the π - π^* and n - π^* bands of azobenzenes), other wavelength-specific extinction coefficients can also be calculated, for example in the tail of an absorption band when it is used for excitation.

Photostationary state distribution (PSD) is determined during or after excitation with a specific wavelength, depending on the thermal isomerisation rate. The most accurate determination methods are quantitative nuclear magnetic resonance spectroscopy (NMR) and high-performance liquid chromatography (HPLC). If thermal isomerisation is negligible on the timescale of minutes, the sample can be irradiated to PSS and then studied with either of these methods, although determining accurate values has certain prerequisites: the NMR signals need to be sufficiently separated and in the case of HPLC, either the ϵ difference of the isomers needs to be known at the recording wavelength or an isosbestic point must exist. In the case of faster-isomerising compounds, HPLC cannot be utilised. ^1H NMR is functional for switches isomerising even on the timescale of seconds if custom-made *in situ* excitation setups are employed. However, at sub-second thermal isomerisation half-lives, the high concentration of an NMR sample typically hampers reaching good PSDs (cf. Equation 2 in Chapter 2.1). Moreover, neither NMR nor HPLC are feasible instruments for characterising solid-state samples. The third way of determining PSDs is based on the isomerisation-induced differences in the absorption spectrum of the compound. If the absorbance at a certain wavelength decreases by a certain factor χ upon isomerisation from a sample constituting of only the stable isomer, the molar fraction of the metastable isomer is equal to or bigger than χ . The value is only absolute if the absorbance of the metastable isomer is zero at the wavelength in question or if the pure metastable isomer spectrum can be determined through deconvolution;¹⁶⁰ otherwise, the value gives a lower limit for

the PSD (Figure 7). Despite this deficiency, the method is valuable when studying photoswitches whose thermal isomerisation is fast, and for probing the photoswitching in solid environments. If the PSD is known, the absorption spectrum of the pure metastable isomer can be calculated from the pure stable isomer and PSS spectra, as the absorbance at the PSS is

$$Abs_{PSS} = \chi_E Abs_E + \chi_Z Abs_Z \Rightarrow Abs_Z = \frac{Abs_{PSS} - \chi_E Abs_E}{\chi_Z}. \quad (3)$$

Through a similar procedure, the pure stable and metastable isomer absorption spectra can be calculated from two PSS spectra if the related PSDs are known.

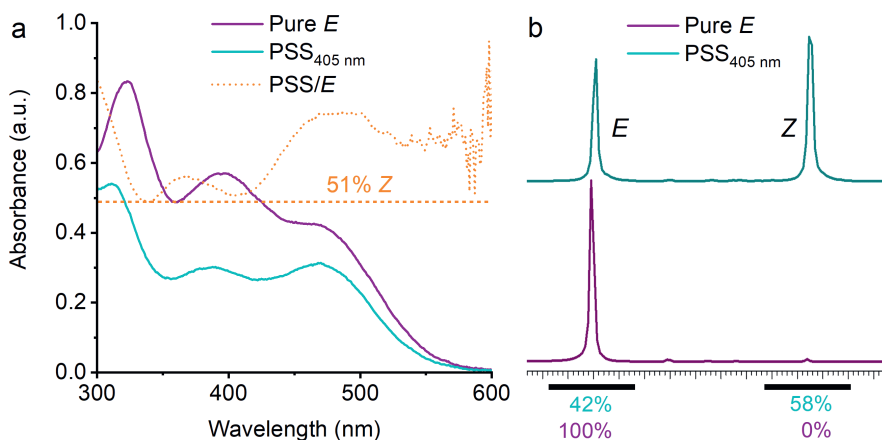


Figure 7. Determination of the PSD with (a) UV-visible absorption spectroscopy and (b) ¹H NMR spectroscopy. The determined lower limit for the PSD from (a) is 51% Z, whereas the absolute value from (b) is 58% Z.

Isomerisation quantum yields and the molar absorptivities of each isomer govern the PSDs. To determine quantum yields, the kinetics of isomerisation need to be monitored.¹⁶¹ For a general photoisomerisation reaction (here, $E \rightarrow Z$ for simplicity) where thermal isomerisation is slow enough to be neglected, the isomerisation rate is expressed by Equation 4: it depends on the quantum yields, excitation intensity and the fraction of light absorbed by each isomer. This equation cannot be solved analytically. If one of the isomers (here, Z) does not absorb at the excitation wavelength, the differential equation is simplified (Equation 5) and can be solved to yield Equation 6. In all cases, I_{exc} is the molar photon flux ($\text{mol dm}^{-3} \text{s}^{-1}$) and can be determined either with a power meter or more accurately through actinometry.

$$\frac{d[Z]}{dt} = -\frac{d[E]}{dt} = \varphi_{E \rightarrow Z} I_{exc} (1 - 10^{-\varepsilon_E l [E]}) - \varphi_{Z \rightarrow E} I_{exc} (1 - 10^{-\varepsilon_Z l [Z]}) \quad (4)$$

$$\frac{d[Z]}{dt} = -\frac{d[E]}{dt} = \varphi_{E \rightarrow Z} I_{exc} (1 - 10^{-\varepsilon_E l [E]}) \quad (5)$$

$$\log_{10}(10^{[E](t)\varepsilon_E l} - 1) - \log_{10}(10^{[E]_0\varepsilon_E l} - 1) = \varepsilon_E l \varphi_{E \rightarrow Z} I_{exc} t \quad (6)$$

In the case of only one absorbing species (here, the E isomer), the PSD can be monitored over time (e.g., with UV-vis spectroscopy) and this data fitted with Equation 6, to yield the quantum yield. The procedure is significantly simplified if the excited sample is concentrated enough to absorb all the irradiated light (i.e. we are operating in the total absorption regime where the absorbance at the excitation wavelength is > 2), as the last term in Equation 5 can now be omitted. In this case, the PSD can be determined before and after an excitation pulse (e.g., with NMR) and the φ value extracted from Equation 7.

$$[Z] = -\Delta[E] = \varphi_{E \rightarrow Z} I_{exc} t \quad (7)$$

However, often both isomers absorb at the excitation region, in which case the so-called initial slope method is utilised. The method approximates that, if starting from a pure isomer, the small fraction of the other isomer formed upon photoisomerisation does not affect the kinetics of the reaction in the beginning of excitation; thus, for the first ca. 10% of the isomerisation, Equations 6 and 7 can be used even when the forming isomer competes for the excitation light. It should be noted that when quantum yields are determined in a cuvette with steady-state spectroscopy, the excitation intensity must be low enough to allow for the sample to mix sufficiently on the timescale of the measurement. Conversely, if time-resolved spectroscopy is used on the millisecond timescale, mixing should not be used to keep the excited molecules inside the observation beam area. Nano- and femtosecond measurements are already fast enough for the mixing not to affect them.

Thermal isomerisation can be followed by any method where the isomers give rise to separate signals, thus enabling the tracking of the signal intensities (isomer distributions) over time. Most commonly, NMR, HPLC or absorption spectroscopy is utilised. As with the PSD determination, NMR and HPLC are only feasible for slow-isomerising systems (half-lives of hours or more) due to the minute-long recording times. Absorption spectroscopy, on the other hand, can be carried out even on the microsecond timescale, with no downsides compared to NMR or HPLC. Typically, either whole spectra are recorded with fixed time intervals and the

absorbance values at a given wavelength over time are extracted from the data (Figure 8), or the absorbance at a fixed wavelength is recorded continuously over time. The data is then fitted with a monoexponential decay function

$$Abs(t) = Abs_{\infty} - (Abs_{\infty} - Abs_0)e^{-\frac{t}{\tau}}, \quad (8)$$

in which Abs_0 and Abs_{∞} are the absorbance values at $t = 0$ and $t = \infty$, and τ is the lifetime of the metastable isomer. Another often used parameter, half-life $t_{1/2}$, can be acquired by multiplying τ by a factor of $\ln(2)$. Full conversion (>99%) is only acquired in the course of almost seven half-lives (Figure 6).

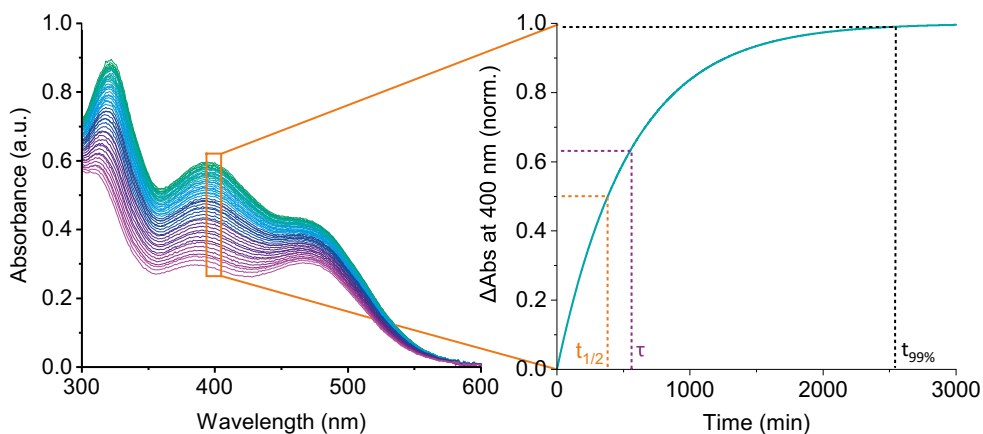


Figure 8. A schematic presentation of the monitoring of thermal isomerisation with UV-vis absorption spectroscopy.

If the environment of the photoswitch is heterogeneous, Equation 8 is modified accordingly. In the case of two distinct environments (e.g., complexed and freely solvated molecules), a biexponential fit (Equation 9) can be used, yielding the lifetimes τ_1 and τ_2 . If the heterogeneous medium is a continuum of different environments, a stretched exponential decay fit (Equation 10) is a better choice. In that case, the stretch factor b ($0 < b < 1$) expresses the amount of heterogeneity, being 1 for a homogeneous system (monoexponential decay).

$$Abs(t) = Abs_{\infty} - (Abs_{\infty} - Abs_0) \left(e^{-\frac{t}{\tau_1}} + e^{-\frac{t}{\tau_2}} \right) \quad (9)$$

$$Abs(t) = Abs_{\infty} - (Abs_{\infty} - Abs_0) e^{\left(\frac{-t}{\tau}\right)^b} \quad (10)$$

3 SPECTRAL TUNING OF AZOBENZENES

Having established the theory and practice of photoswitching, we shall now address the topic of this thesis, red-light photoisomerisation. Due to the success of various azobenzene-based applications, considerable effort has been put into tuning the absorption spectrum of azobenzene through synthetic modifications. Here, we will focus on the different approaches to red-shift the isomerisation wavelengths of azobenzene derivatives. Chapter 3.1 covers the structural designs that can be utilised to shift the π - π^* absorption band to longer wavelengths, while the more recent strategy of excitation at the n - π^* band to induce isomerisation in both directions is presented in Chapter 3.2. Finally, Chapter 3.3 concentrates on the original work of this thesis, a class of visible-light photoswitches, *ortho*-fluoroaminoazobenzenes. Azoheteroarenes are not covered in this chapter, although visible-light-absorbing equivalents have been published.¹⁶²

3.1 Red-shifting the π - π^* absorption band: electron-donating substituents, push-pull systems and protonated azobenzenes

The π - π^* absorption band is readily used for $E \rightarrow Z$ isomerisation, but for parent azobenzene, this requires excitation at ca. 340 nm or below. The introduction of electron-donating alkoxy and especially amino substituents in *ortho* or *para* position relative to the azo bond extends the conjugation of the π -system, thus raising and lowering the energies of the π and π^* orbitals, respectively, leading to a red-shift of the π - π^* band.^{163–165} Azobenzenes with pyrrolidino, piperidino or dialkylamino substituents attached to their *para* positions such as **12** (Figure 9) typically exhibit absorption maxima near 400 nm.^{163,165,166} Conjugated systems can also be built through *ortho* amination (cf. Chapter 3.3), in which case the absorption maximum can be shifted to >500 nm (**13**).^{94,167,168} Visible-light photoisomerisation of such azobenzenes is relatively efficient (PSDs up to >70% *Z*). The absorption band can be further red-shifted by employing an electron-withdrawing unit conjugated to the electron-donating moiety across the azo bridge. Typically these push-pull azobenzenes, exemplified by **14**, absorb at around 500 nm.¹⁶³ Their

photoisomerisation is often relatively inefficient due to reduced spectral resolution between the isomers. Through optimised designs based on multiple electron-donating and -withdrawing units, the absorption band can be shifted to the red region (**15**).¹⁶⁹ In addition, push-pull azobenzenes are solvatochromic, showing most red-shifted absorption spectra in protic solvents that can best stabilise the polarisation of the donor–acceptor molecule.¹⁶³

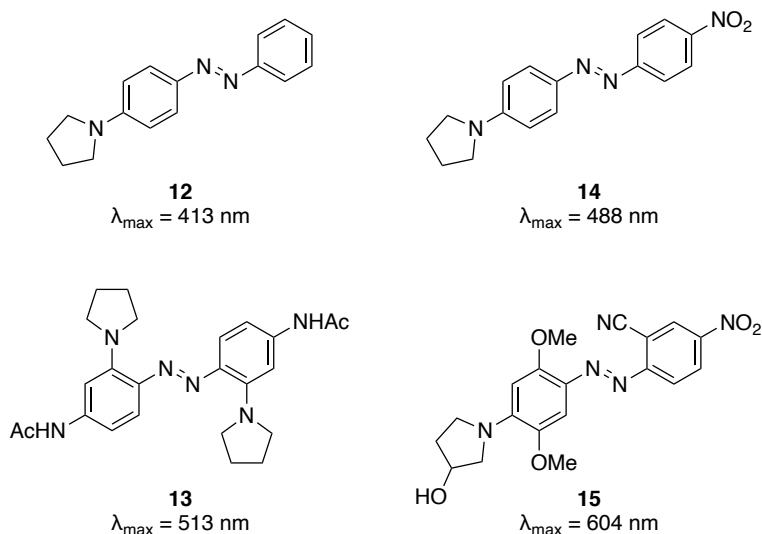


Figure 9. Absorption spectra of selected amino-substituted azobenzenes.

Generally, the energy of the π – π^* transition correlates with the ground-state isomerisation energy barrier,¹⁷⁰ limiting the application areas of aminoazobenzenes and push-pull systems. In aprotic organic solvents the thermal isomerisation of aminoazobenzenes is often relatively slow, half-lives spanning from seconds to tens of minutes. However, in aqueous environments and especially physiological conditions, thermal half-lives are shorter, lying in the sub-second range.¹⁷¹ This kind of instant switching between two states may be beneficial for applications such as photoinduced surface patterning,⁵⁴ vision restoration⁹⁵ and nonlinear optics,⁹⁶ but some azobenzenes isomerise so fast (in milliseconds or less) that efficient photoswitching is rendered practically impossible. These azobenzenes find use as dyes and photothermal converters in, e.g., photoactuation.¹¹¹

To shift the wavelengths further towards red, the azo bridge can be protonated to create azonium compounds (Figure 10). Traditionally, protonation has been utilised to red-shift the absorption maximum of azobenzene dyes¹⁶³ or to catalyse

the $Z \rightarrow E$ reaction since the N=N bond in azonium compounds is weakened.¹⁷² The concept of utilising azonium compounds themselves as photoswitches has been investigated less. Recently, it was shown that when a vast excess of trifluoromethanesulfonic acid is used with 4-methoxyazobenzene, the E isomer of the respective azonium ion **16** is formed.¹⁷³ This isomer can then be converted to the metastable Z -azonium with 520 nm light, albeit with a moderate PSD (36% Z). The Z -azonium is relatively stable in organic solvent ($t_{1/2} \approx 17$ min), although considerably destabilised in comparison with the deprotonated compound ($t_{1/2} \approx 30$ h). Thus, it is possible to switch from E to Z by consecutive acidification, visible-light excitation and neutralisation steps, although the low PSD undermines the strategy. Even near-infrared photoswitching has been enabled for the azonium molecule **17** with *para*-amino and *ortho*-alkoxy substituents. Low-intensity excitation at 720 nm induces fast $E \rightarrow Z$ photoisomerisation; unfortunately, the PSD was not reported.¹⁷⁴ When irradiation is ceased, fast thermal isomerisation restores the original isomer.

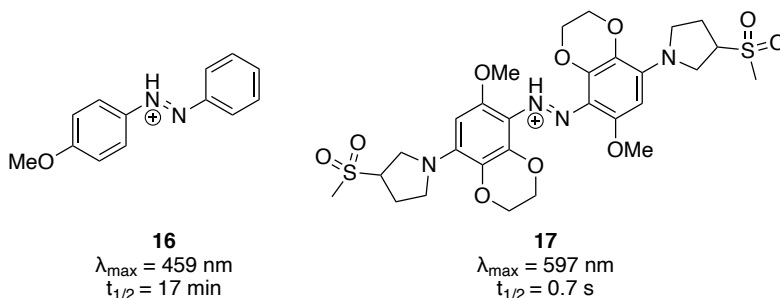
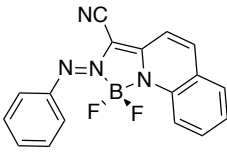


Figure 10. Photochemical properties of selected azonium compounds.

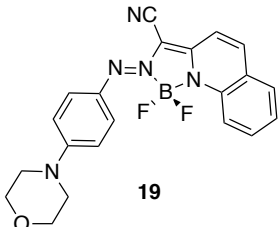
Finally, we shall have a look at azo- BF_2 photoswitches. Strictly speaking, they are not azobenzenes, so it is somewhat questionable whether they fall into the scope of this chapter. The bond between the azo group and boron locks the highly conjugated right-hand side of the molecule in one conformation, thus enabling $E \rightarrow Z$ isomerisation about the N=N bond. Because of the extended π -system of **18**, a low-energy and relatively high-intensity $\pi_{\text{nb}} \rightarrow \pi^*$ transition exists in the green-light regime, enabling efficient isomerisation from E to Z and back with 570 and 450 nm excitation, respectively (Table 1). Considering the absorption wavelengths, the metastable Z isomer is surprisingly stable, showing a half-life of 12.5 hours at room temperature.¹⁷⁵ The absorption band can be further red-shifted by employing electron-donating amino substituents in the *para* position of the left-hand phenyl

ring. In a systematic study of various substituents, it was found that the switch **19** functionalised with a morpholinyl moiety yielded the best combination of red-shifted absorbance (maximum at 680 nm), good $\text{PSD}_{E \rightarrow Z}$ (83% with 710 nm excitation) and reasonable thermal stability (15 min).¹⁷⁶ The right-hand side can also be modified. The compound **20**, despite exhibiting worse photochemical features than its two cousins, is particularly interesting: its thermal isomerisation rate is highly concentration-dependent, the half-life of the *Z* isomer spanning from 6.5 minutes to almost 200 hours on a concentration range from 22 μM to 3.8 mM due to aggregation that hampers the isomerisation.¹⁷⁷ This phenomenon could be exploited by designing pharmaceuticals that remain in their active form at sites where they are able to form aggregates (e.g., upon accumulation to cancer cells), while isomerising to their inactive forms in seconds elsewhere. However, it should be noted that although the azo- BF_2 switches show good photochemical properties, their potential for applications has not yet been demonstrated. One possible downside in utilising the isomerisation is the minor geometry change as compared to azobenzenes.

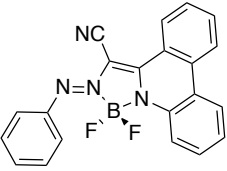
Table 1. Photochemical properties of selected azo- BF_2 complexes.



18



19



20

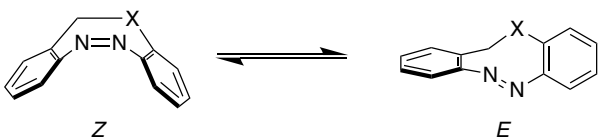
	λ_{max} (<i>E</i>)	λ_{max} (<i>Z</i>)	ϵ_{max} (<i>E</i>)	$\text{PSD}_{E \rightarrow Z}$	$\text{PSD}_{Z \rightarrow E}$	$t_{1/2}$
18	530 nm	480 nm	8,000	97% (570 nm)	80% (450 nm)	12.5 h (21 °C, DCM)
19	680 nm	-	28,000	83% (710 nm)	-	15 min (21 °C, DCM)
20	535 nm	501 nm	12,400	91% (600 nm)	65% (430 nm)	6.5 min (21 °C, DCM) ^a

^a Concentration-dependent: 6.5 min at 22 μM , 195 h at 8.3 mM.

3.2 Utilising the $n-\pi^*$ absorption band: *ortho*-substitution

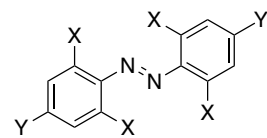
While the energy of the $\pi-\pi^*$ band has been successfully tuned to realise visible-light-switching azobenzenes with fast thermal isomerisation, switching between two stable isomers is not possible via this approach as a red-shift is generally accompanied by a decrease in the *Z* stability.¹⁷⁰ To combine visible light isomerisation with good thermal stability, it is thus necessary to utilise the less

probable but lower-energy $n\text{--}\pi^*$ transition. For most azobenzenes the $n\text{--}\pi^*$ bands of the *E* and *Z* isomers overlap to the extent that efficient bidirectional isomerisation is impossible and somewhat efficient $Z \rightarrow E$ isomerisation is only possible because of the higher molar absorptivity of the *Z* isomer.^{71,72} To overcome this hurdle, structural modifications have been discovered that selectively alter the energy states of only one isomer, thus enabling photoisomerisation in both directions using visible light only. The first such example was the diazocine structure **21** (Table 2). The ethylene bridge between the *ortho* carbons separates the $n\text{--}\pi^*$ bands by 86 nm, allowing switching between PSDs of 92% *Z* and 100% *E* with 520 and 385 nm light, respectively.¹⁷⁸ The structure of the *E* isomer is highly twisted compared to parent azobenzene, thus increasing the molar absorptivity at its $n\text{--}\pi^*$ band compared to the latter ($\epsilon = 750 \text{ M}^{-1} \text{ cm}^{-1}$ vs $405 \text{ M}^{-1} \text{ cm}^{-1}$). Most interestingly, due to its constrained ring structure, the *Z* isomer is stabilised by 6–7 kcal mol⁻¹ compared to what is now a metastable *E* isomer, with a thermal *E*-half-life of 4.5 hours at room temperature. In an effort to improve the photochemical properties, heterodiazocines in which one of the carbon atoms in the ethylene bridge has been replaced with an oxygen, sulphur or nitrogen atom, have been synthesised.^{179,180} Out of these, oxygen (**22**) blue-shifts the $n\text{--}\pi^*$ band of the *Z* isomer while also decreasing the thermal stability of the *E* isomer, whereas sulphur (**23**) retains the $n\text{--}\pi^*$ absorption band of the *Z* isomer at 405 nm and stabilises the metastable isomer significantly, leading to better overall qualities. The tails of the $n\text{--}\pi^*$ absorption bands extend to the far-red region, enabling $E \rightarrow Z$ isomerisation with >650 nm light.¹⁷⁹ Nitrogen-substituted diazocines have also been designed, and as the most intriguing group of compounds, alkylated derivatives (e.g., **24**) show remarkable red-shift in their $n\text{--}\pi^*$ (*E*) bands, enabling quantitative photoisomerisation to *Z* even with 740 nm light.¹⁸⁰ However, the $\text{PSD}_{Z \rightarrow E}$ is only 50% and thermal isomerisation occurs in less than a minute. Using an acetyl-functionalised nitrogen atom (**25**) improves the PSD to 85% and increases the thermal stability of the switch, but at the same time, the narrower absorption band inhibits the use of NIR light. In addition, true for all diazocines reported so far, the $Z \rightarrow E$ isomerisation can only be achieved with UV or purple light, thus limiting the applicability of these switches in biological context. This hampers their use in photopharmacology although quantitative photoisomerisation to the *Z* isomer might offer interesting possibilities, seeing that (i) many azobenzene-based potential photoswitchable pharmaceuticals are active in their linear *E* form and inactive in the more closed *Z* form, and (ii) the ability to get rid of traces of the biologically active isomers is the key to good photoresponsivity in the activity of the drug.²⁸

Table 2. Photochemical properties of selected diazocines.


	X	λ_{\max} (Z)	λ_{\max} (E)	PSD _{E→Z}	PSD _{Z→E}	t _{1/2}
21	CH ₂	404 nm	490 nm	>99% (520 nm)	92% (385 nm)	4.5 h
22	O	385 nm	525 nm	>99% (520 nm)	80% (385 nm)	89 s
23	S	405 nm	525 nm	>99% (520 nm)	70% (405 nm)	3.5 d
24	NMe	401 nm	554 nm	>99% (740 nm)	50% (405 nm)	40 s
25	NAc	400 nm	520 nm	>99% (590 nm)	85% (405 nm)	29 min

Tetra-*ortho*-methoxyazobenzenes (**26** in Table 3) were published in 2011.¹⁸¹ Due to repulsive interactions between the oxygen and nitrogen lone pairs, the *ortho*-methoxy substituents force the molecule out of planarity, thus increasing the probability of the n- π^* transition tenfold compared to the parent azobenzene ($\epsilon = 4,030 \text{ M}^{-1} \text{ cm}^{-1}$). In addition, they raise the n orbital energy of the *E* isomer, which leads to a red-shift of the n- π^* band. This effect is not present in the highly twisted *Z* isomer where the methoxy moieties do not clash with the nitrogen atoms. Thus, the n- π^* absorption bands are separated, although only by 36 nm. This is still enough to enable switching between PSDs of 80% *E* and 85% *Z* with 450 and 530 nm light, respectively. In addition to lowering the excitation energy for the stable \rightarrow metastable state photoisomerisation compared to diazocines (from 405 to 450 nm), this molecular design shows good thermal stability for the *Z* isomer ($t_{1/2} = 2.4$ days).

Table 3. Photochemical properties of *ortho*-methoxy-¹⁸¹ and *ortho*-fluoroazobenzenes.⁹⁹


	X	Y	λ_{\max} (E)	λ_{\max} (Z)	PSD _{E→Z}	PSD _{Z→E}	t _{1/2}
26	OMe	NHAc	480 nm	444 nm	80% (530 nm)	85% (450 nm)	14 d (25 °C, DMSO)
27	F	H	460 nm	417 nm	86% (>500 nm)	91% (410 nm)	1.9 y (25 °C DMSO)
28	F	CO ₂ Me	474 nm	421 nm	90% (>500 nm)	97% (410 nm)	56 h (20 °C, DMSO)

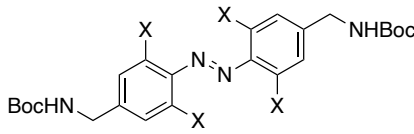
Tetra-*ortho*-fluorinated azobenzenes (e.g., **27**), published a year after their *ortho*-methoxy equivalents, show similar behaviour. Fluorine atoms are considerably smaller than methoxy substituents, and thus the molecule can assume a mostly planar structure. Their strongly electron-withdrawing inductive effect lowers the energies of all frontier molecular orbitals (FMOs) except the n orbital, possibly because of

steric interactions between the nitrogen lone pairs and the fluorine atoms. The n orbital of the *Z* isomer is lower in energy, leading to 42-nm separation of the n- π^* bands. As a downside compared to **26**, the maxima of these bands are located at ca. 30 nm shorter wavelengths compared to the *ortho*-methoxyazobenzenes. On a positive note, near-quantitative bidirectional switching is possible with >500 and 410 nm excitation ($E \rightarrow Z$ and $Z \rightarrow E$, respectively). Even more importantly, the thermal half-lives of their *Z* isomers reach years at room temperature, which was unprecedented at the time and remains a valuable quality for a plethora of applications.⁹⁹ Thermal stability can be tuned by changing the number of *ortho* fluorines to meet the requirements of a given application.¹⁸² Although this degree of stability can nowadays also be accomplished with certain azoarylpyrazoles,¹⁸³ no other azoarene families are known to couple year-long *Z*-half-lives with efficient visible-light activation. The tail of the absorption band extends to the red-light region. Thus, even >600 nm light has been used for the $E \rightarrow Z$ isomerisation of azobenzenes bearing ester¹⁸⁴ or aldehyde¹⁸⁵ moieties in the *para* position. Such π acceptors improve the PSDs in both directions (**28** in Table 3). However, they also destabilise the *Z* isomer drastically.¹⁸²

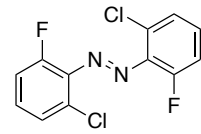
In addition to the second-row elements oxygen and fluorine, heavier chalcogens and halogens have been introduced to the *ortho* position (**29–35**, Table 4).^{186–188} As the atom size increases and steric interactions become stronger, the planarity of the *E* isomer decreases. This effect leads to lessened spectral differences between the isomers and subsequently worse PSDs.¹⁸⁶ At the same time, the increased steric load raises the energies of both isomers, thus lowering the activation energy of isomerisation: the half-life of the *Z* isomer decreases from years to minutes in the halogen series $F > Cl > Br > I$ and from days to seconds in the chalcogen series $O > S > Se$ (photoisomerisation was not observed for tellurium-substituted equivalents).¹⁸⁶ Yet, the heavier-atom derivatives have an advantage over their second-row equivalents: conformational flexibility increases as a function of atom size, which is observed as a broadening of the n- π^* bands – allowing for lower-energy excitation to be used for the $E \rightarrow Z$ isomerisation. The absorption band tails of iodo- and seleno-substituted azobenzenes **32** and **35** extend up to the near-infrared wavelengths.¹⁸⁶ However, in the quest for bistable red-light switches, it is the *ortho*-chlorinated azobenzenes **30** that show most potential, combining red-light $E \rightarrow Z$ isomerisation and relatively high photostationary states with practically bistable character (*Z*-half-lives of days or weeks at room temperature).^{186,188–190} Based on systematic structure–property studies, moderately electron-donating *para* substituents are the key to good PSDs upon red-light excitation, as they improve the

spectral resolution in the absorption tail and also seem to have a positive effect on the quantum yield of isomerisation in the $E \rightarrow Z$ direction.¹⁸⁸ Strongly electron-donating or -withdrawing groups (e.g., amino and nitro), however, are detrimental for the stability of the Z isomer.

Table 4. Photochemical properties of *ortho*-halogeno- and *ortho*-chalcogenoazobenzenes.¹⁸⁶



29–35



36

	X	λ_{\max} (n- π^* , E)	PSD $_{E \rightarrow Z}$	$t_{1/2}$ (DMSO)
29	F	454 nm	84% (530 nm)	1.3 y (25 °C)
30	Cl	463 nm	77% (625 nm)	6.7 d (25 °C)
31	Br	466 nm	66% (625 nm)	12 h (25 °C)
32	I	514 nm	50% (625 nm)	5 min (25 °C)
33	OMe	460 nm	95% (625 nm)	8.2 d (25 °C)
34	SEt	515 nm	46% (625 nm)	3 min (25 °C)
35	SeMe	534 nm	n.d.	34 s (25 °C)
36	-	463 nm	97% (660 nm)	16 h (70 °C)

Mixed *ortho* substitution has been investigated less although it may provide means to combine the favourable qualities of two different azobenzene families. As the sole example in literature, azobenzene **36** carrying two fluorines and two chlorines in *ortho* positions has been studied in detail.¹⁹¹ This substitution pattern yields good Z -stability (half-life of 16 h at 70 °C, corresponding to weeks at room temperature) as well as a bathochromic shift even greater than for *ortho*-chloroazobenzenes. The compound can be isomerised efficiently from E to Z with 660 nm excitation (PSD 97% Z) back to E with 410 nm (PSD 90% E).

3.3 Fluoroaminoazobenzenes

Despite the developments during the last decade or so in the ways to realise visible-light-driven isomerisation via n- π^* excitation, the $Z \rightarrow E$ excitation wavelengths of thermally stable azobenzenes still lie in the blue end of the visible spectrum, which is an obstacle to their use *in vivo*. Furthermore, due to the low molar extinction of the n- π^* band, isomerisation via excitation in this region is often very slow. The issue is most pronounced for *ortho*-chlorinated azobenzenes for which the red-side

tail of the absorption band needs to be used for efficient isomerisation. In some cases, good PSDs are only reached after hours of high-intensity irradiation.^{190,191} The visible-light absorptivity can be enhanced by employing *ortho*-amino substituents: they red-shift the π - π^* band through the interaction of the amino lone pair and the π -system, and increase the intensity of the n - π^* band by breaking the planarity.^{94,167} Unfortunately, this also shortens the thermal *Z*-half-life, even to sub-second timescales in some cases. As their advantage, amino-substituted azobenzenes are resistant to glutathione,¹⁶⁷ a common cellular antioxidant that reduces less electron-rich azobenzenes and compromises their applicability in intracellular systems.^{29,192} In addition, amino substituents such as piperazine and proline derivatives provide additional functionalisation sites in the *ortho* positions, enabling molecular structures unattainable with *ortho*-halogenated compounds.

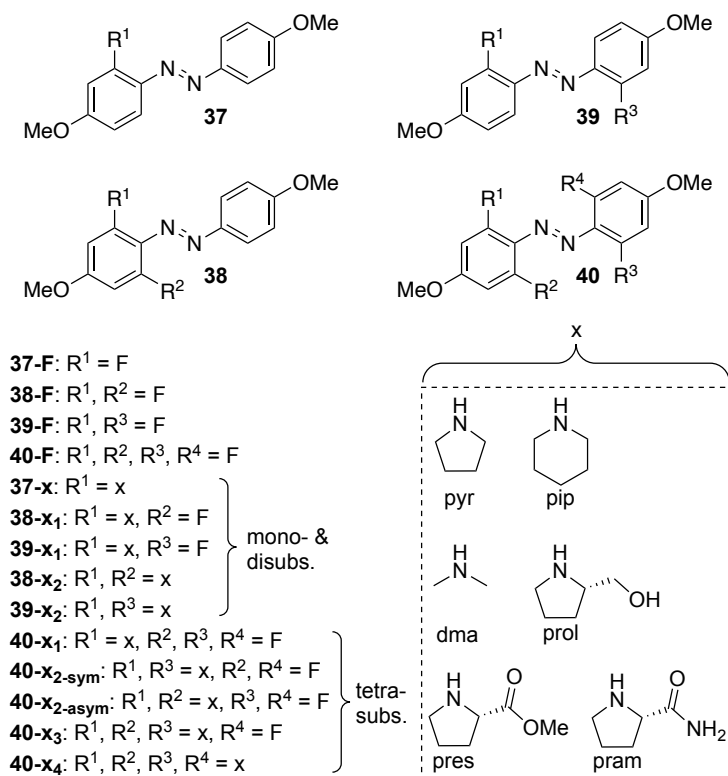
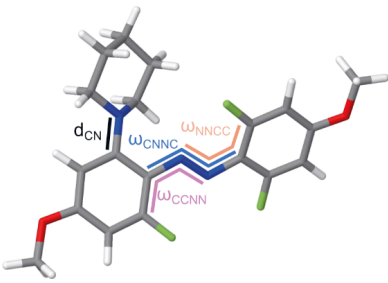


Figure 11. Structures of *ortho*-aminated and -fluorinated azobenzenes (pyr = pyrrolidine, pip = piperidine, dma = dimethylamine, prol = prolinol, pres = proline methyl ester, pram = prolinamide). Modified with permission from ref. 94. Copyright 2022, Springer.

Thus, we set out to investigate whether the good thermal stability of *ortho* fluorination and the high visible-light absorptivity of *ortho* amination can be combined. Starting from *ortho*-fluoroazobenzenes with four different fluorination patterns and utilising an efficient nucleophilic aromatic substitution reaction,¹⁶⁸ one or more fluorines were easily substituted with six secondary amines (pyrrolidine, piperidine, dimethylamine, L-prolinol, L-proline methyl ester and L-prolinamide) in good or moderate yields (Figure 11). In total, we synthesised 41 azobenzene derivatives and studied them in acetonitrile to determine structure–property relationships in this class of photoswitches.⁹⁴ Herein, we shall describe separately (i) the substitution pattern effects in a series of piperidino-substituted compounds and (ii) the effect of the amine within a substitution pattern, restricting our analysis to only three of the amino substituents (pyrrolidino, piperidino and dimethylamino).

Table 5. Selected *ortho*-fluorinated and -aminated azobenzenes along with their measured absorption maxima and molar extinction coefficients, and calculated (B3LYP+D3(BJ)/6-31G*/PCM(MeCN)) dihedral angles and $N_{\text{amine}}\text{--Ar}$ bond lengths. Modified with permission from ref. 94. Copyright 2022, Springer.



	λ_{max} (nm)	ϵ ($\text{M}^{-1} \text{cm}^{-1}$)	ω_{CCNN} ($^{\circ}$)	ω_{CNNC} ($^{\circ}$)	ω_{NNCC} ($^{\circ}$)	d_{CN} (\AA)
37-F	357/432	29110/3608	0	180	0	-
37-pip	341/402/449	14924/10075/6800	16	177	3	1.401
38-pyr₁	335/411/454	16739/8006/7792	23	177	8	1.369
38-pip₁	337/381/453	15930/8911/3493	29	177	4	1.398
38-dma₁	337/390/449	17179/8293/5555	29	177	4	1.399
39-pip₁	349/411/447	16610/10890/9228	15	178	2	1.400
40-pip₁	334/394/457	8503/3975/2340	28	177	7	1.394
40-pip_{2-sym}	321/384/465	5516/3060/2000	20	177	20	1.395

The fluorinated precursors **37-F**, **38-F**, **39-F** and **40-F** are essentially planar and thus show an intense $\pi\text{--}\pi^*$ band at 343–357 nm ($\epsilon \approx 25,000\text{--}29,000 \text{ M}^{-1} \text{cm}^{-1}$) accompanied by a weak $n\text{--}\pi^*$ band at 432–435 nm ($\epsilon \approx 2,200\text{--}3,600 \text{ M}^{-1} \text{cm}^{-1}$). When at least one fluorine is substituted with an amine, the intensities change drastically: the intensity of the $\pi\text{--}\pi^*$ band decreases by half, while a three- to four-fold increase

is observed in the visible-light absorbance (see selected compounds in Table 5). This observation indicates the twisting of the structure. Based on DFT geometry optimisations on the B3LYP+D3(BJ)/6-31G*/PCM(MeCN) level of theory, this is indeed the case, as the dihedral CCNN angle on the amino side is markedly non-zero (15–29°) for all amino-substituted compounds. The twisting is most pronounced for the compounds with two amino groups (e.g., **40-pip**_{2-sym}).

In addition to changes in the relative intensities of the bands, other spectral alterations are observed. Most interestingly, the *ortho*-amino(fluoro)azobenzenes show three absorption bands in the UV-visible region (Table 5), in contrast to the two bands ($\pi\text{--}\pi^*$ and $n\text{--}\pi^*$) that typically form the absorption spectrum of azobenzenes. A frontier molecular orbital analysis based on the aforementioned geometry optimisations reveals that the $S_0 \rightarrow S_1$ and $S_0 \rightarrow S_3$ transitions have $n\text{--}\pi^*$ and $\pi\text{--}\pi^*$ character, respectively, while the $S_0 \rightarrow S_2$ transition can best be described as an $n_{\text{amino}}\text{--}\pi^*$ transition, although the “ n_{amino} ” orbital also has considerable contribution from the π -system (Figure 12). The π orbital (in $S_0 \rightarrow S_3$) is barely at all located on the nitrogen, which explains why the $\pi\text{--}\pi^*$ band is not significantly shifted in comparison to the non-aminated parent compounds.

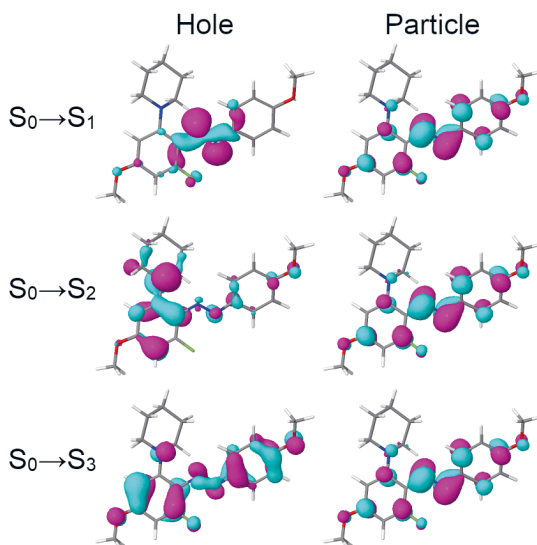


Figure 12. Dominating natural transition orbital (NTO) pairs of the three low-energy transitions of *E*-**38-pip**₁ from “hole” NTO to “particle” NTO, calculated at the B3LYP+D3(BJ)/6-31G*/PCM(MeCN) level of theory. The contributions of the shown hole–particle pairs to the respective transitions are larger than 99%. Adapted with permission from ref. 94. Copyright 2022, Springer.

The spectral changes upon *ortho* amination are visualised in Figure 13ab for a series of switches that all have the same amino (piperidino) substituent, thus allowing the comparison of substitution patterns. The visible-light absorbance is most pronounced in the case of the **39-x₁** and **39-x₂** series that have amino and fluoro substituents or two amino substituents in opposite rings, respectively, with intense ($\epsilon \approx 9,000\text{--}12,000\text{ M}^{-1}\text{ cm}^{-1}$) absorption bands at $>430\text{ nm}$. If amino and fluoro substituents are located in the same aryl ring (**38-x₁**), the visible-light absorption is less pronounced, presumably due to the electron-withdrawing inductive effect of the fluorine atom that lessens the electronic effect of the amino substituent. If two amino substituents are located in the same aryl ring (**39-x₁**, **40-x_{2-asym}**), the aforementioned third transition is not visible in the spectrum, but instead the spectral shape resembles a normal azobenzene with distinctly red-shifted $\pi\text{--}\pi^*$ band (a so-called aminoazobenzene).

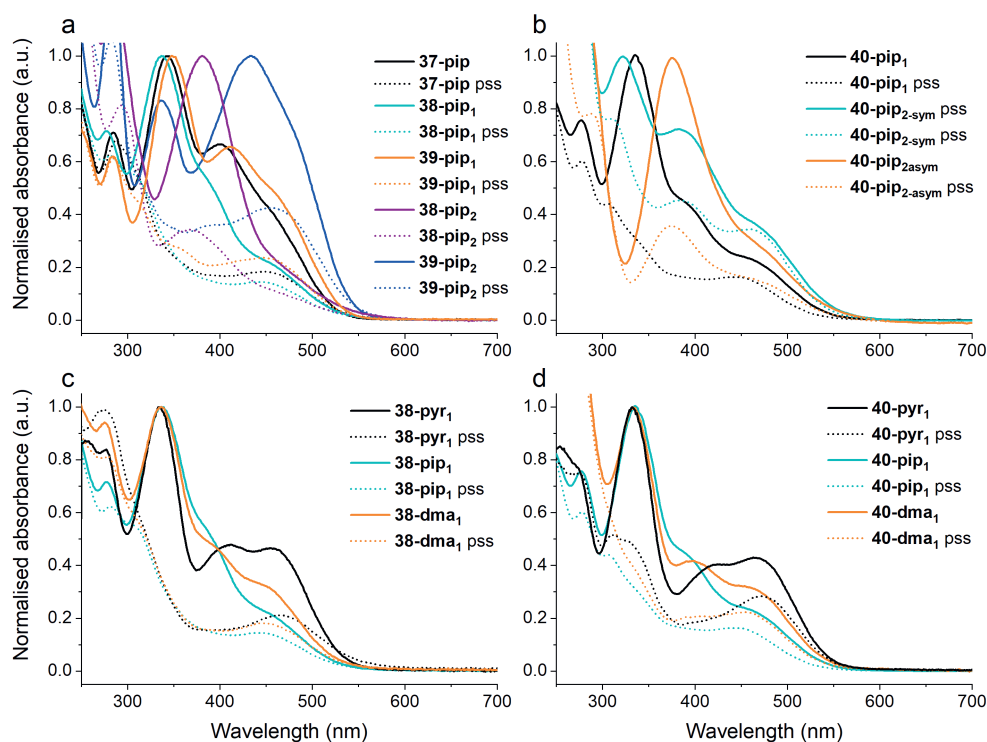


Figure 13. Normalised absorption spectra of (a) mono- and di-*ortho*-functionalised and (b) tetra-*ortho*-functionalised azobenzenes carrying piperidino substituents, and azobenzenes from (c) **38-x₁** and (d) **40-x₁** series carrying either pyrrolidino, piperidino or dimethylamino substituents. Adapted with permission from ref. 94. Copyright 2022, Springer.

The nature of the amine also affects the absorption profile. The intensity of the $n-\pi^*$ band is dramatically higher for the pyrrolidino-substituted compounds (e.g., **38-pyr₁** and **40-pyr₁**) than for the piperidino- and dimethylamino-substituted equivalents (Figure 13cd). This originates from steric interactions: the five-membered pyrrolidino ring adopts a planar geometry and thus has significant steric interactions with the azo nitrogen lone pair, while the larger bond angles in the six-membered piperidino ring and the unconstrained dimethylamino moiety do not allow planar structures at the amino nitrogen, thus lowering the amount of steric clash with the nitrogen bridge. The increased planarity of the pyrrolidino moiety implicates a notable sp^2 character for the nitrogen, which is indeed visible in the length of the $N-C_{Ar}$ bond, being 2.9 pm shorter for the pyrrolidino than for piperidino (Table 5) – i.e., the bond has significant double bond character. Thus, the pyrrolidino substituent is also more capable of donating electron density to the system. Interestingly, also the $n-\pi^*_Z$ band (Z-rich PSS) is notably stronger for pyrrolidino-substituted compounds (Figure 13cd), even exceeding the absorptivity of the $n-\pi^*_E$ band beyond ca. 530 nm for **38-pyr₁**.

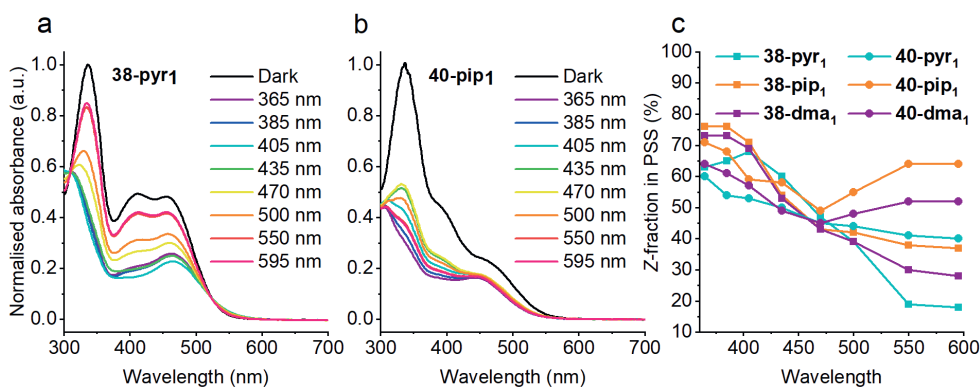


Figure 14. Photostationary state spectra of (a) **38-pyr₁** and (b) **40-pip₁**, and (c) PSDs of **38-x₁** and **40-x₁** upon excitation with 365–595 nm light. Modified with permission from ref. 94. Copyright 2022, Springer.

As the planarity of the azobenzene reduces, the spectral differences between the isomers become less pronounced (Figure 13ab). This has a negative impact on the PSDs. To determine the optimal substitution patterns and amino substituents for efficient bidirectional switching, we screened the PSDs upon excitation with wavelengths ranging from 365 to 595 nm. While for most compounds efficient switching was only possible with UV light and/or thermal back-isomerisation (*vide*

infra) hampered the photoisomerisation,⁹⁴ two particularly intriguing compounds stood out: **38-pyr₁** can be isomerised between PSDs of >85% *E* and >80% *Z* with 595 and 405 nm light, respectively (Figure 14a), while **40-pip₁** is isomerised relatively efficiently from *E* to *Z* with both UV and orange light (PSD_{595 nm} = 72% *Z*) but cannot be photoisomerised efficiently back to *E* (Figure 14b). In general, the substitution pattern **38-x₁** and pyrrolidino substitution are ideal for efficient bidirectional switching, while the series **40-x₁** shows less efficient *Z* → *E* isomerisation but enables low-energy light to be used to drive the equilibrium towards *Z*, especially with the piperidino substituent (Figure 14c).

Finally, we studied the thermal stability of the metastable *Z* isomer. As expected, aminated compounds exhibit markedly shorter half-lives than the parent *ortho*-fluoroazobenzenes. In general, the thermal stability decreased as the number of amino substituents increased (Figure 15). The shortest half-lives were recorded for the azobenzenes with two amino substituents in the same aryl ring (**39-x₂** and **40-x_{2-asy}**), whereas the **40-x₁** series (one amino and three fluoro substituents) exhibited remarkably slow isomerisation. Within a fixed substitution pattern, the half-lives followed a trend pip > dma > pyr. This effect originates from their electron donation ability (*vide supra*). Computational investigation reproduced the trends and suggested a rotational pathway either in the singlet ground-state or partially in the first excited triplet state.⁹⁴ The amino substituents can stabilise a partial positive charge in the system and thus accelerate the rotational isomerisation via (partial) heterolytic N=N bond cleavage, which explains why the most electron-donating pyrrolidino substituent exhibits lowest stability. The most stable compound (**40-pip₁**) had a *Z*-half-life of 56 days at 25 °C.

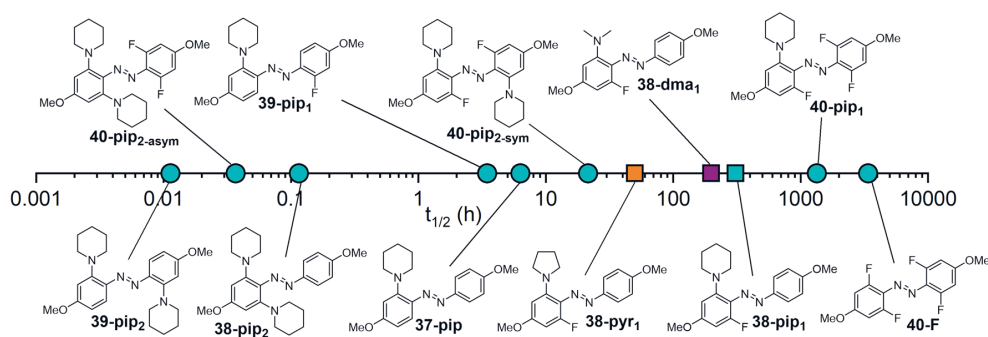


Figure 15. Thermal half-lives of selected *ortho*-fluorinated and *ortho*-aminated azobenzenes. Measured in acetonitrile at 25 °C.

In conclusion, combined *ortho* fluorination and amination promotes visible-light absorptivity, enabling fast switching between *E*- and *Z*-rich PSSs with low-energy excitation. The substitution pattern and choice of the amino substituent dictate the photochemical properties and thermal isomerisation rate, allowing the tuning of the azobenzene photoswitching dynamics. Cyclic amino substituents are in every respect better than acyclic equivalents: compared to the dimethylamino moiety, pyrrolidino substituents are stronger and piperidino substituents weaker donors, thus giving rise to strongest visible-light absorptivity enhancement and conservation of *Z*-stability, respectively. The optimal substitution pattern for bidirectional and relatively bistable switching is **38-pyr₁**, while **40-pip₁** couples low-energy isomerisation with high thermal stability. Moreover, substitution is also feasible with proline derivatives, enabling further *ortho* linkage while controlling the photochemistry. However, (near)quantitative switching is not possible in this class of photoswitches, and despite the enhancement of low-energy-light absorptivity, the absorption bands do not extend to the red region. Further structural modifications are needed to perfect the photochemistry of *ortho*-fluoroaminoazobenzenes. Two clear research lines should be pursued: the functionalisation of *meta* and *para* positions, following the guidelines published for *ortho*-fluoro- and chloroazobenzenes,^{182,186,188} as well as the substitution of fluorines for chlorines.^{189,191}

4 INHERENTLY BLUE: INDIGOID PHOTOSWITCHES

In the previous chapter we focused on how a well-established class of photoswitches can be modified to make it function with visible, even red light. Herein, we will take a different approach and examine a more recently developed family of photoswitches inspired by the structure of a familiar dye that absorbs in the red-light region without any structural modifications. Now, the challenge is to tune the photoswitching dynamics and photoresponsive behaviour towards the state of the art, i.e. azobenzenes. The dye in question is indigo, the abundant compound in textile industry. It comprises two indolinone rings linked by a C=C bond and could, in principle, function as an *E-Z* photoswitch. However, the parent indigo **E-41** undergoes fast proton transfer to **42** upon excitation, followed by ground-state regeneration of the original structure,^{193,194} preventing isomerisation to **Z-41** (Figure 16a).

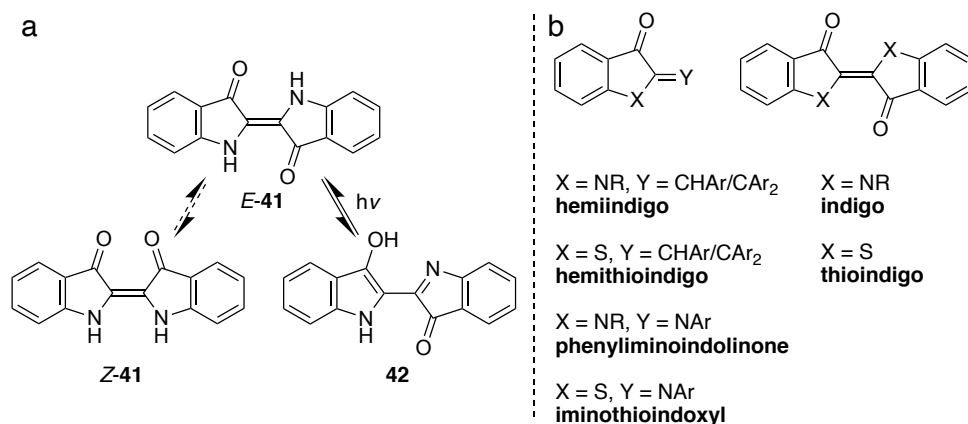


Figure 16. (a) The photoreactivity of indigo. (b) Indigoid photoswitch structures. Aryl substitution is omitted for simplicity.

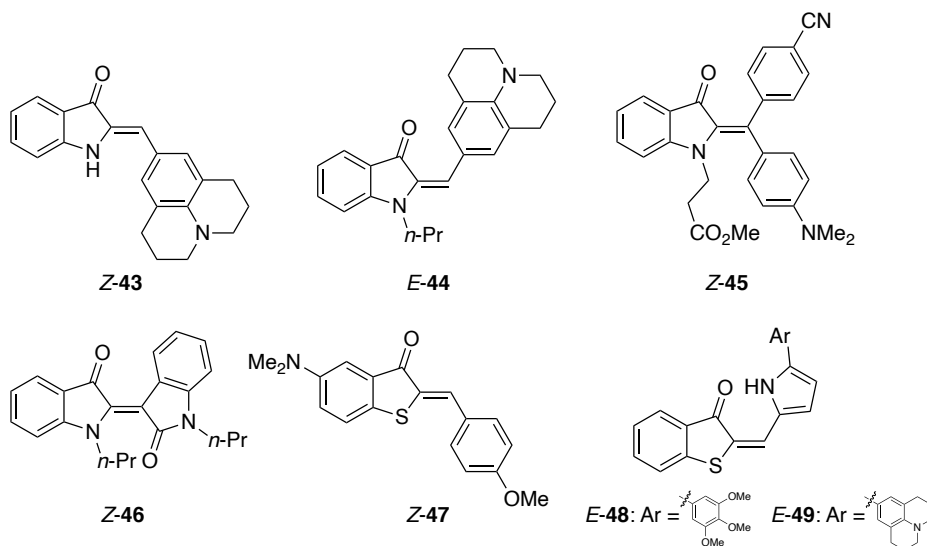
Disabling the excited-state proton transfer is the key to *E-Z* isomerisation.¹⁹⁵ This can be achieved by (i) switching the nitrogen atom for sulphur, (ii) functionalising the nitrogen atom, or (iii) substituting one of the indolinone halves with a CH-Ph

or N–Ph motif – or by combining these strategies (Figure 16b). These so-called indigoid photoswitches absorb visible light by default. If the other photoisomerisation properties of these switches can be optimised, they have potential to accomplish the elusive far-red/near-infrared switching even better than azobenzenes, opening doors to applications in biology and medicine. In addition, contrary to azobenzenes, many indigoids isomerise between two rigid, planar structures, which may prove beneficial for applications where conformational flexibility is disadvantageous.⁷⁵ In this chapter, we will look at the properties, advantages and challenges of indigoid photoswitches, starting with different half-indigo structures (Chapter 4.1), continuing with thioindigos and *N*-functionalised indigos (Chapter 4.2) and finally focusing on the original work of this thesis, indigo photoisomerisation in solid state (Chapter 4.3).

4.1 Hemiindigos and hemithioindigos

If one of the indolinone fractions in indigo is replaced with a different aryl ring, intramolecular proton transfer is disabled and the resulting hemiindigo can operate as a photoswitch. Considering the simplicity of this idea and the fact that hemiindigos have been known as chromophores for more than a century,^{196–199} it is astounding that the first comprehensive study on their photoswitching potential is only a few years old.⁸² Therein, it was established that a strong push-pull character across the isomerisable C=C bond is a prerequisite for clean and efficient isomerisation. This can be achieved by installing an amino substituent to the *para* position of the stilbene fraction, thus conjugated to the carbonyl unit in the indolinone. With this structure, the hemiindigo **43** exhibits efficient switching between the stable *Z* and metastable *E* states with orange-red and green light, respectively, with relatively high thermal stability (Table 6). Through the functionalisation of the indolinone nitrogen, the photochemical properties can be further tuned. As the state-of-the-art example, **44** can be switched almost quantitatively with 505 and 680 nm light and is virtually bistable ($t_{1/2} \approx 1$ year at 25 °C). The increased steric interactions between the *n*-propyl chain and the aryl ring raise the energy of the *Z* isomer so that the energies of the isomers are almost equal, the *E* isomer being slightly more stable. Interestingly, the equilibration half-lives of hemiindigos are strongly solvent-dependent. For instance, for **44**, the half-life is 0.9 years in DMSO but only 1.4 days in toluene.⁸²

Table 6. Photochemical properties of selected hemiindigo, hemithioindigo and indirubin photoswitches. Thermodynamically stable isomers are depicted.



	λ_{\max} (Z)	λ_{\max} (E)	PSD _{Z → E}	PSD _{E → Z}	$t_{1/2}$ (25 °C)
43 ⁸²	522 nm	563 nm	81% (505 nm)	95% (617 nm)	11 d (DMSO)
44 ⁸²	520 nm	570 nm	98% (505 nm)	99% (680 nm)	0.9 years (DMSO)
45 ²⁰²	507 nm	560 nm	90% (490 nm)	88% (625 nm)	40 d (PhMe)
46 ²⁰⁰	617 nm	600 nm	84% (625 nm)	61% (450 nm), 46% (730 nm)	2.6 min (PhMe)
47 ²⁰¹	493 nm	515 nm	82% (625 nm)	89% (505 nm)	30 d (PhMe)
48 ²⁰²	492 nm	555 nm	99% (460 nm)	99% (623 nm)	7.1 h (PhMe) ^a
49 ²⁰²	559 nm	619 nm	>99% (567 nm)	62% (740 nm)	0.3 h (PhMe) ^a

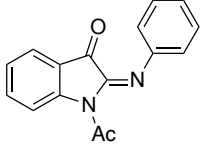
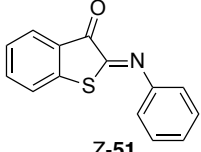
^a Half-life at 80 °C, corresponding to approx. 10–70 days (**48**) and 0.5–3 days (**49**) at 25 °C.

It is also possible to functionalise the “stilbene end” of the C=C bond twice, affording more possibilities for further tuning of the photochemical properties. However, at least so far, the additional functionalisation has not resulted in further improvement of the switching dynamics, with the best combination of good PSDs and thermal stability exhibited by **45**.²⁰³ Yet another way of exploiting the hemiindigo structure is to bind it to its constitutional isomer, forming indirubin. Most favourable photochemical properties exist for derivative **46** in which both nitrogen atoms are functionalised with *n*-propyl chains.²⁰⁰ The compound can be isomerised between relatively high PSDs of the *E* and *Z* states with 625 and 450 nm excitation, which in itself is no improvement from the aforementioned hemiindigos. What makes this switch interesting is that if Schreiner’s thiourea catalyst is applied, the selective supramolecular interactions between the *E* isomer and the catalyst red-shift the absorption band of the *E* isomer, thus enabling *E* → *Z* photoisomerisation with 730

nm light – albeit rather inefficiently (Table 6). Thus, bidirectional isomerisation is possible with red light only. Unfortunately, the thermal stability of the *E* isomer is rather low ($t_{1/2} = 2.6$ min). Nevertheless, this example is closest so far to the universal goal of bistable bidirectional switching in the biooptical window.

Hemithioindigos are the most widespread and best-studied indigoid photoswitches, owing to an unprecedented combination of bidirectional visible-light isomerisation and thermal stability. The isomerisation wavelengths of unsubstituted hemithioindigo lie in the blue–green part of the visible spectrum, enabling switching between PSDs containing 93% *E* and 84% *Z* with 405 and 523 nm excitation, respectively.²⁰² The compound is practically bistable, with $\Delta G^\ddagger = 31.4$ kcal mol⁻¹ for the thermal *E* \rightarrow *Z* isomerisation in toluene, corresponding to a half-life of hundreds of years at room temperature.²⁰⁴ The first hemithioindigo applications date back two to three decades^{205,206} and their fundamental photochemistry has been studied thoroughly.^{207–211} The biggest developments in terms of red-shifting the absorption bands, however, have been taken quite recently.^{75,204} The red-shift can be accomplished through the installation of an electron donor in the *para* position of the stilbene part, but at the same time, this decreases the stability of the *E* isomer significantly (down to 9 minutes for the strongest donor).²⁰¹ This effect can be countered with an electron-donating group in the thioindigo fraction: **47**, carrying a *para* methoxy substituent in the stilbene part and a dimethylamino substituent in the thioindigo ring (*para* to the sulphur atom), shows a good combination of thermal stability and red-shifted absorbance (Table 6). The generally good PSDs can be further improved by substituting the phenyl ring for a five-membered heteroarene. The resulting heteroaryl hemithioindigos exhibit distinctly separate absorption bands, allowing even quantitative switching in many cases, especially with derivatives containing a pyrrole (**48**, **49**) or imidazole moiety due to the isomer-specific intramolecular hydrogen bonding between the NH of the heteroaryl ring and the carbonyl oxygen.^{202,212,213} In addition, if strongly electron-donating substituents are utilised (e.g., **49**), switching is enabled even in the near-infrared light region.²⁰²

Table 7. Photochemical properties of unsubstituted phenyliminoindolinone and iminothioindoxyl photoswitches. Thermodynamically stable isomers are depicted.

 <p>E-50</p>		 <p>Z-51</p>	
	λ_{max} (E)	λ_{max} (Z)	$t_{1/2}$
50 ¹⁵⁹	510 nm	436 nm	77 μ s (PhMe)
51 ⁷⁹	510 nm	430 nm	12 ms (PhMe)

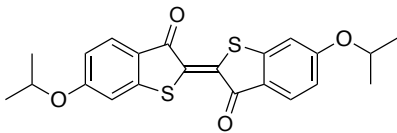
As the final example of half-indigo photoswitches, we shall have a look at two families – phenyliminoindolinone and iminothioindoxyl – that combine indigo and thioindigo fractions, respectively, with an azobenzene half, leading to a C=N bond as the photoisomerisable unit (Table 7). Both the *E* and the *Z* isomer absorb visible light, the *E* isomer in the green–orange light region and the *Z* isomer in the blue regime, and bidirectional switching with visible light is thus possible, much in a similar fashion as for hemi(thio)indigos. In stark contrast to the latter, the metastable isomers of both switches are extremely short-lived, isomerisation occurring on the timescale of milliseconds or even microseconds. What makes these compounds unique (for example, compared to push-pull-type azobenzenes) is the great spectral separation of the isomers, being 74 and 80 nm for **50** and **51**, respectively, and even exceeding 100 nm for some derivatives of **51**.^{79,159} This enables selective excitation of the thermally stable isomer and thus, more efficient photoisomerisation than would be feasible for other existing switches of similar ground-state isomerisation rate. Due to the steric clash by the acetyl group in *Z*-**50** and its derivatives, the *E* isomer is lower in energy, while for iminothioindoxyls that lack the steric interaction, it is the *Z* isomer that is more stable. Thus, the stable \rightarrow metastable state reaction is accompanied by positive photochromism for **51** and negative photochromism for **50**. The thermal isomerisation rate and the location of the absorption bands can be fine-tuned with *para* substituents in the phenyl fraction of the molecule.

4.2 Indigos and thioindigos

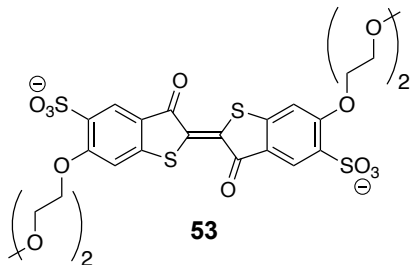
Efficient visible-light isomerisation of thioindigos was demonstrated already in the 1950s: for example, unsubstituted thioindigo exhibits PSDs of 96% *E* and 57% *Z* with <495 and >520 nm excitation, respectively.²¹⁴ Interestingly, in another early

study on 6,6'-diisopropoxythioindigo **52**, the PSDs are reversed: 90% *Z* and 74% *E* with 458 and 515 nm excitation, respectively (Table 8).²¹⁵ Despite a number of spectroscopic studies,^{214,216–219} comprehensive switching studies have not been made, and no attempts to red-shift the absorption bands have been published – probably due to solubility issues. Based on the limited data, the half-lives of the metastable *Z* isomer seem to be typically shorter than those of hemiindigos and hemithioindigos, lying in the range of hours. For some hydrogen-bond-stabilised derivatives the thermal isomerisation is slower, negligible over several hours.²²⁰ Overall, thioindigos do not seem to rival hemiindigos and hemithioindigos in terms of photochemical properties. Yet, some steps have been taken to bring their photoswitching to aqueous environments. As an example, the sulfonate-decorated derivative **53** is well-soluble in water and capable of relatively efficient *E* → *Z* isomerisation in water.²²¹

Table 8. Photochemical properties of selected thioindigos.



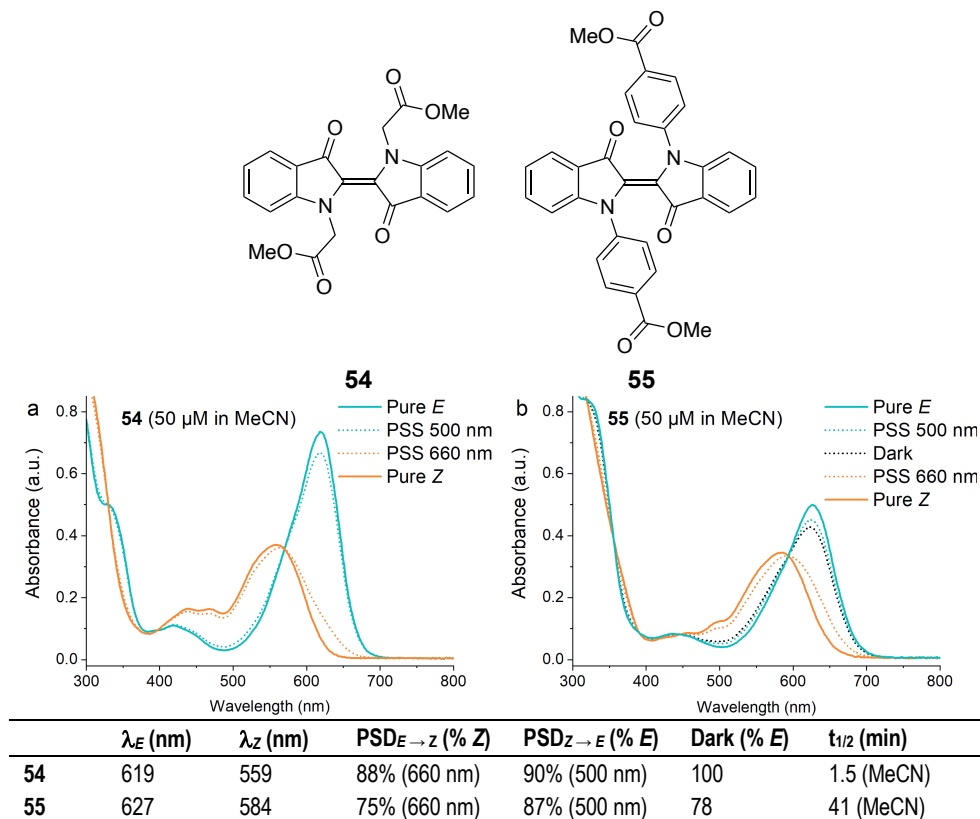
52



53

	λ_{max} (<i>E</i>)	λ_{max} (<i>Z</i>)	PSD _{<i>E</i> → <i>Z</i>}	PSD _{<i>Z</i> → <i>E</i>}	
52	514 nm	459 nm	90% (515 nm)	74% (458 nm)	(epoxy resin)
53	520 nm	476 nm	65% (578 nm)	–	(H ₂ O)

Different *N*-functionalised indigo derivatives have been the subject of extensive spectroscopic studies starting from the mid-20th century.^{222–225} Unsubstituted *E*-indigo is extremely poorly soluble in most solvents, with a slightly solvent-dependent absorption maximum at 595–611 nm. Methylation shifts the spectrum further towards red, up to 648 nm in ethanol, and enables photoisomerisation to the metastable *Z* isomer. However, thermal *Z* → *E* isomerisation takes place on a timescale of seconds.^{80,223} π acceptors such as acetyl or *tert*-butoxycarbonyl groups stabilise the *Z* isomer, but in both cases the absorption maximum is blue-shifted to ca. 550 nm.^{222,225} Unfortunately, neither of these indigo derivatives has been properly characterised in terms of PSDs and thermal isomerisation rates.

Table 9. Photochemical properties of selected *N,N*-difunctionalised indigos.²²⁶

Comprehensive studies on a library of *N,N*-difunctionalised indigos were only carried out relatively recently, revealing the key to combining red-light absorption with improved stability of the *Z* isomer: indeed, electron withdrawal is needed to stabilise the metastable isomer, but through an inductive effect rather than resonance in order to not affect the electronic transitions.⁸⁰ Thus, the indigo **54**, carrying electron-withdrawing ester groups separated from the nitrogen atoms by methylene units, has an absorption maximum (attributed to the π - π^* , i.e. $S_0 \rightarrow S_1$ transition) at 619 nm and can be isomerised efficiently (88%) to the *Z* state by exciting at 660 nm (Table 9). The band is blue-shifted to 559 nm for the *Z* isomer, with a considerable 60-nm separation between the isomers. Back-isomerisation is thus possible with 500 (or 525) nm irradiation. The compound is by no means bistable, but thermal isomerisation is still two magnitudes slower than for the methylated equivalent and slow enough for efficient isomerisation even with low-intensity light. Spectral separation and thermal stability are best in non-polar solvents such as toluene, while the spectra of both isomers are most red-shifted in polar solvents such as DMSO.⁸¹

It should be highlighted here that contrary to most azobenzenes and hemi(thio)indigos, indigo exhibits negative photochromism, which is highly beneficial for efficient isomerisation, especially in concentrated samples.

To further enhance the thermal stability, aryl substituents can be utilised: π,π interactions stabilise the *Z* isomer selectively, increasing the ground-state isomerisation barrier substantially. If electron-withdrawing substituents are installed on the ring, thermal half-lives are prolonged up to hours, depending on the strength of the EWG.⁸⁰ For instance, *Z*-**55** has a half-life of 41 minutes in acetonitrile.²²⁶ Judging from the molecular structure in Table 9, the aromatic π -system and the *para* substituent seem to be conjugated with the nitrogen lone pair, but this is not the case. The aryl rings are perpendicular and the orbitals therein are barely at all involved in the $\pi\text{--}\pi^*$ transition.⁸⁰ Thus, no hypsochromic shift is seen for the absorption band. In fact, the absorption maximum of **55** is slightly red-shifted compared to **54**. However, the arylation affects the energy levels of the *Z* isomer more drastically, worsening the spectral separation down to 43 nm. Therefore, the PSDs are compromised: 75% *Z* and 87% *E* with 660 and 500 nm excitation, respectively. As another downside regarding arylated indigos, the energy difference between the isomers is brought down to the order of 1 kcal mol⁻¹, which results in dark equilibria containing 12–39% of the *Z* isomer in contrast to the quantitative thermal *Z* \rightarrow *E* isomerisation observed for indigos *N*-functionalised with alkyl substituents.⁸⁰ For example, at 25 °C, **55** reaches an equilibrium where the *Z*-fraction is 22%.

Despite these restrictions, indigos are so far the most promising candidates for fast bistable photoswitching with red light. Additionally, especially the aryl-functionalised compounds experience pronounced geometry changes upon isomerisation, exceeding by far the extent of steric displacement in hemi(thio)indigos and even azobenzenes, with a photoinduced 3.5-Å change in the distance between the *para* positions of the aryl rings.⁸⁰ Noteworthy, photoisomerisation is possible (albeit not very efficient) also if only one of the nitrogen atoms is aryl-functionalised.²²⁷ In this case, the rate of thermal isomerisation is highly dependent on the amount of water present in the solvent, which makes monoarylated indigos viable candidates for sensory applications,⁵² similar to what has been demonstrated for hydroxyazobenzenes¹⁰⁰ but operating with red light.

4.3 Indigo photoswitching in the solid

Although the theoretical, mechanistic and practical aspects of indigo photoswitching have been studied quite extensively, no studies existed on whether the favourable photochemical properties can be transferred to a solid environment, the realm of most photoswitch applications. The aforementioned great isomerisation-induced spatial displacements are beneficial for creating photoresponsive systems, but at the same time, substantial strain may be created inside the solid matrix, changing the potential energy surfaces of the switch and perhaps prohibiting the switching altogether.^{116,117} Thus, we investigated the solid-state photoswitching behaviour of six indigo derivatives based on three fundamental substitution patterns: dialkyl-, diaryl- and alkyl-aryl-substituted compounds (Figure 17a).²²⁶ The ester moieties serve both as the EWGs to improve the PSDs and thermal stability, and as synthetic handles for further functionalisation. As the solid matrices, we chose thin films of five amorphous polymers: polystyrene (PS), poly(4-vinylpyridine) (P4VP), poly(methylmethacrylate) (PMMA), poly(butylmethacrylate) (PBMA) and poly(hexylmethacrylate) (PHMA), depicted in Figure 17b. PS, P4VP and PMMA are rigid (T_g values ranging from 100 to 137 °C) polymers often utilised in solid-state photoswitching,^{100,228–230} while PBMA and PHMA were chosen to give information on the switching performance in a softer environment. The indigos were dispersed into the material with no covalent linkage.

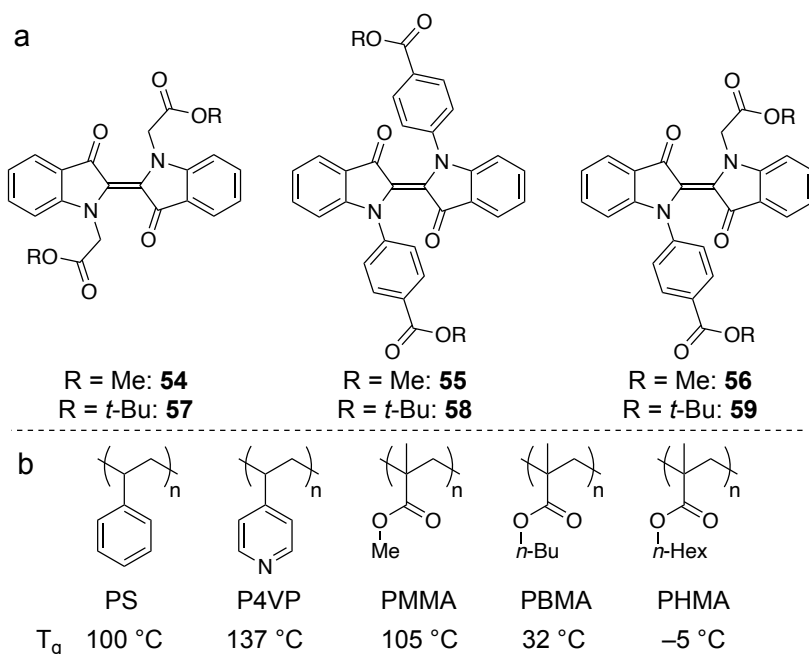


Figure 17. (a) Studied indigos and (b) polymers along with their glass transition temperatures.²²⁶

We started by preparing polymer films containing 2% (w/w) of the indigos **54–56**. Viscous solutions were spin-cast to create uniform and sufficiently thick (5–20 μm) films. The photochemical properties of the indigos in each polymer were then characterised with UV-visible absorption spectroscopy. Only negligible differences were seen in the absorption spectra, with the exception of the polar P4VP in which the π – π^* absorption band was red-shifted by 10 nm.²²⁶ Photoswitching dynamics upon 660 nm irradiation, instead, were drastically different. In the rigid PS and P4VP matrices, switching was very inefficient, with PSDs of only 10–20% *Z* (Figure 18ac). Similar behaviour has been observed for other switches that undergo vast geometry changes upon isomerisation.¹¹⁶ In softer PBMA and PHMA, a markedly bigger fraction of the molecules can be isomerised from *E* to *Z*, up to 55% in the case of **54** in PBMA, so that a pronounced colour change is visible (Figure 18bcf). Compared to PS and P4VP, switching was relatively efficient in PMMA for **54** but the difference was less pronounced for **55** and **56**. Generally, the least bulky compound **54** could be isomerised most efficiently. Switching back with 500 nm excitation worked in all cases as efficiently as in acetonitrile (Figure 18ab). Thermal lifetimes of the *Z* isomer (acquired using a stretched exponential fit) were expectedly longest for the doubly aryl-functionalised **55** and shortest for the dialkyl compound

54 in all polymers, but the difference between these varied greatly: for the rigid P4VP, the lifetimes of **54** and **55** were 2.7 and 4.4 minutes, whereas in the softer PBMA, the respective values were 1.2 and 83 minutes (Figure 18d). It is possible that in a rigid matrix the $E \rightarrow Z$ isomerization of the bulky **55** induces considerable mechanical strain which relaxes upon $Z \rightarrow E$ isomerisation, increasing the rate compared to a softer environment. Interestingly, the PSDs and thermal stabilities of all indigos were lower in PHMA than in PBMA despite the former being even softer. This is probably the result of lessened miscibility and, subsequently, increased aggregation in PHMA (*vide infra*).

The photostability of indigos in the polymer matrices is lower than in acetonitrile: as a representative example, after 250 sequential 660 and 500 nm excitation pulses on **54** in PHMA, ca. 75% of the initial dye concentration is decomposed (Figure 18e). In contrast, in acetonitrile, almost half of the initial dye content is conserved after 1,000 isomerisation cycles. However, in the course of a few cycles, degradation is barely noticeable. Rapid photodecomposition was observed in PMMA and PBMA. To understand the phenomenon, the photodecomposition products in acetonitrile, PBMA and PHMA were studied with UV-visible spectroscopy and mass spectrometry. In acetonitrile and PHMA, a colourless product with a mass signal of $[M+H+16]^+$ was observed, indicating the formation of a well-known oxygen adduct. In PBMA, however, a yellow product was formed, absorbing at 400 nm and giving a mass signal of $[M-2+H]^+$, indicative of some form of cyclisation product.²²⁶ We hypothesised this unexpected product to originate from the end groups or initiator residues found in PMMA and PBMA, as they were purchased from a different vendor than the other polymers.

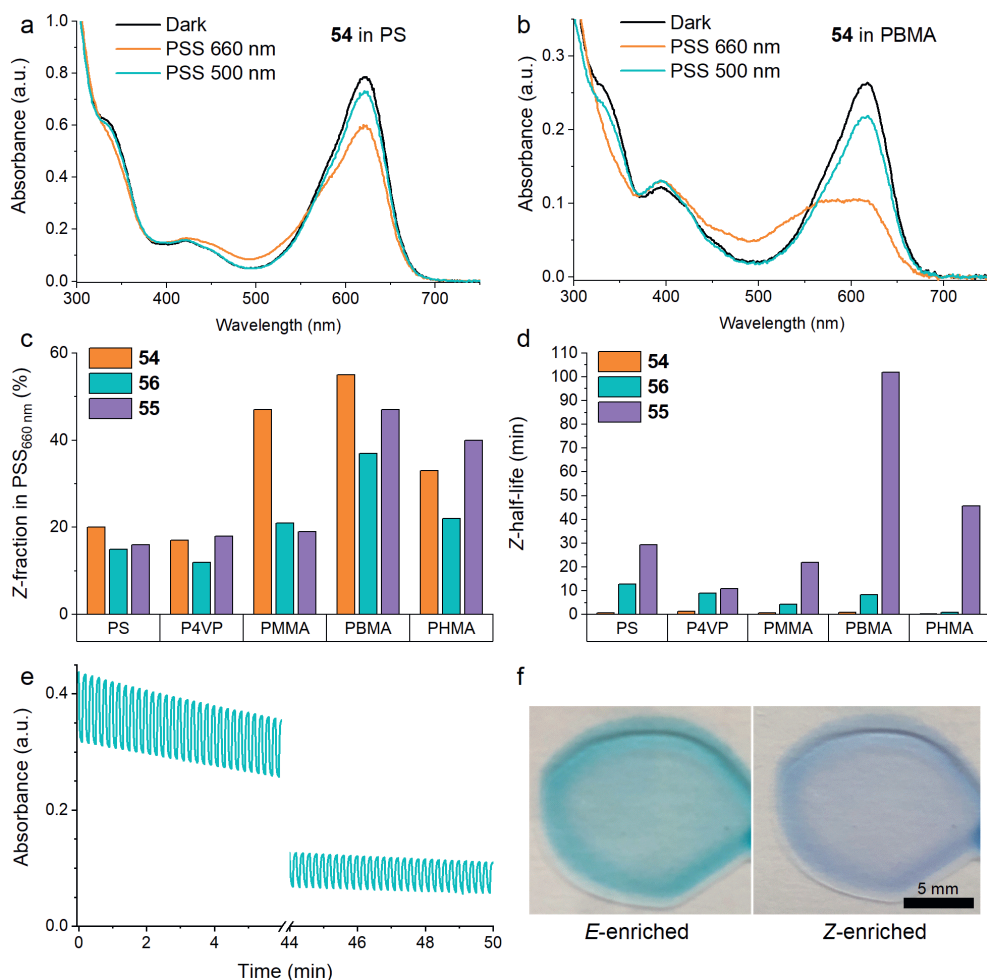


Figure 18. Absorption spectra of **54** at room temperature in dark and upon irradiation with 660 and 500 nm light in (a) PS and (b) PBMA, showing the difference between inefficient and efficient switching. (c) Z-fraction in the photostationary state (illumination with 660 nm light) and (d) Z-lifetime for all indigo–polymer combinations. (e) 250 switching cycles for **54** in PHMA. (f) Photographs of PHMA films with **55** upon irradiation with 500 and 660 nm light. Indigo content: 2% (w/w) except 0.5% in (e) and (f). Excitation intensities: 670 mW cm⁻² (660 nm), 220 mW cm⁻² (500 nm). Modified with permission from ref. 226. Copyright 2023, RSC.

Having established that solid-state photoswitching of indigos is possible in these matrices, we studied the effect of dye loading. PHMA films with 0.25–10% (w/w) of indigo were prepared; this polymer was chosen because it combined relatively efficient switching with good photostability (in contrast to PBMA). Unexpectedly big spectral changes were found in both absorption and fluorescence spectra (Figure 19a) with a clear broadening and red-shift of the bands as a function of increasing

indigo concentration (10 nm between the 2% and 10% samples). We hypothesised this to stem from the aggregation of indigo molecules. To inhibit agglomeration, we prepared **57**, electronically identical to **54** but capped with bulky *tert*-butyl units that should hamper the packing of these molecules. Indeed, the absorption spectra of the whole concentration series were now identical, and only minute changes were observed in their fluorescence spectra (Figure 19b). Concentration dependence was seen in the fluorescence spectra of **55** and **56**, but their absorption spectra were not affected by dye loading, probably because the perpendicular aryl groups inhibit aggregation. Likewise, no shifts were observed in the absorption spectra of **54** in PS or in PBMA, although shifts were visible in the fluorescence spectra (Figure 19c). The π,π interactions between PS and the indigos are an obvious explanation for the inhibited aggregation, but the origin of the aggregation control in PBMA is less clear. Possibly, the longer alkyl chains in PHMA lead to lower miscibility of the indigo. Alternatively, the different end groups in PBMA (*vide supra*) may play a role in breaking the aggregation.

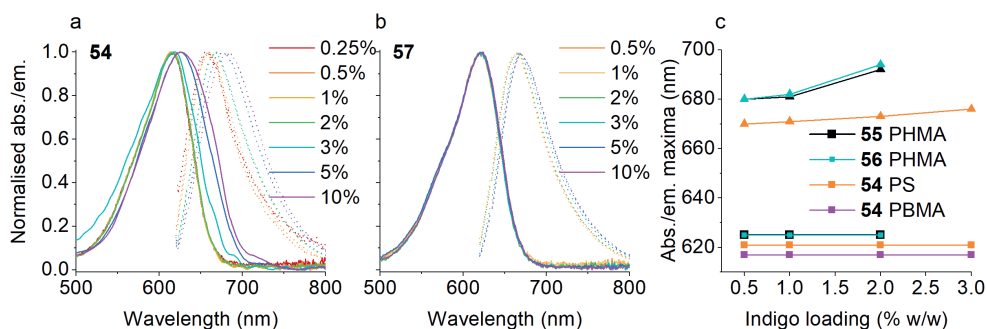


Figure 19. Absorption and emission spectra of (a) **54** and (b) **57**. (c) Absorption and emission maxima of **54** in PS and PBMA, and **55** and **56** in PHMA (squares for absorption, triangles for emission). Modified with permission from ref. 226. Copyright 2023, RSC.

The effects of dye loading are not restricted to spectral properties. To our surprise, both PSDs and thermal isomerisation rates are strongly concentration-dependent, even when using very low indigo concentrations. For example, for **54** in PHMA, the PSD decreases from 67% to 10% when the indigo concentration is increased from 0.5% to 10%. At the same time, the thermal *Z*-lifetime decreases from 61 to 5 seconds (Figure 20a). It should be emphasised that although these two parameters correlate, the deteriorating PSDs do not result from decreased thermal stability, but a common factor drives both changes. The stretch factor in the exponential decay fit (see Chapter 2.3) grows more pronounced as the dye loading increases, which is

an indication of decreased homogeneity, further validating the aggregation hypothesis. However, the same trends are also observed for **55–57** despite the aryl (**55**, **56**) and *tert*-butyl (**57**) units that inhibit aggregation (Figure 20) and also in PBMA and PS where aggregation-induced spectral changes are smaller. Apparently, additional intermolecular interactions contribute to the behaviour.

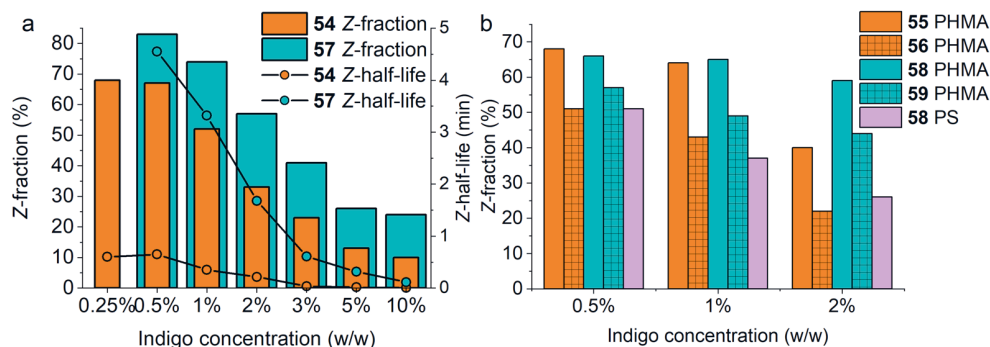


Figure 20. (a) PSD and Z-lifetime of **54** and **57** in PHMA. (b) PSD of **55**, **56**, **58** and **59** in PHMA and **58** in PS. PSDs are measured upon illumination with 660 nm light. Modified with permission from ref. 226. Copyright 2023, RSC.

Increasing the steric bulk of a molecule and thus the free volume around it is a general structural feature for enhancing solid-state switching.^{45,231} Gratifyingly, this is also the case for indigos: both PSDs and thermal stability are better for the *tert*-butyl-capped derivative **57** than the less bulky, electronically equivalent **54** (Figure 20a), reaching a PSD of 83% Z and a thermal Z-lifetime of 5.5 minutes at a dye loading of 0.5%. Similarly, **58–59** isomerise more efficiently than **55–56** (Figure 20b). Using this approach, relatively efficient switching (PSD of 51% Z) is enabled even in the rigid polystyrene (Figure 20b). In this case, the compound exhibits a Z-lifetime of 5.8 hours, far exceeding the value measured in acetonitrile.

In conclusion, indigoid photoswitches offer efficient and fast visible-light isomerisation coupled to good or even excellent thermal stability. Even red light can be utilised in the case of suitably *N,N*-difunctionalised indigo derivatives. However, solid-state switching of these compounds had not been attempted thus far. Herein, we studied the factors that govern the photoswitching dynamics in polymer thin films, a typical solid-state environment for many photoresponsive materials. Utilising different indigo derivatives, we were able to realise *E–Z* isomerisation in a solid matrix with red light for the first time. Best PSDs were acquired in soft matrices. Furthermore, our studies revealed that the *E* → *Z* photoisomerisation efficiency and the thermal stability of the metastable *Z* isomer have a strong dependence on the

indigo loading, probably due to aggregation and other intermolecular interactions of the indigo chromophores. Based on these findings, we propose three factors that promote efficient red-light switching in the solid: (i) a soft matrix, (ii) low (<1%) loading, and (iii) installation of bulky elements that increase the free volume around the switch. Our findings somewhat determine the potential application areas of these switches, as high photoswitch concentrations cannot be utilised. In the future, it should be investigated whether other indigoid families exhibit a similar concentration dependence, and if further bulking of the indigo core could improve the photoswitching parameters. The addition of alkoxy (or other) substituents in the 5 or 6 positions of the aryl rings has been shown to further red-shift the absorption band of indigo²³² and would thus enable additional tuning of the spectral properties as well as thermal isomerisation rates, in addition to inhibiting the aggregation of the molecules.

5 INDIRECT ISOMERISATION OF AZOBENZENES

In this thesis, the need for red-light photoisomerisation has so far been addressed with structural modifications. However, while red-light-induced isomerisation in one direction (typically, from stable to metastable state) is nowadays possible with multiple molecular structures, the reversed reaction is realised with higher-energy excitation.^{80,185,190} Thus, the complete switching cycle is not confined within the biooptical window (>650 nm). However, there is a way to circumvent this deficiency: indirect isomerisation via photocatalysis in which a catalytic species is activated with near-infrared light (i.e., in a region where neither isomer of the photoswitch absorbs) to induce the back-isomerisation. The working principle of an ideal photoswitch system is depicted in Figure 21. In this system, red light (650 nm) is utilised to isomerise the switch from stable to metastable, while 750 nm near-infrared light brings about the catalytic isomerisation back to the stable state. Here, it is important that the spectral separation of the catalyst and photoswitch is sufficient.

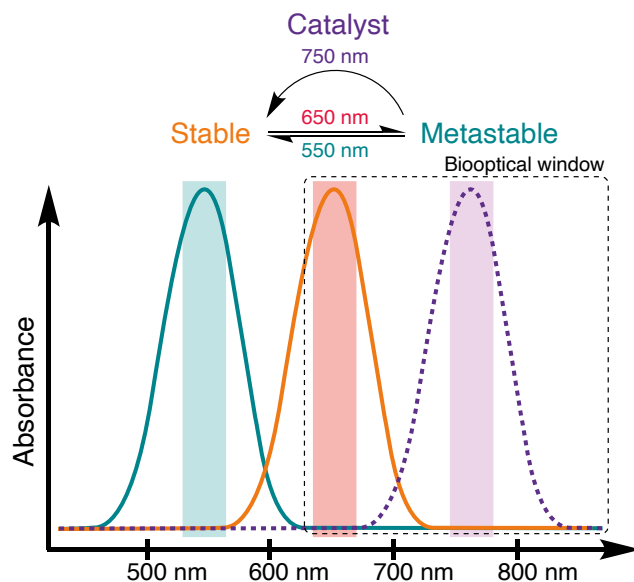


Figure 21. A schematic illustration of an optimal spectral profile of a catalyst-driven photoswitch system operating inside the biooptical window.

Herein, we shall explore different catalytic systems that can be exploited to induce the $Z \rightarrow E$ isomerisation of azobenzenes. Considering how thoroughly azobenzenes and photocatalysis have been investigated,^{233–236} catalytic photoswitch systems are surprisingly scarce. Chapter 5.1 will cover catalytic isomerisation mechanisms based on photoinduced electron transfer and triplet energy transfer, with a particular emphasis on examples that function via excitation with low-energy light. For clarity, indirect isomerisation processes featuring photon upconversion (formation of one high-energy photon from two low-energy photons)^{237–239} or two-photon excitation (simultaneous absorption of two low-energy photons to cover an energy gap of the sum of their energies)^{240,241} are not discussed in detail. Chapter 5.2 will then focus on the original work of this thesis where the azobenzene isomerisation is catalysed by molecular iodine and mediated by oxygen. It should be mentioned that even though this chapter focuses solely on azobenzenes, similar principles have also been utilised with other photoswitch families.^{242–245}

5.1 Catalytic isomerisation mechanisms

The longest-known way to accelerate the thermodynamically favourable $Z \rightarrow E$ isomerisation of azobenzenes relies on binding one of the azo group lone pairs to a proton or a Lewis acid and thus decreasing the double bond character.¹⁷² Also both electron donors and acceptors,²⁴⁶ phosphines²⁴⁷ and transition metal complexes²⁴⁸ were shown to accelerate the thermal isomerisation already in the 20th century. In the last decade gold nanoparticles were proven effective for this purpose, working via electron transfer from the azobenzene to the gold nanoparticle.^{249–251} Building on these findings, reductive²⁵² and oxidative²⁵³ electrocatalytic isomerisation methods have been developed. These routes depend on the formation of anionic and cationic azobenzene radicals, respectively. Both radicals isomerise at an extremely fast rate, 10^{12} to 10^{15} times faster than the respective neutral molecules. As a consequence, the overall isomerisation rate is governed by diffusion and the initial intermolecular electron transfer step.^{251–255} This redox reaction can be induced by applying a current or, in the case of the oxidative pathway, chemically by utilising suitable ground-state electron donors/acceptors. Moreover, and most importantly in the context of this thesis, both routes are accessible photochemically via photoinduced electron transfer (PET).

To understand the PET-catalysed isomerisation (and alternative mechanisms discussed below), we need to establish the basic photochemistry of a general

photocatalyst molecule and the interactions that are possible between an excited catalyst (Cat^*) and a ground-state azobenzene molecule (AB). Upon absorption of a photon, the catalyst is excited from its singlet ground state to its singlet excited state $^1\text{Cat}^*$, much in the same fashion as we discussed the excitation of azobenzene in Chapter 2.1. Note that the notations S_0 , S_1 and T_1 used therein are interchangeable with the notations ^1AB , $^1\text{AB}^*$ and $^3\text{AB}^*$ (or, in the case of the catalyst, ^1Cat , $^1\text{Cat}^*$ and $^3\text{Cat}^*$); here, the latter form is used to distinguish between the catalyst and azobenzene molecules. In the case of an excited azobenzene, we only considered the isomerisation pathway for deactivation. As isomerisation is not possible for the excited catalyst, we are left with three relaxation mechanisms: non-radiative internal conversion to the ground state, radiative transition to the ground state (fluorescence), and intersystem crossing (ISC) into the slightly lower-energy triplet-excited state $^3\text{Cat}^*$ that can further relax radiatively (phosphorescence) or thermally (external conversion) back into the singlet ground state.²⁵⁶ These processes are depicted schematically in Figure 22.

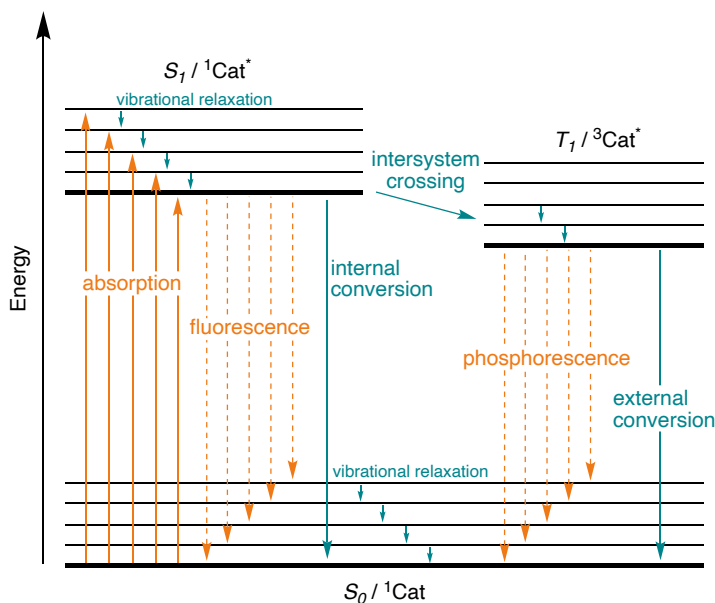


Figure 22. A Jablonski diagram depicting the energy states of a photocatalyst (Cat) and the related transitions. Radiative transitions are coloured orange and non-radiative turquoise.

Since we are interested in a process involving an excited catalyst molecule, the pathways leading back to the ground state will not be discussed further. Instead, we will focus on ISC as it determines whether the catalyst interacting with our

azobenzene is in a singlet or a triplet state – which, as we will soon see, will have an effect on the range of possible interactions. While singlet \rightarrow singlet transitions are typically fast, transitions between different spin states (e.g., ISC) are slower.²⁵⁷ This difference arises from the requisite of conserving the spin angular momentum during any transition, making singlet \rightarrow triplet and triplet \rightarrow singlet transitions improbable.^{258,259} However, the coupling between spin and orbital angular momentum and, in some cases, molecular vibrations, increases the efficiency of ISC.^{257,260} The theoretical background of spin-orbit and spin-vibration coupling lies outside the scope of this thesis. In this context, it suffices to know that heavy atoms (such as palladium and iodine) in the catalyst structure and a small energy difference between the $^1\text{Cat}^*$ and $^3\text{Cat}^*$ states promote ISC.^{257,261} Because the energy gap between $^3\text{Cat}^*$ and ^1Cat is substantially larger, any form of relaxation from the triplet-excited state to ground state is very slow compared to ISC, and naturally also to $^1\text{Cat}^* \rightarrow ^1\text{Cat}$. Thus, the triplet excited state is typically many orders of magnitude longer-living than the respective singlet state.²⁵⁷ In other words, the catalyst has more time to interact with the azobenzene if it can efficiently cross into the triplet state.

Regardless of the spin state the excited catalyst is in, a collision with an azobenzene can result in either reductive or oxidative charge transfer. From the viewpoint of the initially excited molecule (here, the catalyst), these are respectively called electron and hole transfer (Figure 23). Both reactions require the reduction/oxidation potentials of the catalyst and azobenzene to be sufficiently matched, and the mechanism is promoted by a polar medium that can stabilise the pair of radical ions formed.²⁶² Returning to the aforementioned oxidative photocatalytic system, 4,4-dimethoxyazobenzene **2** has an oxidation potential of 1.41 V, matching well the reduction potential of a red-light photocatalyst methylene blue (**60**, MB) in either singlet or triplet excited state (1.56 and 1.60 V, respectively).^{235,253,263} Thus, MB can be used as a red-light photocatalyst to bring about quantitative and fast $Z \rightarrow E$ isomerisation (full conversion in 6 minutes at a MB loading of 10%).²⁵³ However, UV or blue light is needed for the $E \rightarrow Z$ photoisomerisation since MB absorbs in most of the visible spectrum, differing from the ideal photoswitch–catalyst system presented in Figure 21.

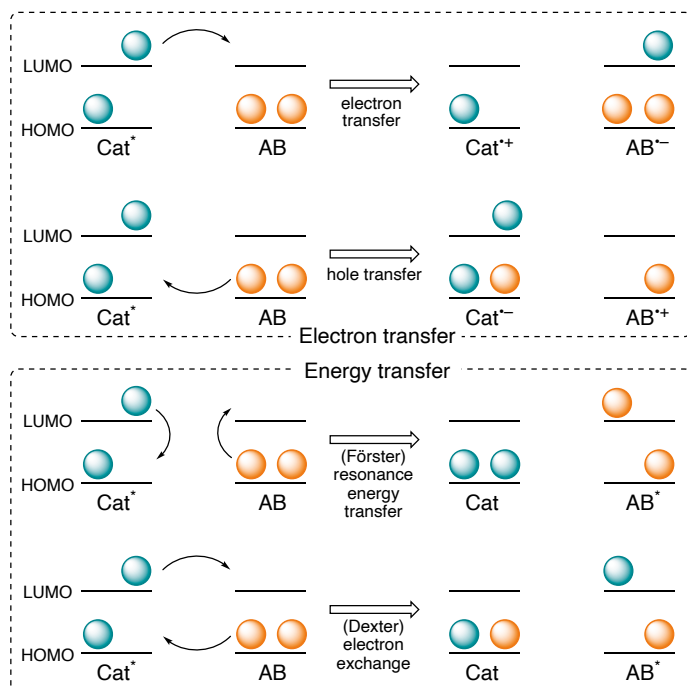
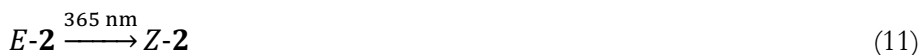
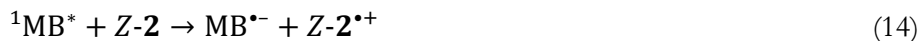


Figure 23. A schematic representation of photoinduced electron and energy transfer mechanisms from a photoexcited catalyst (Cat^*) to a ground-state azobenzene (AB). Turquoise and orange spheres represent the frontier molecular orbitals without assigned spin signs.

The catalytic cycle is described with Equations 11–17. After initial excitation with 660 nm light, MB is able to abstract an electron from the *Z*-azobenzene, which undergoes rapid thermal *Z* \rightarrow *E* isomerisation before retrieving an electron from another azobenzene molecule, thus continuing a free radical chain reaction that allows the quantum yield of photocatalysed isomerisation to exceed unity.²⁵³ Equations 14 and 15 are equally plausible and probably both reactions take place. The reaction tolerates oxygen, albeit with diminished quantum yields. As molecular oxygen is infamous for quenching triplet excited states (*vide infra*), this indicates that a triplet state is involved in the mechanism – but also that the mechanism does not fully depend on the triplet-excited MB.





Another possible interaction between the catalyst and azobenzene molecules is energy transfer. In contrast to charge transfer, no changes occur in the oxidation states of the two interacting species: only energy (excitation) is transferred. In addition to the trivial radiative energy transfer (emission by one molecule and consequent absorption by the other), two distinct mechanisms exist (Figure 23). (Förster) resonance energy transfer is based on coulombic dipole–dipole coupling between the transition state dipoles of the interacting species and is the short-range equivalent of radiative energy transfer, energy transferred in the form of an imaginary photon.^{264–266} It is conventionally considered to occur mainly between singlet states, although exceptions are found when spin-orbit coupling is strong.^{266–268} (Dexter) exchange energy transfer, instead, is caused by FMO interactions and has no restrictions regarding the spin states of the two species: energy can be transferred from an excited singlet or triplet to a ground-state singlet or triplet.^{269,270} All the energy transfer processes discussed henceforth follow the Dexter mechanism and, more specifically, involve energy transfer from a triplet-excited catalyst molecule (triplet sensitizer) to a ground-state AB, resulting in a triplet-excited ${}^3\text{AB}^*$. Azobenzenes have a low-lying triplet state, so this interaction, triplet energy transfer (TET), can be induced with a plethora of sensitizers.^{88,271–275}

The reason we are interested in this form of interaction is that unlike azobenzene radicals, also triplet-excited azobenzenes isomerise extremely fast. The triplet state is completely barrierless (see Figure 4 in Chapter 2.1) and thus, sensitisation from either *E* or *Z* isomer yields the same ${}^3\text{AB}^*$ state where the molecules cannot be assigned as *E* or *Z* (Equation 18).²⁷⁴ Due to the degeneracy of the triplet-excited state and the singlet ground state, intersystem crossing to the ground state is extremely fast: $k_{\text{ISC}} \approx 10^{11} \text{ s}^{-1}$.⁸³ Moreover, the *E* isomer is produced almost exclusively, in a 98–99% yield, due to a >50-time difference in the rates of the reactions in Equations 19 and 20.^{88,276}



As a result of these properties, triplet sensitisation can be utilised to catalyse the $Z \rightarrow E$ isomerisation. Contrary to charge transfer photocatalysis where the redox potentials of the catalyst and azobenzene need to match, triplet sensitisation is relatively universal as the triplet energy of azobenzenes is little affected by structural modifications^{84,88,253,275} and efficient sensitisation is possible regardless of whether the reaction is exothermic or endothermic.²⁷⁶ In fact, MB, the red-light photocatalyst used to initiate the oxidative PET-based isomerisation pathway, functions as a TET agent for azobenzenes where charge transfer is unfavourable.²⁵³ Also porphyrin-based triplet sensitisers such as **61** can be used (Figure 24).²⁷⁶ Thus, red light can be utilised to indirectly isomerise a wide range of azobenzenes. Even the use of near-infrared light is possible, although the rate is slower due to the increased endothermic energy difference between the triplet states of the azobenzene and the deeply conjugated sensitizer **62**.²⁷⁶ Because **61** and **62** do not absorb in the blue end of the visible spectrum, blue or green light can be used to isomerise the compounds to the Z state (in contrast to UV light used with MB). Recently, TET-catalysed isomerisation with far-red light was accomplished also in a solid bioplastic material.²⁷⁷

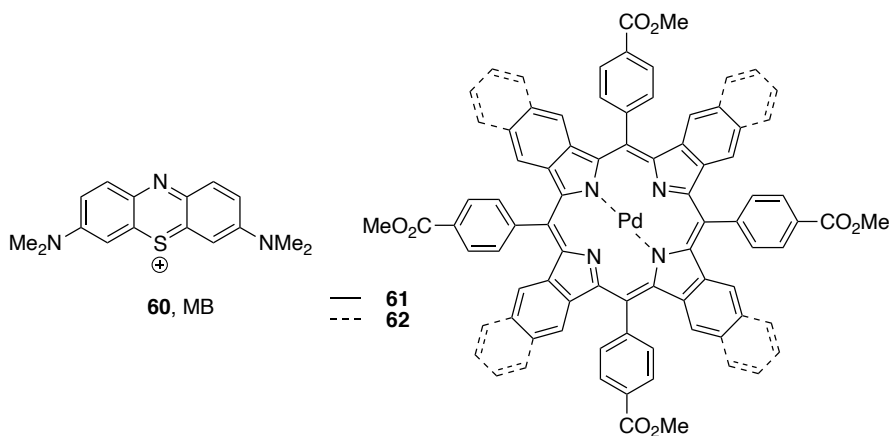


Figure 24. Selected low-energy-light triplet sensitizers.

The biggest drawback in indirect isomerisation via TET is its susceptibility to quenching by molecular oxygen, the phenomenon already mentioned in the context of redox catalysis. Dioxygen O_2 is a species that exists as a triplet in its ground state.^{278,279} It is readily sensitised to the excited singlet state by visible-light triplet sensitisers,²⁸⁰ which in turn hampers the sensitisation of the azobenzene molecules. In addition, singlet oxygen is extremely reactive and may degrade either the azobenzene or the catalyst. As the concentration of oxygen in ambient solutions lies in the range of millimoles per litre,^{281,282} any experiments featuring micromolar concentrations of the catalyst–azobenzene system are seriously affected without precautions. Common measures to tackle the problem include the deaeration of the solvent via freeze-pump-thaw cycles or bubbling with an inert gas, and the use of oxygen scavengers.^{88,253,271,274,276} In the aforementioned solid-state study, the catalyst and azobenzene molecules were confined within a gelatine matrix that blocks the diffusion of oxygen, thus removing the need for further deaeration steps.²⁷⁷

5.2 Isomerisation catalysed by iodine and molecular oxygen

One catalyst we have not discussed yet is molecular iodine, a species that has found use in both thermal and photochemical processes,^{283–287} including the isomerisation of azobenzenes.^{288,289} It absorbs in the visible-light region, the absorption maximum ranging from 410–470 nm in solvents with nucleophilic electron pairs to ca. 520 nm in inert solvents. In an inert solvent, the absorption spectrum is governed by an intense $S_0 \rightarrow S_1$ transition which, after crossing to a dissociative unbound triplet state, leads to the formation of two I^\bullet radicals. This forms the basis of most photocatalytic processes where iodine is utilised.^{290–295} The mechanism has been demonstrated also for azobenzene isomerisation: after dissociation, the iodine radical forms a bond to one of the nitrogen atoms in the azo group, weakening the double bond in a similar fashion as in acid-catalysed isomerisation. Following the accelerated $Z \rightarrow E$ isomerisation, the iodine atom cleaves off, regenerating the radical and yielding E -AB.²⁸⁸ In the presence of a strong-enough electron donor, also photoinduced electron transfer through the excitation of a charge transfer complex is possible. This transition is evident as an additional band on the blue side of the molecular excitation band, and thus, is of little interest to us.

However, one more transition is visible in the absorption spectrum of I_2 , a weak and broad shoulder peak on the red side of the absorption maximum, extending even to the near-infrared regime. This band is associated with a transition to a low-

lying bound triplet state which is not crossed by dissociative states.²⁹⁶ Instead, a relatively stable triplet-excited iodine molecule $^3\text{I}_2^*$ is formed. Probably because of the low intensity of this spin-forbidden transition, the notion of utilising this band for catalytic function had not been pursued, but we speculated that it might have potential in, for example, indirect photoswitching of azobenzenes. To investigate this idea, we studied the isomerisation of a moderately electron-rich 4,4'-dimethoxyazobenzene **2** in *n*-hexane, dichloromethane and carbon tetrachloride. **2** was chosen since it had been used successfully in previous studies²⁵³ and the inert solvents of varying polarity and density were used to retain the absorption band in the red part of the spectrum while acquiring information on the mechanism.²⁹⁷ We started with dichloromethane. The absorption bands of *E*-**2** and *Z*-**2** + I_2 , as well as pure I_2 , are depicted in Figure 25. Since iodine barely absorbs any light at around 365 nm where the π - π^* band of **2** is located, we used this wavelength for the direct *E* \rightarrow *Z* isomerisation. The pure *Z*-**2** has an n - π^* band at around 440 nm, and this band does not extend to the red-light region. The absorption of iodine, however, does extend to the red and even beyond the visible range, albeit with low absorptivity: $\epsilon_{660} = 41 \text{ M}^{-1} \text{ cm}^{-1}$ and $\epsilon_{770} = 8.6 \text{ M}^{-1} \text{ cm}^{-1}$.²⁹⁸ Thus, irradiation at $>650 \text{ nm}$ can only excite iodine.

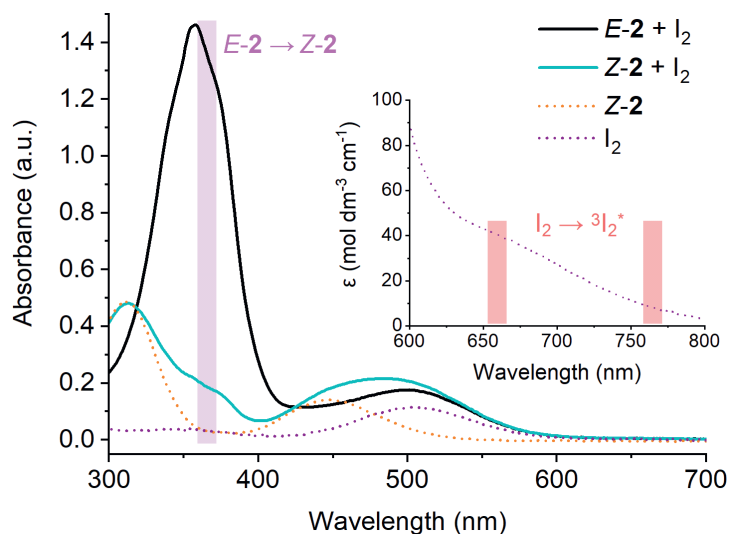


Figure 25. Absorption spectra of a mixture of **2** (50 μM) and I_2 (200 μM) in dichloromethane in dark and upon 365 nm excitation, and of **2** and I_2 separately upon 365 nm excitation. The absorption tail of I_2 is shown in the inset. The wavelengths used for *E* \rightarrow *Z* (365 nm) and *Z* \rightarrow *E* (660 or 770 nm) isomerisation are illustrated with purple and red shading, respectively.

We then proceeded to studying the iodine-catalysed back-isomerisation with varying amounts of iodine. The kinetics of the isomerisation are visualised in Figure 26a by plotting the absorbance at 372 nm (the π - π^* band of *E*-2) as a function of time. After initial *E* \rightarrow *Z* isomerisation with 365 nm excitation (purple shading), the absorbance value increased slightly, probably due to diffusion from unilluminated parts of the solution. When 770 nm excitation was then started (red shading), quantitative *Z* \rightarrow *E* isomerisation took place. Due to the extremely low molar extinction value, the reaction is only fast when stoichiometric amounts of iodine are used. However, the reaction takes place also with a catalyst loading of 10% (Figure 26b), and the reaction with a low catalyst loading can be made reasonably fast by using 660 nm light instead of the 770 nm light. We also tested the robustness of the reaction. Gratifyingly, the system was fully functional even after 1,000 cycles (Figure 26c).

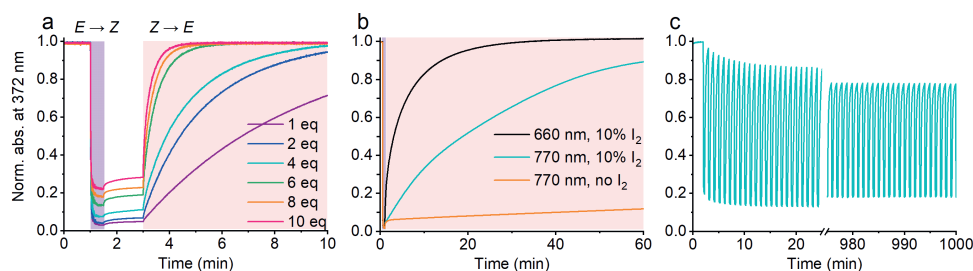


Figure 26. (a) Photoisomerisation curves of **2** with varying amounts of iodine; excitation pulses with 365 and 770 nm are illustrated with purple (1–1.5 min) and red (3–10 min) shading, respectively. (b) Photoisomerisation curves of **2** with low iodine loading. Excitation (660 or 770 nm) starts at 1.0 min. (c) Recurring isomerisation cycles with pulses of 365 and 770 nm excitation (15+45 s).

To determine whether the reaction is driven by TET, PET or I^\bullet radicals, we compared the reaction rates in the three solvents (Figure 27a). The photocatalysed reaction was 3.3 times faster in CCl_4 than in hexane although the rate of homolytic dissociation of I_2 is 5-fold in the latter.²⁹⁹ Thus, the I^\bullet -mediated mechanism was refuted. The lifetime of $^3I_2^*$ is longer in CCl_4 than in DCM (2.7 vs 0.51 ns)²⁹⁶ and thus, TET should be more efficient in CCl_4 , especially given that the molar absorptivity at 770 nm is higher in CCl_4 .²⁹⁸ However, the reaction rate was 2.1-fold in DCM compared to CCl_4 (Figure 27a). Thus, the rate seems to be determined rather by the polarity of the solvent than any other parameter, which is indicative of a formation of a charged species during the reaction, i.e. PET.²⁶² Furthermore, we tested the reaction with three other azobenzenes and found that the catalytic

isomerisation only takes place with sufficiently electron-rich substrates; no reaction was observed with unsubstituted azobenzene **1** and the electron-poor **64**, and the rate was significantly lower for the 4-methoxyazobenzene **63** (Figure 27b). Thus, we concluded that oxidative PET lies behind the catalytic behaviour.

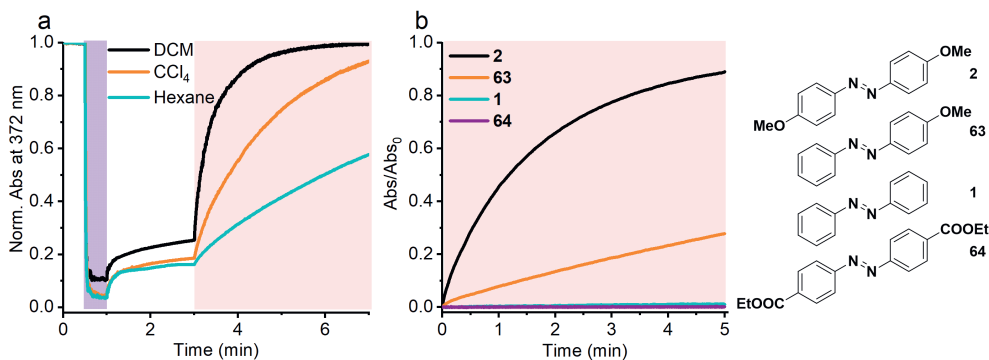


Figure 27. (a) Photoisomerisation curves of **2** in dichloromethane, carbon tetrachloride and *n*-hexane. Excitation with 365 nm at 0.5–1.0 min and with 770 nm at 3–7 min. (b) Photoisomerisation curves of **2**, **63**, **1** and **64** in dichloromethane. Excitation with 770 nm at 0–5 min. In both cases 4 equivalents of iodine was used.

As we postulated the reaction to proceed via a triplet state, the catalysed isomerisation was also studied in a freeze-pump-thaw-deaerated solution and solutions bubble-degassed with either argon or nitrogen, hypothesising that an oxygen-free environment might make the isomerisation more efficient. To our great surprise, the reaction was pronouncedly *slower* in these (partly) deoxygenated solutions as compared to the respective cases under an ambient atmosphere (Figure 28a). This is remarkable, as in all previous TET- and PET-mediated systems the presence of oxygen has been an impediment to efficient isomerisation.^{253,276} In our system, the oxygen instead proved to hold a central role in the mechanism. Iodine is known to sensitise singlet oxygen,³⁰⁰ which in turn has been demonstrated to isomerise certain alkenes,³⁰¹ so we hypothesised this to be involved in the mechanism. Due to the low concentration of ³I₂^{*}, we were unable to directly show the formation of singlet oxygen or other oxygen species. Singlet oxygen scavengers were not successful as they have nucleophilic lone pairs that can interact with iodine.²⁹⁸ Hence, we probed the oxygen-mediated mechanism indirectly, by utilising palladium (II) phthalocyanine (**65**, PdPc), an efficient near-infrared-light singlet oxygen sensitizer with a low triplet energy and relatively short triplet lifetime; due to these properties, direct TET to **Z-2** is improbable.³⁰² When the optical density of

PdPc at 770 nm was matched with that of iodine in the earlier measurement, no catalytic behaviour was observed although the [$^1\text{O}_2$] produced is undisputedly higher based on the reported quantum yields.^{300,302} When the concentrations of iodine and PdPc were matched, photocatalysed isomerisation occurred – but even then, slower than for iodine despite the fact that now the fraction of excited sensitisers was considerably higher. Moreover, also the PdPc-mediated isomerisation was oxygen-dependent, and contrary to the iodine-catalysed reaction, it was faster in CCl_4 than in DCM (Figure 28b).

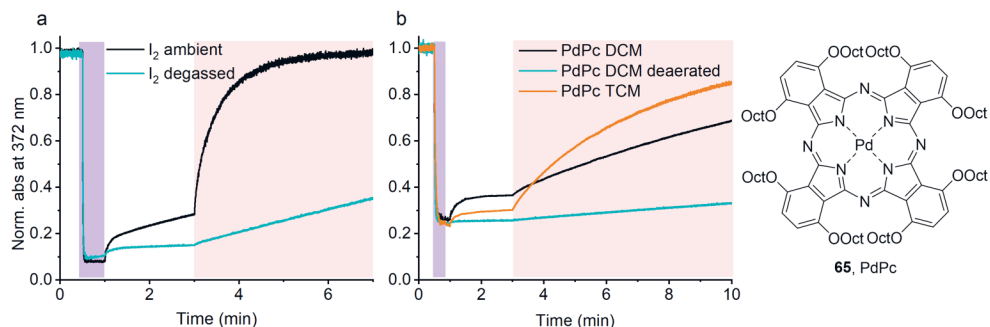
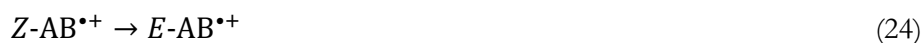


Figure 28. Photoisomerisation curves of **2** with (a) iodine under ambient conditions and after freeze-pump-thaw deaeration, and (b) with PdPc in DCM and CCl_4 under ambient conditions and in DCM after freeze-pump-thaw deaeration. Excitation with 365 nm at 0.5–1.0 min and with 770 nm from 3.0 min.

Building on these results, we proposed that the mechanism does indeed involve the formation of singlet oxygen which subsequently oxidises the *Z*-azobenzene, forming a radical cation $Z\text{-AB}^{\bullet+}$ and a superoxide radical anion $\text{O}_2^{\bullet-}$.^{303,304} After rapid isomerisation,²⁵³ a reverse electron transfer reaction takes place, regenerating the ground-state triplet oxygen and *E*-AB. These reactions are shown in Equations 21–25; although I_2 is used as a sensitizer, the same steps apply to PdPc.





In the case of PdPc, its triplet lifetime (highest in CCl_4 ³⁰⁵) and the solubility of oxygen (higher in CCl_4 than in dichloromethane^{281,282}) seem to determine the rate of the catalytic isomerisation. Clearly, some additional reaction is possible with iodine, based on the different solvent dependency and markedly higher rates. We proposed that both of these observations are explained by an additional electron transfer step between ground-state iodine and the anionic oxygen radical,³⁰⁶ in which case the formed oxygen would be singlet-excited and thus further accelerate the reaction (Equation 26).³⁰⁷ It is also possible for reactive oxygen species to cause the dissociation of iodine,³⁰⁸ creating neutral I^\bullet radicals that would catalyse the reaction.²⁸⁸ However, the observed solvent effect does not support this possibility.



To conclude, indirect $Z \rightarrow E$ isomerisation pathways have been demonstrated with red- or near-infrared-light TET or PET agents, even coupled to visible-light $E \rightarrow Z$ isomerisation in one case.²⁷⁶ Molecular oxygen, abundant in most media of interest, hampers the use of triplet sensitisers. PET is less sensitive to oxygen. Interestingly, molecular iodine can be used as a near-infrared photocatalyst to induce the $Z \rightarrow E$ isomerisation of suitably electron-rich azobenzenes. The reaction is not only tolerated but in fact mediated by oxygen, which is unprecedented in photoswitching. Based on our studies and existing literature, we propose that the reaction proceeds via singlet oxygen produced by triplet-excited iodine and subsequent electron transfer from the azobenzene to singlet oxygen, resulting in a radical cation that rapidly isomerises to the E form. In addition, another PET step featuring iodine and further accelerating the reaction seems probable. However, additional spectroscopic and computational studies are required to accurately determine the mechanism. It should also be noted that although the catalytic system functions with near-infrared light and tolerates ambient conditions, it only functions with selected azobenzenes and inert solvents and absorbs across the whole visible spectrum, disabling the use of low-energy light for the $E \rightarrow Z$ isomerisation. Furthermore, iodine can also catalyse organic reactions in the ground state, limiting its suitability. Thus, in order to make the photoswitching system practically useful, other singlet oxygen sensitisers with appropriate redox properties should be found. In this light, the fact that PdPc can be used (although inefficiently) in the place of iodine is encouraging. Another viewpoint is that near-infrared excitation of iodine and the subsequent production

of reactive oxygen might have yet unexplored uses in organic synthesis or other applications. For both photoswitching and other prospects, a better understanding of the underlying mechanism is integral.

6 BEYOND SWITCHES: MOLECULAR MOTORS DRIVEN BY VISIBLE LIGHT

In the last three chapters we have investigated ways to realise photoswitching with red or even near-infrared light. In addition to photoswitch-specific approaches such as the *ortho* substitution of azobenzenes, general strategies have been introduced: tuning established switches by extending the π -system or creating push-pull character, taking advantage of less-explored molecular structures such as indigoids, or inducing the switching indirectly with photocatalysts. Herein, we shall see how these approaches are also applicable to light-driven molecular motors, a special class of photoswitches where the switching between multiple states occurs via unidirectional rotation around a double bond. Chapter 6.1 introduces the fundamentals of photochemically-driven single-molecule motors, followed by an account of different steps taken towards systems operating with visible light. In Chapter 6.2, we shall present the final original piece of this thesis, the synthesis and characterisation of a barbituric-acid-based molecular motor that absorbs in the visible light regime. It should be highlighted that Chapter 6.1 can barely scratch the surface of the beautiful chemistry built around molecular motors and should only be regarded as essential background information for our work. Comprehensive reviews on the theoretical and practical aspects of molecular motors, as well as a broader scope of rotatory molecular structures, may be consulted for further information.^{11–13,309–312}

6.1 Molecular motors based on rotation around a double bond

The chemistry of *E*–*Z* photoswitches was reviewed in Chapter 2.1. Stiff-stilbenes are an exemplary family of compounds that can be interconverted between their stable *E* and metastable *Z* isomers photochemically or thermally. What makes this class of photoswitches particularly intriguing is that through the addition of steric bulk around the central double bond (in the fjord region), the molecule is forced out of planarity into a helical structure, and if a (pseudo)stereogenic centre is located in this region, the helicity of this compound, aptly named overcrowded alkene, is

predetermined by the non-symmetrical steric interactions (Figure 29).³⁰⁹ As a consequence, photoexcitation of the compound results in unidirectional rotation, in contrast to the stochastic motion of photoswitches. Three generations of molecular motors based on overcrowded alkenes have been designed so far. The original first-generation motor **66** features two symmetric halves separated by a C=C axle, both of which have a stereogenic centre.³¹³ In the second-generation motors (e.g., **67**), the top and bottom halves differ and the molecules have only one stereogenic centre.^{314,315} The half with a higher moment of inertia is defined as the stator, while the smaller half is called a rotor (or rotator).³¹⁶ Finally, third-generation motors such as **68** lacking any point chirality at all but instead carrying a pseudo-asymmetric centre have been contrived, now featuring two rotating units.³¹⁷ There are also motors based on other structures which will be covered later in this chapter.

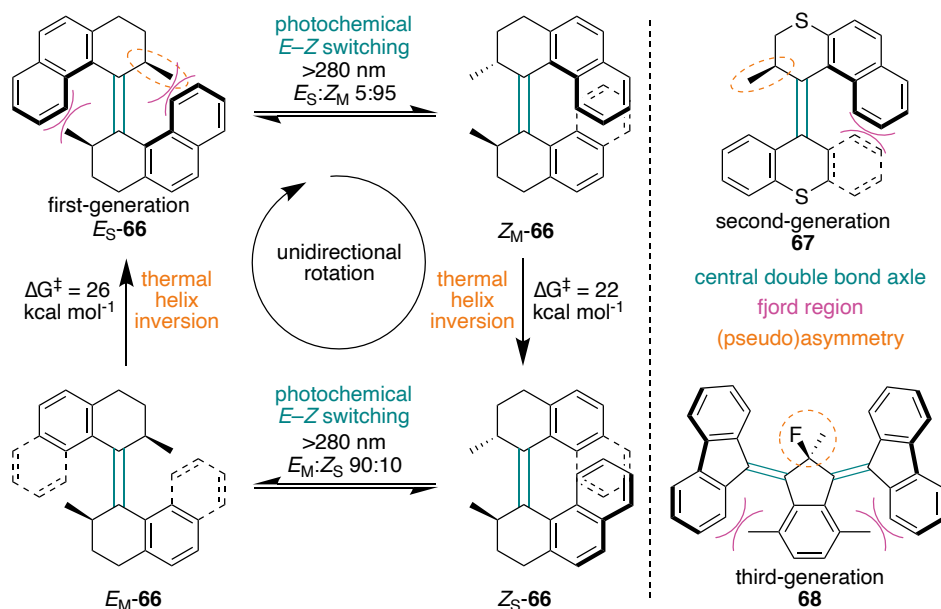


Figure 29. The rotation cycle of a first-generation molecular motor and the structures of representative second- and third-generation motors.

The key to unidirectional net rotation is a closed cycle consisting of an oriented sequence of propagating steps. As a representative example, the rotation cycle of a first-generation motor **66** is depicted in Figure 29 and discussed herein.³⁰⁹ Four distinct isomers can be identified: the *E* and *Z* isomers can both have either *M* or *P* helicity, one of which is more stable than the other due to differences in the steric strain. Starting from the stable helical form of the *E* isomer (*E_S*), excitation at the π –

π^* band of the motor brings the molecule into its first excited state where relaxation from the Frank-Condon state to the S_1 minimum takes place with a lifetime on the order of 100 fs and subsequent relaxation to ground state in 5–10 ps.³¹⁸ In total, this photochemical $E \rightarrow Z$ isomerisation (PEZI) step has a quantum yield of up to 85%, resulting in the metastable state of the Z isomer (Z_M).³¹⁹ Thermal helix inversion (THI) to the stable Z isomer (Z_S) has a half-life of ca. 15 minutes at room temperature.³⁰⁹ It can in turn be photoisomerised, yielding the metastable E isomer (E_M). Finally, another THI step refurnishes the original E_S state. This step has a considerably higher energy barrier, corresponding to a half-life of months at room temperature; thus, heating is required to induce the last isomerisation step.^{309,313} Although a PSS is formed during both PEZ steps and hence, a fraction of the molecules does not proceed to the next THI step, no molecules rotate in the reverse direction as the THI steps are irreversible^a and the barriers for thermal $Z \rightarrow E$ isomerisation (TEZI) are typically even higher. Thus, THI acts as a ratchet to ensure net unidirectional rotation. However, competing thermal back-isomerisation is a real possibility when $\Delta G^\ddagger_{\text{THI}}$ is high or $\Delta G^\ddagger_{Z \rightarrow E}$ low.³²⁰ In such cases, the molecules are rendered switches instead of motors.³²¹

The rotation cycles of second- and third-generation motors follow the same fundamentals, although differences exist: the E and Z isomers of second-generation motors with a symmetrical bottom half (e.g., **67**) are interchangeable and thus these molecules have only two states, stable and metastable. This design simplifies the characterisation of such motors, but at the same time, makes proving the unidirectionality of the rotation impossible without desymmetrisation of the symmetric half or the preparation of an enantiomerically pure sample. Third-generation motors share the same fundamental steps, but because of two independently moving rotors, they exhibit at least four states even if the individual rotor parts are symmetrical, and with desymmetrised rotors even more states are observed.³¹⁷ Herein, we will focus on second-generation motors. As an advantage over first-generation motors, both THI barriers are the same ($\Delta G^\ddagger \approx 25 \text{ kcal mol}^{-1}$ for **67**), which results in a steady rotation speed over the whole cycle.³¹⁶ The excited-state dynamics is also different, the $S_1 \rightarrow S_0$ relaxation occurring on a 1 ps timescale (cf. 5–10 ps for first-generation motors).^{322,323} Concurrently, quantum yields of isomerisation are significantly lower, ranging from <1% to 20%^{315,324–326} and even the theoretical upper limits lie below 30%.³²⁷ Electron-withdrawing units conjugated

^a Although THI is in principle an equilibrium process, the energy difference between the stable and metastable states is large enough (8.6 and 11 kcal mol⁻¹ for *E*-**66** and *Z*-**66**, respectively) for the reaction to be considered irreversible.

to the C=C axle often improve these values,^{324,326} and push-pull systems promote quantum efficiency even more.³²⁸ This effect arises from the geometry of the S_1 minimum and the conical intersection between the S_1 and S_0 states. After initial homolytic cleavage of the central C=C bond upon photoexcitation, electron density is shifted towards one side of the π bond as the molecule traverses to the conical intersection, and to stabilise the forming anionic electron pair, the atom at the central carbon axle pyramidalises. This charge transfer causes the motion about the central axis to be precessional (Figure 30a).^{322,327,329,330} If an electron-withdrawing group can delocalise the electron pair, less pyramidalisation takes place and the rotation is more axial. This geometry, in turn, has been linked to higher PEZI quantum yields.^{328,329} Thus, to efficiently harness photonic energy for rotation instead of simply dissipating it as heat, structures with sufficient push-pull character are favourable. In the quest for optimal properties, chemists have designed (i) biomimetic motors^{331–333} inspired by the natural unidirectional motor rhodopsin³³⁴ and (ii) theoretical motors constituting of minimal rotor and stator parts,^{335–339} both equipped with sufficient push-pull character. Computational studies have revealed high quantum yields up to 90% for some of the theoretical motors,³³⁹ although many of them suffer from reduced rotation directionality. These structures can be used as inspiration for synthetic motors, as we will see in Chapter 6.2.

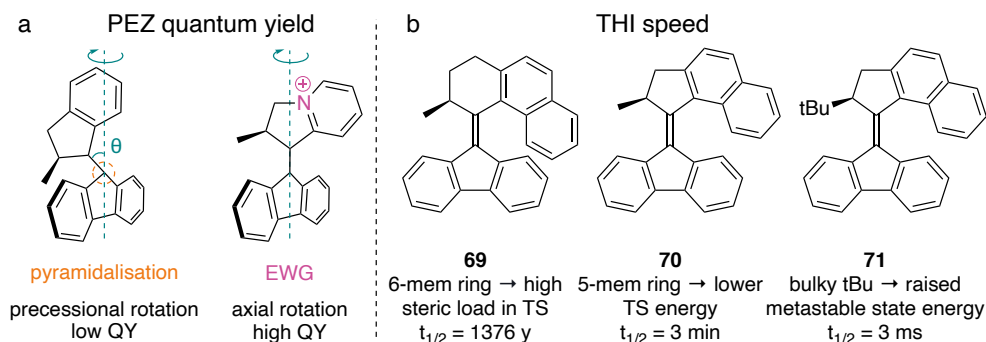


Figure 30. (a) Schematic TS geometries showing a pyramidalised and non-pyramidalised structure, leading to precessional and axial rotation, respectively. (b) Selected second-generation motors and their THI half-lives, demonstrating the features that speed up the reaction.

Since the THI steps of the molecular motors **66** and **67** are slow, the characterisation and even isolation of each isomer is rather easy. This also means that elevated temperatures are required for fast rotation. To speed up the thermal ratcheting steps, the steric hindrance in the transition state structure can be reduced by switching the six-membered rings attached to the C=C axle to five-membered rings, thus making

the fjord region less crowded (Figure 30b, **69** vs **70**).^{315,340,341} Alternatively, heteroatoms can be installed in the place of the bridging carbons for the same effect.^{315,342} Motors with such structures exhibit THI half-lives of seconds or less.³⁰⁹ Another approach to make rotation faster is to switch the methyl group in the stereogenic centre for a larger alkyl group (**70** vs **71**). Due to the perpendicular arrangement in the THI transition state, the alkyl substituent does not affect the energy of the transition state. Instead, it selectively raises the energy of the metastable state through increased steric load.³⁴³ It should be noted that the aforementioned modifications have predictable effects in second-generation motors, but the structure–property relationships are less easily anticipated for the first generation due to the two different THI steps. Finally, also fully photochemical switches have been designed.^{344–346} Since all steps are driven by photonic energy, the rotation does not rely on heat and can, in principle, occur on a picosecond timescale.

The motors discussed thus far function upon irradiation with ultraviolet light. Second-generation motors are somewhat red-shifted compared to first-generation compounds (operation wavelengths shifted from 280 to 365 nm between **66** and **67**), but additional measures are needed to bring the wavelengths to the visible part of the spectrum. Direct two-photon absorption of the motor core enables excitation with 710 nm light, but it is not practically feasible for most applications due to the enormous irradiation intensities required (TW cm^{-2}).³⁴⁷ The energy gap for one-photon absorption can be reduced by extending the π -system with additional aromatic rings on either half.^{348,349} For instance, the second-generation motor **72** can be rotated with 490 nm excitation because of its red-shifted and broadened absorption band as compared to the otherwise identical parent motor **70** (Figure 31).³⁴⁸ As a disadvantage, these motors exhibit lower isomerisation quantum yields and worse PSDs. Also the application of push-pull substituents has been utilised.^{326,350} As an example, the methoxy and cyano substituents conjugated across the C=C axle in **73** lower the HOMO–LUMO gap sufficiently for the motor to be efficiently isomerised with 530 nm light.³²⁶ The PSDs and quantum efficiencies are also good. The motor **74**, featuring a pyrrolidino moiety as the electron donor, has an even further red-shifted absorption band, extending to the red part of the visible spectrum in polar solvents where the polarisation of the molecule is strongest. Due to this effect, the compound actually only functions as a motor in non-polar solvents. In polar solvents the C=C bond is weakened to a point where thermal $Z \rightarrow E$ isomerisation outcompetes THI, rendering **74** to a switch.³⁵¹

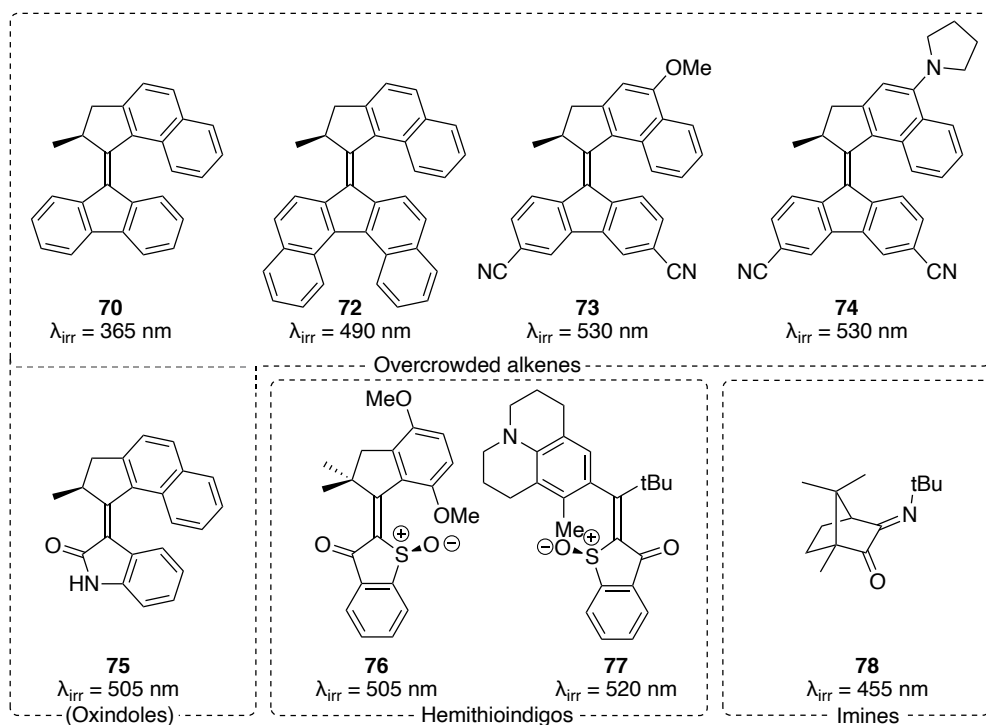


Figure 31. Selected red-shifted molecular motors along with the irradiation wavelengths used to induce the photochemical isomerisation steps.

Like with switches, the absorption of motors can also be shifted towards the red end of the visible spectrum by employing novel molecular structures instead of individual small modifications. One such family are oxindole-based motors, a subclass of second-generation overcrowded alkene motors.^{315,328,352} Because of the intrinsically electron-withdrawing nature of the lower half, compounds such as **75** absorb well in the visible range, and further red-shift as well as enhancement of photoisomerisation quantum efficiency can be realised with small synthetic modifications.³⁵²

Stepping further away from the conventional overcrowded-alkene-based motors, structures featuring hemithioindigos can also perform unidirectional rotation about a C=C double bond. The earliest hemithioindigo motor **76** resembles oxindole motors, except for the origin of chirality: contrary to hemithioindigo photoswitches, the sulphur atom is oxidised into a sulfoxide, thus creating an asymmetric centre in the lower half (thioindigo part) of the molecule. The rotation mechanism itself is identical to that of a second-generation motor, and like oxindole motors, also hemithioindigo motors are intrinsically red-shifted.³⁵³ PEZI occurs on a timescale of 0.3–10 ps, depending on the substitution pattern, and the lifetimes of the THI steps

range from 3 ns to 40 ms.^{354,355} Further structural developments led to the discovery of an entirely different working mechanism, the figure-of-eight motion by **77**.³⁵⁶ The rotation cycle features four steps: two PEZI steps, each followed by a thermal so-called hula twist step that consists of concerted *E*–*Z* isomerisation and single bond rotation.³⁵⁷ The latter is only allowed in this kind of structure where the C–C bonds connected to the C=C axle are not bound inside a ring structure. Because of the strong push-pull character caused by the julolidine unit in the top half conjugated to the carbonyl group in the lower half, the absorption band is even more red-shifted, enabling the operation of the motor with 530 nm excitation. Unfortunately, the photochemical steps are only efficient in apolar solvents, whereas the thermal steps are only fast in strongly polar solvents, and continuous irradiation in moderately polar solvents leads to a decrease in the directionality of the rotation.³⁵⁶ Following a similar molecular design, fully photochemical rotation has been realised. In this case, the rotation cycle consists of sequential PEZI and single bond rotation steps or hula twists combining the two thereof, all of which are induced photochemically. However, multiple possible photoreactions are possible from each isomeric species and although the quantum yields of individual steps are biased towards one cycle (with a probability of 86% against all possible outcomes), the rotation is not completely unidirectional. It can, however, be made almost unidirectional at low temperatures where the competing photoreactions become less probable.³⁵⁸ This finding is in stark contrast to conventional motors that lose their unidirectionality when the thermal ratcheting steps cannot operate at reduced temperatures. Finally, it should be mentioned that motors based on rotation around a C=N bond have also been designed and synthesised, **78** absorbing in the visible range.^{359–361} Depending on the structure, the rotation cycle consists of either two or four parts. In a two-stroke mechanism, PEZI is followed by thermal inversion of the nitrogen stereocentre that restores the original conformation. The four-stroke mechanism contains two sets of consecutive PEZI and ring inversion steps. More detailed descriptions of the hemithioindigo and imine motor rotation cycles are presented in an excellent recent review.³⁰⁹

Also indirect excitation has been exploited to avoid high-energy light, using palladium (II) porphyrin as a sensitiser to bring the motor into its triplet-excited state, from where relaxation may lead to *E*–*Z* isomerisation.³⁶² The process was most efficient for **79** which has the sensitiser covalently linked to the motor core (Figure 32). A PSD of 67:33 **79**_M:**79**_S was recorded upon excitation with 532 nm light, with a quantum efficiency of 11% (cf. 14% upon direct excitation). This may seem odd, remembering how triplet sensitisation was used to drive azobenzene isomerisation

almost quantitatively from *Z* to *E* in Chapter 5.²⁷⁶ However, the T_1 state of azobenzene is inherently different because of its $n\text{--}\pi^*$ nature. From the T_1 state of stilbene that has $\pi\text{--}\pi^*$ nature, external conversion to the ground state yields both isomers with almost the same probability, the *Z* isomer slightly favoured in most conditions.^{243,363,364} The same fundamentals apply to overcrowded alkenes. Despite the difference to azobenzene sensitisation, the same drawback is present: the system functions only in strongly deaerated conditions.³⁶²

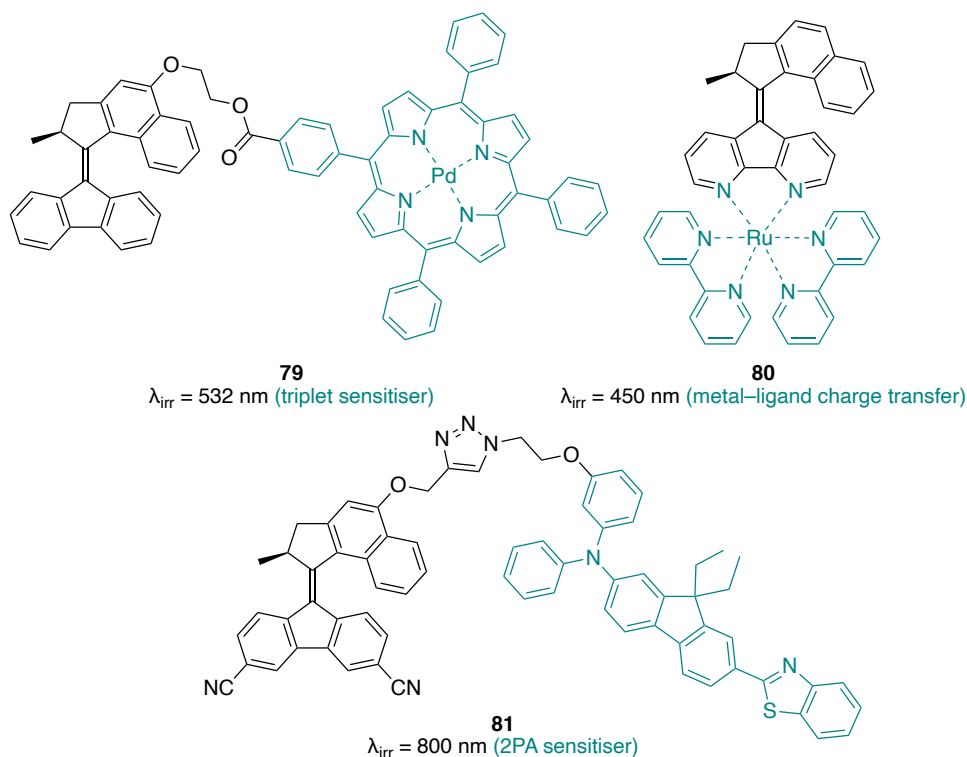


Figure 32. Molecular motors operating upon indirect excitation.

Also using the motor as a ligand in a transition metal complex such as **80** has been demonstrated as a way to induce the excitation indirectly. The complex can be excited with 450 nm light, leading to charge transfer to the ligand and subsequently PEZI to a PSD of 36:64 $\mathbf{80_M}:\mathbf{80_S}$. Although the PSD is low, the following THI step is faster than without coordination to the metal, leading to overall faster rotation and allowing visible light to be used.³⁶⁵ Finally, although direct two-photon excitation requires extreme light intensities which are detrimental to living cells, indirect two-photon absorption with a well-designed antenna sensitizer is feasible. The motor **81**

features a two-photon absorber with a large absorption cross-section. It can be efficiently excited to its singlet-excited state upon irradiation with 800 nm light, keeping the intensity at 150 mW cm⁻², which is below the threshold for cell degradation. Förster-type resonance energy transfer from the sensitiser and the motor may now take place, resulting in the singlet-excited motor, from which the PEZI step proceeds like upon direct excitation.³⁶⁶

6.2 Molecular motors based on barbituric acid

Despite the steps taken towards motors operating with visible light, these molecular designs often suffer from relatively low photoisomerisation quantum yields and PSDs as well as synthetic complexity. Taking inspiration from the biomimetic and theoretical motors and switches that feature high quantum efficiencies and fast rotation kinetics (e.g., **82**),^{367,368} we were searching for a simple structural design that would yield a visible-light-absorbing motor with considerable push-pull character. Barbituric acid is a strong electron acceptor, ideal for different donor-acceptor (push-pull) systems such as DASAs (see Chapter 2.2). Its alpha hydrogens are remarkably acidic ($\text{pK}_a \approx 4$), which enables efficient reactions with various electrophiles under mild conditions. Recently, a library of ultrafast visible-light-responsive photo-oscillators (e.g., **83**) based on barbituric acid was synthesised via a Knoevenagel condensation in water.³⁶⁹ We envisioned that coupling barbituric acid with a moderately electron-rich top half might yield a molecular motor with desirable properties. Thus, we designed the structure **84** that was expected to function as a second-generation motor (Figure 33a). Efforts to synthesise the compound from **85** and **86** using conditions reported for barbituric acid condensations with ketones^{370–372} failed, so we reverted to the procedure utilised for oxindoles with similar top halves (Figure 33b).³⁵² Surprisingly, instead of the expected product, we consistently and exclusively acquired the compound **87** featuring an additional hydroxy group in the asymmetric centre.³⁷³ Since this site is intrinsically nucleophilic in both **84** and **85** and oxygen electrophiles are notoriously elusive, the reaction is truly astonishing. Under standard conditions, **87** was acquired in a 15% yield, accompanied by recovered starting material (65%) and traces of an elimination product **88**.

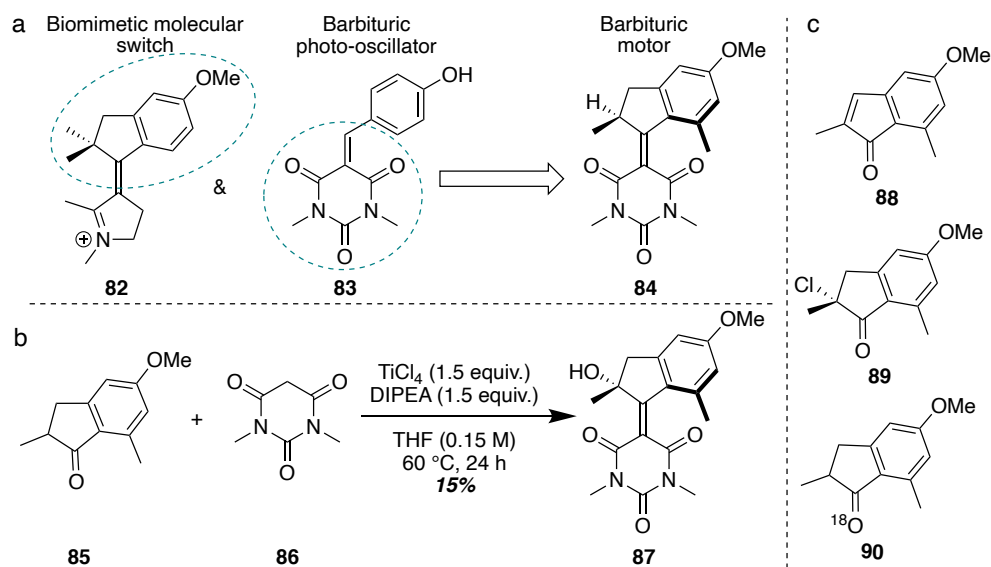


Figure 33. (a) Molecular design and (b) synthesis of a molecular motor based on barbituric acid. (c) Side products and starting materials of mechanistic studies.

To understand the unexpected formation of **87**, we probed the reaction with a range of parallel control experiments, changing one parameter at a time. Because of prominent side products arising from a reaction between THF and TiCl_4 ,³⁷⁴ the isolation of **87** was difficult and could not be done quantitatively. Thus, the reaction yields were estimated with ^1H NMR. The reaction was carried out in dry solvent under a nitrogen atmosphere by default, and its outcome was independent of whether residual moisture was removed with molecular sieves or ambient light blocked. Pristine reagents were used to eliminate the possibility of phantom reactivity by degraded or contaminated reagents, with no effect on the product composition. Interestingly, the reaction proceeded only when both a Lewis acid (TiCl_4) and a non-nucleophilic base (DIPEA) were present although the acidity of barbituric acid should allow the condensation without any base. When the amount of base was increased, the elimination product **88** became prominent. Because of this side product, we considered an alpha-chlorinated intermediate **89** (Figure 33c) but refuted it as no product was formed when starting from this substrate. Furthermore, when the reaction was carried out with an oxygen-18-labelled ketone **90**, no ^{18}O was found in the product; thus, the oxygen must come from outside, as opposed to a rearrangement of the initial carbonyl structure. Next, we considered that the hydroxy moiety would form during the quenching step, but the product composition was unaffected by whether the reaction mixture was quenched with

aqueous ammonium chloride, water, deuterium oxide or methanol. We tried to observe the reactive intermediate directly by carrying out the reaction in THF- d_8 , but recording the NMR spectra from an unquenched reaction mixture was not possible, presumably because of paramagnetic titanium species formed during the reaction. However, we were able to get some insight into the mechanism by recording a mass spectrum immediately after quenching the reaction, before further work-up. We observed a mass signal for $[M+H+16]^+$, i.e. containing an extra oxygen atom. The same signal was observed when starting from **90**. This signal was replaced by the correct $[M+H]^+$ value after full work-up. Thus, we postulate that a peroxide-type intermediate is initially formed before decomposition to **87** when heated up in the rotary evaporator. The most obvious peroxide source would be O_2 , but we observed no difference in the product composition when using carefully degassed THF solutions. The finer details of the mechanism remain unclear to us.

Regardless of its formation mechanism, **87** turned out to absorb well within the visible spectrum with reasonable molar absorptivity values, λ_{max} ranging from 421 to 444 nm and ϵ_{max} from 12,800 to 20,100 $dm^3\ mol^{-1}\ cm^{-1}$ in different solvents (Figure 34a, Table 10). Moreover, an X-ray diffraction analysis of single crystals (grown from an ethyl acetate/pentane solution) revealed that the molecules adopt a twisted, helical structure, a prerequisite for unidirectional rotation (Figure 34b). Interestingly, an intramolecular hydrogen bond is found between the OH group and one of the carbonyl oxygens of the lower half. Since the lower half of the molecule is symmetric, only two states, stable and metastable, can potentially be observed. We studied the possible photoisomerisation process first with 1H NMR at $-90\ ^\circ C$ where thermal processes do not compete with photochemical pathways. Starting from the stable state, a PSD of 63:37 **87_M**:**87_S** was observed (in MeOD) upon excitation at 420 nm (Figure 34c). After heating the sample to $-45\ ^\circ C$ for 15 minutes, the stable state was repopulated with no sign of photodegradation.

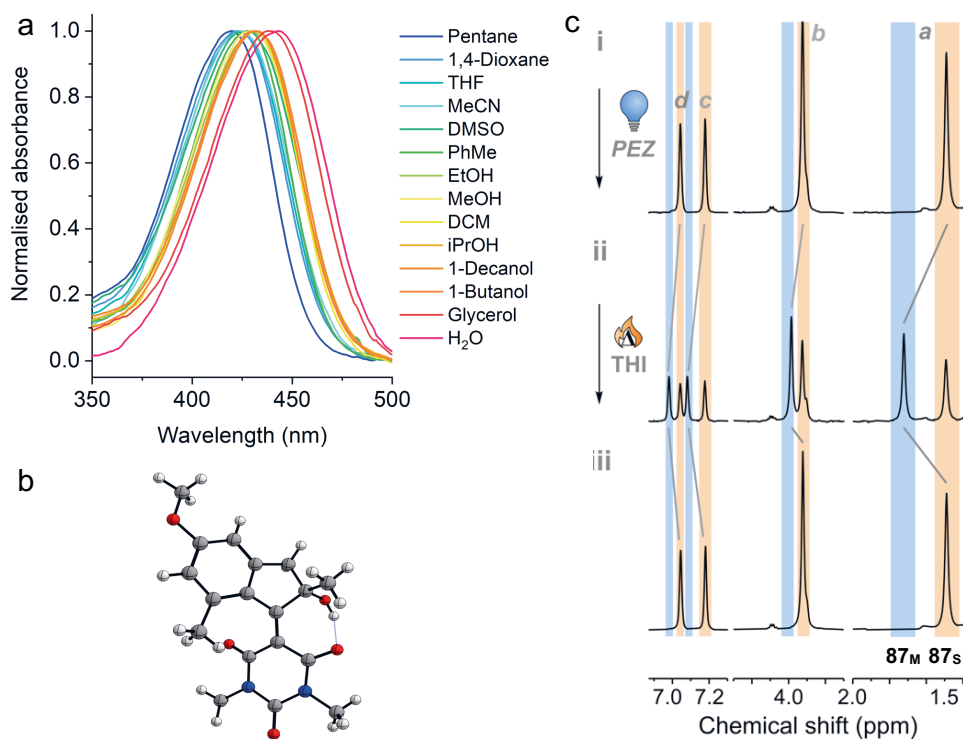
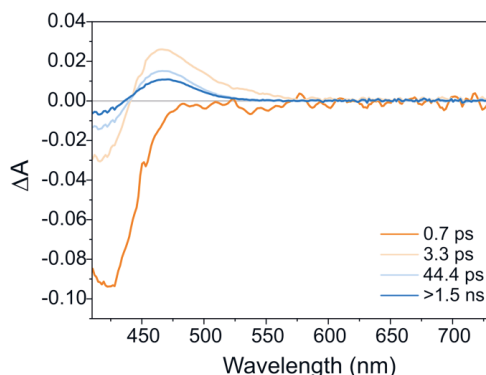


Figure 34. (a) Absorption spectra of **87** in different solvents. (b) ORTEP image (ellipsoid probability of 50%) of the crystal structure of **87**; only one molecule of a two-molecule conglomerate is shown for clarity. (c) ¹H NMR spectra of **87** (i) in dark, (ii) upon excitation with 410 nm light, and (iii) after 15 minutes at -45 °C, all measured at -90 °C in MeOD. Modified with permission from ref. 373. Copyright 2023, RSC.

Femtosecond transient absorption spectroscopy revealed that after initial excitation to the S_1 state, the **87_S** \rightarrow **87_M** photoreaction occurs with a lifetime of less than 1 ps (τ_1 ; 0.5 ps in *n*-hexane), which is visible as ground state bleach at around 410–430 nm and subsequently as product absorption at 460–480 nm. This event is followed by vibrational and solvent-induced relaxation (τ_2 and τ_3) to the metastable state energy minimum (Table 10). This relaxation is slower and depends on the polarity, polarisability and viscosity of the solvent.

Table 10. Absorption maxima λ_{\max} and molar coefficients ϵ , excited state lifetimes τ_1 – τ_3 and $\mathbf{87_M} \rightarrow \mathbf{87_S}$ isomerisation lifetimes for $\mathbf{87}$ in various solvents. Evolution-associated difference spectra obtained from global analysis of the transient absorption data of $\mathbf{87}$ is shown for MeOH. Modified with permission from ref. 373. Copyright 2023, RSC.



	λ_{\max} (nm)	ϵ (M ⁻¹ cm ⁻¹)	τ_1 $\mathbf{87_S^*}$ (ps)	τ_2 $\mathbf{87_S^*}$ (ps)	τ_3 $\mathbf{87_S^*}$ (ps)	τ $\mathbf{87_M} \rightarrow \mathbf{87_S}$ (ms)
Pentane	425	19200				12.3
Hexane			0.5	10.5		
1,4-dioxane	421	18900				19.7
Toluene	441	18500	0.6	8.5	38.2	28.8
DCM	432	20400	0.7	6.6	30.3	75.0
THF	428	18300				11.7
Decanol	433	18100				14.6
<i>i</i> PrOH	435	19100				5.88
EtOH	428	20100				1.81
MeOH	432	19100	0.7	3.3	44.4	1.34
MeCN	424	18600	0.6	1.5	13.7	34.2
Glycerol	430	15300				1.81
DMSO	432	14400	0.7	6.8	170.9	75.5
H ₂ O	444	12800				$7.87 \cdot 10^{-3}$

To gain insight into the photoisomerisation mechanism, we carried out excited state molecular dynamics simulations of $\mathbf{87_S}$ at the OM2/MRCI level of theory. The simulations correctly predict the unidirectional $\mathbf{87_S} \rightarrow \mathbf{87_M}$ step to be ultrafast, with an excited-state lifetime of 0.53 ps (well in accordance with the experimental value in *n*-hexane) and a quantum yield of 68% (Figure 35a). The latter value is high compared to second-generation molecular motors, which is probably caused by two factors: (i) the electron-withdrawing nature of barbituric acid that inhibits pyramidalisation in the excited state and leads to axial rotation, and (ii) hydrogen

bonding that actively promotes rotation. Upon excitation, the intramolecular hydrogen bond found in **87_s** is broken. After the molecule reaches the perpendicular orientation at the conical intersection, a new hydrogen bond is formed between the OH and the other carbonyl, creating a “lasso” effect that pulls the rotation forward (Figure 35a). This effect is a unique feature for this serendipitous molecular structure.

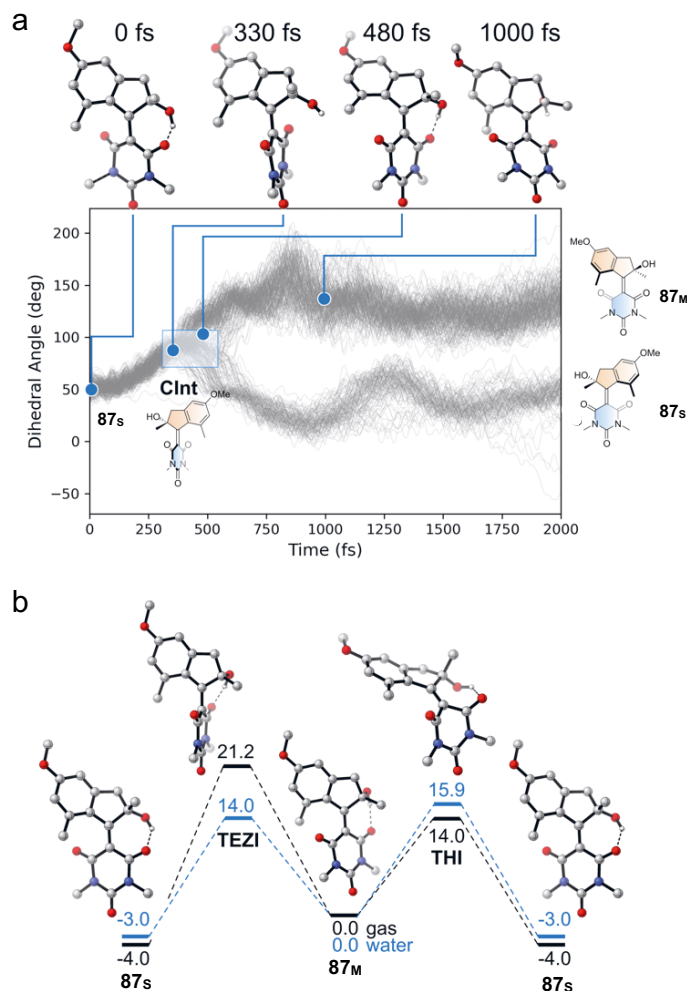


Figure 35. (a) Evolution of the dihedral angle associated with the rotation about the central C=C bond over time obtained at the OM2/MRCI level and snapshots of the isomerisation of **87** selected from a productive MD simulation that led to the formation of **87_M** underlining the hydrogen bond “lasso” effect. (b) Gibbs free energies (DSD-BLYP-D3BJ/def2-QZVP//r²SCAN-3c level, in kcal mol⁻¹) for the thermal processes of motor **87** on the ground state surface. The black and blue surfaces depict the energies of the structures in gas phase and using water as implicit solvent (conductor-like polarisable continuum model), respectively. Modified with permission from ref. 373. Copyright 2023, RSC.

The kinetics of the thermal $87_M \rightarrow 87_S$ isomerisation was further investigated with nanosecond transient absorption spectroscopy, yielding room-temperature isomerisation lifetimes ranging from 1.3 to 76 ms without a strong correlation to solvent polarity (Table 10). However, in water the lifetime was significantly shorter, only 7.9 μ s, which may hint at an alternative isomerisation mechanism in an aqueous environment. At the same time, we also observed relatively rapid decomposition of the motor in water; thus, further investigation of the isomerisation mechanism was restricted to other solvents. We also synthesised the motor **91** (Figure 36) with a desymmetrised lower half, which enables observing sequential steps of the rotation cycle. The molecule was initially isolated in a 1:1 ratio of the E_S and Z_S isomers, and using supercritical fluid chromatography, this was enriched to a 73:27 mixture. We were not able to unequivocally determine the exact stereochemistry; thus, we call these the isomers a and c, respectively. Starting from this mixture, excitation with 420 nm light at -90 °C in MeOD resulted in a PSS mixture with four isomers, a:b:c:d = 12:61:9:19, and after 70 minutes in dark at -90 °C, a new dark equilibrium with 77:23 a:c was reached. Based on this data, the molecule does not seem to function as an (efficient) motor; the small change in the a:c integral ratio may be a sign of some degree of directionality but is within the error margin of integration. To further assess the directionality of the cycle, we also studied the two possible thermal isomerisation reactions computationally in gas phase at the DSD-BLYP-D3BJ/def2-QZVP//r²SCAN-3c level of theory. We optimised the structures of 87_S , 87_M and the THI transition state in gas phase and using water as the implicit solvent (conductor-like polarisable continuum model). According to these results, THI is more favourable than TEZI in gas phase where the energy difference of the thermal barriers is 7.2 kcal mol⁻¹, favouring THI by a $\sim 10^5$ -time difference in the respective reaction rates. This is also the case in non-polar solvents. However, in polar solvents such as methanol or water, the situation is reversed: polar solvents stabilise the polarisation of the push-pull structure in the molecule, leading to diminished double bond character in the central C=C axle. Thus, in water the ΔG^\ddagger of TEZI is lowered down to 14 kcal mol⁻¹. Simultaneously, polar solvents weaken intramolecular hydrogen bonding, which raises the $\Delta G^\ddagger_{\text{THI}}$ by 2 kcal mol⁻¹. Overall, due to these effects, TEZI is favoured over THI in polar solvents, similarly as in the case of another recent motor that had a strong push-pull character.³⁵¹ This explains the observed lack of directionality for **91** in methanol-d₄.

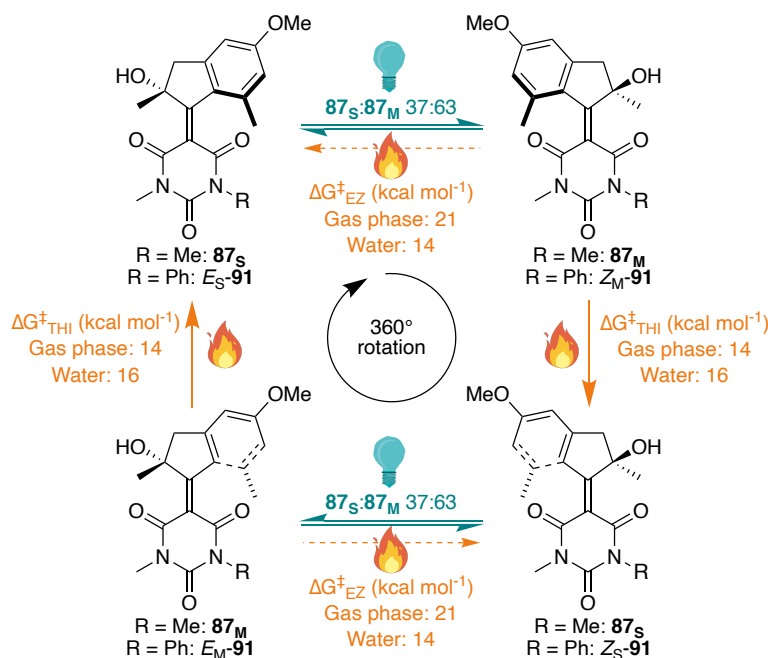


Figure 36. The rotation cycle of **87** and **91** and the thermal barriers of THI and TEZI, calculated at the DSD-BLYP-D3BJ/def2-QZVP//r²SCAN-3c level of theory.

In conclusion, we synthesised a new molecular motor scaffold based on barbituric acid, featuring high absorptivity in the visible-light regime, sub-picosecond photoisomerisation kinetics and unidirectional thermal helix inversion on a millisecond timescale. Surprising reactivity in a Knoevenagel condensation yielded a quaternary stereocentre fitted with a hydroxy group alpha to the C=C axle. Molecular dynamics simulations suggest that this serendipitous OH unit forms a hydrogen bond to a C=O unit in the barbituric acid during the photoreaction and thus actively pulls the rotation forward. Owing to this feature, as well as the electron-withdrawing nature of barbituric acid that stabilises the excited state structure, the predicted photoisomerisation quantum yield was high, 68%, more than double the theoretical maxima of conventional second-generation molecular motors. Based on experimental and computational studies, the compound seems to function as a motor only in non-polar media where intramolecular hydrogen bonding lowers the thermal barrier of the ratcheting THI step, while in polar solvents the backwards TEZI step becomes more favourable, reducing the efficiency of unidirectional rotation. Several questions should be answered in future research. Despite our best efforts to elucidate the oxidation mechanism, the fine details of the reaction pathway

remain to be determined. The generality of the reaction with different ketones (potentially yielding motors with different properties) should also be screened. Furthermore, it should be tested whether hydrogen bonding can be utilised to improve the photochemical performance of other molecular motors as well. For example, a retinal-based theoretical motor design exploiting hydrogen bonding was proposed already a decade ago³⁷⁵ but has not been realised.

7 CONCLUSIONS AND OUTLOOK

Photoswitches and molecular motors hold great potential in creating revolutionary nanoscopic devices and intelligent materials. However, conventional photoswitch systems operate almost exclusively with ultraviolet light, which hampers their applicability in environments where short wavelengths cause damage to the surrounding material or suffer from poor penetration, especially in the context of biosciences and medicine. In this thesis we have studied different approaches to realise photoswitching with benign lower-energy excitation, preferably with light from the red end of the visible spectrum. We have identified three distinct strategies that can be employed to accomplish this goal and progressed each of these research fronts with one original study. Finally, we have shown how these ideas may be applied to molecular motors, enabling unidirectional rotation on a molecular level with visible light. The common theme in this thesis is to apply molecular orbital theory and mechanistic thinking to photoswitching systems in order to understand the fundamental chemistry behind successful molecular designs.

The most common approach towards photoswitching with visible light is to shift the absorption bands of well-established photoswitches via synthetic modifications. For instance, azobenzenes can be functionalised in the *ortho* positions to tune the photoswitching dynamics. In **Publication I** we established structure–property relationships in *ortho*-fluoroaminoazobenzenes in search of an optimal combination of enhanced visible-light absorptivity and retained thermal stability of the metastable *Z* isomer. We showed that it is possible to obtain fast and efficient bidirectional photoisomerisation with visible light while simultaneously providing further functionalisation sites in the *ortho* positions. While we were unable to shift the isomerisation wavelengths to the biooptical window, the boosted absorptivity makes isomerisation very fast compared to the state-of-the-art *ortho*-fluorinated azobenzenes. Further tuning of the photochemical properties might be feasible through functionalisation of the *meta* and *para* positions, and thus far unexplored *ortho*-chloroaminoazobenzenes would, potentially, yield switches whose absorption band extends to the red-light regime. As an interesting detail, with one molecular design the isomer distribution in the photostationary state was virtually unaffected by the excitation wavelength, yielding ca. 50–70% *Z* in all cases, while also exhibiting

a Z-half-life on the month timescale. This might be beneficial for the storage of solar energy, as the whole UV-visible spectrum could be utilised without any need for filters. To this end, the energy storage capability (the energy difference of the *E* and *Z* forms) and the possibility to release the energy at will through sensitised back-isomerisation should be studied.

In **Publication II** we utilised indigos, an emerging photoswitch family that inherently absorbs red light. Instead of tuning the absorption bands, the challenge is to achieve the same level of photoswitching as with more conventional switches. In our case, we set out to accomplish efficient switching of indigos in a polymeric (semi)solid matrix, the environment of most materials applications. We discovered three ways to promote the switching parameters of indigo photoswitches: creating free volume around the switches through the addition of bulky substituents, choosing a soft matrix to minimise physical strain upon isomerisation, and keeping the indigo loading low to avoid aggregation. When all of these are implemented in concert, switching can be made as efficient as in solution. The obstacle to further use seems to be the aggregation tendency at high loadings. Efficient switching with up to 10% of the indigo is a prerequisite for, e.g., photochemical actuation of polymer films, while in our case the best PSDs were acquired when <1% of the indigo was utilised. To tackle this problem, further synthetic modifications in the indigo core could be beneficial to suppress the stacking of the molecules. If suitable long-chained substituents were installed on opposite sides of the core, this might even promote the incorporation of these molecules into liquid-crystalline systems, enabling the design of novel red-light-responsive functional materials. Core functionalisation provides also an additional means to tune the photochemical properties of these switches. Last, the same design principles could be applied to the solid-state switching of other indigoid photoswitches.

Indirect isomerisation of azobenzenes with low-energy irradiation was investigated in **Publication III**, utilising molecular iodine as a near-infrared light photocatalyst. The catalytic system is robust but only functional with selected, moderately electron-rich azobenzenes, as it requires an electron to be abstracted from the azobenzene. Most intriguingly, the catalytic isomerisation reaction is mediated by singlet oxygen and can be catalysed without iodine by using other singlet oxygen sensitisers. Thus, we envision that the catalysis can be made more efficient and practical by designing a singlet oxygen sensitiser with optimal photo- and electrochemical properties, although the approach might still be limited to selected azobenzenes. To continue on this line of research, the underlying mechanism of the oxygen-mediated catalysis should first be unravelled through time-resolved

spectroscopy studies and computational considerations, which would give insight into the properties of an ideal photocatalyst for this reaction. In terms of generality, triplet sensitisation and hole catalysis remain the best choices for catalytic isomerisation, although sensitisation requires work in terms of improving the oxygen tolerance of the systems. Finally, a catalytic method to induce $E \rightarrow Z$ isomerisation is waiting to be developed.

In the final piece of this thesis, **Publication IV**, we turned our attention beyond switches, to single-molecule motors that function upon absorption of visible light. During the preparation of a barbituric-acid-based motor we encountered unexpected reactivity in a Knoevenagel condensation, resulting in an additional hydroxy group near the central axle of rotation. This turned out to be highly fortuitous, as the hydroxy group enhances the quantum yield of rotation through hydrogen bonding during the photochemical isomerisation step. This, combined with the electron-withdrawing nature of the barbiturate unit, makes the rotation highly efficient compared to any conventional second-generation motor. Further studies are needed to determine whether hydrogen bonding could be applied to boost the performance of other motor structures as well. The barbituric-acid-based motor features ultrafast sub-picosecond photochemistry and millisecond-scale thermal rotation steps. It absorbs strongly inside the visible spectrum, being the synthetically simplest example of a visible-light-driven molecular motor. It is, however, worth noting that direct isomerisation wavelengths are still restricted to below 600 nm, both with our design and with earlier examples. In this sense, motors are clearly less developed than switches. Whether motors that can be excited directly with red light are within reach using the design principles covered in this thesis is not certain and remains a challenge for future research.

While we have herein focused on shifting the excitation wavelengths to the red part of the visible spectrum and even beyond, it is important to remember that not all applications require this feature. For most uses, blue–green light is just as good, and in some cases even ultraviolet light can be utilised. However, the use of red light is crucial for most potential applications in biosciences and medicine. Despite our own studies and the efforts of the whole photoswitching community to optimise red-light photoswitching systems, near-quantitative bidirectional switching within the biooptical window remains elusive, especially when coupled to good thermal stability. The steps taken towards this ultimate goal seem promising for all of the three directions covered in this thesis. Because of the vast variety of potential applications, it is likely that numerous different approaches are needed, probably representing all of the covered strategies and even mixing them: for instance, using

a near-infrared-light photosensitiser with a red-light photoswitch (such as a modified azobenzene or an indigo derivative) would enable switching in both directions with low-energy light. It is also clear that one molecular design or even one photoswitch family cannot meet the requirements of all potential applications, and that insight into structure–property relationships and various isomerisation mechanisms of different photoswitches is crucial for the future of responsive, even intelligent molecular systems. Thus, further optimisation of the aforementioned (and perhaps altogether new) strategies for photoswitching with low-energy light is needed. Only then may photoswitchable systems finally take the final step from proof-of-concept to real-world applications. We believe that through this work, we have done our share to progress this objective.

BIBLIOGRAPHY

- 1 C. Kaspar, B. J. Ravoo, W. G. van der Wiel, S. V Wegner and W. H. P. Pernice, The rise of intelligent matter, *Nature*, 2021, **594**, 345–355.
- 2 A. Walther, Viewpoint: From Responsive to Adaptive and Interactive Materials and Materials Systems: A Roadmap, *Adv. Mater.*, 2020, **32**, 1905111.
- 3 F. Huang, X. Zhang and B. Z. Tang, Stimuli-responsive materials: a web themed collection, *Mater. Chem. Front.*, 2019, **3**, 10–11.
- 4 A. Priimagi and S. Hecht, From Responsive Molecules to Interactive Materials, *Adv. Mater.*, 2020, **32**, 2000215.
- 5 S. Bahl, H. Nagar, I. Singh and S. Sehgal, Smart materials types, properties and applications: A review, *Mater. Today Proc.*, 2020, **28**, 1302–1306.
- 6 X. Xia, C. M. Spadaccini and J. R. Greer, Responsive materials architected in space and time, *Nat. Rev. Mater.*, 2022, **7**, 683–701.
- 7 Z. L. Pianowski, Ed., *Molecular Switches: Chemistry, Properties, and Applications*, Wiley-VCH Verlag GmbH, 2022.
- 8 A. Goulet-Hanssens, F. Eisenreich and S. Hecht, Enlightening Materials with Photoswitches, *Adv. Mater.*, 2020, **32**, 1905966.
- 9 J. Boelke and S. Hecht, Designing Molecular Photoswitches for Soft Materials Applications, *Adv. Opt. Mater.*, 2019, **7**, 1900404.
- 10 M. M. Russew and S. Hecht, Photoswitches: From molecules to materials, *Adv. Mater.*, 2010, **22**, 3348–3360.
- 11 B. L. Feringa, The Art of Building Small: From Molecular Switches to Motors (Nobel Lecture), *Angew. Chemie Int. Ed.*, 2017, **56**, 11060–11078.
- 12 J. C. M. Kistemaker, A. S. Lubbe and B. L. Feringa, Exploring molecular motors, *Mater. Chem. Front.*, 2021, **5**, 2900–2906.
- 13 R. Iino, K. Kinbara and Z. Bryant, Introduction: Molecular Motors, *Chem. Rev.*, 2020, **120**, 1–4.
- 14 E. Moulin, L. Faour, C. C. Carmona-Vargas and N. Giuseppone, From Molecular Machines to Stimuli-Responsive Materials, *Adv. Mater.*, 2020, **32**, 1906036.
- 15 F. Lancia, A. Ryabchun and N. Katsonis, Life-like motion driven by artificial molecular machines, *Nat. Rev. Chem.*, 2019, **3**, 536–551.
- 16 S. Billiet, K. De Bruycker, F. Driessen, H. Goossens, V. Van Speybroeck, J. M. Winne and F. E. Du Prez, Triazolinediones enable ultrafast and reversible click chemistry for the design of dynamic polymer systems, *Nat. Chem.*, 2014, **6**, 815–821.

- 17 K. L. Diehl, I. V. Kolesnichenko, S. A. Robotham, J. L. Bachman, Y. Zhong, J. S. Brodbelt and E. V. Anslyn, Click and chemically triggered declick reactions through reversible amine and thiol coupling via a conjugate acceptor, *Nat. Chem.*, 2016, **8**, 968–973.
- 18 J. Zhuang, B. Zhao, X. Meng, J. D. Schiffman, S. L. Perry, R. W. Vachet and S. Thayumanavan, A programmable chemical switch based on triggerable Michael acceptors, *Chem. Sci.*, 2020, **11**, 2103–2111.
- 19 R. A. Bissell, E. Córdova, A. E. Kaifer and J. F. Stoddart, A chemically and electrochemically switchable molecular shuttle, *Nature*, 1994, **369**, 133–137.
- 20 L. Gerhard, K. Edelmann, J. Homberg, M. Valášek, S. G. Bahoosh, M. Lukas, F. Pauly, M. Mayor and W. Wulfhchel, An electrically actuated molecular toggle switch, *Nat. Commun.*, 2017, **8**, 14672.
- 21 Y. Han, C. Nickle, Z. Zhang, H. P. A. G. Astier, T. J. Duffin, D. Qi, Z. Wang, E. del Barco, D. Thompson and C. A. Nijhuis, Electric-field-driven dual-functional molecular switches in tunnel junctions, *Nat. Mater.*, 2020, **19**, 843–848.
- 22 A. Albini and M. Fagnoni, Green chemistry and photochemistry were born at the same time, *Green Chem.*, 2004, **6**, 1–6.
- 23 N. Hoffmann, Photochemical reactions of aromatic compounds and the concept of the photon as a traceless reagent, *Photochem. Photobiol. Sci.*, 2012, **11**, 1613–1641.
- 24 W. A. Velema, W. Szymanski and B. L. Feringa, Photopharmacology: Beyond proof of principle, *J. Am. Chem. Soc.*, 2014, **136**, 2178–2191.
- 25 J. Broichhagen, J. A. Frank and D. Trauner, A Roadmap to Success in Photopharmacology, *Acc. Chem. Res.*, 2015, **48**, 1947–1960.
- 26 M. M. Lerch, M. J. Hansen, G. M. van Dam, W. Szymanski and B. L. Feringa, Emerging Targets in Photopharmacology, *Angew. Chemie - Int. Ed.*, 2016, **55**, 10978–10999.
- 27 K. Hüll, J. Morstein and D. Trauner, In Vivo Photopharmacology, *Chem. Rev.*, 2018, **118**, 10710–10747.
- 28 M. J. Fuchter, On the Promise of Photopharmacology Using Photoswitches: A Medicinal Chemist's Perspective, *J. Med. Chem.*, 2020, **63**, 11436–11447.
- 29 A. A. Beharry and G. A. Woolley, Azobenzene photoswitches for biomolecules, *Chem. Soc. Rev.*, 2011, **40**, 4422–4437.
- 30 W. Szymański, J. M. Beierle, H. A. V. Kistemaker, W. A. Velema and B. L. Feringa, Reversible Photocontrol of Biological Systems by the Incorporation of Molecular Photoswitches, *Chem. Rev.*, 2013, **113**, 6114–6178.
- 31 V. M. Lechner, M. Nappi, P. J. Deneny, S. Folliet, J. C. K. Chu and M. J. Gaunt, Visible-Light-Mediated Modification and Manipulation of Biomacromolecules, *Chem. Rev.*, 2022, **122**, 1752–1829.
- 32 C. Fedele, P. A. Netti and S. Cavalli, Azobenzene-based polymers: emerging applications as cell culture platforms, *Biomater. Sci.*, 2018, **6**, 990–995.
- 33 S. P. Ihrig, F. Eisenreich and S. Hecht, Photoswitchable polymerization catalysis: state of the art, challenges, and perspectives, *Chem. Commun.*, 2019, **55**, 4290–4298.

- 34 R. Dorel and B. L. Feringa, Photoswitchable catalysis based on the isomerisation of double bonds, *Chem. Commun.*, 2019, **55**, 6477–6486.
- 35 R. Liu, X. Zhang, F. Xia and Y. Dai, Azobenzene-based photoswitchable catalysts: State of the art and perspectives, *J. Catal.*, 2022, **409**, 33–40.
- 36 D. Majee and S. Presolski, Dithienylethene-Based Photoswitchable Catalysts: State of the Art and Future Perspectives, *ACS Catal.*, 2021, **11**, 2244–2252.
- 37 B. M. Neilson and C. W. Bielawski, Illuminating photoswitchable catalysis, *ACS Catal.*, 2013, **3**, 1874–1885.
- 38 H. Zeng, P. Wasylczyk, D. Wiersma and A. Priimagi, Light Robots: Bridging the Gap between Microrobotics and Photomechanics in Soft Materials, *Adv. Mater.*, 2018, **30**, 1703554.
- 39 Y. Chen, J. Yang, X. Zhang, Y. Feng, H. Zeng, L. Wang and W. Feng, Light-driven bimorph soft actuators: design, fabrication, and properties, *Mater. Horizons*, 2021, **8**, 728–757.
- 40 M. da Cunha, M. G. Debye and A. P. H. J. Schenning, Bioinspired light-driven soft robots based on liquid crystal polymers, *Chem. Soc. Rev.*, 2020, **49**, 6568–6578.
- 41 Z. Wang, P. Erhart, T. Li, Z.-Y. Zhang, D. Sampedro, Z. Hu, H. A. Wegner, O. Brummel, J. Libuda, M. B. Nielsen and K. Moth-Poulsen, Storing energy with molecular photoisomers, *Joule*, 2021, **5**, 3116–3136.
- 42 C.-L. Sun, C. Wang and R. Boulatov, Applications of Photoswitches in the Storage of Solar Energy, *ChemPhotoChem*, 2019, **3**, 268–283.
- 43 M. Mansø, A. U. Petersen, Z. Wang, P. Erhart, M. B. Nielsen and K. Moth-Poulsen, Molecular solar thermal energy storage in photoswitch oligomers increases energy densities and storage times, *Nat. Commun.*, 2018, **9**, 1945.
- 44 M. A. Gerkman, R. S. L. Gibson, J. Calbo, Y. Shi, M. J. Fuchter and G. G. D. Han, Arylazopyrazoles for Long-Term Thermal Energy Storage and Optically Triggered Heat Release below 0 °C, *J. Am. Chem. Soc.*, 2020, **142**, 8688–8695.
- 45 E. N. Cho, D. Zhitomirsky, G. G. D. Han, Y. Liu and J. C. Grossman, Molecularly Engineered Azobenzene Derivatives for High Energy Density Solid-State Solar Thermal Fuels, *ACS Appl. Mater. Interfaces*, 2017, **9**, 8679–8687.
- 46 L. Dong, Y. Feng, L. Wang and W. Feng, Azobenzene-based solar thermal fuels: design, properties, and applications, *Chem. Soc. Rev.*, 2018, **47**, 7339–7368.
- 47 Y. Shi, M. A. Gerkman, Q. Qiu, S. Zhang and G. G. D. Han, Sunlight-activated phase change materials for controlled heat storage and triggered release, *J. Mater. Chem. A*, 2021, **9**, 9798–9808.
- 48 Y. Ru, Z. Shi, J. Zhang, J. Wang, B. Chen, R. Huang, G. Liu and T. Yu, Recent progress of photochromic materials towards photocontrollable devices, *Mater. Chem. Front.*, 2021, **5**, 7737–7758.
- 49 Y. Wakayama, R. Hayakawa, K. Higashiguchi and K. Matsuda, Photochromism for optically functionalized organic field-effect transistors: a comprehensive review, *J. Mater. Chem. C*, 2020, **8**, 10956–10974.

- 50 L. Zheng, J. Li, Y. Wang, X. Gao, K. Yuan, X. Yu, X. Ren, X. Zhang and W. Hu, High-performance optical memory transistors based on a novel organic semiconductor with nanosprouts, *Nanoscale*, 2019, **11**, 7117–7122.
- 51 L. A. Frolova, P. A. Troshin, D. K. Susarova, A. V Kulikov, N. A. Sanina and S. M. Aldoshin, Photoswitchable organic field-effect transistors and memory elements comprising an interfacial photochromic layer, *Chem. Commun.*, 2015, **51**, 6130–6132.
- 52 C. Fedele, T.-P. Ruoko, K. Kuntze, M. Virkki and A. Priimagi, New tricks and emerging applications from contemporary azobenzene research, *Photochem. Photobiol. Sci.*, 2022, **21**, 1719–1734.
- 53 S. L. Oscurato, F. Reda, M. Salvatore, F. Borbone, P. Maddalena and A. Ambrosio, Shapeshifting Diffractive Optical Devices, *Laser Photon. Rev.*, 2022, **16**, 2100514.
- 54 A. Priimagi and A. Shevchenko, Azopolymer-based micro- and nanopatterning for photonic applications, *J. Polym. Sci. Part B Polym. Phys.*, 2014, **52**, 163–182.
- 55 J. M. Taskinen, A. J. Moilanen, H. Rekola, K. Kuntze, A. Priimagi, P. Törmä and T. K. Hakala, All-Optical Emission Control and Lasing in Plasmonic Lattices, *ACS Photonics*, 2020, **7**, 2850–2858.
- 56 H. J. Meteling, F. Bosse, L. Schlichter, B. J. Tyler, H. F. Arlinghaus and B. J. Ravoo, Versatile Surface Patterning with Low Molecular Weight Photoswitches, *Small*, 2022, **18**, 2203245.
- 57 M. Regehly, Y. Garmshausen, M. Reuter, N. F. König, E. Israel, D. P. Kelly, C.-Y. Chou, K. Koch, B. Asfari and S. Hecht, Xolography for linear volumetric 3D printing, *Nature*, 2020, **588**, 620–624.
- 58 Z. Zhang, W. Wang, M. O'Hagan, J. Dai, J. Zhang and H. Tian, Stepping Out of the Blue: From Visible to Near-IR Triggered Photoswitches, *Angew. Chemie Int. Ed.*, 2022, **61**, e202205758.
- 59 J. Volarić, W. Szymanski, N. A. Simeth and B. L. Feringa, Molecular photoswitches in aqueous environments, *Chem. Soc. Rev.*, 2021, **50**, 12377–12449.
- 60 T. Kusukawa and M. Fujita, “Ship-in-a-Bottle” Formation of Stable Hydrophobic Dimers of cis-Azobenzene and -Stilbene Derivatives in a Self-Assembled Coordination Nanocage, *J. Am. Chem. Soc.*, 1999, **121**, 1397–1398.
- 61 D. Samanta, D. Galaktionova, J. Gemen, L. J. W. Shimon, Y. Diskin-Posner, L. Avram, P. Král and R. Klajn, Reversible chromism of spiropyran in the cavity of a flexible coordination cage, *Nat. Commun.*, 2018, **9**, 641.
- 62 D. Samanta, J. Gemen, Z. Chu, Y. Diskin-Posner, L. J. W. Shimon and R. Klajn, Reversible photoswitching of encapsulated azobenzenes in water, *Proc. Natl. Acad. Sci.*, 2018, **115**, 9379–9384.
- 63 L. Pesce, C. Perego, A. B. Grommet, R. Klajn and G. M. Pavan, Molecular Factors Controlling the Isomerization of Azobenzenes in the Cavity of a Flexible Coordination Cage, *J. Am. Chem. Soc.*, 2020, **142**, 9792–9802.
- 64 M. Canton, A. B. Grommet, L. Pesce, J. Gemen, S. Li, Y. Diskin-Posner, A. Credi, G. M. Pavan, J. Andréasson and R. Klajn, Improving Fatigue Resistance of Dihydropyrene by Encapsulation within a Coordination Cage, *J. Am. Chem. Soc.*, 2020, **142**, 14557–14565.

- 65 J. Wang, L. Avram, Y. Diskin-Posner, M. J. Białek, W. Stawski, M. Feller and R. Klajn, Altering the Properties of Spiropyran Switches Using Coordination Cages with Different Symmetries, *J. Am. Chem. Soc.*, 2022, **144**, 21244–21254.
- 66 J. Fregoni, G. Granucci, M. Persico and S. Corni, Strong Coupling with Light Enhances the Photoisomerization Quantum Yield of Azobenzene, *Chem*, 2020, **6**, 250–265.
- 67 A.-L. Leistner and Z. L. Pianowski, Smart Photochromic Materials Triggered with Visible Light, *European J. Org. Chem.*, 2022, **2022**, e202101271.
- 68 D. Bléger and S. Hecht, Visible-Light-Activated Molecular Switches, *Angew. Chemie Int. Ed.*, 2015, **54**, 11338–11349.
- 69 Y. Norikane, S. Tanaka and E. Uchida, Azobenzene crystals swim on water surface triggered by light, *CrystEngComm*, 2016, **18**, 7225–7228.
- 70 G. S. Hartley, 113. The cis-form of azobenzene and the velocity of the thermal cis→trans-conversion of azobenzene and some derivatives, *J. Chem. Soc.*, 1938, 633–642.
- 71 H. Rau, in *Photoreactive Organic Thin Films*, eds. Z. Sekkat and W. B. T.-P. O. T. F. Knoll, Academic Press, San Diego, 2002, pp. 3–47.
- 72 H. M. D. Bandara and S. C. Burdette, Photoisomerization in different classes of azobenzene, *Chem. Soc. Rev.*, 2012, **41**, 1809–1825.
- 73 S. Crespi, N. A. Simeth and B. König, Heteroaryl azo dyes as molecular photoswitches, *Nat. Rev. Chem.*, 2019, **3**, 133–146.
- 74 D. Villarón and S. J. Wezenberg, Stiff-Stilbene Photoswitches: From Fundamental Studies to Emergent Applications, *Angew. Chemie Int. Ed.*, 2020, **59**, 13192–13202.
- 75 C. Petermayer and H. Dube, Indigoid Photoswitches: Visible Light Responsive Molecular Tools, *Acc. Chem. Res.*, 2018, **51**, 1153–1163.
- 76 S. Kirchner, A.-L. Leistner, P. Gödtel, A. Seliwjorstow, S. Weber, J. Karcher, M. Nieger and Z. Pianowski, Hemipiperazines as peptide-derived molecular photoswitches with low-nanomolar cytotoxicity, *Nat. Commun.*, 2022, **13**, 6066.
- 77 G. Wald, Molecular Basis of Visual Excitation, *Science (80-)*, 1968, **162**, 230–239.
- 78 I. Aprahamian, Hydrazone switches and things in between, *Chem. Commun.*, 2017, **53**, 6674–6684.
- 79 M. W. H. Hoorens, M. Medved', A. D. Laurent, M. Di Donato, S. Fanetti, L. Slappendel, M. Hilbers, B. L. Feringa, W. Jan Buma and W. Szymanski, Iminothioindoxyl as a molecular photoswitch with 100 nm band separation in the visible range, *Nat. Commun.*, 2019, **10**, 2390.
- 80 C.-Y. Huang, A. Bonasera, L. Hristov, Y. Garmshausen, B. M. Schmidt, D. Jacquemin and S. Hecht, N,N'-Disubstituted Indigos as Readily Available Red-Light Photoswitches with Tunable Thermal Half-Lives, *J. Am. Chem. Soc.*, 2017, **139**, 15205–15211.
- 81 Š. Budzák, J. Jovaišaitė, C.-Y. Huang, P. Baronas, K. Tulaitė, S. Juršėnas, D. Jacquemin and S. Hecht, Mechanistic Insights into the Photoisomerization of N,N'-Disubstituted Indigos, *Chem. – A Eur. J.*, 2022, **28**, e202200496.
- 82 C. Petermayer, S. Thumser, F. Kink, P. Mayer and H. Dube, Hemiindigo: Highly Bistable Photoswitching at the Biooptical Window, *J. Am. Chem. Soc.*, 2017, **139**, 15060–15067.

- 83 A. Cembran, F. Bernardi, M. Garavelli, L. Gagliardi and G. Orlandi, On the Mechanism of the cis–trans Isomerization in the Lowest Electronic States of Azobenzene: S0, S1, and T1, *J. Am. Chem. Soc.*, 2004, **126**, 3234–3243.
- 84 L. Gagliardi, G. Orlandi, F. Bernardi, A. Cembran and M. Garavelli, A theoretical study of the lowest electronic states of azobenzene: the role of torsion coordinate in the cis–trans photoisomerization, *Theor. Chem. Acc.*, 2004, **111**, 363–372.
- 85 C. R. Crecca and A. E. Roitberg, Theoretical Study of the Isomerization Mechanism of Azobenzene and Disubstituted Azobenzene Derivatives, *J. Phys. Chem. A*, 2006, **110**, 8188–8203.
- 86 L. Wang, W. Xu, C. Yi and X. Wang, Isomerization and electronic relaxation of azobenzene after being excited to higher electronic states., *J. Mol. Graph. & Model.*, 2009, **27**, 792–796.
- 87 J. Casellas, M. J. Bearpark and M. Reguero, Excited-State Decay in the Photoisomerisation of Azobenzene: A New Balance between Mechanisms, *ChemPhysChem*, 2016, **17**, 3068–3079.
- 88 P. Bortolus and S. Monti, Cis-trans photoisomerization of azobenzene. Solvent and triplet donors effects, *J. Phys. Chem.*, 1979, **83**, 648–652.
- 89 G. Tiberio, L. Muccioli, R. Berardi and C. Zannoni, How Does the Trans–Cis Photoisomerization of Azobenzene Take Place in Organic Solvents?, *ChemPhysChem*, 2010, **11**, 1018–1028.
- 90 I. C. D. Merritt, D. Jacquemin and M. Vacher, cis → trans photoisomerisation of azobenzene: a fresh theoretical look., *Phys. Chem. Chem. Phys.*
- 91 S. Shinkai, Y. Kusano, K. Shigematsu and O. Manabe, On the rotation versus the inversion mechanism in the thermal isomerization of cis-azobenzenes, *Chem. Lett.*, 1980, **9**, 1303–1306.
- 92 M. Reimann, E. Teichmann, S. Hecht and M. Kaupp, Solving the Azobenzene Entropy Puzzle: Direct Evidence for Multi-State Reactivity, *J. Phys. Chem. Lett.*, 2022, **13**, 10882–10888.
- 93 S. Crespi, N. A. Simeth, A. Bellisario, M. Fagnoni and B. König, Unraveling the Thermal Isomerization Mechanisms of Heteroaryl Azoswitches: Phenylazaindoles as Case Study, *J. Phys. Chem. A*, 2019, **123**, 1814–1823.
- 94 K. Kuntze, J. Viljakka, E. Titov, Z. Ahmed, E. Kalenius, P. Saalfrank and A. Priimagi, Towards low-energy-light-driven bistable photoswitches: ortho-fluoroaminoazobenzenes, *Photochem. Photobiol. Sci.*, 2022, **21**, 159–173.
- 95 M. A. Kienzler, A. Reiner, E. Trautman, S. Yoo, D. Trauner and E. Y. Isacoff, A Red-Shifted, Fast-Relaxing Azobenzene Photoswitch for Visible Light Control of an Ionotropic Glutamate Receptor, *J. Am. Chem. Soc.*, 2013, **135**, 17683–17686.
- 96 S. K. Yesodha, C. K. Sadashiva Pillai and N. Tsutsumi, Stable polymeric materials for nonlinear optics: a review based on azobenzene systems, *Prog. Polym. Sci.*, 2004, **29**, 45–74.
- 97 S. Kobayashi, H. Yokoyama and H. Kamei, Substituent and solvent effects on electronic absorption spectra and thermal isomerization of push-pull-substituted cis-azobenzenes,

- Chem. Phys. Lett.*, 1987, **138**, 333–338.
- 98 J. Garcia-Amorós, B. Maerz, M. Reig, A. Cuadrado, L. Blancafort, E. Samoylova and D. Velasco, Picosecond Switchable Azo Dyes, *Chem. – A Eur. J.*, 2019, **25**, 7726–7732.
 - 99 D. Bléger, J. Schwarz, A. M. Brouwer and S. Hecht, o-Fluoroazobenzenes as Readily Synthesized Photoswitches Offering Nearly Quantitative Two-Way Isomerization with Visible Light, *J. Am. Chem. Soc.*, 2012, **134**, 20597–20600.
 - 100 M. Poutanen, Z. Ahmed, L. Rautkari, O. Ikkala and A. Priimagi, Thermal Isomerization of Hydroxyazobenzenes as a Platform for Vapor Sensing, *ACS Macro Lett.*, 2018, **7**, 381–386.
 - 101 C. Barrett, A. Natansohn and P. Rochon, Cis-Trans Thermal Isomerization Rates of Bound and Doped Azobenzenes in a Series of Polymers, *Chem. Mater.*, 1995, **7**, 899–903.
 - 102 T. Murase, S. Sato and M. Fujita, Switching the Interior Hydrophobicity of a Self-Assembled Spherical Complex through the Photoisomerization of Confined Azobenzene Chromophores, *Angew. Chemie Int. Ed.*, 2007, **46**, 5133–5136.
 - 103 R. Reuter and H. A. Wegner, Switchable 3D networks by light controlled π -stacking of azobenzene macrocycles, *Chem. Commun.*, 2013, **49**, 146–148.
 - 104 Z. Ye, Z. Yang, L. Wang, L. Chen, Y. Cai, P. Deng, W. Feng, X. Li and L. Yuan, A Dynamic Hydrogen-Bonded Azo-Macrocyclic for Precisely Photo-Controlled Molecular Encapsulation and Release, *Angew. Chemie Int. Ed.*, 2019, **58**, 12519–12523.
 - 105 R. G. DiNardi, A. O. Douglas, R. Tian, J. R. Price, M. Tajik, W. A. Donald and J. E. Beves, Visible-Light-Responsive Self-Assembled Complexes: Improved Photoswitching Properties by Metal Ion Coordination**, *Angew. Chemie Int. Ed.*, 2022, **61**, e202205701.
 - 106 A. D. W. Kennedy, R. G. DiNardi, L. L. Fillbrook, W. A. Donald and J. E. Beves, Visible-Light Switching of Metallosupramolecular Assemblies**, *Chem. – A Eur. J.*, 2022, **28**, e202104461.
 - 107 M. Ovalle, M. Kathan, R. Toyoda, C. N. Stindt, S. Crespi and B. L. Feringa, Light-Fueled Transformations of a Dynamic Cage-Based Molecular System, *Angew. Chemie Int. Ed.*, 2023, **n/a**, e202214495.
 - 108 S. Yagai and A. Kitamura, Recent advances in photoresponsive supramolecular self-assemblies, *Chem. Soc. Rev.*, 2008, **37**, 1520–1529.
 - 109 M. Saccone, K. Kuntze, Z. Ahmed, A. Siiskonen, M. Giese and A. Priimagi, ortho-Fluorination of azophenols increases the mesophase stability of photoresponsive hydrogen-bonded liquid crystals, *J. Mater. Chem. C*, 2018, **6**, 9958–9963.
 - 110 M. Saccone, M. Spengler, M. Pfletscher, K. Kuntze, M. Virkki, C. Wölper, R. Gehrke, G. Jansen, P. Metrangolo, A. Priimagi and M. Giese, Photoresponsive Halogen-Bonded Liquid Crystals: The Role of Aromatic Fluorine Substitution, *Chem. Mater.*, 2019, **31**, 462–470.
 - 111 M. Lahikainen, H. Zeng and A. Priimagi, Reconfigurable photoactuator through synergistic use of photochemical and photothermal effects, *Nat. Commun.*, 2018, **9**, 4148.
 - 112 J. Li, X. Zhou and Z. Liu, Recent Advances in Photoactuators and Their Applications in Intelligent Bionic Movements, *Adv. Opt. Mater.*, 2020, **8**, 2000886.

- 113 T. Hugel, N. B. Holland, A. Cattani, L. Moroder, M. Seitz and H. E. Gaub, Single-Molecule Optomechanical Cycle, *Science* (80-.), 2002, **296**, 1103–1106.
- 114 T. Ikeda and O. Tsutsumi, Optical Switching and Image Storage by Means of Azobenzene Liquid-Crystal Films, *Science* (80-.), 1995, **268**, 1873–1875.
- 115 F. A. Jerca, V. V. Jerca and R. Hoogenboom, Advances and opportunities in the exciting world of azobenzenes, *Nat. Rev. Chem.*, 2022, **6**, 51–69.
- 116 A. Gonzalez, E. S. Kengmana, M. V Fonseca and G. G. D. Han, Solid-state photoswitching molecules: structural design for isomerization in condensed phase, *Mater. Today Adv.*, 2020, **6**, 100058.
- 117 A. B. Grommet, L. M. Lee and R. Klajn, Molecular Photoswitching in Confined Spaces, *Acc. Chem. Res.*, 2020, **53**, 2600–2610.
- 118 A. K. Gaur, D. Gupta, A. Mahadevan, P. Kumar, H. Kumar, D. N. Nampoothiry, N. Kaur, S. K. Thakur, S. Singh, T. Slanina and S. Venkataramani, Bistable Aryl Azopyrazolium Ionic Photoswitches in Water, *J. Am. Chem. Soc.*, , DOI:10.1021/jacs.2c13733.
- 119 Y. Yokoyama, Fulgides for Memories and Switches, *Chem. Rev.*, 2000, **100**, 1717–1740.
- 120 M. Abedi, M. Pápai, K. V Mikkelsen, N. E. Henriksen and K. B. Møller, Mechanism of Photoinduced Dihydroazulene Ring-Opening Reaction, *J. Phys. Chem. Lett.*, 2019, **10**, 3944–3949.
- 121 N. Shahzad, R. U. Nisa and K. Ayub, Substituents effect on thermal electrocyclic reaction of dihydroazulene–vinylheptafulvene photoswitch: a DFT study to improve the photoswitch, *Struct. Chem.*, 2013, **24**, 2115–2126.
- 122 R. S. Becker and J. Michl, Photochromism of Synthetic and Naturally Occurring 2H-Chromenes and 2H-Pyrans, *J. Am. Chem. Soc.*, 1966, **88**, 5931–5933.
- 123 K. Arai, Y. Kobayashi and J. Abe, Rational molecular designs for drastic acceleration of the color-fading speed of photochromic naphthopyrans, *Chem. Commun.*, 2015, **51**, 3057–3060.
- 124 Y. Kobayashi, T. Katayama, T. Yamane, K. Setoura, S. Ito, H. Miyasaka and J. Abe, Stepwise Two-Photon-Induced Fast Photoswitching via Electron Transfer in Higher Excited States of Photochromic Imidazole Dimer, *J. Am. Chem. Soc.*, 2016, **138**, 5930–5938.
- 125 I. Yonekawa, K. Mutoh, Y. Kobayashi and J. Abe, Intensity-Dependent Photoresponse of Biphotochromic Molecule Composed of a Negative and a Positive Photochromic Unit, *J. Am. Chem. Soc.*, 2018, **140**, 1091–1097.
- 126 A. Tokunaga, L. M. Uriarte, K. Mutoh, E. Fron, J. Hofkens, M. Sliwa and J. Abe, Photochromic Reaction by Red Light via Triplet Fusion Upconversion, *J. Am. Chem. Soc.*, 2019, **141**, 17744–17753.
- 127 A. Kometani, Y. Inagaki, K. Mutoh and J. Abe, Red or Near-Infrared Light Operating Negative Photochromism of a Binaphthyl-Bridged Imidazole Dimer, *J. Am. Chem. Soc.*, 2020, **142**, 7995–8005.
- 128 N. Moriyama and J. Abe, Negative Photochromic 3-Phenylperylene-Bridged Imidazole Dimer Offering Quantitative and Selective Bidirectional Photoisomerization with Visible

- and Near-Infrared Light, *J. Am. Chem. Soc.*, DOI:10.1021/jacs.2c13331.
- 129 M. Irie, Diarylethenes for Memories and Switches, *Chem. Rev.*, 2000, **100**, 1685–1716.
 - 130 M. Irie, T. Fukaminato, K. Matsuda and S. Kobatake, Photochromism of diarylethene molecules and crystals: Memories, switches, and actuators, *Chem. Rev.*, 2014, **114**, 12174–12277.
 - 131 S. Nakamura and M. Irie, Thermally irreversible photochromic systems. A theoretical study, *J. Org. Chem.*, 1988, **53**, 6136–6138.
 - 132 R. B. Woodward and R. Hoffmann, The Conservation of Orbital Symmetry, *Angew. Chemie Int. Ed. English*, 1969, **8**, 781–853.
 - 133 M. Herder, B. M. Schmidt, L. Grubert, M. Pätzelt, J. Schwarz and S. Hecht, Improving the Fatigue Resistance of Diarylethene Switches, *J. Am. Chem. Soc.*, 2015, **137**, 2738–2747.
 - 134 M. Carroli, A. G. Dixon, M. Herder, E. Pavlica, S. Hecht, G. Bratina, E. Orgiu and P. Samori, Multiresponsive Nonvolatile Memories Based on Optically Switchable Ferroelectric Organic Field-Effect Transistors, *Adv. Mater.*, 2021, **33**, 2007965.
 - 135 M. Irie, S. Kobatake and M. Horichi, Reversible Surface Morphology Changes of a Photochromic Diarylethene Single Crystal by Photoirradiation, *Science (80-.)*, 2001, **291**, 1769–1772.
 - 136 L. Kuroki, S. Takami, K. Yoza, M. Morimoto and M. Irie, Photoinduced shape changes of diarylethene single crystals: correlation between shape changes and molecular packing, *Photochem. Photobiol. Sci.*, 2010, **9**, 221–225.
 - 137 J. I. Mamiya, A. Kuriyama, N. Yokota, M. Yamada and T. Ikeda, Photomobile polymer materials: Photoresponsive behavior of cross-linked liquid-crystalline polymers with mesomorphic diarylethenes, *Chem. - A Eur. J.*, 2015, **21**, 3174–3177.
 - 138 T. Arai, T. Oguchi, T. Wakabayashi, M. Tsuchiya, Y. Nishimura, S. Oishi, H. Sakuragi and K. Tokumaru, Mechanistic Approach to the Sensitization Process of Aromatic Ketones in the Isomerization between Norbornadiene and Quadricyclane, *Bull. Chem. Soc. Jpn.*, 1987, **60**, 2937–2943.
 - 139 J. Orrego-Hernández, A. Dreos and K. Moth-Poulsen, Engineering of Norbornadiene/Quadricyclane Photoswitches for Molecular Solar Thermal Energy Storage Applications, *Acc. Chem. Res.*, 2020, **53**, 1478–1487.
 - 140 M. Quant, A. Lennartson, A. Dreos, M. Kuisma, P. Erhart, K. Börjesson and K. Moth-Poulsen, Low Molecular Weight Norbornadiene Derivatives for Molecular Solar-Thermal Energy Storage, *Chem. – A Eur. J.*, 2016, **22**, 13265–13274.
 - 141 Z. Wang, A. Roffey, R. Losantos, A. Lennartson, M. Jevric, A. U. Petersen, M. Quant, A. Dreos, X. Wen, D. Sampedro, K. Börjesson and K. Moth-Poulsen, Macroscopic heat release in a molecular solar thermal energy storage system, *Energy Environ. Sci.*, 2019, **12**, 187–193.
 - 142 T. Luchs, P. Lorenz and A. Hirsch, Efficient Cyclization of the Norbornadiene-Quadricyclane Interconversion Mediated by a Magnetic [Fe₃O₄-CoSalphen] Nanoparticle Catalyst, *ChemPhotoChem*, 2020, **4**, 52–58.
 - 143 B. S. Lukyanov and M. B. Lukyanova, Spiropyrans: Synthesis, Properties, and Application, *Chem. Heterocycl. Compd.*, 2005, **41**, 1–31.

- 144 L. Kortekaas and W. R. Browne, The evolution of spiropyran: fundamentals and progress of an extraordinarily versatile photochrome, *Chem. Soc. Rev.*, 2019, **48**, 3406–3424.
- 145 A. Mustafa, The Chemistry of Spiropyrans., *Chem. Rev.*, 1948, **43**, 509–523.
- 146 R. Klajn, Spiropyran-based dynamic materials, *Chem. Soc. Rev.*, 2014, **43**, 148–184.
- 147 M. Bletz, U. Pfeifer-Fukumura, U. Kolb and W. Baumann, Ground- and First-Excited-Singlet-State Electric Dipole Moments of Some Photochromic Spirobenzopyrans in Their Spiropyran and Merocyanine Form, *J. Phys. Chem. A*, 2002, **106**, 2232–2236.
- 148 L. Wimberger, S. K. K. Prasad, M. D. Peeks, J. Andréasson, T. W. Schmidt and J. E. Beves, Large, Tunable, and Reversible pH Changes by Merocyanine Photoacids, *J. Am. Chem. Soc.*, 2021, **143**, 20758–20768.
- 149 M. Mandal, D. Banik, A. Karak, S. K. Manna and A. K. Mahapatra, Spiropyran–Merocyanine Based Photochromic Fluorescent Probes: Design, Synthesis, and Applications, *ACS Omega*, 2022, **7**, 36988–37007.
- 150 S. Helmy, S. Oh, F. A. Leibfarth, C. J. Hawker and J. Read de Alaniz, Design and Synthesis of Donor–Acceptor Stenhouse Adducts: A Visible Light Photoswitch Derived from Furfural, *J. Org. Chem.*, 2014, **79**, 11316–11329.
- 151 J. R. Hemmer, S. O. Poelma, N. Treat, Z. A. Page, N. D. Dolinski, Y. J. Diaz, W. Tomlinson, K. D. Clark, J. P. Hooper, C. Hawker and J. Read de Alaniz, Tunable Visible and Near Infrared Photoswitches, *J. Am. Chem. Soc.*, 2016, **138**, 13960–13966.
- 152 M. M. Lerch, S. J. Wezenberg, W. Szymanski and B. L. Feringa, Unraveling the Photoswitching Mechanism in Donor–Acceptor Stenhouse Adducts, *J. Am. Chem. Soc.*, 2016, **138**, 6344–6347.
- 153 M. Di Donato, M. M. Lerch, A. Lapini, A. D. Laurent, A. Iagatti, L. Bussotti, S. P. Ihrig, M. Medved', D. Jacquemin, W. Szymański, W. J. Buma, P. Foggi and B. L. Feringa, Shedding Light on the Photoisomerization Pathway of Donor–Acceptor Stenhouse Adducts, *J. Am. Chem. Soc.*, 2017, **139**, 15596–15599.
- 154 M. M. Lerch, M. Medved', A. Lapini, A. D. Laurent, A. Iagatti, L. Bussotti, W. Szymański, W. J. Buma, P. Foggi, M. Di Donato and B. L. Feringa, Tailoring Photoisomerization Pathways in Donor–Acceptor Stenhouse Adducts: The Role of the Hydroxy Group, *J. Phys. Chem. A*, 2018, **122**, 955–964.
- 155 M. M. Lerch, W. Szymański and B. L. Feringa, The (photo)chemistry of Stenhouse photoswitches: guiding principles and system design, *Chem. Soc. Rev.*, 2018, **47**, 1910–1937.
- 156 N. Mallo, P. T. Brown, H. Iranmanesh, T. S. C. MacDonald, M. J. Teusner, J. B. Harper, G. E. Ball and J. E. Beves, Photochromic switching behaviour of donor–acceptor Stenhouse adducts in organic solvents, *Chem. Commun.*, 2016, **52**, 13576–13579.
- 157 J. R. Hemmer, Z. A. Page, K. D. Clark, F. Stricker, N. D. Dolinski, C. J. Hawker and J. Read de Alaniz, Controlling Dark Equilibria and Enhancing Donor–Acceptor Stenhouse Adduct Photoswitching Properties through Carbon Acid Design, *J. Am. Chem. Soc.*, 2018, **140**, 10425–10429.
- 158 R. Berraud-Pache, E. Santamaría-Aranda, B. de Souza, G. Bistoni, F. Neese, D. Sampedro and R. Izsák, Redesigning donor–acceptor Stenhouse adduct photoswitches

- through a joint experimental and computational study, *Chem. Sci.*, 2021, **12**, 2916–2924.
- 159 S. Crespi, N. A. Simeth, M. Di Donato, S. Doria, C. N. Stindt, M. F. Hilbers, F. L. Kiss, R. Toyoda, S. Wesseling, W. J. Buma, B. L. Feringa and W. Szymański, Phenylimino Indolinone: A Green-Light-Responsive T-Type Photoswitch Exhibiting Negative Photochromism, *Angew. Chemie Int. Ed.*, 2021, **60**, 25290–25295.
 - 160 K. Rustler, P. Nitschke, S. Zahnbrecher, J. Zach, S. Crespi and B. König, Photochromic Evaluation of 3(5)-Arylazo-1H-pyrazoles, *J. Org. Chem.*, 2020, **85**, 4079–4088.
 - 161 K. Stranius and K. Börjesson, Determining the Photoisomerization Quantum Yield of Photoswitchable Molecules in Solution and in the Solid State, *Sci. Rep.*, 2017, **7**, 41145.
 - 162 A. K. Gaur, H. Kumar, D. Gupta, I. P. Tom, D. N. Nampoothiry, S. K. Thakur, A. Mahadevan, S. Singh and S. Venkataramani, Structure–Property Relationship for Visible Light Bidirectional Photoswitchable Azoheteroarenes and Thermal Stability of Z-Isomers, *J. Org. Chem.*, 2022, **87**, 6541–6551.
 - 163 G. Hallas, R. Marsden, J. D. Hepworth and D. Mason, The effects of cyclic terminal groups in 4-aminoazobenzene and related azo dyes. Part 1. Electronic absorption spectra of some monoazo dyes derived from N-phenylpyrrolidine and N-phenylpiperidine, *J. Chem. Soc. Perkin Trans. 2*, 1984, 149–153.
 - 164 J. D. Hepworth, D. Mason, G. Hallas and R. Marsden, The Effects of Cyclic Terminal Groups in 4-Aminoazobenzene and Related Azo Dyes: Part 2 Values of Some Monoazo Dyes Derived from IV-Phenylpyrrolidine and N-Phenylpiperidine, *Dye. Pigment.*, 1985, **6**, 389–396.
 - 165 G. Hallas, The Effects of Terminal Groups in 4-Aminoazobenzene and Disperse Dyes Related Thereto, *J. Soc. Dye. Colour.*, 1979, **95**, 285–294.
 - 166 T. J. Sørensen, K. Kjaer, D. W. Breiby and B. W. Laursen, Synthesis of Novel Amphiphilic Azobenzenes and X-ray Scattering Studies of Their Langmuir Monolayers, *Langmuir*, 2008, **24**, 3223–3227.
 - 167 O. Sadovskii, A. A. Beharry, F. Zhang and G. A. Woolley, Spectral tuning of azobenzene photoswitches for biological applications, *Angew. Chemie - Int. Ed.*, 2009, **48**, 1484–1486.
 - 168 Z. Ahmed, A. Siiskonen, M. Virkki and A. Priimagi, Controlling azobenzene photoswitching through combined: Ortho -fluorination and -amination, *Chem. Commun.*, 2017, **53**, 12520–12523.
 - 169 T. Eom and A. Khan, Push-pull azobenzene chromophores with negative halochromism, *Dye. Pigment.*, 2021, **188**, 109197.
 - 170 J. Dokić, M. Gothe, J. Wirth, M. V Peters, J. Schwarz, S. Hecht and P. Saalfrank, Quantum Chemical Investigation of Thermal Cis-to-Trans Isomerization of Azobenzene Derivatives: Substituent Effects, Solvent Effects, and Comparison to Experimental Data, *J. Phys. Chem. A*, 2009, **113**, 6763–6773.
 - 171 L. Chi, O. Sadovskii and G. A. Woolley, A Blue-Green Absorbing Cross-Linker for Rapid Photoswitching of Peptide Helix Content, *Bioconjug. Chem.*, 2006, **17**, 670–676.
 - 172 S. Ciccone and J. Halpern, Catalysis of the cis-trans isomerization of azobenzene by acids and cupric salts, *Can. J. Chem.*, 1959, **37**, 1903–1910.
 - 173 J. Rickhoff, N. B. Arndt, M. Böckmann, N. L. Doltsinis, B. J. Ravoo and L. Korteckaas,

- Reversible, Red-Shifted Photoisomerization in Protonated Azobenzenes, *J. Org. Chem.*, 2022, **87**, 10605–10612.
- 174 M. Dong, A. Babalhavaeji, C. V Collins, K. Jarrah, O. Sadovski, Q. Dai and G. A. Woolley, Near-Infrared Photoswitching of Azobenzenes under Physiological Conditions, *J. Am. Chem. Soc.*, 2017, **139**, 13483–13486.
 - 175 Y. Yang, R. P. Hughes and I. Aprahamian, Visible light switching of a BF₂-coordinated azo compound, *J. Am. Chem. Soc.*, 2012, **134**, 15221–15224.
 - 176 Y. Yang, R. P. Hughes and I. Aprahamian, Near-Infrared Light Activated Azo-BF₂ Switches, *J. Am. Chem. Soc.*, 2014, **136**, 13190–13193.
 - 177 H. Qian, Y.-Y. Wang, D.-S. Guo and I. Aprahamian, Controlling the Isomerization Rate of an Azo-BF₂ Switch Using Aggregation, *J. Am. Chem. Soc.*, 2017, **139**, 1037–1040.
 - 178 R. Siewertsen, H. Neumann, B. Buchheim-Stehn, R. Herges, C. Näther, F. Renth and F. Temps, Highly efficient reversible Z-E photoisomerization of a bridged azobenzene with visible light through resolved S(1)(n pi*) absorption bands., *J. Am. Chem. Soc.*, 2009, **131**, 15594–15595.
 - 179 M. Hammerich, C. Schütt, C. Stähler, P. Lenters, F. Röhricht, R. Höppner and R. Herges, Heterodiazocines: Synthesis and Photochromic Properties, Trans to Cis Switching within the Bio-optical Window, *J. Am. Chem. Soc.*, 2016, **138**, 13111–13114.
 - 180 P. Lenters, E. Stadler, F. Röhricht, A. Brahms, J. Gröbner, F. D. Sönnichsen, G. Gescheidt and R. Herges, Nitrogen Bridged Diazocines: Photochromes Switching within the Near-Infrared Region with High Quantum Yields in Organic Solvents and in Water, *J. Am. Chem. Soc.*, 2019, **141**, 13592–13600.
 - 181 A. A. Beharry, O. Sadovski and G. A. Woolley, Azobenzene photoswitching without ultraviolet light, *J. Am. Chem. Soc.*, 2011, **133**, 19684–19687.
 - 182 C. Knie, M. Utecht, F. Zhao, H. Kulla, S. Kovalenko, A. M. Brouwer, P. Saalfrank, S. Hecht and D. Bléger, ortho-Fluoroazobenzenes: Visible Light Switches with Very Long-Lived Z Isomers, *Chem. – A Eur. J.*, 2014, **20**, 16492–16501.
 - 183 C. E. Weston, R. D. Richardson, P. R. Haycock, A. J. P. White and M. J. Fuchter, Arylazopyrazoles: Azoheteroarene Photoswitches Offering Quantitative Isomerization and Long Thermal Half-Lives, *J. Am. Chem. Soc.*, 2014, **136**, 11878–11881.
 - 184 D. Ditter, L. B. Braun and R. Zentel, Influences of Ortho-Fluoroazobenzenes on Liquid Crystalline Phase Stability and 2D (Planar) Actuation Properties of Liquid Crystalline Elastomers, *Macromol. Chem. Phys.*, 2020, **221**, 1900265.
 - 185 A.-L. Leistner, S. Kirchner, J. Karcher, T. Bantle, M. L. Schulte, P. Gödtel, C. Fengler and Z. L. Pianowski, Fluorinated Azobenzenes Switchable with Red Light, *Chem. – A Eur. J.*, 2021, **27**, 8094–8099.
 - 186 A. Kerckhoffs, K. E. Christensen and M. J. Langton, Fast relaxing red and near-IR switchable azobenzenes with chalcogen and halogen substituents: periodic trends, tuneable thermal half-lives and chalcogen bonding, *Chem. Sci.*, 2022, **13**, 11551–11559.
 - 187 S. Samanta, T. M. McCormick, S. K. Schmidt, D. S. Seferos and G. A. Woolley, Robust visible light photoswitching with ortho-thiol substituted azobenzenes, *Chem. Commun.*, 2013, **49**, 10314–10316.

- 188 L. N. Lameijer, S. Budzak, N. A. Simeth, M. J. Hansen, B. L. Feringa, D. Jacquemin and W. Szymanski, General Principles for the Design of Visible-Light-Responsive Photoswitches: Tetra-ortho-Chloro-Azobenzenes, *Angew. Chemie Int. Ed.*, 2020, **59**, 21663–21670.
- 189 D. B. Konrad, J. A. Frank and D. Trauner, Synthesis of Redshifted Azobenzene Photoswitches by Late-Stage Functionalization, *Chem. – A Eur. J.*, 2016, **22**, 4364–4368.
- 190 M. Wegener, M. J. Hansen, A. J. M. Driessen, W. Szymanski and B. L. Feringa, Photocontrol of Antibacterial Activity: Shifting from UV to Red Light Activation, *J. Am. Chem. Soc.*, 2017, **139**, 17979–17986.
- 191 D. B. Konrad, G. Savasci, L. Allmendinger, D. Trauner, C. Ochsenfeld and A. M. Ali, Computational Design and Synthesis of a Deeply Red-Shifted and Bistable Azobenzene, *J. Am. Chem. Soc.*, 2020, **142**, 6538–6547.
- 192 M. Dong, A. Babalhavaeji, S. Samanta, A. A. Beharry and G. A. Woolley, Red-Shifting Azobenzene Photoswitches for in Vivo Use, *Acc. Chem. Res.*, 2015, **48**, 2662–2670.
- 193 S. Yamazaki, A. L. Sobolewski and W. Domcke, Molecular mechanisms of the photostability of indigo, *Phys. Chem. Chem. Phys.*, 2011, **13**, 1618–1628.
- 194 J. Pina, D. Sarmiento, M. Accoto, P. L. Gentili, L. Vaccaro, A. Galvão and J. S. Seixas de Melo, Excited-State Proton Transfer in Indigo, *J. Phys. Chem. B*, 2017, **121**, 2308–2318.
- 195 G. M. Wyman, The cis-trans isomerization of conjugated compounds, *Chem. Rev.*, 1955, **55**, 625–657.
- 196 A. Baeyer, Ueber die Verbindungen der Indigogruppe, *Berichte der Dtsch. Chem. Gesellschaft*, 1883, **16**, 2188–2204.
- 197 M. Mostoslavski and V. A. Izmailskii, Absorption spectra of 3-keto-2, 3-dihydrothionaphene and its derivatives. 3., *Zhurnal Obs. Khimii*, 1961, **31**, 17-.
- 198 M. Hooper and W. N. Pitkethly, 2-Arylmethylideneindolin-3-ones: stereochemistry and reduction with sodium borohydride, *J. Chem. Soc. Perkin Trans. 2*, 1972, 1607–1613.
- 199 A. R. Katritzky, Q. Li and W. Fan, Color and constitution. Part 8. Some novel dyestuffs containing indoxyl residues, *J. Heterocycl. Chem.*, 1988, **25**, 1287–1292.
- 200 S. Thumser, L. Köttner, N. Hoffmann, P. Mayer and H. Dube, All-Red-Light Photoswitching of Indirubin Controlled by Supramolecular Interactions, *J. Am. Chem. Soc.*, 2021, **143**, 18251–18260.
- 201 F. Kink, M. P. Collado, S. Wiedbrauk, P. Mayer and H. Dube, Bistable Photoswitching of Hemithioindigo with Green and Red Light: Entry Point to Advanced Molecular Digital Information Processing, *Chem. – A Eur. J.*, 2017, **23**, 6237–6243.
- 202 J. E. Zweig and T. R. Newhouse, Isomer-Specific Hydrogen Bonding as a Design Principle for Bidirectionally Quantitative and Redshifted Hemithioindigo Photoswitches, *J. Am. Chem. Soc.*, 2017, **139**, 10956–10959.
- 203 M. Sacherer, F. Hampel and H. Dube, Fourfold Double-Bond Substituted Hemiindigo: Highly Functionalized Red-Light Responsive Photoswitches, *ChemRxiv*, , DOI:10.26434/chemrxiv-2022-xfbfc.
- 204 S. Wiedbrauk and H. Dube, Hemithioindigo—an emerging photoswitch, *Tetrahedron*

- Lett.*, 2015, **56**, 4266–4274.
- 205 T. Seki, T. Tamaki, T. Yamaguchi and K. Ichimura, Photochromism of hemithioindigo derivatives. II. Photochromic behaviors in bilayer membranes and related systems, *Bull. Chem. Soc. Jpn.*, 1992, **65**, 657–663.
 - 206 K. Eggers, T. M. Fyles and P. J. Montoya-Pelaez, Synthesis and Characterization of Photoswitchable Lipids Containing Hemithioindigo Chromophores, *J. Org. Chem.*, 2001, **66**, 2966–2977.
 - 207 T. Cordes, T. Schadendorf, B. Priewisch, K. Rück-Braun and W. Zinth, The Hammett Relationship and Reactions in the Excited Electronic State: Hemithioindigo Z/E-Photoisomerization, *J. Phys. Chem. A*, 2008, **112**, 581–588.
 - 208 T. Cordes, T. Schadendorf, K. Rück-Braun and W. Zinth, Chemical control of Hemithioindigo-photoisomerization – Substituent-effects on different molecular parts, *Chem. Phys. Lett.*, 2008, **455**, 197–201.
 - 209 A. Nenov, T. Cordes, T. T. Herzog, W. Zinth and R. de Vivie-Riedle, Molecular Driving Forces for Z/E Isomerization Mediated by Heteroatoms: The Example Hemithioindigo, *J. Phys. Chem. A*, 2010, **114**, 13016–13030.
 - 210 B. Maerz, S. Wiedbrauk, S. Oesterling, E. Samoylova, A. Nenov, P. Mayer, R. de Vivie-Riedle, W. Zinth and H. Dube, Making Fast Photoswitches Faster—Using Hammett Analysis to Understand the Limit of Donor–Acceptor Approaches for Faster Hemithioindigo Photoswitches, *Chem. – A Eur. J.*, 2014, **20**, 13984–13992.
 - 211 S. Wiedbrauk, B. Maerz, E. Samoylova, P. Mayer, W. Zinth and H. Dube, Ingredients to TICT Formation in Donor Substituted Hemithioindigo, *J. Phys. Chem. Lett.*, 2017, **8**, 1585–1592.
 - 212 J. E. Zweig, T. A. Ko, J. Huang and T. R. Newhouse, Effects of π -extension on pyrrole hemithioindigo photoswitches, *Tetrahedron*, 2019, **75**, 130466.
 - 213 V. Josef, F. Hampel and H. Dube, Heterocyclic Hemithioindigos: Highly Advantageous Properties as Molecular Photoswitches**, *Angew. Chemie Int. Ed.*, 2022, **61**, e202210855.
 - 214 G. M. Wyman and W. R. Brode, The Relation between the Absorption Spectra and the Chemical Constitution of Dyes XXII. cis-trans Isomerism in Thioindigo Dyes1, *J. Am. Chem. Soc.*, 1951, **73**, 1487–1493.
 - 215 D. L. Ross, Photochromic Indigoids. III: A Photochromic Element Based on the cis-trans Photoisomerization of a Thioindigo Dye, *Appl. Opt.*, 1971, **10**, 571–576.
 - 216 W. R. Brode and G. M. Wyman, Absorption Spectra of Thioindigo Dyes in Benzene and Chloroform, *J. Res. Natl. Bur. Stand. (1934)*, 1951, **47**, 170–178.
 - 217 J. Sühnel and K. Gustav, Spektroskopie und Photochemie indigoider Verbindungen. V. Quantenchemische Berechnungen zum unterschiedlichen UV/S-Spektralverhalten der trans- und cis-Isomeren thioindigoider Verbindungen, *J. für Prakt. Chemie*, 1978, **320**, 917–921.
 - 218 J. Z. Vlahakis, K. E. Maly and R. P. Lemieux, Thioindigo-containing organosiloxane liquid crystals with electroclinic properties, *J. Mater. Chem.*, 2001, **11**, 2459–2464.
 - 219 D. Jacquemin, J. Preat, V. Wathelet, M. Fontaine and E. A. Perpète, Thioindigo Dyes: Highly Accurate Visible Spectra with TD-DFT, *J. Am. Chem. Soc.*, 2006, **128**, 2072–2083.

- 220 B. Koeppe, S. Rühl and F. Römpf, Towards More Effective, Reversible pH Control by Visible Light Alone: A Thioindigo Photoswitch Undergoing a Strong pK_a Modulation by Isomer-Specific Hydrogen Bonding, *ChemPhotoChem*, 2019, **3**, 71–74.
- 221 B. Koeppe and F. Römpf, Reversible Spatial Control in Aqueous Media by Visible Light: A Thioindigo Photoswitch that is Soluble and Operates Efficiently in Water, *Chem. – A Eur. J.*, 2018, **24**, 14382–14386.
- 222 W. R. Brode, E. G. Pearson and G. M. Wyman, The relation between the absorption spectra and the chemical constitution of dyes. XXVII. cis-trans isomerism and hydrogen bonding in Indigo Dyes1, *J. Am. Chem. Soc.*, 1954, **76**, 1034–1036.
- 223 J. Weinstein and G. M. Wyman, Spectroscopic Studies on Dyes. II. The Structure of N,N'-Dimethylindigo1, *J. Am. Chem. Soc.*, 1956, **78**, 4007–4010.
- 224 G. M. Wyman and A. F. Zenhäusern, Spectroscopic Studies on Dyes. V. Derivatives of cis-Indigo1, *J. Org. Chem.*, 1965, **30**, 2348–2352.
- 225 D. Farka, M. Scharber, E. D. Głowacki and N. S. Sariciftci, Reversible Photochemical Isomerization of N,N'-Di(t-butoxycarbonyl)indigos, *J. Phys. Chem. A*, 2015, **119**, 3563–3568.
- 226 K. Kuntze, J. Viljakka, M. Virkki, C.-Y. (Dennis) Huang, S. Hecht and A. Priimagi, Red-light photoswitching of indigos in polymer thin films, *Chem. Sci.*, 2023, **14**, 2482–2488.
- 227 L. A. Huber, P. Mayer and H. Dube, Photoisomerization of Mono-Arylated Indigo and Water-Induced Acceleration of Thermal cis-to-trans Isomerization, *ChemPhotoChem*, 2018, **2**, 458–464.
- 228 S. Hisham, N. Muhamad Sarih, H. A. Tajuddin, Z. H. Zainal Abidin and Z. Abdullah, Unraveling the surface properties of PMMA/azobenzene blends as coating films with photoreversible surface polarity, *RSC Adv.*, 2021, **11**, 15428–15437.
- 229 C. Pakula, C. Hanisch, V. Zaporozhchenko, T. Strunskus, C. Bornholdt, D. Zargarani, R. Herges and F. Faupel, Optical switching behavior of azobenzene/PMMA blends with high chromophore concentration, *J. Mater. Sci.*, 2011, **46**, 2488–2494.
- 230 G. Clavier, F. Ilhan and V. M. Rotello, Photochemical Control of the Macroconformation of Polystyrene Using Azobenzene Side Chains, *Macromolecules*, 2000, **33**, 9173–9175.
- 231 M. El Gemayel, K. Börjesson, M. Herder, D. T. Duong, J. A. Hutchison, C. Ruzié, G. Schweicher, A. Salleo, Y. Geerts, S. Hecht, E. Orgiu and P. Samorì, Optically switchable transistors by simple incorporation of photochromic systems into small-molecule semiconducting matrices, *Nat. Commun.*, 2015, **6**, 6330.
- 232 C.-Y. D. Huang and S. Hecht, A Blueprint for Transforming Indigos to Photoresponsive Molecular Tools, *Chem. – A Eur. J.*, 2023, **n/a**, e202300981.
- 233 T. Noël and E. Zysman-Colman, The promise and pitfalls of photocatalysis for organic synthesis, *Chem Catal.*, 2022, **2**, 468–476.
- 234 S. Reischauer and B. Pieber, Emerging concepts in photocatalytic organic synthesis, *iScience*, 2021, **24**, 102209.
- 235 N. A. Romero and D. A. Nicewicz, Organic Photoredox Catalysis, *Chem. Rev.*, 2016, **116**, 10075–10166.

- 236 M. H. Shaw, J. Twilton and D. W. C. MacMillan, Photoredox Catalysis in Organic Chemistry, *J. Org. Chem.*, 2016, **81**, 6898–6926.
- 237 Z. Jiang, M. Xu, F. Li and Y. Yu, Red-Light-Controllable Liquid-Crystal Soft Actuators via Low-Power Excited Upconversion Based on Triplet–Triplet Annihilation, *J. Am. Chem. Soc.*, 2013, **135**, 16446–16453.
- 238 L. Wang, H. Dong, Y. Li, C. Xue, L.-D. Sun, C.-H. Yan and Q. Li, Reversible Near-Infrared Light Directed Reflection in a Self-Organized Helical Superstructure Loaded with Upconversion Nanoparticles, *J. Am. Chem. Soc.*, 2014, **136**, 4480–4483.
- 239 C. Yao, P. Wang, X. Li, X. Hu, J. Hou, L. Wang and F. Zhang, Near-Infrared-Triggered Azobenzene-Liposome/Upconversion Nanoparticle Hybrid Vesicles for Remotely Controlled Drug Delivery to Overcome Cancer Multidrug Resistance, *Adv. Mater.*, 2016, **28**, 9341–9348.
- 240 J. Moreno, M. Gerecke, L. Grubert, S. A. Kovalenko and S. Hecht, Sensitized Two-NIR-Photon $Z \rightarrow E$ Isomerization of a Visible-Light-Addressable Bistable Azobenzene Derivative, *Angew. Chemie Int. Ed.*, 2016, **55**, 1544–1547.
- 241 M. Izquierdo-Serra, M. Gascón-Moya, J. J. Hirtz, S. Pittolo, K. E. Poskanzer, È. Ferrer, R. Alibés, F. Busqué, R. Yuste, J. Hernando and P. Gorostiza, Two-Photon Neuronal and Astrocytic Stimulation with Azobenzene-Based Photoswitches, *J. Am. Chem. Soc.*, 2014, **136**, 8693–8701.
- 242 G. M. Wyman, B. M. Zarnegar and D. G. Whitten, Excited-state chemistry of indigoid dyes. III. Interaction of indigo and thioindigo with tin(IV) tetraphenyltetrahydroporphyrin triplets. Photosensitized isomerization of thioindigo, *J. Phys. Chem.*, 1973, **77**, 2584–2586.
- 243 J. A. Mercer-Smith and D. G. Whitten, Photosensitization of stilbene isomerization by palladium and platinum porphyrins, an intermolecular quantum chain process, *J. Am. Chem. Soc.*, 1978, **100**, 2620–2625.
- 244 G. Gescheidt, A. Lamprecht, J. Heinze, B. Schuler, M. Schmittel, S. Kiau and C. Rüchardt, Electron-Transfer-Catalyzed $cis \rightarrow trans$ Isomerization of 1,1'-Azonorborane. Prototype of a reversible two-stage storage system, *Helv. Chim. Acta*, 1992, **75**, 1607–1612.
- 245 S. Fredrich, T. Morack, M. Sliwa and S. Hecht, Mechanistic Insights into the Triplet Sensitized Photochromism of Diarylethenes, *Chem. – A Eur. J.*, 2020, **26**, 7672–7677.
- 246 D. Schulte-Frohlinde, Über den Mechanismus der Katalytischen $cis \rightarrow trans$ -Umlagerung von Azobenzol, *Justus Liebigs Ann. Chem.*, 1958, **612**, 131–138.
- 247 C. D. Hall and P. D. Beer, Trico-ordinate phosphorus compounds as catalysts for the isomerization of (Z)-to (E)-azobenzene, *J. Chem. Soc. Perkin Trans. 2*, 1991, 1947 – 1950.
- 248 A. Nakamura, K. Doi, K. Tatsumi and S. Otsuka, Catalysis by low-valent diamagnetic transition-metal complexes of the cis — $trans$ isomerization of azobenzenes, *J. Mol. Catal.*, 1976, **1**, 417–429.
- 249 G. L. Hallett-Tapley, C. D'Alfonso, N. L. Pacioni, C. D. McTiernan, M. González-Béjar, O. Lanzalunga, E. I. Alarcon and J. C. Scaiano, Gold nanoparticle catalysis of the cis — $trans$ isomerization of azobenzene, *Chem. Commun.*, 2013, **49**, 10073–10075.

- 250 S. Simoncelli and P. F. Aramendía, Mechanistic insight into the Z–E isomerization catalysis of azobenzenes mediated by bare and core–shell gold nanoparticles, *Catal. Sci. Technol.*, 2015, **5**, 2110–2116.
- 251 E. Titov, L. Lysyakova, N. Lomadze, A. V Kabashin, P. Saalfrank and S. Santer, Thermal Cis-to-Trans Isomerization of Azobenzene-Containing Molecules Enhanced by Gold Nanoparticles: An Experimental and Theoretical Study, *J. Phys. Chem. C*, 2015, **119**, 17369–17377.
- 252 A. Goulet-Hanssens, M. Utecht, D. Mutruc, E. Titov, J. Schwarz, L. Grubert, D. Bléger, P. Saalfrank and S. Hecht, Electrocatalytic Z → E Isomerization of Azobenzenes, *J. Am. Chem. Soc.*, 2017, **139**, 335–341.
- 253 A. Goulet-Hanssens, C. Rietze, E. Titov, L. Abdullahu, L. Grubert, P. Saalfrank and S. Hecht, Hole Catalysis as a General Mechanism for Efficient and Wavelength-Independent Z → E Azobenzene Isomerization, *Chem*, 2018, **4**, 1740–1755.
- 254 P. Neta and H. Levanon, Spectrophotometric study of the radicals produced by the reduction of syn- and anti-azobenzene, *J. Phys. Chem.*, 1977, **81**, 2288–2292.
- 255 E. Laviron and Y. Mugnier, A study of the isomerization of cis-azobenzene anion radical in dimethylformamide, *J. Electroanal. Chem. Interfacial Electrochem.*, 1978, **93**, 69–73.
- 256 P. A. M. Dirac and N. H. D. Bohr, The quantum theory of the emission and absorption of radiation, *Proc. R. Soc. London. Ser. A, Contain. Pap. a Math. Phys. Character*, 1927, **114**, 243–265.
- 257 D. S. McClure, Triplet-Singlet Transitions in Organic Molecules. Lifetime Measurements of the Triplet State, *J. Chem. Phys.*, 1949, **17**, 905–913.
- 258 E. Wigner, Über die Erhaltungssätze in der Quantenmechanik, *Nachrichten von der Gesellschaft der Wissenschaften zu Göttingen, Math. Klasse*, 1927, **1927**, 375–381.
- 259 E. P. Wigner and E. E. Witmer, Über die Struktur der zweiatomigen Molekelspektren nach der Quantenmechanik, *Zeitschrift für Phys.*, 1928, **51**, 859–886.
- 260 T. J. Penfold, E. Gindensperger, C. Daniel and C. M. Marian, Spin-Vibronic Mechanism for Intersystem Crossing, *Chem. Rev.*, 2018, **118**, 6975–7025.
- 261 R. Englman and J. Jortner, The energy gap law for radiationless transitions in large molecules, *Mol. Phys.*, 1970, **18**, 145–164.
- 262 M. Berberich, A.-M. Krause, M. Orlandi, F. Scandola and F. Würthner, Toward Fluorescent Memories with Nondestructive Readout: Photoswitching of Fluorescence by Intramolecular Electron Transfer in a Diaryl Ethene-Perylene Bisimide Photochromic System, *Angew. Chemie Int. Ed.*, 2008, **47**, 6616–6619.
- 263 T. Shen, Z.-G. Zhao, Q. Yu and H.-J. Xu, Photosensitized reduction of benzil by heteroatom-containing anthracene dyes, *J. Photochem. Photobiol. A Chem.*, 1989, **47**, 203–212.
- 264 T. Forster, Energiewanderung und Fluoreszenz, *Naturwissenschaften*, 1946, **33**, 166–175.
- 265 T. Förster, Zwischenmolekulare energiewanderung und fluoreszenz, *Ann. Phys.*, 1948, **437**, 55–75.
- 266 D. L. Andrews, A unified theory of radiative and radiationless molecular energy transfer,

- Chem. Phys.*, 1989, **135**, 195–201.
- 267 R. G. Bennett, Radiationless Intermolecular Energy Transfer. I. Singlet→Singlet Transfer, *J. Chem. Phys.*, 1964, **41**, 3037–3040.
 - 268 R. G. Bennett, R. P. Schwenker and R. E. Kellogg, Radiationless Intermolecular Energy Transfer. II. Triplet→Singlet Transfer, *J. Chem. Phys.*, 1964, **41**, 3040–3041.
 - 269 K. Razi Naqvi and C. Steel, Exchange-induced resonance energy transfer, *Chem. Phys. Lett.*, 1970, **6**, 29–32.
 - 270 K. R. Naqvi, Spin selection rules concerning intermolecular energy transfer. Energy-transfer studies using doublet-state acceptors. Comments, *J. Phys. Chem.*, 1981, **85**, 2303–2304.
 - 271 L. B. Jones and G. S. Hammond, Mechanisms of Photochemical Reactions in Solution. XXX.1 Photosensitized Isomerization of Azobenzene, *J. Am. Chem. Soc.*, 1965, **87**, 4219–4220.
 - 272 J. Ronayette, R. Arnaud, P. Lebourgeois and J. Lemaire, Isomérisation photochimique de l'azobenzène en solution. I, *Can. J. Chem.*, 1973, **52**, 1848–1857.
 - 273 J. Ronayette, R. Arnaud and J. Lemaire, Isomérisation photosensibilisée par des colorants et photoréduction de l'azobenzène en solution. II, *Can. J. Chem.*, 1973, **52**, 1858–1867.
 - 274 S. Monti, E. Gardini, P. Bortolus and E. Amouyal, The triplet state of azobenzene, *Chem. Phys. Lett.*, 1981, **77**, 115–119.
 - 275 S. Monti, S. Dellonte and P. Bortolus, The lowest triplet state of substituted azobenzenes: An energy transfer investigation, *J. Photochem.*, 1983, **23**, 249–256.
 - 276 J. Isokuorti, K. Kuntze, M. Virkki, Z. Ahmed, E. Vuorimaa-Laukkanen, M. A. Filatov, A. Turshatov, T. Laaksonen, A. Priimagi and N. A. Durandin, Expanding excitation wavelengths for azobenzene photoswitching into the near-infrared range via endothermic triplet energy transfer, *Chem. Sci.*, 2021, **12**, 7504–7509.
 - 277 P. Bharmoria, S. Ghasemi, F. Edhborg, R. Losantos, Z. Wang, A. Mårtensson, M. Morikawa, N. Kimizuka, Ü. İsci, F. Dumoulin, B. Albinsson and K. Moth-Poulsen, Far-red triplet sensitized Z-to-E photoswitching of azobenzene in bioplastics, *Chem. Sci.*, 2022, **13**, 11904–11911.
 - 278 R. S. Mulliken, Interpretation of the Atmospheric Oxygen Bands; Electronic Levels of the Oxygen Molecule, *Nature*, 1928, **122**, 505.
 - 279 R. P. Wayne, in *Advances in Photochemistry*, 1969, pp. 311–371.
 - 280 C. Schweitzer and R. Schmidt, Physical Mechanisms of Generation and Deactivation of Singlet Oxygen, *Chem. Rev.*, 2003, **103**, 1685–1758.
 - 281 S. R. Bakalyar, M. P. T. Bradley and R. Honganen, The role of dissolved gases in high-performance liquid chromatography, *J. Chromatogr. A*, 1978, **158**, 277–293.
 - 282 T. Sato, Y. Hamada, M. Sumikawa, S. Araki and H. Yamamoto, Solubility of Oxygen in Organic Solvents and Calculation of the Hansen Solubility Parameters of Oxygen, *Ind. Eng. Chem. Res.*, 2014, **53**, 19331–19337.
 - 283 M. S. Yusubov and V. V. Zhdankin, Iodine catalysis: A green alternative to transition metals in organic chemistry and technology, *Resour. Technol.*, 2015, **1**, 49–67.

- 284 M. Breugst and D. von der Heiden, Mechanisms in Iodine Catalysis, *Chem. - A Eur. J.*, 2018, **24**, 9187–9199.
- 285 K. Ishihara, in *Iodine Catalysis in Organic Synthesis*, 2022, pp. 11–26.
- 286 R. L. Sutar and S. M. Huber, in *Iodine Catalysis in Organic Synthesis*, 2022, pp. 27–67.
- 287 A. E. Bosnidou and R. M. Romero, in *Iodine Catalysis in Organic Synthesis*, 2022, pp. 121–149.
- 288 S. Yamashita, D. P. Cosgrave, H. Ono and O. Toyama, The Photoisomerization of cis-Azobenzene in the Presence of Iodine, *Bull. Chem. Soc. Jpn.*, 1963, **36**, 688–692.
- 289 R. Arnaud and J. Lemaire, Isomerisation cis-trans de l'azobenzene catalysee par l'iode. III, *Can. J. Chem.*, 1973, **52**, 1868–1871.
- 290 A. R. Gangloff, T. M. Judge and P. Helquist, Light-induced, iodine-catalyzed aerobic oxidation of unsaturated tertiary amines, *J. Org. Chem.*, 1990, **55**, 3679–3682.
- 291 A. Itoh, T. Kodama and Y. Masaki, New Synthetic Method of Benzaldehydes and α,β -Unsaturated Aldehydes with I₂ under Photoirradiation, *Chem. Lett.*, 2001, **30**, 686–687.
- 292 A. Itoh, T. Kodama, Y. Masaki and S. Inagaki, Oxidative Cleavage of the Double Bonds of Styrenes with a Combination of Mesoporous Silica FSM-16 and I₂ under Photoirradiation, *Synlett*, 2002, **2002**, 522–524.
- 293 S. Farhadi, A. Zabardasti and Z. Babazadeh, Aerobic photocatalytic oxidation of activated benzylic and allylic alcohols to carbonyl compounds catalyzed by molecular iodine, *Tetrahedron Lett.*, 2006, **47**, 8953–8957.
- 294 M. Hu, Y. Wang, Z. Xiong, D. Bi, Y. Zhang and Y. Xu, Iodine-Sensitized Degradation of 2,4,6-Trichlorophenol under Visible Light, *Environ. Sci. Technol.*, 2012, **46**, 9005–9011.
- 295 Y. Sudo, E. Yamaguchi and A. Itoh, Photo-oxidative Cross-Dehydrogenative Coupling-Type Reaction of Thiophenes with α -Position of Carbonyls Using a Catalytic Amount of Molecular Iodine, *Org. Lett.*, 2017, **19**, 1610–1613.
- 296 A. L. Harris, M. Berg and C. B. Harris, Studies of chemical reactivity in the condensed phase. I. The dynamics of iodine photodissociation and recombination on a picosecond time scale and comparison to theories for chemical reactions in solution, *J. Chem. Phys.*, 1986, **84**, 788–806.
- 297 E. M. Voigt, Absorption maxima of the visible band of iodine in different groups of solvents, *J. Phys. Chem.*, 1968, **72**, 3300–3305.
- 298 K. Kuntze, J. Isokuoritti, A. Siiskonen, N. Durandin, T. Laaksonen and A. Priimagi, Azobenzene Photoswitching with Near-Infrared Light Mediated by Molecular Oxygen, *J. Phys. Chem. B*, 2021, **125**, 12568–12573.
- 299 F. W. Lampe and R. M. Noyes, Absolute Quantum Yields for Dissociation of Iodine in Inert Solvents, *J. Am. Chem. Soc.*, 1954, **76**, 2140–2144.
- 300 J. Olmsted and G. Karal, Iodine-sensitized photoformation of singlet oxygen, *J. Am. Chem. Soc.*, 1972, **94**, 3305–3310.
- 301 O. Turque, A. Greer and O. R. Wauchope, Synthetic feasibility of oxygen-driven photoisomerizations of alkenes and polyenes, *Org. Biomol. Chem.*, 2020, **18**, 9181–9190.

- 302 B. D. Rihter, M. E. Kenney, W. E. Ford and M. A. J. Rodgers, Synthesis and photoproperties of diamagnetic octabutoxyphthalocyanines with deep red optical absorbance, *J. Am. Chem. Soc.*, 1990, **112**, 8064–8070.
- 303 K. Krumova and G. Cosa, in *Singlet Oxygen: Applications in Biosciences and Nanosciences, Volume 1*, The Royal Society of Chemistry, London, 2016, vol. 1, pp. 1–21.
- 304 M. Krumb, T. Lucas and T. Opatz, Visible Light Enables Aerobic Iodine Catalyzed Glycosylation, *European J. Org. Chem.*, 2019, **2019**, 4517–4521.
- 305 M. Niemi, N. V Tkachenko, A. Efimov, H. Lehtivuori, K. Ohkubo, S. Fukuzumi and H. Lemmetyinen, Exciplex Mediated Photoinduced Electron Transfer Reactions of Phthalocyanine-Fullerene Dyads, *J. Phys. Chem. A*, 2008, **112**, 6884–6892.
- 306 H. A. Schwarz and B. H. J. Bielski, Reactions of HO₂ and O₂⁻ with iodine and bromine and the I₂⁻ and I atom reduction potentials, *J. Phys. Chem.*, 1986, **90**, 1445–1448.
- 307 F. E. J. Scully, in *Biochemical and clinical aspects of oxygen*, ed. W. S. Caughey, Academic Press, 1979, pp. 627–634.
- 308 M. H. Van Benthem and S. J. Davis, Detection of vibrationally excited molecular iodine in the dissociation region of chemical oxygen-iodine lasers, *J. Phys. Chem.*, 1986, **90**, 902–905.
- 309 D. R. S. Pooler, A. S. Lubbe, S. Crespi and B. L. Feringa, Designing light-driven rotary molecular motors, *Chem. Sci.*, 2021, **12**, 14964–14986.
- 310 M. Baroncini, S. Silvi and A. Credi, Photo- and Redox-Driven Artificial Molecular Motors, *Chem. Rev.*, 2020, **120**, 200–268.
- 311 A. S. Lubbe, D. R. S. Pooler and B. L. Feringa, in *Photochemistry: Volume 50*, The Royal Society of Chemistry, 2022.
- 312 S. Kassem, T. van Leeuwen, A. S. Lubbe, M. R. Wilson, B. L. Feringa and D. A. Leigh, Artificial molecular motors, *Chem. Soc. Rev.*, 2017, **46**, 2592–2621.
- 313 N. Koumura, R. W. J. Zijlstra, R. A. van Delden, N. Harada and B. L. Feringa, Light-driven monodirectional molecular rotor, *Nature*, 1999, **401**, 152–155.
- 314 N. Koumura, E. M. Geertsema, A. Meetsma and B. L. Feringa, Light-Driven Molecular Rotor: Unidirectional Rotation Controlled by a Single Stereogenic Center, *J. Am. Chem. Soc.*, 2000, **122**, 12005–12006.
- 315 D. Roke, M. Sen, W. Danowski, S. J. Wezenberg and B. L. Feringa, Visible-Light-Driven Tunable Molecular Motors Based on Oxindole, *J. Am. Chem. Soc.*, 2019, **141**, 7622–7627.
- 316 G. S. Kottas, L. I. Clarke, D. Horinek and J. Michl, Artificial Molecular Rotors, *Chem. Rev.*, 2005, **105**, 1281–1376.
- 317 J. C. M. Kistemaker, P. Štacko, J. Visser and B. L. Feringa, Unidirectional rotary motion in achiral molecular motors, *Nat. Chem.*, 2015, **7**, 890–896.
- 318 A. S. Sardjan, P. Roy, W. Danowski, G. Bressan, L. Nunes dos Santos Comprido, W. R. Browne, B. L. Feringa and S. R. Meech, Ultrafast Excited State Dynamics in a First Generation Photomolecular Motor, *ChemPhysChem*, 2020, **21**, 594–599.
- 319 T. E. Wiley, A. Konar, N. A. Miller, K. G. Spears and R. J. Sension, Primed for Efficient Motion: Ultrafast Excited State Dynamics and Optical Manipulation of a Four Stage

- Rotary Molecular Motor, *J. Phys. Chem. A*, 2018, **122**, 7548–7558.
- 320 J. C. M. Kistemaker, S. F. Pizzolato, T. van Leeuwen, T. C. Pijper and B. L. Feringa, Spectroscopic and Theoretical Identification of Two Thermal Isomerization Pathways for Bistable Chiral Overcrowded Alkenes, *Chem. – A Eur. J.*, 2016, **22**, 13478–13487.
- 321 J. Sheng, W. Danowski, S. Crespi, A. Guinart, X. Chen, C. Stähler and B. L. Feringa, Designing P-type bi-stable overcrowded alkene-based chiroptical photoswitches, *Chem. Sci.*, 2023, **14**, 4328–4336.
- 322 J. Conyard, K. Addison, I. A. Heisler, A. Cnossen, W. R. Browne, B. L. Feringa and S. R. Meech, Ultrafast dynamics in the power stroke of a molecular rotary motor, *Nat. Chem.*, 2012, **4**, 547–551.
- 323 C. R. Hall, J. Conyard, I. A. Heisler, G. Jones, J. Frost, W. R. Browne, B. L. Feringa and S. R. Meech, Ultrafast Dynamics in Light-Driven Molecular Rotary Motors Probed by Femtosecond Stimulated Raman Spectroscopy, *J. Am. Chem. Soc.*, 2017, **139**, 7408–7414.
- 324 J. Conyard, A. Cnossen, W. R. Browne, B. L. Feringa and S. R. Meech, Chemically Optimizing Operational Efficiency of Molecular Rotary Motors, *J. Am. Chem. Soc.*, 2014, **136**, 9692–9700.
- 325 A. Cnossen, J. C. M. Kistemaker, T. Kojima and B. L. Feringa, Structural Dynamics of Overcrowded Alkene-Based Molecular Motors during Thermal Isomerization, *J. Org. Chem.*, 2014, **79**, 927–935.
- 326 L. Pfeifer, M. Scherübl, M. Fellert, W. Danowski, J. Cheng, J. Pol and B. L. Feringa, Photoefficient 2nd generation molecular motors responsive to visible light, *Chem. Sci.*, 2019, **10**, 8768–8773.
- 327 A. Kazaryan, Z. Lan, L. V Schäfer, W. Thiel and M. Filatov, Surface Hopping Excited-State Dynamics Study of the Photoisomerization of a Light-Driven Fluorene Molecular Rotary Motor, *J. Chem. Theory Comput.*, 2011, **7**, 2189–2199.
- 328 D. R. S. Pooler, R. Pierron, S. Crespi, R. Costil, L. Pfeifer, J. Léonard, M. Olivucci and B. L. Feringa, Effect of charge-transfer enhancement on the efficiency and rotary mechanism of an oxindole-based molecular motor, *Chem. Sci.*, 2021, **12**, 7486–7497.
- 329 M. Filatov and M. Olivucci, Designing Conical Intersections for Light-Driven Single Molecule Rotary Motors: From Precessional to Axial Motion, *J. Org. Chem.*, 2014, **79**, 3587–3600.
- 330 A. Kazaryan, J. C. M. Kistemaker, L. V Schäfer, W. R. Browne, B. L. Feringa and M. Filatov, Understanding the Dynamics Behind the Photoisomerization of a Light-Driven Fluorene Molecular Rotary Motor, *J. Phys. Chem. A*, 2010, **114**, 5058–5067.
- 331 G. Marchand, J. Eng, I. Schapiro, A. Valentini, L. M. Frutos, E. Pieri, M. Olivucci, J. Léonard and E. Gindensperger, Directionality of Double-Bond Photoisomerization Dynamics Induced by a Single Stereogenic Center, *J. Phys. Chem. Lett.*, 2015, **6**, 599–604.
- 332 I. Schapiro, M. Gueye, M. Paolino, S. Fusi, G. Marchand, S. Haacke, M. E. Martin, M. Huntress, V. P. Vysotskiy, V. Veryazov, J. Léonard and M. Olivucci, Synthesis, spectroscopy and QM/MM simulations of a biomimetic ultrafast light-driven molecular motor, *Photochem. Photobiol. Sci.*, 2019, **18**, 2259–2269.
- 333 M. Paolino, T. Giovannini, M. Manathunga, L. Latterini, G. Zampini, R. Pierron, J.

- Léonard, S. Fusi, G. Giorgi, G. Giuliani, A. Cappelli, C. Cappelli and M. Olivucci, On the Transition from a Biomimetic Molecular Switch to a Rotary Molecular Motor, *J. Phys. Chem. Lett.*, 2021, **12**, 3875–3884.
- 334 A. Strambi, B. Durbeej, N. Ferré and M. Olivucci, *Anabaena* sensory rhodopsin is a light-driven unidirectional rotor, *Proc. Natl. Acad. Sci.*, 2010, **107**, 21322–21326.
- 335 A. Nikiforov, J. A. Gamez, W. Thiel and M. Filatov, Computational Design of a Family of Light-Driven Rotary Molecular Motors with Improved Quantum Efficiency, *J. Phys. Chem. Lett.*, 2016, **7**, 105–110.
- 336 B. Oruganti, J. Wang and B. Durbeej, Computational Insight to Improve the Thermal Isomerisation Performance of Overcrowded Alkene-Based Molecular Motors through Structural Redesign, *ChemPhysChem*, 2016, **17**, 3399–3408.
- 337 B. Oruganti, J. Wang and B. Durbeej, Excited-State Aromaticity Improves Molecular Motors: A Computational Analysis, *Org. Lett.*, 2017, **19**, 4818–4821.
- 338 M. Filatov, M. Paolino, S. K. Min and K. S. Kim, Fulgides as Light-Driven Molecular Rotary Motors: Computational Design of a Prototype Compound, *J. Phys. Chem. Lett.*, 2018, **9**, 4995–5001.
- 339 M. Filatov, M. Paolino, S. K. Min and C. H. Choi, Design and photoisomerization dynamics of a new family of synthetic 2-stroke light driven molecular rotary motors, *Chem. Commun.*, 2019, **55**, 5247–5250.
- 340 M. K. J. ter Wiel, R. A. van Delden, A. Meetsma and B. L. Feringa, Light-Driven Molecular Motors: Stepwise Thermal Helix Inversion during Unidirectional Rotation of Sterically Overcrowded Biphenanthrylidenes, *J. Am. Chem. Soc.*, 2005, **127**, 14208–14222.
- 341 J. Vicario, A. Meetsma and B. L. Feringa, Controlling the speed of rotation in molecular motors. Dramatic acceleration of the rotary motion by structural modification, *Chem. Commun.*, 2005, 5910–5912.
- 342 N. Koumura, E. M. Geertsema, M. B. van Gelder, A. Meetsma and B. L. Feringa, Second Generation Light-Driven Molecular Motors. Unidirectional Rotation Controlled by a Single Stereogenic Center with Near-Perfect Photoequilibria and Acceleration of the Speed of Rotation by Structural Modification, *J. Am. Chem. Soc.*, 2002, **124**, 5037–5051.
- 343 J. Vicario, M. Walko, A. Meetsma and B. L. Feringa, Fine Tuning of the Rotary Motion by Structural Modification in Light-Driven Unidirectional Molecular Motors, *J. Am. Chem. Soc.*, 2006, **128**, 5127–5135.
- 344 G. B. Boursalian, E. R. Nijboer, R. Dorel, L. Pfeifer, O. Markovitch, A. Blokhuis and B. L. Feringa, All-Photochemical Rotation of Molecular Motors with a Phosphorus Stereoelement, *J. Am. Chem. Soc.*, 2020, **142**, 16868–16876.
- 345 M. Filatov (Gulak), M. Paolino, R. Pierron, A. Cappelli, G. Giorgi, J. Léonard, M. Huix-Rotlant, N. Ferré, X. Yang, D. Kaliakin, A. Blanco-González and M. Olivucci, Towards the engineering of a photon-only two-stroke rotary molecular motor, *Nat. Commun.*, 2022, **13**, 6433.
- 346 A. Gerwien, P. Mayer and H. Dube, Photon-Only Molecular Motor with Reverse Temperature-Dependent Efficiency, *J. Am. Chem. Soc.*, 2018, **140**, 16442–16445.
- 347 D. Liu, V. García-López, R. S. Gunasekera, L. Greer Nilewski, L. B. Alemany, A. Aliyan,

- T. Jin, G. Wang, J. M. Tour and R. Pal, Near-Infrared Light Activates Molecular Nanomachines to Drill into and Kill Cells, *ACS Nano*, 2019, **13**, 6813–6823.
- 348 T. van Leeuwen, J. Pol, D. Roke, S. J. Wezenberg and B. L. Feringa, Visible-Light Excitation of a Molecular Motor with an Extended Aromatic Core, *Org. Lett.*, 2017, **19**, 1402–1405.
- 349 D. Roke, B. L. Feringa and S. J. Wezenberg, A Visible-Light-Driven Molecular Motor Based on Pyrene, *Helv. Chim. Acta*, 2019, **102**, e1800221.
- 350 R. A. van Delden, N. Koumura, A. Schoevaars, A. Meetsma and B. L. Feringa, A donor–acceptor substituted molecular motor: unidirectional rotation driven by visible light, *Org. Biomol. Chem.*, 2003, **1**, 33–35.
- 351 L. Pfeifer, S. Crespi, P. van der Meulen, J. Kemmink, R. M. Scheek, M. F. Hilbers, W. J. Buma and B. L. Feringa, Controlling forward and backward rotary molecular motion on demand, *Nat. Commun.*, 2022, **13**, 2124.
- 352 D. R. S. Pooler, D. Doellerer, S. Crespi and B. L. Feringa, Controlling rotary motion of molecular motors based on oxindole, *Org. Chem. Front.*, 2022, **9**, 2084–2092.
- 353 M. Guentner, M. Schildhauer, S. Thumser, P. Mayer, D. Stephenson, P. J. Mayer and H. Dube, Sunlight-powered kHz rotation of a hemithioindigo-based molecular motor, *Nat. Commun.*, 2015, **6**, 8406.
- 354 R. Wilcken, M. Schildhauer, F. Rott, L. A. Huber, M. Guentner, S. Thumser, K. Hoffmann, S. Oesterling, R. de Vivie-Riedle, E. Riedle and H. Dube, Complete Mechanism of Hemithioindigo Motor Rotation, *J. Am. Chem. Soc.*, 2018, **140**, 5311–5318.
- 355 R. Wilcken, L. Huber, K. Grill, M. Guentner, M. Schildhauer, S. Thumser, E. Riedle and H. Dube, Tuning the Ground and Excited State Dynamics of Hemithioindigo Molecular Motors by Changing Substituents, *Chem. – A Eur. J.*, 2020, **26**, 13507–13512.
- 356 A. Gerwien, P. Mayer and H. Dube, Green light powered molecular state motor enabling eight-shaped unidirectional rotation, *Nat. Commun.*, 2019, **10**, 4449.
- 357 R. S. H. Liu and G. S. Hammond, Photochemical reactivity of polyenes: from dienes to rhodopsin, from microseconds to femtoseconds, *Photochem. Photobiol. Sci.*, 2003, **2**, 835–844.
- 358 A. Gerwien, M. Schildhauer, S. Thumser, P. Mayer and H. Dube, Direct evidence for hula twist and single-bond rotation photoproducts, *Nat. Commun.*, 2018, **9**, 2510.
- 359 J.-M. Lehn, Conjecture: Imines as Unidirectional Photodriven Molecular Motors—Motional and Constitutional Dynamic Devices, *Chem. – A Eur. J.*, 2006, **12**, 5910–5915.
- 360 L. Greb and J.-M. Lehn, Light-Driven Molecular Motors: Imines as Four-Step or Two-Step Unidirectional Rotors, *J. Am. Chem. Soc.*, 2014, **136**, 13114–13117.
- 361 L. Greb, A. Eichhöfer and J.-M. Lehn, Synthetic Molecular Motors: Thermal N Inversion and Directional Photoinduced C–N Bond Rotation of Camphorquinone Imines, *Angew. Chemie Int. Ed.*, 2015, **54**, 14345–14348.
- 362 A. Cnossen, L. Hou, M. M. Pollard, P. V Wesenhagen, W. R. Browne and B. L. Feringa, Driving Unidirectional Molecular Rotary Motors with Visible Light by Intra- And Intermolecular Energy Transfer from Palladium Porphyrin, *J. Am. Chem. Soc.*, 2012, **134**, 17613–17619.

- 363 K. Nakatani, H. Sato and R. Fukuda, A catalyzed E/Z isomerization mechanism of stilbene using para-benzoquinone as a triplet sensitizer, *Phys. Chem. Chem. Phys.*, 2022, **24**, 1712–1721.
- 364 D. Beery, E. Stanisauskis, G. M. McLeod, A. Das, G. A. Guillory, J. G. Kennemur, W. S. Oates and K. Hanson, Enabling Lower Energy Light Harvesting in Stilbene-Based Photomechanical Polymers via Triplet Sensitization, *ACS Appl. Polym. Mater.*, 2022, **4**, 4081–4086.
- 365 S. J. Wezenberg, K.-Y. Chen and B. L. Feringa, Visible-Light-Driven Photoisomerization and Increased Rotation Speed of a Molecular Motor Acting as a Ligand in a Ruthenium(II) Complex, *Angew. Chemie Int. Ed.*, 2015, **54**, 11457–11461.
- 366 L. Pfeifer, N. V. Hoang, M. Scherübl, M. S. Pshenichnikov and B. L. Feringa, Powering rotary molecular motors with low-intensity near-infrared light, *Sci. Adv.*, 2020, **6**, eabb6165.
- 367 A. Sinicropi, E. Martin, M. Ryazantsev, J. Helbing, J. Briand, D. Sharma, J. Léonard, S. Haacke, A. Cannizzo, M. Chergui, V. Zanirato, S. Fusi, F. Santoro, R. Basosi, N. Ferré and M. Olivucci, An artificial molecular switch that mimics the visual pigment and completes its photocycle in picoseconds, *Proc. Natl. Acad. Sci.*, 2008, **105**, 17642–17647.
- 368 A. D. Dunkelberger, R. D. Kieda, J. Y. Shin, R. Rossi Paccani, S. Fusi, M. Olivucci and F. Fleming Crim, Photoisomerization and Relaxation Dynamics of a Structurally Modified Biomimetic Photoswitch, *J. Phys. Chem. A*, 2012, **116**, 3527–3533.
- 369 T. T. Abiola, B. Rioux, J. M. Toldo, J. Alarcán, J. M. Woolley, M. A. P. Turner, D. J. L. Coxon, M. do Casal, C. Peyrot, M. M. Mention, W. J. Buma, M. N. R. Ashfold, A. Braeuning, M. Barbatti, V. G. Stavros and F. Allais, Towards developing novel and sustainable molecular light-to-heat converters, *Chem. Sci.*, 2021, **12**, 15239–15252.
- 370 K. Görlitzer and D. Hölscher, Anellierte Thiopyrone, 1. Mitt. Thiopyrano[3,2-b]indol-4(5H)-one, Thiopyrano[2,3-b]indol-4(9H)-one als Nebenprodukte, *Arch. Pharm. (Weinheim)*, 1986, **319**, 120–125.
- 371 S. Naya, Y. Yamaguchi and M. Nitta, Novel Synthesis, Properties, and Oxidizing Ability of 11,13-Disubstituted 3,8-Methanocycloundeca[8,9-b]pyrimido[5,4-d]-furan-12(11H),14(13H)-dionylum Tetrafluoroborates, *J. Org. Chem.*, 2003, **68**, 9284–9291.
- 372 X. Chen, M. K. Thøgersen, L. Yang, R. F. Lauridsen, X.-S. Xue, K. A. Jørgensen and K. N. Houk, [8+2] vs [4+2] Cycloadditions of Cyclohexadienamines to Tropone and Heptafulvenes—Mechanisms and Selectivities, *J. Am. Chem. Soc.*, 2021, **143**, 934–944.
- 373 K. Kuntze, D. R. S. Pooler, M. Di Donato, M. Hilbers, P. van der Meulen, W. J. Buma, A. Priimagi, B. L. Feringa and S. Crespi, A Visible-Light-Driven Molecular Motor Based on Barbituric Acid, *Chem. Sci.*, 2023.
- 374 P. A. Delaney, R. A. W. Johnstone and I. D. Entwistle, Metal-assisted reactions. Part 17. Ring-opening and dimerization of cyclic ethers by titanium halides, *J. Chem. Soc. Perkin Trans. 2*, 1986, 1855–1860.
- 375 C. García-Iriepa, M. Marazzi, F. Zapata, A. Valentini, D. Sampedro and L. M. Frutos, Chiral Hydrogen Bond Environment Providing Unidirectional Rotation in Photoactive Molecular Motors, *J. Phys. Chem. Lett.*, 2013, **4**, 1389–1396.

PUBLICATIONS

- Publication I Kuntze, K., Viljakka, J., Titov, E., Ahmed, Z., Kalenius, E., Saalfrank, P. & Priimägi, A. Towards low-energy-light-driven bistable photoswitches: *ortho*-fluoroaminoazobenzenes. *Photochemical & Photobiological Sciences* **2022**, 21, 2, 159–173.
- Publication II Kuntze, K., Viljakka, J., Virkki, M., Huang, C.-Y., Hecht, S. & Priimägi, A. Red-light photoswitching of indigos in polymer thin films. *Chemical Science* **2023**, 14, 10, 2482–2488.
- Publication III Kuntze, K., Isokuortti, J., Siiskonen, A., Durandin, N. A., Laaksonen, T. & Priimägi, A. Azobenzene photoswitching with near-infrared light mediated by molecular oxygen. *Journal of Physical Chemistry B* **2021**, 125, 45, 12568–12573.
- Publication IV Kuntze, K.,[†] Pooler, D. R. S.,[†] Di Donato, M., Hilbers, M. F., van der Meulen, P., Buma, W. J., Priimägi, A., Feringa, B. L. & Crespi, S. A visible-light-driven molecular motor based on barbituric acid. *Chemical Science*, **2023**.

[†] Equal contribution.

PUBLICATION I

Towards low-energy-light-driven bistable photoswitches: *ortho*-fluoroaminoazobenzenes

Kuntze, K., Viljakka, J., Titov, E., Ahmed, Z., Kalenius, E., Saalfrank, P. & Priimägi, A.

Photochemical and Photobiological Sciences, vol. 21, p. 159, 2022

DOI: <https://doi.org/10.1007/s43630-021-00145-4>

Publication reprinted with the permission of the copyright holders.



Towards low-energy-light-driven bistable photoswitches: *ortho*-fluoroaminoazobenzenes

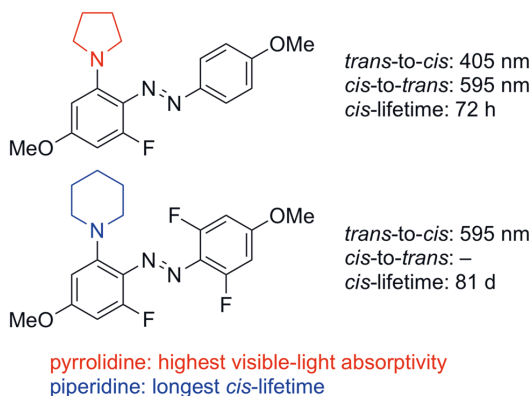
Kim Kuntze¹ · Jani Viljakka¹ · Evgenii Titov² · Zafar Ahmed¹ · Elina Kalenius³ · Peter Saalfrank² · Arri Priimagi¹

Received: 23 September 2021 / Accepted: 17 November 2021 / Published online: 10 December 2021
© The Author(s) 2021

Abstract

Thermally stable photoswitches that are driven with low-energy light are rare, yet crucial for extending the applicability of photoresponsive molecules and materials towards, *e.g.*, living systems. Combined *ortho*-fluorination and -amination couples high visible light absorptivity of *o*-aminoazobenzenes with the extraordinary bistability of *o*-fluoroazobenzenes. Herein, we report a library of easily accessible *o*-aminofluoroazobenzenes and establish structure–property relationships regarding spectral qualities, visible light isomerization efficiency and thermal stability of the *cis*-isomer with respect to the degree of *o*-substitution and choice of amino substituent. We rationalize the experimental results with quantum chemical calculations, revealing the nature of low-lying excited states and providing insight into thermal isomerization. The synthesized azobenzenes absorb at up to 600 nm and their thermal *cis*-lifetimes range from milliseconds to months. The most unique example can be driven from *trans* to *cis* with any wavelength from UV up to 595 nm, while still exhibiting a thermal *cis*-lifetime of 81 days.

Graphical abstract



✉ Evgenii Titov
titov@uni-potsdam.de

✉ Arri Priimagi
arri.priimagi@tuni.fi

¹ Smart Photonic Materials, Faculty of Engineering and Natural Sciences, Tampere University, P.O. Box 541, 33101 Tampere, Finland

² Theoretical Chemistry, Institute of Chemistry, University of Potsdam, Karl-Liebknecht-Straße 24-25, 14476 Potsdam, Germany

³ Department of Chemistry, University of Jyväskylä, P.O. Box 35, 40014 Jyväskylä, Finland

1 Introduction

Photochromic molecular switches such as azobenzenes [1], diarylethenes [2, 3] and spiropyrans [4–6] pave the way towards next-generation pharmaceuticals [7–11], catalysts [12–14] and functional materials [15–18] that can be activated or controlled with a spatially and temporally precise external stimulus–light. Azobenzene derivatives, whose geometry, dipole moment and other physical properties change drastically upon *cis*–*trans* isomerization around the

N=N bond, are particularly attractive photoswitches due to their synthetic versatility, good fatigue resistance and high isomerization quantum yields [1]. The photochemical properties of azobenzene photoswitches can be tuned with simple structural modifications to meet the requirements of a given application. In particular, many applications benefit from switching with low-energy and low-intensity light as well as from high thermal stability of the metastable *cis*-isomer. These attributes are crucial for switches used in living systems [19] or memories [20] and often times advantageous for applications in solar thermal fuel systems [21, 22] and soft-robotic materials [23–25] as well: high-energy irradiation generally has a degrading effect on the switch and its surroundings [26, 27] and, on the other hand, constant illumination is not always possible.

The observed absorption of azobenzene in the UV–Visible range is a combination of two transitions, the symmetry-allowed $\pi\text{--}\pi^*$ and the symmetry-forbidden $n\text{--}\pi^*$. While many substitution patterns red-shift the $\pi\text{--}\pi^*$ band significantly [19, 28, 29], this is accompanied by a drastic drop in the thermal stability of the *cis*-isomer [30], rendering these azobenzenes unsuitable for applications in photobiology where constant irradiation is not possible and near-bistable systems are, therefore, required. *ortho*-Substitution with suitable moieties, in turn, decouples the $n\text{--}\pi^*$ absorption bands of the *cis* and *trans* isomers, red-shifting it for the *trans*-form while simultaneously prolonging the *cis*-lifetime [31, 32]. However, while *ortho*-methoxylated [33], fluorinated [31, 34–36] and chlorinated [37–39] compounds enable efficient switching between two essentially bistable forms with visible light, high irradiation intensities or long illumination periods (hours for *ortho*-chlorinated compounds [38, 39]) are required for efficient switching because of the low molar absorptivity of the $n\text{--}\pi^*$ band. This is a drawback particularly when the photoswitch is illuminated through tissue or other light-scattering or -absorbing material. *ortho*-Amination increases the molar absorptivity but concurrently decreases the *cis*-lifetime to the time scale of seconds [19]. However, as their advantage, amino-substituted azobenzenes are resistant to glutathione that reduces less electron-rich compounds and hampers their applicability in biological systems [40, 41]. In addition, compared to halogens, amino substituents such as piperazine and proline derivatives provide additional functionalization sites in the *ortho* positions, enabling molecular structures unattainable with *ortho*-fluorinated or chlorinated compounds. Thus, it would be highly desirable to combine the best qualities of both *o*-amino- and *o*-halosubstituents.

Recently, we have shown that combined *ortho*-fluorination and amination yields azobenzenes with high molar absorptivity at visible wavelengths and tunable *cis*-lifetimes [42]. Starting from mono- or di-*ortho*-fluorinated precursors, we selectively substituted one or both of the fluorines with

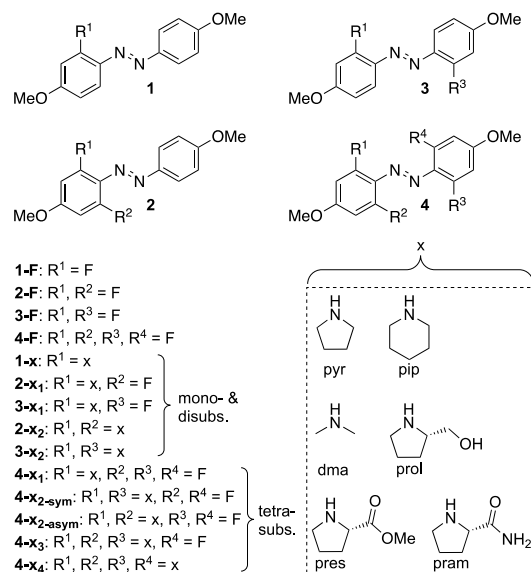
pyrrolidine via a high-yielding nucleophilic aromatic substitution reaction, producing azobenzenes with a relatively long (3 days) or extremely short (1 s) *cis*-lifetime depending on the substitution pattern. However, the studied library of molecules did not include tetra-*ortho*-substituted azobenzenes that have widely shown the best isomerization efficiencies and *cis*-lifetimes among different classes of *ortho*-substituted azobenzenes [31, 34]. The study also gave no information on how the choice of amine affects the photochemical properties of the *ortho*-functionalized azobenzenes. Furthermore, even though the molar absorptivity in the visible region was high, efficient *trans*–*cis* isomerization was only achieved at relatively short wavelengths (365–405 nm). Hence, there is a need for systematic studies to better understand and utilize this class of azobenzenes.

Herein, we present a library of 41 *ortho*-aminofluoroazobenzenes acquired by substituting one or more of the fluorine atoms in mono-, di- and tetra-*ortho*-fluorinated azobenzenes with different secondary amines. Through a systematic survey of the photochemical properties of each compound, we explore the effects of (i) degree of substitution and (ii) choice of amine, searching for the optimal molecular structures that can be isomerized efficiently with low-energy light while maintaining long *cis*-lifetimes. The observed structure–property relationships are further rationalized with density functional theory (DFT) and time-dependent DFT (TD-DFT) calculations which provide electronic insight into low-lying excited states and shed light on thermal isomerization. Additionally, we show that commercial and inexpensive L-proline derivatives can be used to create azobenzenes with similar photoswitching properties as the pyrrolidine-substituted ones, while enhancing water solubility and providing easy synthetic access to *ortho*-linkage to, e.g., bioactive molecules or polymer networks.

2 Results and discussion

2.1 Synthesis

Starting from the *ortho*-mono- and difluorinated azobenzene precursors **1**–**3-F** and utilizing previously reported synthetic procedures [42], we complemented the mono- and di-*ortho*-substituted series with piperidino- and dimethylamino-substituted azobenzenes (Scheme 1); pyrrolidino-substituted equivalents were already published [42]. The degree of substitution can be easily controlled for the difluorinated precursors **2-F** and **3-F**, yielding series **2-x₁** and **2-x₂**, and **3-x₁** and **3-x₂**, respectively, x standing for the amine and subscript for the number of fluorines that have been substituted. This is because the activation Gibbs free energy for the second substitution is significantly greater than for the first reaction due to electron-donating nature of the amino



Scheme 1 Substitution patterns of studied azobenzene derivatives and the abbreviations used for different secondary amines. (*pyr* pyrrolidine, *pip* piperidine, *dma* dimethylamine, *prol* L-prolinol, *pres* L-proline methyl ester, *pram* L-prolinamide)

moiety, leading to excellent yields for either mono- or diaminated product [42]. The reaction proved to be less selective for the tetra-fluorinated **4-F**, creating a mixture of **4-x₁**, **4-x_{2-sym}** and **4-x_{2-asy}** (monoaminated, symmetrically diaminated and asymmetrically diaminated products, respectively) despite our efforts to optimize the reaction conditions. As an example, the optimized yields for **4-pip₁** and **4-pip_{2-sym}** only reached 58% (85% based on recovered starting material) and 54%, respectively. The diaminated products **4-pip_{2-sym}** and **4-pip_{2-asy}** were acquired in a 5:1 ratio. The selectivity of the pyrrolidine and piperidine substitution for **2-F**, **3-F** and **4-F** is illustrated in Table 1. For the reactions of **4-F** with other amines, the conditions were chosen so that all the products were acquired simultaneously.

The series **1-x**, **2-x₁**, **3-x₁**, **3-x₂**, **4-x₁** and **4-x_{2-sym}** were stable enough to be isolated and studied regardless of the chosen amine, but **2-pyr₂** and **4-pyr_{2-sym}** degraded over time. Of the three amines, piperidine produced the most stable products, demonstrated by the fact that the only stable products of higher degree of substitution were **4-pip₃** and **4pip₄**; for pyrrolidine and dimethylamine, no stable products were acquired when more than two fluorines were substituted. Similar decomposition has been reported in earlier studies of *ortho*-amination [40, 42]. Conversely, the reaction times were longer for piperidine than for pyrrolidine and/or the former required heating in order to progress (Table 1),

Table 1 Selectivity of the amination of **2-F**, **3-F** and **4-F**, the reaction scheme of entry 2 as an example

Substrate	Reaction conditions	Product(s) and yield(s)
2-F + pyr^a	5 eq. in MeCN, rt, 2.5 h	2-pyr₁ (92%)
2-F + pip	2 eq. in MeCN, 50 °C, 20 h	2-pip₁ (95%)
3-F + pyr^a	neat, rt, 20 h	3-pyr₁ (81%), 3-pyr₂ (15%)
3-F + pip	20 eq. in MeCN, rt, 20 h	3-pip₁ (94%)
4-F + pyr	2 eq. in MeCN, rt, 2 h	4-pyr₁ (56%), 4-pyr_{2-sym} (11%)
4-F + pyr	4 eq. in MeCN, rt, 20 h	4-pyr_{2-sym} (28%), 4-pyr₁ (10%)
4-F + pip	2 eq. in MeCN, 50 °C, 2 h	4-pip₁ (58%), 4-pip_{2-sym} (9%), recovered 4-F (25%)
4-F + pip	4 eq. in MeCN, 50 °C, 20 h	4-pip_{2-sym} (54%), 4-pip₁ (11%), 4pip_{2-asy} (11%), 4pip₃ (6.7%)

rt room temperature

^aPreviously published [42] reaction

probably due to greater steric interactions in the transition state of the piperidine substitution.

Next, we investigated L-prolinol (prol), L-proline methyl ester (pres), and L-prolinamide (pram), using these pyrrolidine-resembling molecules to elaborate the series **2-x₁**, **3-x₁**, **4-x₁** and **4-x_{2-sym}**. The proline derivatives were consistently less reactive towards the fluorinated precursor than pyrrolidine (see Supporting Information), probably due to increased steric interactions and decreased nucleophilicity of the nitrogen lone pair. We also attempted to synthesize the L-proline-substituted products from **2-F** to **4-F** with the parent amino acid, but these could not be isolated, presumably because of intramolecular protonation of the azo bridge and subsequent decomposition. DFT calculations verify that the carboxylic proton is perfectly poised towards one of the nitrogen lone pairs at a hydrogen bonding distance (Fig. S142).

2.2 Spectral properties

Overall, 41 synthesized compounds were stable enough to be studied. The absorption wavelengths and molar extinction coefficients of the *trans*-isomer, *cis*-fractions in the photostationary state (PSS) and thermal lifetimes of the *cis*-to-*trans* isomerization of the compounds are presented in Table 2. The *ortho*-fluorinated azobenzenes **1–3-F** exhibit typical

Table 2 Photochemical properties and thermal *cis*-to-*trans* isomerization lifetime of synthesized azobenzenes^a

	λ (nm)	ϵ (l mol ⁻¹ cm ⁻¹)	PSS (% Z) ^b	τ_{cis} ^c		λ (nm)	ϵ (l mol ⁻¹ cm ⁻¹)	PSS (% Z) ^b	τ_{cis} ^c
1-F^f	357/432	29,110/3608	93 [365]	42 h	4-F	343/435	27,815/3086	91 [365]	204 ^d
2-F^f	350/432	24,652/2286	93 [365]	60 h	4-pyr₁	332/419/463	10,686/4840/4956	60 [365]	244 h
3-F^f	343/435	27,815/3086	94 [365]	430 h	4-pip₁	334/394/457	8503/3975/2340	71 [365]	81 ^d
1-pyr^f	340/430/462	12,693/10818/12749	72 [470]	15 s	4-dma₁	332/395/457	15,219/6778/5064	64 [365]	257 h
1-pip^f	341/402/449	14,924/10075/6800	75 [405]	9.1 h	4-prol₁	331/393/457	5184/2824/2011	39 [405]	276 h
1-dma	341/415/449	11,421/7730/6943	75 [405]	219 s	4-pres₁	329/400/465	15,818/6722/7227	58 [405]	260 h
2-pyr₁^f	335/411/454	16,739/8006/7792	80 ^d [405]	72 h	4-pram₁	329/394/466	11,525/4717/4326	55 [405]	270 h
2-pip₁	337/381/453	15,930/8911/3493	76 [385]	445 h	4-pyr_{2-sym}	318/408/488	7680/5661/5538	54 [405]	7.4 h
2-dma₁	337/390/449	17,179/8293/5555	73 [385]	286 h	4-pip_{2-sym}	321/384/465	5516/3060/2000	43 [405]	31 h
2-prol₁	333/405/456	4955/2526/2307	75 [385]	131 h	4-dma_{2-sym}	324/403/457	13,103/9225/7178	56 [385]	31 h
2-pres₁	339/396/447	14,010/8144/7368	62 [405]	8.5 h	4-prol_{2-sym}	317/387/487	6111/3822/4084	44 [405]	75 h
2-pram₁	338/400/437	13,362/7322/6544	69 [385]	6.9 h	4-pres_{2-sym}	324/388/482	5175/5274/4346	47 [405]	24 h
3-pyr₁^f	344/479	13,777/15042	71 [405]	258 s	4-pram_{2-sym}	325/392/482	5778/4039/3406	60 [405]	29 h
3-pip₁	349/411/447	16,610/10890/9228	71 [365]	5 h	4-pyr_{2-asym}	365/445	5466/6200	45 [405]	1.1 s
3-dma₁	346/436/456	16,315/11589/11804	69 [405]	165 s	4-pip_{2-asym}	374/? ^g	19,726/? ^g	64 [405]	192 s
3-prol₁	344/446/468	9404/7590/8571	61 [405]	219 s	4-dma_{2-asym}	388/? ^g	10,350/? ^g	39 [405]	0.2 s
3-pres₁	354/436/464	14,391/7205/8159	64 [405]	74 s	4-pram_{2-asym}	360/448	6872/5770	40 [405]	0.05 s
3-pram₁	343/436/462	7068/6323/6777	67 [405]	64 s	4-pip₃	366/460	.. ^e	28 [405]	3.8 s
2-pip₂	380	13,480	69 [365]	10 min	4-pip₄	356/471	.. ^e	5 [405]	0.2 s
2-dma₂	389	10,330	55 [365]	0.4 s					
3-pyr₂^f	488/514	3701/3456	62 [365]	1.2 s					
3-pip₂	336/434	10,110/12160	61 [365]	59 min					

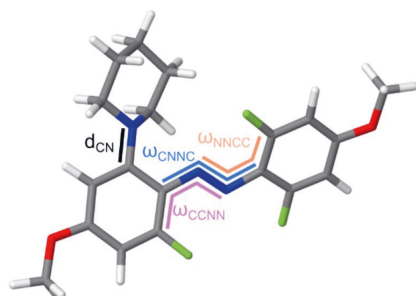
^aStudied in 50–150 μ M acetonitrile solutions. Spectral properties belong to the *trans* isomer^bMinimum values estimated from the difference in absorbance. Irradiation wavelength is specified in square brackets^cThermal lifetime of the *cis*-isomer at 25 °C, determined as an inverse of the rate constant in an exponential fit^dMeasured with ¹H NMR^ePoorly soluble, accurate concentration not known^fPreviously published [42] data^gHard to extract peak value

azobenzene absorption spectra, strong π - π^* peaks at ca. 350 nm accompanied by weak n - π^* bands at ca. 430 nm. When fluorines are substituted with amines, the absorption spectrum changes significantly: the molar absorptivity in the π - π^* band is lowered by half, while the absorptivity in the visible wavelengths (the n - π^* band, > 400 nm) increases multifold and is shifted towards red.

To explain the enhanced visible range absorption, we optimized the geometries of selected compounds at the B3LYP [43, 44] + D3(BJ)[45]/6-31G*[46] level of theory, using the polarizable continuum model [47, 48] (PCM) to account for the solvation effects by acetonitrile (see sect 4.4). The *ortho*-fluorinated precursor **1-F** is perfectly planar with orthogonal n and π^* orbitals, which accounts for the almost negligible absorbance in the n - π^* band (Table 2), only non-zero due to molecular vibrations coupled with the electronic transitions [49]. The fact that the absorbance for the *ortho*-aminated compounds is relatively high in the n - π^* band (the nature of the electronic

transitions is discussed later in this section) would suggest that the planarity is broken. Optimized geometries indeed show that the amino-substituted compounds are twisted compared to their planar parent precursors. The degree of twisting can be quantified with three dihedral angles (Table 3): ω_{CCNN} , ω_{CNCC} and ω_{NNCC} . For symmetrical azobenzenes, the first and third angle have the same value, and for asymmetrical ones, we have assigned ω_{CCNN} to the amino-substituted side. While **1F** is completely planar, its aminated derivatives exhibit dihedral angles of up to ca. 30° on the side of the aminated ring. This improves the overlap between the n and π^* orbitals and explains the increased absorbance. We note, however, that the CCNN values of Table 3 alone cannot explain changes in absorbance observed when going, e.g., from **1-x** to **2-x₁**. Apart from an effect of further CN torsion out of the equilibrium (discussed below), there is an intrinsic electronic effect of fluorine (see Supporting Information, p. S69). The red shift can be attributed to donation of electron density from

Table 3 Dihedral angles and C–N bond length of selected azobenzenes, calculated at the B3LYP+D3(BJ)/6-31G*/PCM(ACN) level of theory. The dihedral angles of interest are shown on the example of **4-pip1**



	ω_{CCNN} (°)	ω_{CNNC} (°)	ω_{NNCC} (°)	d_{CN} (Å)
1-F	0	180	0	–
1-pyr	2	180	3	1.368
1-pip	16	177	3	1.401
2-pyr₁	23	177	8	1.369
2-pip₁	29	177	4	1.398
2-dma₁	29	177	4	1.399
3-pip₁	15	178	2	1.400
4-pip₁	28	177	7	1.394
4-pip_{2-sym}	20	177	20	1.395

the amino substituent, demonstrated by bond lengths of ca. 1.37–1.40 Å between the amino substituent and the aromatic ring, displaying significant double bond character (Table 3).

The effect that the substitution pattern has on the spectral properties is illustrated in Fig. 1a and b by comparing the spectra of different piperidino-substituted compounds. Piperidine was chosen because of the remarkable stability of the products, thus enabling the comparison of all relevant substitution patterns. Relative to *ortho*-fluoroazobenzenes, the absorptivity in the visible wavelength range increases the least for **2-pip₁**, *i.e.*, when the fluorine and piperidine are located on the same aryl ring (red curve). Having only one piperidino substituent (**1-pip**, black curve) or a piperidine and a fluorine in opposite rings (**3-pip₁**, blue curve) promotes visible light absorptivity more, with the absorption spectrum of **3-pip₁** slightly red-shifted compared to **1-pip**. Having two piperidines in the same ring (**2-pip₂**, magenta curve) or in opposite rings (**3-pip₂**, green curve) red-shifts the spectrum more pronouncedly, and the greatest visible range absorbance is exhibited by **3-pip₂**. The spectral shape is different for the asymmetrically diaminated molecules **2-pip₂** and **4-pip_{2-asym}** compared to the symmetrical **3-pip₂** and **4-pip_{2-sym}**, the former showing only one major

absorption band in the visible range due to strong one-sided electron donation. The absorption maxima of the tetrasubstituted **4-pip₁**, **4-pip_{2-sym}** and **4-pip_{2-asym}** are shifted by only a few nanometers compared to the respective disubstituted series, but the tail of the absorption band reaches significantly further on the red side, especially for **4-pip_{2-sym}** (Fig. 1b, red curve). Same trends were observed with other amines as well (Fig. S128–S138).

The choice of amine has a consistent effect on the absorption spectra: the compounds substituted with pyrrolidine or its derivatives show strong absorptivity from 400 to 550 nm, whereas these peaks are smaller for piperidino- and dimethylamino-substituted molecules (Fig. 1c). The phenomenon is known for amino-substituted azobenzenes and arises from the degree of delocalization of the nitrogen lone pair, the nitrogen in the pyrrolidino moiety having more sp^2 character than the ones in piperidino and dimethylamino substituents [50], as also demonstrated by shorter C–N bond lengths for pyrrolidino-substituted compounds (Table 3). This difference is explained by steric interactions between the α protons of the amino group and the *meta*-proton in the aromatic ring that are stronger for piperidine and dimethylamine [50]. In addition, *exo* double bonds stabilize five-membered rings but destabilize six-membered rings [51]. Another trend is found in the photostationary state spectra: even though the compounds have almost equal *cis*-fractions upon illumination, the $n \rightarrow \pi^*$ absorbance in the *cis*-rich mixture is highest for pyrrolidine, exceeding the absorbance of the pure *trans* isomer (and creating an isosbestic point) at the red end.

To further rationalize the experimental spectral data, we computed the excitation energies and oscillator strengths of the electronic transitions from the ground state to the low-lying excited states of selected molecules using linear response time-dependent density functional theory (TD-DFT) [52] and PCM (in the non-equilibrium regime [53]) to account for solvent (ACN). We used B3LYP and ω B97X-D [54] density functional approximations as representatives of the global hybrid and long-range corrected families, respectively, as they are expected to give different results, in particular, not only different excitation energies but also ordering of excited states when intramolecular charge-transfer states are present [55, 56]. The nature of excited states was analyzed by means of natural transition orbital [57] (NTO) analysis.

The structure–property relationships are reproduced on a semi-quantitative level computationally (see Fig. 2 for comparison of experimental and computational trends as well as Table S1 and Fig. S139 for calculated transitions and broadened absorption spectra, respectively). For the *trans* isomer, the amino substituents induce the splitting of the $\pi \rightarrow \pi^*$ transition in two, one of which ($S_0 \rightarrow S_2$, the second band from the red side) is red-shifted and the other one ($S_0 \rightarrow S_3$, the third band) is blue-shifted with respect to

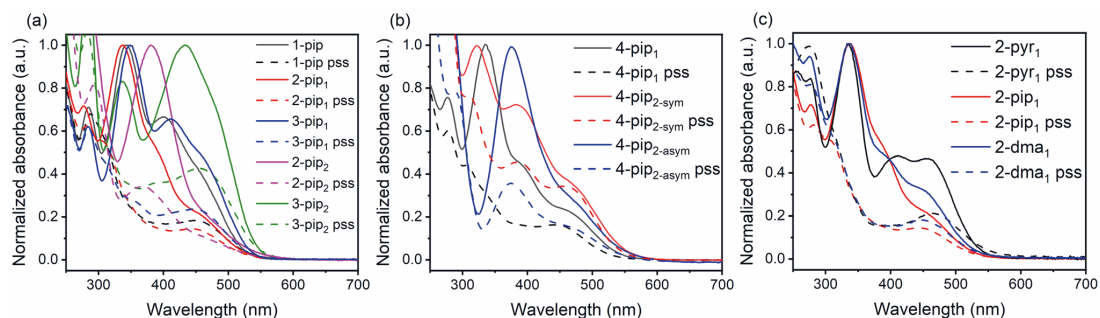


Fig. 1 Absorption spectra of **a** 1-**pip**, 2-**pip**₁, 3-**pip**₁, 2-**pip**₂ and 3-**pip**₂, **b** 4-**pip**₁, 4-**pip**_{2-sym} and 4-**pip**_{2-asm}, and **c** 2-**pyr**₁, 2-**pip**₁ and 2-**dma**₁ in dark and in PSS, the most intense band normalized to 1

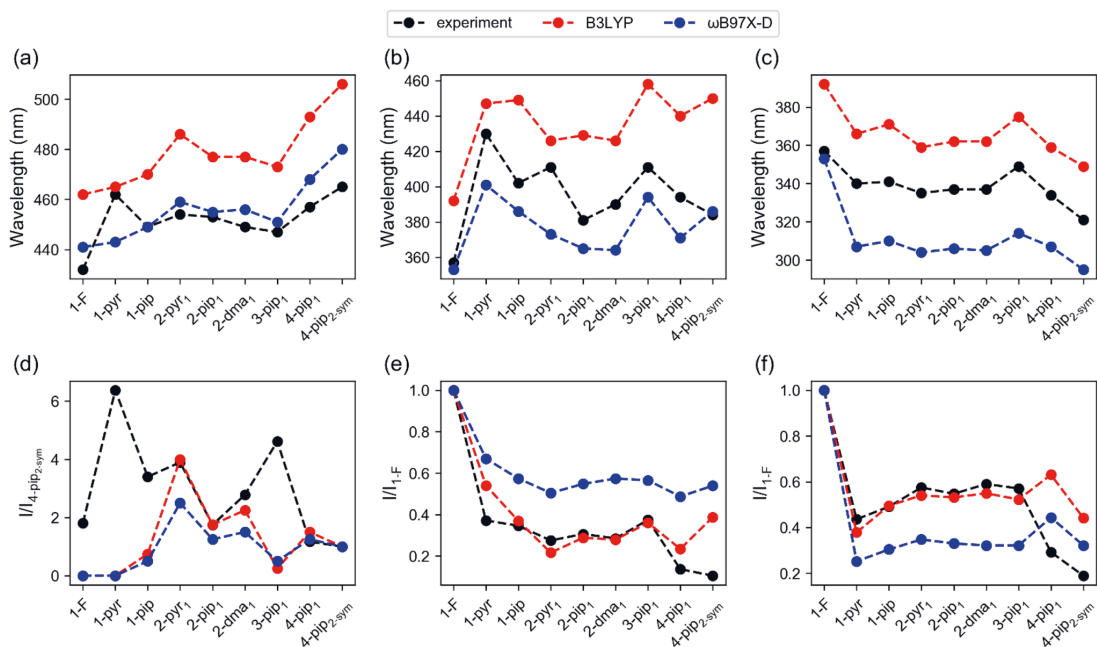


Fig. 2 Comparison of experimental and calculated peak positions (**a–c**) and relative intensities (**d–f**) for first three absorption bands of *trans* isomers (panels **a,d** for band 1; panels **b,e** for band 2; and panels **c,f** for band 3). The relative intensity is calculated as the ratio

of extinction coefficients (taken from Table 2) for the experimental trends and as the ratio of oscillator strengths (taken from Table S1) for the computational trends, relative to 4-**pip**_{2-sym} in (**d**) and to 1-**F** in (**e**) and (**f**)

the $\pi-\pi^*$ transition ($S_0 \rightarrow S_2$) of the parent molecule 1-**F**. The hole NTOs of these transitions reveal considerable contribution of the nitrogen lone pair orbital of the amino substituent, especially for the second band (see Fig. 3 for the case of 2-**pip**₁ and Table S2 for other molecules), giving the nitrogen substantial sp^2 character. Moreover, the $n-\pi^*$ transition ($S_0 \rightarrow S_1$) acquires a non-zero oscillator strength for all the considered aminoazobenzenes except

1-**pyr**. When using B3LYP, the $S_0 \rightarrow S_3$ transition is usually more intense than the $S_0 \rightarrow S_2$ transition. This trend is reversed when using $\omega B97X-D$. The B3LYP trend appears to better reproduce experimental intensities, especially for the second and third bands (Fig. 2 e,f). We also note that B3LYP red-shifts the spectra with respect to the measured ones, whereas $\omega B97X-D$ blue-shifts the $\pi-\pi^*$ transitions and either slightly red-shifts or blue-shifts the $n-\pi^*$

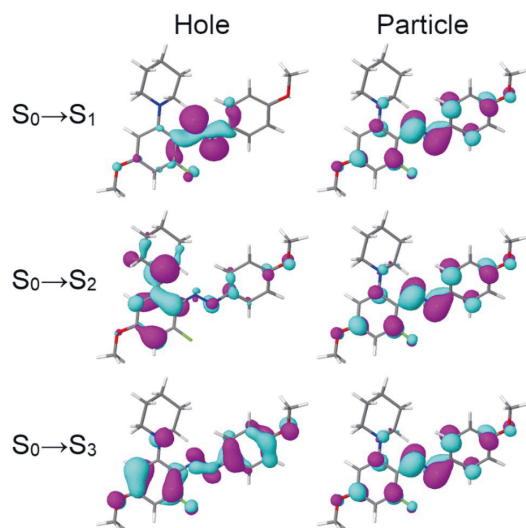


Fig. 3 Dominant natural transition orbital pairs for the first three transitions ($S_0 \rightarrow S_1$, $S_0 \rightarrow S_2$, and $S_0 \rightarrow S_3$) of the *trans*-2-**pip**₁ calculated at the TD-B3LYP+D3(BJ)/6-31G*/PCM(ACN) level of theory. Upon a given transition an electron is transferred from the “Hole” NTO to the “Particle” NTO. The contributions of the shown hole-particle pairs to the respective transitions are larger than 99%

transition depending on the molecule in question (Fig. 2 a–c).

The $S_0 \rightarrow S_1$ oscillator strengths of **2-pyr**₁, **2-pip**₁ and **2-dma**₁ show the same trend as the experimental extinction coefficients (Fig. 2d). The $S_0 \rightarrow S_1$ transition is also red-shifted for **2-pyr**₁ compared to the other two compounds. In addition, the computations reproduce the red shift **1-pip** **p** < **2-pip**₁ < **4-pip**₁ < **4-pip**_{2-sym} (Fig. 2a). The experimental spectral differences in intensity between **2-pip**₁ and **3-pip**₁, however, are only reproduced computationally in the case of $S_0 \rightarrow S_2$ and not for $S_0 \rightarrow S_1$ (Fig. 2 d,e and Fig. S139). Explaining this would require computational studies beyond single geometries, e.g., molecular dynamics simulations or Wigner distributions [58]. Judging the performance of the two used functionals by comparing with the experiment, we find that TD- ω B97X-D performs particularly well for the excitation energies of the first band (Fig. 2a) and TD-B3LYP works very well for the relative intensities of the second and third bands (Fig. 2 e,f). It is worth noting, however, that these results are obtained using an implicit solvation model (PCM in our case), which simplifies the complexity of the environment.

Interestingly, the $n-\pi^*$ absorption band of **1-pyr** is strong in the measured spectrum (Table 2), while zero $S_0 \rightarrow S_1$ oscillator strength is found computationally (Table S1). To explain this discrepancy, we analyzed the change in the

oscillator strength of the lowest transitions upon torsion around the C–N bond (varying ω_{CCNN}), since this type of motion is expected to occur at room temperature. We found that this torsion does not require much energy and causes the increase in the $S_0 \rightarrow S_1$ oscillator strength (Fig. S140), thus explaining the experimental results.

For the *cis*-isomer, we also observed the appearance of additional transitions in the low-energy region. Whereas for **1-F** the $S_0 \rightarrow S_2$ transition bears the largest oscillator strength (out of four lowest transitions), it is either the $S_0 \rightarrow S_3$ or $S_0 \rightarrow S_4$ transition which is the most intense one in the case of aminoazobenzenes, depending on the density functional in use and the molecule under consideration (Table S1). For most molecules, it is $S_0 \rightarrow S_4$ with B3LYP and $S_0 \rightarrow S_3$ with ω B97X-D. The oscillator strengths of the $S_0 \rightarrow S_1$ transition of *cis*-**2-pyr**₁, *cis*-**2-pip**₁ and *cis*-**2-dma**₁ reproduce the experimentally observed trend in the absorbances of the *cis*-rich photostationary state mixtures (*pyr* > *dma* > *pip*) with both functionals (Table S1 and Fig. S139). The NTOs of the *cis*-isomers are shown in Table S3.

2.3 Photoisomerization efficiency

To determine how efficiently the products can be switched from *trans* to *cis*, we estimated the *cis*-fraction in the most *cis*-rich PSS mixture by comparing the UV–Vis spectra in the PSS upon illumination (365, 385 or 405 nm) and in the dark after sufficient heating, *i.e.*, with only *trans*-isomer present (see sect 4.2). The molar fractions should be viewed as minimum values, as the method assumes the *cis*-absorbance to be zero at the wavelength in question. As a representative example, the minimum *cis*-fraction in the PSS for **2-pyr**₁ upon irradiation with 405 nm light calculated with this method is 68%, but with ¹H NMR measurements, 80% *trans*-to-*cis* switching is observed [42]. Similarly, upon 405 nm irradiation, the *cis*-fraction of **4-pip**₁ was determined as 66% with ¹H NMR (Fig. S94c), compared to the 59% calculated from the UV–Vis spectra. The efficiency is best for the series **1-x**, **2-x**₁ and **3-x**₁, all of which can be driven to > 70% *cis*. The tetrasubstituted compounds cannot generally be isomerized as efficiently (Table 2).

We were particularly interested in switching with low-energy illumination and screened excitation wavelengths from 365 to 595 nm for each product in the series **1-x**, **2-x**₁, **3-x**₁, **4-x**₁ and **4-x**_{2-sym}, *i.e.*, the series that are stable with all amino substituents. The *cis*-fractions upon illumination with specific wavelengths are presented in Table S5. It turns out that even though most compounds absorb strongly from 400 to 500 nm, not all of them can be efficiently driven to the *cis*-state with > 435 nm illumination. For instance, the highly absorbing **2-pyr**₁ is efficiently driven to *cis* with 365–435 nm, but longer wavelengths drive the equilibrium towards *trans* (Fig. 4a). This holds true for many other

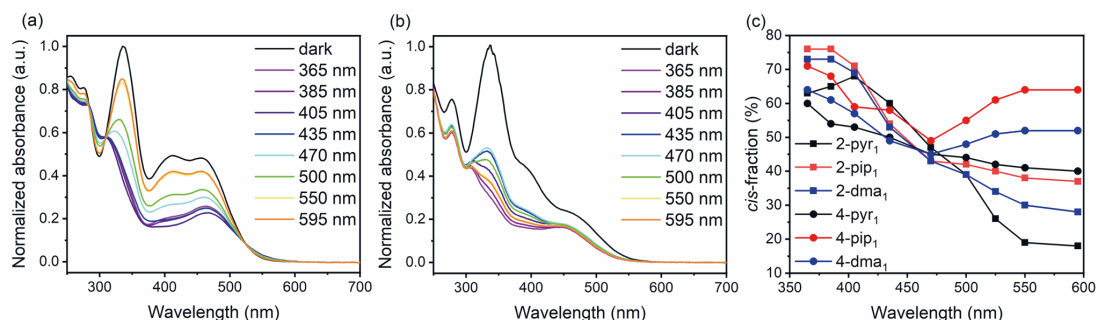


Fig. 4 Normalized absorption spectra of **a** 2-pyr₁ and **b** 4-pip₁ upon illumination with 365–595 nm light, and **c** the photostationary state compositions of selected azobenzenes with different illumination wavelengths

ortho-aminoazobenzenes as well, especially pyrrolidino- or proline-derivative-substituted ones that even exhibit an isobestic point at ca. 520 nm (Fig. 1c, Fig. S134). Even though efficient isomerization is not possible at the absorbance maximum of the $n\text{-}\pi^*$ region, this feature enables switching from *trans* to *cis* with short wavelengths (365–435 nm) and in the opposite direction with lower energy light (525–595 nm). For piperidino- and dimethylamino-substituted compounds the back-isomerization is less effective (Fig. 4c), probably due to spectral differences for the *cis*-isomer (Fig. 1c). We wish to highlight that the photostationary states were acquired fast (< 30 s) with illumination intensities ranging from 11 to 77 mW cm⁻² depending on the wavelength (Table S5).

The *cis*-to-*trans* photoisomerization is less efficient for the series 4-x₁ and 4-x_{2-sym}, hampering the switching between the isomers (Table 2). This is likely due to worse spectral separation of the isomers caused by increased twisting of the *trans*-isomer (Table 3). However, driving the equilibrium towards *cis* with low-energy light (435–595 nm) is more efficient than in the case of the disubstituted series. As the most promising example, 4-pip₁ can be driven to > 64% *cis* state with 550 and 595 nm illumination (Fig. 4 b, c), a unique feature for thermally stable azobenzenes (*cis*-lifetime of 81 days at 25 °C, see next section). In fact, with ¹H NMR studies, a *cis*-fraction of 72% was observed (Fig. S94d). Direct photoisomerization in the opposite direction is not effective, but the back-isomerization can be accomplished with, e.g., a red- or near-infrared-activated triplet sensitizer [59] or via electron transfer [60–63].

Considering the strong molar absorptivity of the pyrrolidino-substituted compounds in the visible range, it is interesting that the *cis*-to-*trans* isomerization is more efficient for piperidino- and dimethylamino-substituted azobenzenes at 400–500 nm (Fig. 4c). This is a good reminder that high molar absorptivity alone is not an indication of efficient switching if the spectral separation of the isomers and ratio

of quantum yields are not favorable. The trend correlates with the absorbance of the *cis*-isomer at 400–600 nm which is highest for pyrrolidino- and lowest for piperidino-substituted azobenzenes (Fig. 1c, Fig. S139). As an interesting detail, the *cis*-fractions of 4-pyr₁ and 4-pyr_{2-sym} decrease monotonically with increasing excitation wavelength, whereas for the piperidine and dimethylamine equivalents, the *cis*-fraction decreases from 405 to 470 nm but increases when moving further to the red (Fig. 4c, Table S5).

2.4 Thermal *cis*–*trans* isomerization rate

The *cis*-lifetimes were determined by monitoring the absorbance values after *trans*-to-*cis* photoisomerization and fitting a monoexponential formula to the kinetic data. The lifetime τ is an inverse of the rate constant (see Sect 4.3). The thermal stability of the *cis*-isomer is inversely correlated with the degree of π donation from the amino group: when compounds with the same substitution pattern but different amino substituents are compared, the order in *cis*-lifetimes is piperidine > dimethylamine > pyrrolidine, reversed to the order seen for the molar absorptivity in the visible range. In effect, this means that the molecular design is often a trade-off between long *cis*-lifetimes and high absorptivity in the visible range, a typical dilemma of azobenzenes. In the series 1-x, 3-x₁, 2-x₂ and 3-x₂, only piperidino products can be described as near-bistable, whereas the pyrrolidino- and dimethylamino-substituted azobenzenes isomerize in minutes or seconds. The series 2-x₁ and 2-pyr₁ in particular, provides a compromise: the *cis*-lifetimes range from 7 to 445 h (72 h for 2-pyr₁), while the molar absorptivity remains high above 450 nm.

In the earlier studies of *ortho*-fluorinated azobenzenes, tetra-*ortho*-fluorinated compounds exhibited the best *cis*-stability [31]. When compared to series 2-x₁, the *cis*-lifetimes are indeed increased for series 4-x₁ (up to 81 days at 25 °C for 4-pip₁) with the exception of 4-dma₁, for

which the thermal isomerization is actually faster than for **2-dma₁**, although remaining in the time scale of hours (Table 2). The stability of the *cis*-isomers in the series **4-x_{2-asym}** is even lower than in the series **2-x₂** (from 0.05 to 192 s), probably due to a push–pull effect by the amino- and fluoro-substituents on opposite rings.

To corroborate our experimental findings, we studied the thermal isomerization kinetics computationally by Eyring's transition state theory [64] using the B3LYP functional which has been found to perform well for kinetics of azobenzene [65]. We considered both inversion and rotation pathways for the *cis* → *trans* isomerization. Spin-restricted DFT (RDFT) calculations were done to locate inversion transition states and broken-symmetry spin-unrestricted (UDFT) calculations were performed to find rotation transition states (we note that for **1-pyr** we also found a rotation transition state using RDFT).

In the case of the inversion path, the linearization of the CNN unit may occur on either side from the azo group (Tables S10–S12). The intrinsic reaction coordinate (IRC) calculations [66, 67] with subsequent geometry optimizations showed that the *cis*-isomers corresponding to these two types of inversion transition states generally differ in geometry (conformation) from one another (Tables S10–S12). We note that these different *cis*-isomers of a given molecule have different ground-state energies (Table S6) but they may, in principle, be populated photochemically. See further discussion of different *cis*-isomer conformations in Supporting Information (pp. S83–S85).

In the case of the RDFT treatment (inversion pathways), we performed calculations with and without solvent (PCM(ACN)) and dispersion (D3(BJ)) corrections. The calculated lifetimes increase in the order gas phase < PCM(ACN) < PCM(ACN) + D3(BJ), with the latter being too long in comparison with the experimental values (Table S6). The too long lifetimes can be attributed to too large calculated activation Gibbs free energies. Interestingly, the too large calculated inversion barriers (in comparison with experimental activation energies) when accounting for dispersion and solvation have recently been found for azobispyrazoles [68].

The lifetimes corresponding to the two inversion pathways are different, allowing one to assign a faster and a slower pathway (Fig. 5). That being said, the lifetime for the faster pathway (calculated taking into account PCM and D3 corrections) is still longer than the experimental lifetime.

For **1-pyr**, we found an inversion and a rotation transition states (on the RDFT level) with virtually the same activation barrier. These two transition states correspond to the same *cis* conformation. In this case, the total rate constant was calculated as the sum of rate constants corresponding to rotation and inversion, and the lifetime was calculated as the

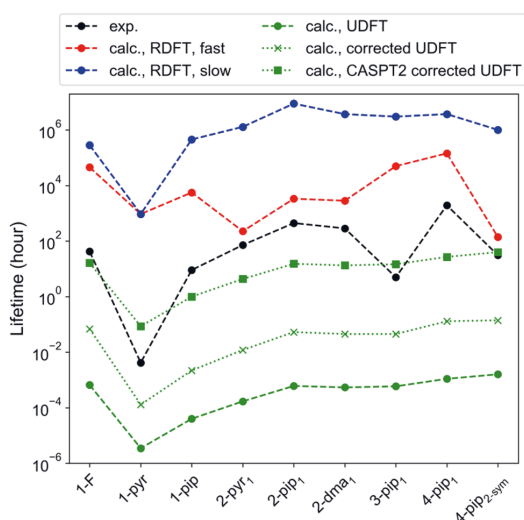


Fig. 5 Comparison of experimental and calculated lifetimes of thermal $Z \rightarrow E$ isomerization. The rotational pathway was treated with the UB3LYP+D3(BJ)/6-31G*/PCM(ACN) method (green curves) and the inversion pathway with RB3LYP+D3(BJ)/6-31G*/PCM(ACN) (red and blue curves). “Corrected UDFT” corresponds to the activation barriers corrected using the approach by Yamaguchi et al. [69] “CASPT2 corrected UDFT” corresponds to $\Delta G_{UDFT}^\ddagger + 0.26$ eV barriers, where 0.26 eV comes from the difference in UDFT and CASPT2 energies of parent azobenzene (taken from ref [70]). See text for the details

inverse of the total rate constant. Yet, this lifetime is much larger than that found in experiment (Fig. 5).

We also considered the rotational pathway for all selected molecules applying broken-symmetry UDFT. The rotational transition states (with the CNNC dihedral of about 90° and both CNN units bent) are expected to exhibit homolytic cleavage of the azo bond and, therefore, RDFT is expected to fail [70, 71]. Interestingly, for the recently introduced azobispyrazole family mentioned above, the rotational barriers calculated with UDFT were found to be lower than the experimental ones, in contrast to the inversion barriers (see above)[68].

We were able to locate rotation transition states for all selected molecules using the broken-symmetry UDFT, namely UB3LYP+D3(BJ)/6-31G*/PCM(ACN). The corresponding lifetimes calculated using UDFT barriers are too short (by a factor of 10^{-3} – 10^{-6}) when comparing to the experiment (Fig. 5). Yet, the $\langle S^2 \rangle$ values (at the rotational TS geometries) are slightly above 1 for all the studied molecules, meaning that the electronic state is a mixed-spin state of singlet and higher multiplets. To estimate the energy of a pure-singlet state, with $\langle S^2 \rangle = 0$, (at the rotational TS geometry) we used the approach proposed by Yamaguchi et al. (see sect 4.4) [69]. The lifetimes calculated from the

corrected barriers, while being shorter than the experimental ones, are closer to the experiment than the uncorrected UDFT lifetimes (Fig. 5). Moreover, for azobenzene, the difference between energies calculated with broken-symmetry UB3LYP and CASPT2 (at the rotational TS geometry) was found to be $E_{\text{CASPT2}} - E_{\text{UB3LYP}} \approx 0.26$ eV (6 kcal/mol) [70]. Therefore, we also tried to correct $\Delta G_{\text{UDFT}}^\ddagger$ as $\Delta G_{\text{UDFT}}^\ddagger + 0.26$ eV, to estimate the correction coming from a multireference treatment. The lifetimes calculated using this approach (called “CASPT2 corrected UDFT”) are in fairly good agreement with the experimental lifetimes. Moreover, the trend in experimental lifetimes with changing the amine is qualitatively reproduced (Fig. 5). In particular, for series **1-x** and **2-x₁** the experimental and computational trends coincide. We note that, while quantitative lifetimes may be wrong, the correct trends are also followed by the other theoretical treatments reported in Fig. 5.

Finally, several reports proposed that the thermal *cis* → *trans* isomerization may proceed via a nonadiabatic pathway involving the ground (lowest) singlet and triplet states, *i.e.* $S_0 \rightarrow T_1 \rightarrow S_0$ transitions [70, 72, 73]. This hypothesis is based on (i) the fact that for azobenzene, the T_1 state is located below the S_0 state at the geometries close to the rotational transition state, and (ii) sufficiently large spin–orbit coupling along the rotational pathway [72].

To check the triplet energetics for our molecules, we calculated the energy of the T_1 state at the rotational TS geometry. We also optimized the geometry in the T_1 state (starting from the rotational transition state). Similar to the parent azobenzene, the triplet state (T_1) was found to be lower than the singlet state (S_0) at the geometries near the rotational transition state for all the molecules (Table S8). One thus cannot exclude the nonadiabatic pathway from consideration. We also note that the optimized triplet geometries are similar to the optimized UDFT rotational transition states, *i.e.* the minimum of the T_1 PES is located on the rotational pathway.

In summary, our calculations indicate that for the investigated molecules, the thermal isomerization proceeds via rotation, which, in turn, may occur on the ground-state singlet PES or, probably, involves the nonadiabatic singlet–triplet pathway.

2.5 Proline derivatives

The spectral properties and photoswitching dynamics of the prolinol, proline ester and prolinamide series are close to those of the respective pyrrolidine-substituted azobenzenes: for example, **2-prol₁**, **2-pres₁** and **2-pram₁** can all be cycled with 405 and 595 nm the same way as **2-pyr₁** (Table S5), and the *cis*-lifetime of **2-prol₁** is actually even longer than for **2-pyr₁** (131 vs 72 h, Table 2). Similarly, **3-pram₁** is

isomerized to both directions even more efficiently than **3-pyr₁**. As an unexpected benefit, prolinamido-substituted products proved to be particularly robust towards decomposition over time, a problem especially associated with pyrrolidine-substituted azobenzenes.

In this light, the utilization of the proline derivatives for *ortho*-linkage to, *e.g.*, biologically active molecules or polymeric materials while simultaneously gaining good photochemical properties seems feasible. We also noticed that the introduction of two prolinamido units into the system (**4-pram_{2sym}**) was enough to promote water solubility from 0 to > 500 μM (Fig. S143) without compromising the photoswitching qualities. When more hydrophilic moieties are linked to the amines, even better water solubility will be attained.

3 Conclusions

We have synthesized and characterized 41 *ortho*-fluorinated and -aminated azobenzenes, varying the substitution pattern, degree of amination and choice of amine. Our simple synthetic routes yield *ortho*-aminofluoroazobenzenes, new photoswitches that combine the exceptionally long *cis*-lifetimes of *ortho*-fluorinated azobenzenes with the high visible-range absorptivity of *ortho*-aminated azobenzenes. Through systematic studies, we have determined how the aforementioned structural factors affect the photochemical properties. Compared to the parent *ortho*-fluoroazobenzenes, the degree to which the properties of the amino-substituted products differ depends on the π donation strength of the amino substituent: a strong donor such as pyrrolidine promotes the visible light absorptivity more than other amines, whereas piperidine, a weaker donor, preserves the long *cis*-lifetime better. DFT calculations revealed non-planarity of the *trans*-isomers and TD-DFT calculations disclosed the nature of three absorption bands. The experimental trends for band shifts and changes in absorbance upon varying the substituents were semi-quantitatively reproduced. Moreover, the calculations indicated a preference for the rotational pathway for thermal *cis* → *trans* isomerization and corroborated trends within a given class of molecules.

Three of the studied substitution patterns (series **2-x₁**, **4-x₁** and **4-x_{2sym}**) yielded nearly bistable photoswitches, *cis*-lifetimes in solution ranging from several hours to weeks at 25 °C. Of these, the most promising switches were **2-pyr₁** that could be switched efficiently to both directions with 405 and 595 nm (*trans*-to-*cis* and *cis*-to-*trans*, respectively), and **4-pip₁** that could be driven efficiently to *cis* with as long wavelengths as 595 nm. For applications where relatively fast (seconds to minutes) thermal isomerization is desired, series **1-x** and **3-x₁** provide systems that can be driven with visible light to either direction. In all cases, the

photostationary state is reached extremely fast compared to, e.g., reported *ortho*-chlorinated azobenzenes. Lastly, we have shown that inexpensive L-proline derivatives can be used to synthesize switches with similar photochemical properties as the respective pyrrolidino-substituted compounds, paving the way towards easy *ortho*-linkage.

4 Methods

4.1 Synthetic procedures

Synthetic work was carried out in Tampere University. All reagents and solvents were commercial and purchased from Sigma Aldrich, TCI Europe, VWR or FluoroChem. The *ortho*-aminated azobenzenes were synthesized by stirring an *ortho*-fluorinated precursor and the selected amine in acetonitrile in ambient conditions. The amount of amine, reaction time and temperature were chosen with respect to the reactivity of the precursor and the desired degree of substitution (see Table 1 and Supplementary Methods). The synthesis of **4-pip₁**, **4-pip_{2-sym}** and **4-pip_{2-asy}** is exemplary: Tetra-*ortho*-fluorinated precursor **4-F** (31.1 mg, 0.1 mmol) and pyrrolidine (16.5 μ l, 0.2 mmol) were stirred in acetonitrile (1 ml) at room temperature for 2 h. The reaction mixture was then concentrated under reduced pressure and purified by column chromatography (10–20% ethyl acetate in hexane) to yield **4-pyr₁** (19 mg, 52%) as an orange solid, **4-pyr_{2-sym}** (4.0 mg, 9.6%) as a red solid and **4-pyr_{2-asy}** (4.0 mg, 9.6%) as an orange-brown solid. Unreacted **4-F** (5 mg, 16%) was also recovered. Reactions were monitored with thin-layer chromatography (TLC) on commercial Merck Silica 60 F₂₅₄ TLC plates, and the developed plates were visualized with UV irradiation (254 nm) or with potassium permanganate and cerium ammonium molybdate stains. The nuclear magnetic resonance (NMR) and high-resolution mass spectroscopy results are given in Supplementary Methods and NMR spectra are depicted in Fig. S1–S94.

Accurate mass experiments were performed with Agilent 6560 Ion mobility Q-TOF mass spectrometer, which was equipped with dualAJS ESI ion source. The compounds were dissolved in DCM (1 mg/ml) and samples were prepared with 1 μ M concentration in methanol. Samples were injected from syringe pump generally with 5 μ l/min flowrate. ES tuning mix (Agilent technologies) was used for calibration. The exact mass values were calculated using Isotope Distribution Calculator (part of Agilent MassHunter Data Analysis Core) and the data was analyzed using MassHunter Workstation Software B08.00 from Agilent Technologies, USA. Characterization was done using accurate mass values (limit values < 3 mDa or < 5 ppm) and fit of isotopic distributions. In case of overlapping distributions, the result was

verified with measurement of ion mobility mass spectra (IM-MS).

The NMR spectra were measured with a 500 MHz JEOL ECZR 500 (125 MHz for ¹³C) at 25 °C and processed with the JEOL Delta NMR software version 5.3.1 (Windows).

4.2 Photochemical studies

UV–Visible absorption spectra were recorded with an Agilent Cary 60 spectrophotometer equipped with an Ocean Optics Qpod 2e Peltier-thermostated cell holder whose temperature accuracy is 0.1 °C. Photoexcitation was conducted using a Prior Lumen 1600 light source containing multiple narrow-band LEDs at different wavelengths. The spectra of the LEDs were measured with the aforementioned spectrophotometer without taking into account the wavelength dependency in the sensitivity of the sensor. The illumination intensities were acquired by measuring the illumination powers with a Coherent LabMax thermal power meter and dividing the number by the area of the cuvette being illuminated (0.78 cm²). Full-width-half-maximum values and illumination intensities are shown in Table S5. Quartz fluorescence cuvettes with an optical path of 1.0 cm were used for all measurements. The molar absorption coefficients were calculated with the Beer–Lambert law for each distinguishable absorption peak. For figures the absorption spectra were normalized to 1 with respect to the π – π^* band.

Photostationary state (PSS) refers to the mixture of isomers upon constant illumination with a chosen excitation wavelength. Dark, in turn, refers to the mixture of isomers after an elongated period in a dark cavity at room temperature or at an elevated temperature. Based on the thermal relaxation lifetime of the molecules, the time and temperature were chosen so that the mixture would consist of azobenzenes only in the *trans* state.

The photostationary state compositions were determined by comparing the absorbance values of the photostationary state mixture with those in the dark spectrum. The *cis*-fraction was calculated from the wavelength that had the greatest difference in the absorbance values. If the *cis*-absorbance at this wavelength is assumed zero and the dark spectrum is assumed to equal to that of pure *trans* isomer, the *cis*-fraction is $1 - Abs_{pss}/Abs_{dark}$. This is a minimum value, as the *cis*-absorbance is typically non-zero. If the dark spectrum is not entirely *trans* (i.e., the mixture has not been in dark for long enough to isomerize completely to *trans*), this will also lower the calculated *cis*-fraction compared to the true value. However, these values are relatively accurate: for instance, for **4-dma_{2-sym}** the isomer composition calculated from an NMR sample

after prolonged irradiation is 58% *cis* and 42% *trans* (Fig. S94a), exactly the composition estimated from the UV–Vis spectra.

4.3 Thermal isomerization studies

The thermal isomerization rates were determined with the same methodology as in our earlier study [42]. The 50–150 μM acetonitrile solutions were illuminated with 365, 385 or 405 nm light until a photostationary state was reached. The illumination was then stopped and the absorbance near the absorption maximum of the *trans* isomer was monitored as a function of time. The measured absorbance values were fitted with a monoexponential function. If the thermal *cis*-to-*trans* isomerization was fast, one measurement at 25 °C was carried out. Otherwise, the rates were determined at 50, 60 and 70 °C and extrapolated to 25 °C using the Arrhenius equation. The analyses are presented for all new compounds in Fig. S95–S127.

4.4 Computational studies

All calculations were done with Gaussian 16, revision C.01 [74]. The B3LYP functional [43, 44] with D3(BJ) [45] dispersion correction and PCM(ACN) [47, 48] has been used for geometry optimizations to produce structures for spectra calculations. Low-lying electronically excited states have been calculated with TD-DFT [52] using B3LYP and $\omega\text{B97X-D}$ [54] functionals, with PCM(ACN). Natural transition orbitals (NTOs) [57] have been computed (using Gaussian) to visualize the nature of the excited states.

NTO analysis allows one to simplify an orbital description of electronic transitions. Often, a single NTO hole–particle pair may describe the transition in question whereas several conventional occupied–virtual orbital pairs are needed to characterize the same transition. Upon the electronic transition the excited electron goes from the hole NTO to the particle NTO.

The geometries of the transition states (TSs) and the *cis* (Z) isomers have been optimized using spin-restricted (R) and spin-unrestricted (U) B3LYP+D3(BJ)/6-31G*/PCM(ACN) calculations. In the case of spin-restricted calculations, we have also performed calculations without dispersion correction and without PCM to determine the influence of these corrections on thermal lifetimes. Reaction rate constants for the thermal *cis* \rightarrow *trans* isomerization have been calculated using Eyring's transition state theory [64]:

$$k = \frac{k_B T}{h} \exp\left(-\frac{\Delta G^\ddagger}{k_B T}\right)$$

and the corresponding thermal lifetime as:

$$\tau = \frac{1}{k}.$$

Here, k_B and h are the Boltzmann and Planck constants, respectively, and T is the temperature. We used $T = 298.15\text{ K}$ (25 °C). $\Delta G^\ddagger = G(\text{TS}) - G(\text{Z})$ is the activation Gibbs free energy.

We located transition states using the Berny algorithm as implemented in Gaussian (TS keyword). Intrinsic reaction coordinate [66, 67] calculations (IRC keyword) have been done to locate the corresponding *cis* isomers, which have been further reoptimized. We have located two transition states and two *cis* isomers for each molecule. Energy differences between different *cis* isomers of the same molecule were calculated with respect to the lowest energy *cis*-isomer (of two isomers) of this molecule:

$$\Delta B_{ZZ}^{\text{rel}} = B(Z_i) - B(Z_{\text{lowest energy}}); B = G, E;$$

G is Gibbs free energy; E is energy, *i.e.* a point on the potential energy surface (PES). Thus, $\Delta B_{ZZ}^{\text{rel}} = 0$ for the lowest energy *cis*-isomer, and positive for the second isomer.

Normal mode analysis has been performed to confirm the nature of minima (no imaginary frequency) and transition states (one imaginary frequency).

In the case of spin-unrestricted calculations (performed at the UB3LYP+D3(BJ)/6-31G*/PCM(ACN) level), the Guess(Mix) keyword was used to generate an initial orbital guess, and the broken-symmetry solution was found for all considered molecules. The $\langle S^2 \rangle$ values (at the rotational TS geometries) were slightly above 1 for all the molecules.

To estimate the energy of a pure-singlet state $\Delta E_{\text{UDFT}}^{(S,\ddagger)}$ (at the rotational TS geometry), we used an approach proposed by Yamaguchi et al. [69]

$$\Delta E_{\text{UDFT}}^{(S,\ddagger)} = \Delta E_{\text{UDFT}}^\ddagger + \frac{\langle S^2 \rangle}{2 - \langle S^2 \rangle} \left(\Delta E_{\text{UDFT}}^\ddagger - \Delta E_{\text{UDFT}}^{(T,\ddagger)} \right).$$

Here, the $\langle S^2 \rangle$ values are for rotational TSs, *i.e.*, about 1; $\Delta E_{\text{UDFT}}^\ddagger$ is the energy of the mixed-spin state, and $\Delta E_{\text{UDFT}}^{(T,\ddagger)}$ is the energy of the triplet state at the rotational TS geometry. The second term on the r.h.s. was added to the UDFT activation Gibbs free energies $\Delta G_{\text{UDFT}}^\ddagger$ to obtain the corrected activation Gibbs free energies $\Delta G_{\text{UDFT}}^{(S,\ddagger)}$ corresponding to the pure-singlet state.

The lowest triplet state was optimized starting from the rotational TS structures using the same level of theory, *i.e.*, UB3LYP+D3(BJ)/6-31G*/PCM(ACN). The $\langle S^2 \rangle$ values were slightly above 2, for the optimized triplets. The optimized triplet geometries are similar to the rotational TS structures.

In all the calculations, the 6-31G* basis set [46] has been used.

The molecular structures and NTOs have been visualized using Jmol, an open-source Java viewer for chemical structures in 3D (<http://www.jmol.org/>).

Supplementary Information The online version contains supplementary material available at <https://doi.org/10.1007/s43630-021-00145-4>.

Acknowledgements Financial support of the European Research Council (Starting Grant Project PHOTOTUNE, Decision Number 679646) is gratefully acknowledged. The work is conducted as part of the Academy of Finland Flagship Programme, Photonics Research and Innovation (PREIN), Decision Number 321065. K.K. is grateful for the financial support of Tampere University graduate school. E.T. is grateful to the Deutsche Forschungsgemeinschaft (DFG, German Research Foundation) for the financial support (project number 454020933). (Gefördert durch die Deutsche Forschungsgemeinschaft (DFG) – Projekt Nummer 454020933.) The authors would like to thank Prof. Stefan Hecht for many fruitful discussions on azobenzenes.

Author contributions KK, JV and ZA carried out the experimental work, except for the mass spectra that were measured by EK, ET carried out the computational studies. KK and ET wrote the manuscript with the help of all authors. AP and PS initiated, supervised and funded the work, with partial funding acquired by KK and ET.

Funding H2020 European Research Council, 679646, Arri Priimägi, Luonnontieteiden ja Tekniikan Tutkimuksen Toimikunta, 321065, Graduate School, Tampere University, Deutsche Forschungsgemeinschaft, 454020933, Evgenii Titov

Data availability The datasets generated during and/or analyzed during the current study are available from the corresponding author on reasonable request.

Declarations

Conflict of interest The authors declare no competing interests.

Open Access This article is licensed under a Creative Commons Attribution 4.0 International License, which permits use, sharing, adaptation, distribution and reproduction in any medium or format, as long as you give appropriate credit to the original author(s) and the source, provide a link to the Creative Commons licence, and indicate if changes were made. The images or other third party material in this article are included in the article's Creative Commons licence, unless indicated otherwise in a credit line to the material. If material is not included in the article's Creative Commons licence and your intended use is not permitted by statutory regulation or exceeds the permitted use, you will need to obtain permission directly from the copyright holder. To view a copy of this licence, visit <http://creativecommons.org/licenses/by/4.0/>.

References

- Bandara, H. M. D., & Burdette, S. C. (2012). Photoisomerization in different classes of azobenzene. *Chemical Society Reviews*, 41, 1809–1825. <https://doi.org/10.1039/c1cs15179g>.
- Irie, M., Fukaminato, T., Matsuda, K., & Kobatake, S. (2014). Photochromism of diarylethene molecules and crystals: memories, switches, and actuators. *Chemical Reviews*, 114, 12174–12277. <https://doi.org/10.1021/cr500249p>.
- Zhang, J., & Tian, H. (2018). The endeavor of diarylethenes: new structures, high performance, and bright future. *Advanced Optical Materials*, 6, 1701278. <https://doi.org/10.1002/adom.201701278>.
- Kortekaas, L., & Browne, W. R. (2019). The evolution of spiropyran: fundamentals and progress of an extraordinarily versatile photochrome. *Chemical Society Reviews*, 48, 3406–3424. <https://doi.org/10.1039/C9CS00203K>.
- Klajn, R. (2014). Spiropyran-based dynamic materials. *Chemical Society Reviews*, 43, 148–184. <https://doi.org/10.1039/C3CS60181A>.
- Lukyanov, B. S., & Lukyanova, M. B. (2005). Spiropyrans: synthesis, properties, and application. *Chemistry of Heterocyclic Compounds*, 41, 1–31.
- Velema, W. A., Szymanski, W., & Feringa, B. L. (2014). Photopharmacology: beyond proof of principle. *Journal of the American Chemical Society*, 136, 2178–2191. <https://doi.org/10.1021/ja413063e>.
- Broichhagen, J., Frank, J. A., & Trauner, D. (2015). A roadmap to success in photopharmacology. *Accounts of Chemical Research*, 48, 1947–1960. <https://doi.org/10.1021/acs.accounts.5b00129>.
- Lerch, M. M., Hansen, M. J., van Dam, G. M., et al. (2016). Emerging targets in photopharmacology. *Angewandte Chemie International Edition*, 55, 10978–10999. <https://doi.org/10.1002/anie.201601931>.
- Hüll, K., Morstein, J., & Trauner, D. (2018). In vivo photopharmacology. *Chemical Reviews*, 118, 10710–10747. <https://doi.org/10.1021/acs.chemrev.8b00037>.
- Fuchter, M. J. (2020). On the promise of photopharmacology using photoswitches: a medicinal chemist's perspective. *Journal of Medicinal Chemistry*, 63, 11436–11447. <https://doi.org/10.1021/acs.jmedchem.0c00629>.
- Neilson, B. M., & Bielawski, C. W. (2013). Illuminating photo-switchable catalysis. *ACS Catalysis*, 3, 1874–1885. <https://doi.org/10.1021/cs4003673>.
- Göstl, R., Senf, A., & Hecht, S. (2014). Remote-controlling chemical reactions by light: towards chemistry with high spatio-temporal resolution. *Chemical Society Reviews*, 43, 1982–1996. <https://doi.org/10.1039/c3cs60383k>.
- Stoll, R. S., & Hecht, S. (2010). Artificial light-gated catalyst systems. *Angewandte Chemie—International Edition*, 49, 5054–5075. <https://doi.org/10.1002/anie.201000146>.
- Zhang, J., Zou, Q., & Tian, H. (2013). Photochromic materials: more than meets the eye. *Advanced Materials*, 25, 378–399. <https://doi.org/10.1002/adma.201201521>.
- Goulet-Hanssens, A., Eisenreich, F., & Hecht, S. (2020). Enlightening materials with photoswitches. *Advanced Materials*, 32, 1905966. <https://doi.org/10.1002/adma.201905966>.
- Moulin, E., Faour, L., Carmona-Vargas, C. C., & Giuseppone, N. (2020). From molecular machines to stimuli-responsive materials. *Advanced Materials*, 32, 1906036. <https://doi.org/10.1002/adma.201906036>.
- Lancia, F., Ryabchun, A., & Katsonis, N. (2019). Life-like motion driven by artificial molecular machines. *Nature Reviews Chemistry*, 3, 536–551. <https://doi.org/10.1038/s41570-019-0122-2>.
- Dong, M., Babalhavaeji, A., Samanta, S., et al. (2015). Red-shifting Azobenzene Photoswitches for in vivo use. *Accounts of Chemical Research*, 48, 2662–2670. <https://doi.org/10.1021/acs.accounts.5b00270>.
- Mosciatti, T., Bonacchi, S., Gobbi, M., et al. (2016). Optical input/electrical output memory elements based on a liquid crystalline azobenzene polymer. *ACS Applied Materials & Interfaces*, 8, 6563–6569. <https://doi.org/10.1021/acsami.5b12430>.
- Shi, Y., Gerkman, M. A., Qiu, Q., et al. (2021). Sunlight-activated phase change materials for controlled heat storage and triggered

- release. *Journal of Materials Chemistry A*, 9, 9798–9808. <https://doi.org/10.1039/D1TA01007G>.
22. Gerkman, M. A., Gibson, R. S. L., Calbo, J., et al. (2020). Arylazopyrazoles for long-term thermal energy storage and optically triggered heat release below 0 °C. *Journal of the American Chemical Society*, 142, 8688–8695. <https://doi.org/10.1021/jacs.0c00374>.
 23. Lahikainen, M., Zeng, H., & Priimagi, A. (2018). Reconfigurable photoactuator through synergistic use of photochemical and photothermal effects. *Nature Communications*, 9, 4148. <https://doi.org/10.1038/s41467-018-06647-7>.
 24. Iamsaard, S., Anger, E., Abhoff, S. J., et al. (2016). Fluorinated azobenzenes for shape-persistent liquid crystal polymer networks. *Angewandte Chemie—International Edition*, 55, 9908–9912. <https://doi.org/10.1002/anie.201603579>.
 25. Ryabchun, A., Li, Q., Lancia, F., et al. (2019). Shape-persistent actuators from hydrazone photoswitches. *Journal of the American Chemical Society*, 141, 1196–1200. <https://doi.org/10.1021/jacs.8b11558>.
 26. Lauer, A., Fast, D. E., Steinkoenig, J., et al. (2017). Wavelength-dependent photochemical stability of photoinitiator-derived macromolecular Chain Termini. *ACS Macro Letters*, 6, 952–958. <https://doi.org/10.1021/acsmacrolett.7b00499>.
 27. Yousif, E., & Haddad, R. (2013). Photodegradation and photostabilization of polymers, especially polystyrene: Review. *Springerplus*, 2, 398. <https://doi.org/10.1186/2193-1801-2-398>.
 28. Aleotti, F., Nenov, A., Salvigni, L., et al. (2020). Spectral tuning and photoisomerization efficiency in push-pull azobenzenes: designing principles. *Journal of Physical Chemistry A*, 124, 9513–9523. <https://doi.org/10.1021/acs.jpca.0c08672>.
 29. Eom, T., & Khan, A. (2021). Push-pull azobenzene chromophores with negative halochromism. *Dyes and Pigments*, 188, 109197. <https://doi.org/10.1016/j.dyepig.2021.109197>.
 30. Dokić, J., Gothe, M., Wirth, J., et al. (2009). Quantum chemical investigation of thermal Cis-to-Trans isomerization of azobenzene derivatives: Substituent effects, solvent effects, and comparison to experimental data. *Journal of Physical Chemistry A*, 113, 6763–6773. <https://doi.org/10.1021/jp9021344>.
 31. Knie, C., Utecht, M., Zhao, F., et al. (2014). Ortho-fluoroazobenzenes: Visible light switches with very long-lived Z isomers. *Chemistry—A European Journal*, 20, 16492–16501. <https://doi.org/10.1002/chem.201404649>.
 32. Siewertsen, R., Neumann, H., Buchheim-Stehn, B., et al. (2009). Highly efficient reversible Z-E photoisomerization of a bridged azobenzene with visible light through resolved S(1)(n pi*) absorption bands. *Journal of the American Chemical Society*, 131, 15594–15595. <https://doi.org/10.1021/ja906547d>.
 33. Beharry, A. A., Sadoski, O., & Woolley, G. A. (2011). Azobenzene photoswitching without ultraviolet light. *Journal of the American Chemical Society*, 133, 19684–19687. <https://doi.org/10.1021/ja209239m>.
 34. Bléger, D., Schwarz, J., Brouwer, A. M., & Hecht, S. (2012). o-Fluoroazobenzenes as readily synthesized photoswitches offering nearly quantitative two-way isomerization with visible Light. *Journal of the American Chemical Society*, 134, 20597–20600. <https://doi.org/10.1021/ja310323y>.
 35. Ditter, D., Braun, L. B., & Zentel, R. (2020). Influences of ortho-fluoroazobenzenes on liquid crystalline phase stability and 2D (Planar) actuation properties of liquid crystalline elastomers. *Macromolecular Chemistry and Physics*, 221, 1900265. <https://doi.org/10.1002/macp.201900265>.
 36. Leistner, A.-L., Kirchner, S., Karcher, J., et al. (2021). Fluorinated azobenzenes switchable with red light. *Chemistry—A European Journal*, 27, 8094–8099. <https://doi.org/10.1002/chem.202005486>.
 37. Wegener, M., Hansen, M. J., Driessen, A. J. M., et al. (2017). Photocontrol of antibacterial activity: shifting from UV to Red Light Activation. *Journal of the American Chemical Society*, 139, 17979–17986. <https://doi.org/10.1021/jacs.7b09281>.
 38. Konrad, D. B., Savasci, G., Allmendinger, L., et al. (2020). Computational design and synthesis of a deeply red-Shifted and bistable azobenzene. *Journal of the American Chemical Society*, 142, 6538–6547. <https://doi.org/10.1021/jacs.9b10430>.
 39. Lameijer, L. N., Budzak, S., Simeth, N. A., et al. (2020). General principles for the design of visible-light-responsive photoswitches: tetra- ortho -chloro-azobenzenes. *Angewandte Chemie*. <https://doi.org/10.1002/ange.202008700>.
 40. Sadoski, O., Beharry, A. A., Zhang, F., & Woolley, G. A. (2009). Spectral tuning of azobenzene photoswitches for biological applications. *Angewandte Chemie International Edition*, 48, 1484–1486. <https://doi.org/10.1002/anie.200805013>.
 41. Boulègue, C., Löwenek, M., Renner, C., & Moroder, L. (2007). Redox potential of azobenzene as an amino acid residue in peptides. *ChemBioChem*, 8, 591–594. <https://doi.org/10.1002/cbic.200600495>.
 42. Ahmed, Z., Siiskonen, A., Virkki, M., & Priimagi, A. (2017). Controlling azobenzene photoswitching through combined: Ortho -fluorination and -amination. *Chemical Communications*, 53, 12520–12523. <https://doi.org/10.1039/c7cc07308a>.
 43. Becke, A. D. (1993). Density-functional thermochemistry. III. The role of exact exchange. *The Journal of Chemical Physics*, 98, 5648–5652. <https://doi.org/10.1063/1.464913>.
 44. Stephens, P. J., Devlin, F. J., Chabalowski, C. F., & Frisch, M. J. (1994). Ab initio calculation of vibrational absorption and circular dichroism spectra using density functional force fields. *Journal of Physical Chemistry*, 98, 11623–11627. <https://doi.org/10.1021/j100096a001>.
 45. Grimme, S., Ehrlich, S., & Goerigk, L. (2011). Effect of the damping function in dispersion corrected density functional theory. *Journal of Computational Chemistry*, 32, 1456–1465. <https://doi.org/10.1002/jcc.21759>.
 46. Hariharan, P. C., & Pople, J. A. (1973). The influence of polarization functions on molecular orbital hydrogenation energies. *Theoretica Chimica Acta*, 28, 213–222. <https://doi.org/10.1007/BF00533485>.
 47. Miertuš, S., Scrocco, E., & Tomasi, J. (1981). Electrostatic interaction of a solute with a continuum. A direct utilization of AB initio molecular potentials for the prevision of solvent effects. *Chemical Physics*, 55, 117–129. [https://doi.org/10.1016/0301-0104\(81\)85090-2](https://doi.org/10.1016/0301-0104(81)85090-2).
 48. Scalmani, G., & Frisch, M. J. (2010). Continuous surface charge polarizable continuum models of solvation I. General formalism. *The Journal of Chemical Physics*, 132, 114110. <https://doi.org/10.1063/1.3359469>.
 49. Cusati, T., Granucci, G., Persico, M., & Spighi, G. (2008). Oscillator strength and polarization of the forbidden n→π* band of trans-azobenzene: a computational study. *The Journal of Chemical Physics*, 128, 194312. <https://doi.org/10.1063/1.2925678>.
 50. Hepworth, J. D., Mason, D., Hallas, G., & Marsden, R. (1985). The effects of cyclic terminal groups in 44minoazo-benzene and related Azo dyes: Part 2'f-p& values of some monoazo dyes derived from IV-phenylpyrrolidine and N-Phenylpiperidine. *Dyes and Pigments*, 6, 389–396.
 51. Brown, H. C., Brewster, J. H., & Shechter, H. (1954). An interpretation of the chemical behavior of Five- and Six-membered Ring compounds. *Journal of the American Chemical Society*, 76, 467–474. <https://doi.org/10.1021/ja01631a041>.
 52. Casida, M. E. (1995). Time-dependent density functional response theory for molecules. in *Recent advances in density functional methods* (pp. 155–192). World Scientific.

53. Mennucci, B. (2015). Modeling absorption and fluorescence solvatochromism with QM/Classical approaches. *International Journal of Quantum Chemistry*, 115, 1202–1208. <https://doi.org/10.1002/qua.24889>.
54. Chai, J.-D., & Head-Gordon, M. (2008). Long-range corrected hybrid density functionals with damped atom–atom dispersion corrections. *Physical Chemistry Chemical Physics: PCCP*, 10, 6615–6620. <https://doi.org/10.1039/B810189B>.
55. Titov, E., & Saalfrank, P. (2016). Exciton splitting of adsorbed and Free 4-Nitroazobenzene dimers: a quantum chemical study. *Journal of Physical Chemistry A*, 120, 3055–3070. <https://doi.org/10.1021/acs.jpca.5b10376>.
56. Titov, E., Hummert, J., Ikonnikov, E., et al. (2021). Electronic relaxation of aqueous aminoazobenzenes studied by time-resolved photoelectron spectroscopy and surface hopping TDDFT dynamics calculations. *Faraday Discussions*. <https://doi.org/10.1039/D0FD00111B>.
57. Martin, R. L. (2003). Natural transition orbitals. *The Journal of Chemical Physics*, 118, 4775–4777. <https://doi.org/10.1063/1.1558471>.
58. Sršeň, Š., Sita, J., Slavíček, P., et al. (2020). Limits of the nuclear ensemble method for electronic spectra simulations: temperature dependence of the (E)-azobenzene spectrum. *Journal of Chemical Theory and Computation*, 16, 6428–6438. <https://doi.org/10.1021/acs.jctc.0c00579>.
59. Isokuortti, J., Kuntze, K., Virkki, M., et al. (2021). Expanding excitation wavelengths for azobenzene photoswitching into the near-infrared range via endothermic triplet energy transfer. *Chemical Science*. <https://doi.org/10.1039/D1SC01717A>.
60. Goulet-Hanssens, A., Utecht, M., Mutruc, D., et al. (2017). Electrocatalytic Z → E Isomerization of Azobenzenes. *Journal of the American Chemical Society*, 139, 335–341. <https://doi.org/10.1021/jacs.6b10822>.
61. Goulet-Hanssens, A., Rietze, C., Titov, E., et al. (2018). Hole catalysis as a general mechanism for efficient and wavelength-independent Z → E azobenzene isomerization. *Chem*, 4, 1740–1755. <https://doi.org/10.1016/j.chempr.2018.06.002>.
62. Hallett-Tapley, G. L., D'Alfonso, C., Pacioni, N. L., et al. (2013). Gold nanoparticle catalysis of the cis–trans isomerization of azobenzene. *Chemical Communications*, 49, 10073–10075. <https://doi.org/10.1039/C3CC41669K>.
63. Titov, E., Lysyakova, L., Lomadze, N., et al. (2015). Thermal Cis-to-Trans isomerization of azobenzene-containing molecules enhanced by gold nanoparticles: an experimental and theoretical study. *Journal of Physical Chemistry C*, 119, 17369–17377. <https://doi.org/10.1021/acs.jpcc.5b02473>.
64. Eyring, H. (1935). The activated complex and the absolute rate of chemical reactions. *Chemical Reviews*, 17, 65–77. <https://doi.org/10.1021/cr60056a006>.
65. Rietze, C., Titov, E., Lindner, S., & Saalfrank, P. (2017). Thermal isomerization of azobenzenes: on the performance of Eyring transition state theory. *Journal of Physics: Condensed Matter*, 29, 314002. <https://doi.org/10.1088/1361-648x/aa75bd>.
66. Fukui, K. (1981). The path of chemical reactions—the IRC approach. *Accounts of Chemical Research*, 14, 363–368. <https://doi.org/10.1021/ar00072a001>.
67. Hratchian, H. P., & Schlegel, H. B. (2005). Chapter 10 Finding minima, transition states, and following reaction pathways on ab initio potential energy surfaces. In C. E. Dykstra, G. Frenking, & K. S. Kim (Eds.), *Scuseria GEBT-T and A of CC* (pp. 195–249). Amsterdam: Elsevier.
68. He, Y., Shanguan, Z., Zhang, Z.-Y., et al. (2021). Azobispyrazole family as photoswitches combining (Near-) Quantitative bidirectional isomerization and widely tunable thermal half-lives from hours to years. *Angewandte Chemie International Edition*. <https://doi.org/10.1002/anie.202103705>.
69. Yamaguchi, K., Jensen, F., Dorigo, A., & Houk, K. N. (1988). A spin correction procedure for unrestricted Hartree-Fock and Møller-Plesset wavefunctions for singlet diradicals and polyradicals. *Chemical Physics Letters*, 149, 537–542. [https://doi.org/10.1016/0009-2614\(88\)80378-6](https://doi.org/10.1016/0009-2614(88)80378-6).
70. Gagliardi, L., Orlandi, G., Bernardi, F., et al. (2004). A theoretical study of the lowest electronic states of azobenzene: The role of torsion coordinate in the cis–trans photoisomerization. *Theoretical Chemistry Accounts*, 111, 363–372. <https://doi.org/10.1007/s00214-003-0528-1>.
71. Vela, S., Scheidegger, A., Fabregat, R., & Corminboeuf, C. (2021). Tuning the thermal stability and photoisomerization of azoheteroarenes through Macrocyclic Strain. *Chemistry—A European Journal*, 27, 419–426. <https://doi.org/10.1002/chem.202003926>.
72. Cembran, A., Bernardi, F., Garavelli, M., et al. (2004). On the mechanism of the cis–trans isomerization in the lowest electronic States of Azobenzene: S0, S1, and T1. *Journal of the American Chemical Society*, 126, 3234–3243. <https://doi.org/10.1021/ja038327y>.
73. Heindl, A. H., & Wegner, H. A. (2020). Rational design of azothiophenes—substitution effects on the switching properties. *Chemistry—A European Journal*, 26, 13730–13737. <https://doi.org/10.1002/chem.202001148>.
74. Frisch, M. J., Trucks, G. W., Schlegel, H. B., Scuseria, G. E., Robb, M. A., Cheeseman, J. R., Scalmani, G., Barone, V., Petersson, G. A., Nakatsuji, H., Li, X., Caricato, M., Marenich, A. V., Bloino, J., Janesko, B. G., Gomperts, R., Mennucci, B., Hratchian, H. P., Ortiz, J. V., Izmaylov, A. F., Sonnenberg, J. L., Williams-Young, D., Ding, F., Lipparini, F., Egidi, F., Goings, J., Peng, B., Petrone, A., Henderson, T., Ranasinghe, D., Zakrzewski, V. G., Gao, J., Rega, N., Zheng, G., Liang, W., Hada, M., Ehara, M., Toyota, K., Fukuda, R., Hasegawa, J., Ishida, M., Nakajima, T., Honda, Y., Kitao, O., Nakai, H., Vreven, T., Throssell, K., Montgomery, J. A., Jr., Peralta, J. E., Ogliaro, F., Bearpark, M. J., Heyd, J. J., Brothers, E. N., Kudin, K. N., Staroverov, V. N., Keith, T. A., Kobayashi, R., Normand, J., Raghavachari, K., Rendell, A. P., Burant, J. C., Iyengar, S. S., Tomasi, J., Cossi, M., Millam, J. M., Klene, M., Adamo, C., Cammi, R., Ochterski, J. W., Martin, R. L., Morokuma, K., Farkas, O., Foresman, J. B. & Fox, D. J. (2016). *Gaussian 16, Revision C.01*. Wallingford CT: Gaussian Inc.

PUBLICATION II

Red-light photoswitching of indigos in polymer thin films

Kuntze, K., Viljakka, J., Virkki, M., Huang, C.-Y., Hecht, S. & Priimägi, A.

Chemical Science, vol. 14, p. 2842, 2023

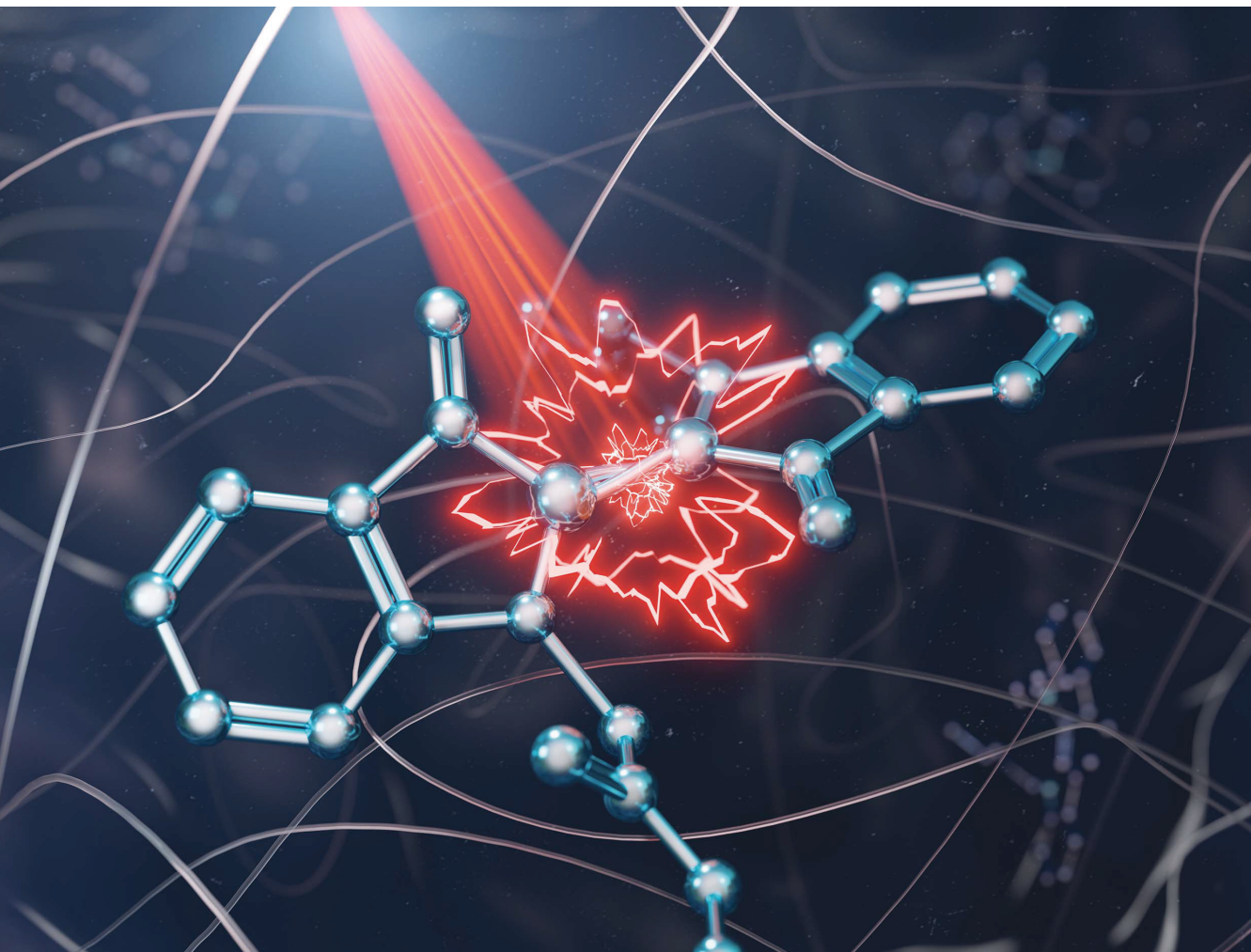
DOI: <https://doi.org/10.1039/D2SC06790K>

Publication reprinted with the permission of the copyright holders.

Chemical Science

Volume 14
Number 10
14 March 2023
Pages 2471–2764

rsc.li/chemical-science



ISSN 2041-6539



ROYAL SOCIETY
OF CHEMISTRY

EDGE ARTICLE

Chung-Yang (Dennis) Huang,
Stefan Hecht, Arri Priimagi *et al.*
Red-light photoswitching of indigos in polymer thin films

Cite this: *Chem. Sci.*, 2023, 14, 2482

All publication charges for this article have been paid for by the Royal Society of Chemistry

Red-light photoswitching of indigos in polymer thin films†

Kim Kuntze,^a Jani Viljakka,^a Matti Virkki,^a Chung-Yang (Dennis) Huang,^b Stefan Hecht^{c,d} and Arri Priimagi^{b,*}

Through simple synthetic derivatisation, the parent indigo dye becomes a red-light *E*–*Z* photoswitch exhibiting negative photochromism and tuneable thermal isomerisation kinetics. These attributes make indigo derivatives extremely attractive for applications related to materials and living systems. However, there is a lack of knowledge in translating indigo photoswitching dynamics from solution to solid state – the environment crucial for most applications. Herein, we study the photoswitching performance of six structurally distinct indigo derivatives in five polymers of varying rigidity. Three key strategies are identified to enable efficient photoswitching under red (660 nm) light: (i) choosing a soft polymer matrix to minimise its resistance toward the isomerisation, (ii) creating free volume around the indigo molecules through synthetic modifications, and (iii) applying low dye loading (<1% w/w) to inhibit aggregation. These strategies are shown to improve both photostationary state distributions and the thermal stability of the *Z* isomer. When all three strategies are implemented, the isomerisation performance (>80% *Z* form in the photostationary state) is nearly identical to that in solution. These findings thus pave the way for designing new red-light photochromic materials based on indigos.

Received 9th December 2022
Accepted 29th January 2023

DOI: 10.1039/d2sc06790k

rsc.li/chemical-science

Introduction

The focus of materials research is steadily shifting towards interactive, “intelligent” materials that adapt to environmental changes and can be controlled with (multiple) external stimuli.^{1,2} Light is arguably the most attractive external stimulus for this purpose as it is non-invasive, waste-free, and can be applied in a highly controllable fashion with superior temporal, spatial and spectral resolution. Thus, systems responding to light are increasingly investigated,^{3,4} with applications emerging in a wide range of research fields from optics^{5,6} and (opto)electronics^{7,8} to photobiology^{9–13} and photomechanics.^{14,15} Among other strategies, photoresponsive materials can be designed by incorporating photochromic molecules (photoswitches) onto the surface of a metal particle¹⁶ or into the bulk

of a macroscopic material. Photoswitches are organic compounds that upon excitation with light of a suitable wavelength interconvert reversibly between two or more isomeric ground state species, inducing changes to the macroscopic properties of a material when the physicochemical characteristics of the involved isomers differ.⁴ A multitude of photoswitches has been developed over the last few decades, mostly based on *E*–*Z* isomerisation around $C=C$,^{17,18} $C=N^{19–21}$ and $N=N^{22,23}$ double bonds or cyclisation reactions.^{24–27}

The wide array of photoswitches with their unique properties has so far provided chemists with flexible options when designing photoresponsive systems with the desired functions. Beyond solution studies, the performance of various photoswitches has been investigated in different solid-like matrices,^{28,29} especially in thin polymer and hydrogel films, where the photochromic molecules can either be covalently bound or simply blended with the polymer matrix.³⁰ Azobenzene thin films, in particular, are increasingly used in the development of smart materials that are reversibly deformed or patterned thanks to the *E*–*Z* switching of photoisomerisable units.^{4–6}

On the other hand, most photoswitches isomerise upon excitation in the ultraviolet region. UV irradiation is absorbed by various materials, causing damage to many polymers and especially to living tissue in addition to suffering from low penetration depth.^{31–33} Hence, extensive research has been carried out to red-shift the isomerisation wavelengths, ultimately aiming for the therapeutic window above 650 nm.^{9,12,34,35}

^aSmart Photonic Materials, Faculty of Engineering and Natural Sciences, Tampere University, FI-33101 Tampere, Finland. E-mail: arri.priimagi@tuni.fi

^bInstitute for Chemical Reaction Design and Discovery (WPI-ICReDD), Hokkaido University, Kita 21, Nishi 10, Kita-ku, Sapporo, Hokkaido 001-0021, Japan. E-mail: dcyluang@icredd.hokudai.ac.jp

^cDepartment of Chemistry & IRIS Adlershof, Humboldt-Universität zu Berlin, Brook-Taylor-Strasse 2, 12489 Berlin, Germany. E-mail: sh@hu-berlin.de

^dDWI – Leibniz Institute for Interactive Materials, Forckenbeckstrasse 50, 52074 Aachen, Germany

† Electronic supplementary information (ESI) available: Supporting results, synthetic details, ¹H NMR, ¹³C NMR and UV-vis spectra of synthesised compounds, sample preparation details, UV-vis spectra and thermal isomerisation graphs of the studied indigo–polymer combinations. See DOI: <https://doi.org/10.1039/d2sc06790k>

To this end, progress has been made by (i) changing the electronic properties of conventional photoswitches such as azobenzenes through structural changes,^{36–41} (ii) designing new photoswitchable scaffolds and structures that intrinsically absorb low-energy light,^{25,42–44} and (iii) exploiting indirect isomerisation using photocatalysts.^{45–47} Yet, the vast majority of these investigations has been restricted to solution, and switching with red or near-infrared light in solid matrices has remained largely unexplored.^{48,49}

With its long history in providing blue colour, indigo is nowadays one of the most widely used dyes (Scheme 1). Structurally, it is composed of two indole-type subunits connected by a central C=C bond. This central double bond conjugates two push-pull pairs of nitrogen/carbonyl groups, and as a result, indigo intrinsically absorbs in the red-light region. Although photoisomerisation of the parent indigo is inhibited by fast excited-state proton transfer,⁵⁰ it is possible to enable photoswitching through *N*-functionalisation. Upon *N*-arylation and/or *N*-alkylation of the parent indigo, efficient isomerisation from the stable *E* isomer to the metastable *Z* form can be realised by red light.⁴⁴ The rate of thermal *Z* → *E* isomerisation can be tuned from seconds to hours, being the slowest for compounds with electron-poor *N*-aryl substituents.⁴⁴ Perhaps most importantly, indigos are negative photochromic compounds: the prominent visible light absorption band is blue-shifted upon *E* → *Z* isomerisation, which enables an increasing amount of red light to penetrate the sample as the content of the photo-generated *Z* isomer increases. These features combined make indigo derivatives attractive candidates for the design of smart materials.

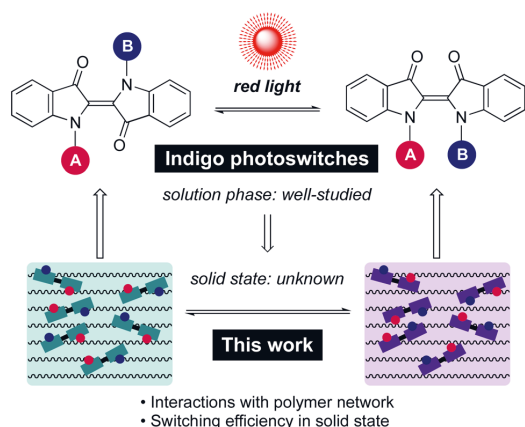
Although the isomerisation of indigo derivatives has been studied extensively in solution,^{51–54} only scattered observations have been made regarding their isomerisation in the solid state.^{55,56} Importantly, no information is available on their photoswitching in organic polymers, which represent a ubiquitous chemical host in materials science. At the outset, it is unclear whether photoisomerisation of indigos can be

successfully translated from solution to polymers. One potential hurdle is that the *E* ↔ *Z* isomerisation of indigos brings about a greater spatial displacement as compared to other steric switches such as azobenzenes. While it is a desirable trait in the view of applications where the molecular-level geometrical changes are utilised to trigger macroscopic transformations in a bulk material, the isomerisation process in a rigid environment may also be more hindered, rendering switching of the indigos in the solid state more challenging than for other classes of photoswitches. Thus, there is a need for a systematic investigation of the solid-state switching behaviour of indigo derivatives to determine criteria enabling their good performance and successful application.

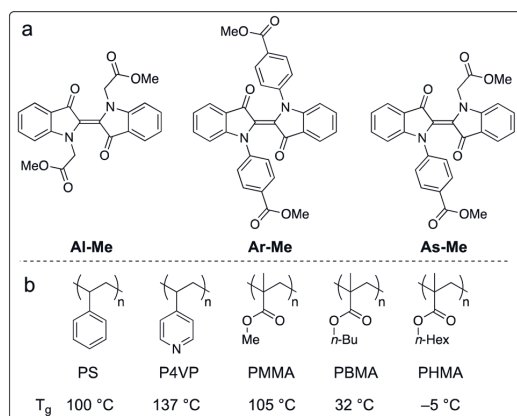
Herein, we present the first example of efficient photo-switching of indigo derivatives in polymer matrices under red light. The effects of *N*-substituents as well as supporting polymer network on the photoswitching dynamics are elucidated. Moreover, we reveal a strong dependence between indigo concentration and the switching properties, critical for the range of applications these switches can best be exploited in. Based on these findings, we demonstrate a strategy by which the photoswitching performance in the solid can be enhanced dramatically – to reach the same level as in solution.

Results and discussion

We chose to study the indigo derivatives **Al-Me**, **Ar-Me** and **As-Me** (Scheme 2a) that represent the three principal substitution patterns yielding functional red-light photoswitches.⁴⁴ The ester moieties have a dual purpose: they function as electron-withdrawing substituents that stabilise the metastable *Z* isomer through an inductive effect, while also providing a linkage for further functionalisation with, *e.g.*, polymerisable groups. The compounds were prepared in one or two steps in moderate to good yields from unsubstituted indigo by utilising the previously published mild nucleophilic substitution reaction⁴⁴ for **Al-Me** and a copper-catalysed coupling⁵⁷ for **Ar-Me**.



Scheme 1 *E*–*Z* isomerisation of indigo photoswitches and the focus of this work.



Scheme 2 (a) Studied indigo derivatives. (b) Studied polymer environments and their glass transition temperatures (*T*_g).

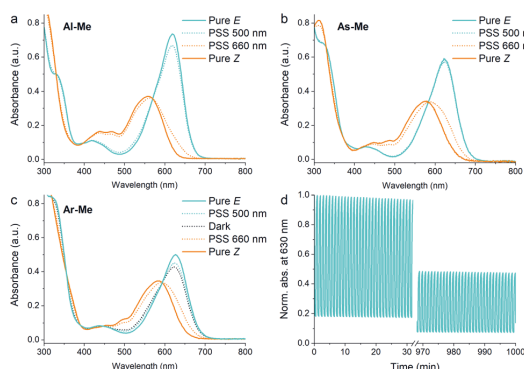


Fig. 1 Absorption spectra of (a) **Al-Me**, (b) **As-Me** and (c) **Ar-Me** in solution (50 μM in acetonitrile, 25 $^{\circ}\text{C}$). (d) 1000 switching cycles with alternating 660 and 500 nm light pulses for **Al-Me**.

The non-symmetric derivative **As-Me** was prepared through a selective mono-arylation followed by an alkylation reaction. Detailed synthetic protocols are given in the ESI†

To confirm that the compounds have similar photochemical properties to the electronically analogous derivatives reported before, we first studied their photoswitching in dilute acetonitrile solutions. As expected, the compounds form photostationary states (PSS) with 75–88% and 3–11% *Z* upon excitation with 660 nm (250 mW cm^{-2} , ≤ 30 s) and 500 nm light (85 mW cm^{-2} , ≤ 2 min), respectively. Their *Z* half-lives range from 1.4 min (**Al-Me**) to 41 min (**Ar-Me**) (Fig. 1, Table 1). Whereas **Al-Me** and **As-Me** exist exclusively as their *E* isomers in the dark, **Ar-Me** reached an equilibrium with 22% *Z* in darkness, irrespective of whether starting from *E*- or *Z*-enriched solutions. The same phenomenon has been reported for other indigos functionalised with two *N*-aryl substituents, originating from the fact that this substitution pattern renders the ground state energy difference between the *E* and *Z* isomers down to *ca.* 1 kcal mol^{-1} .⁴⁴ Overall, all three compounds exhibit very similar photochemical properties to their previously reported analogues.⁵¹ The switching is relatively robust: 82% of **As-Me** and 90% of **Ar-Me** were conserved after 1000 cycles and more than 16 hours of continuous irradiation with alternating 660 and 500 nm light pulses (Fig. S1†) under ambient conditions. **Al-Me** seems, however, less fatigue resistant, with 46% of the original concentration remaining after an identical experiment (Fig. 1d).

Table 1 Photochemical properties of the studied compounds in solution (50 μM in acetonitrile, 25 $^{\circ}\text{C}$)

	λ_E (nm)	λ_Z (nm)	PSS _{660 nm} (% <i>Z</i>)	PSS _{500 nm} (% <i>E</i>)	Dark (% <i>E</i>)	$t_{1/2}$ (min)
Al-Me	619	559	88	90	100	1.4
As-Me	623	577	75	97	100	3.8
Ar-Me	627	584	75	87	78	41

Next, we proceeded to studying whether the compounds switch when doped into polymer matrices. We focused our studies on five amorphous polymers: polystyrene (PS), poly(4-vinylpyridine) (P4VP) and polyacrylates with methyl (PMMA), *n*-butyl (PBMA), and *n*-hexyl (PHMA) side chains (Scheme 1b). PS, P4VP and PMMA are rigid (T_g values between +100 and +137 $^{\circ}\text{C}$) matrices often utilised as scaffolds for photoswitches,^{58–61} differing in polarity and aromaticity. PBMA and PHMA (T_g values +32 and -5 $^{\circ}\text{C}$) were chosen to give information on the photoswitching behaviour in a softer polymeric environment. We began our studies by preparing thin polymer films containing 2% (w/w) of the indigo derivatives. After optimising the spin-casting procedure for each polymer, we were able to create uniform and sufficiently thick (5–20 μm) polymer films from viscous solutions of different polymer–indigo combinations (see the ESI† for details). Each sample was studied with UV-visible absorption spectroscopy. The *Z*-fraction in the photostationary state was estimated by comparing the absorbance values of the dark and PSS spectra (see the ESI† for details). The half-life of thermal isomerisation was determined by recording the absorbance values at a chosen wavelength over time after ceasing the excitation, using a stretched exponential function⁶² to account for the continuum of different microenvironments inside the polymer matrix. Since indigos are known to emit light,⁵¹ we also recorded the fluorescence spectra of the samples.

The polymer environment induced only minute changes in the absorption spectra of the studied compounds (Fig. S2†) with the exception of P4VP in which the major absorption band of all three switches was red-shifted by *ca.* 10 nm, presumably due to the more polar environment.⁵¹ Their photoswitching behaviour, however, proved to be highly polymer-dependent. In the rigid PS and P4VP matrices, only 15–20% of the switches isomerised from *E* to *Z* upon irradiation with 660 nm light (Fig. 2a). Similarly inefficient switching in rigid matrices has been observed for other switches that undergo a large geometric change upon isomerisation.²⁸ In less rigid environments the PSS distribution improved notably, up to 55% *Z* for **Al-Me** in PBMA (Fig. 2b). The *Z*-fraction was typically largest for **Al-Me** and smallest for **As-Me**, the difference being most pronounced in PMMA (Fig. 2c).

Surprisingly, photodegradation leading to a yellow-coloured decomposition product was observed in PMMA and PBMA (visible in Fig. 2b as a missing isosbestic point) but was almost negligible in the other three polymers unless repeated switching cycles were carried out. Furthermore, even though bleaching did eventually take place in all surroundings, in the case of PS, P4VP and PHMA the films turned colourless without any yellow hue. To gain insight into the degradation mechanisms, an LC-MS (liquid chromatography coupled to high-resolution mass spectrometry) analysis was carried out after prolonged irradiation of the indigo switches in solution, in a PHMA film, and in a PBMA film (see the ESI† for details). In solution and in PHMA, the irradiation yielded exclusively a product with a mass of $M + 16$ (Fig. S3†) and no absorption in the visible range, most probably the well-known oxygen adduct.⁶³ In PBMA, we also observed a species absorbing at around 400 nm with a mass corresponding to $M - 2$ (Fig. S3†), hinting towards a cyclisation

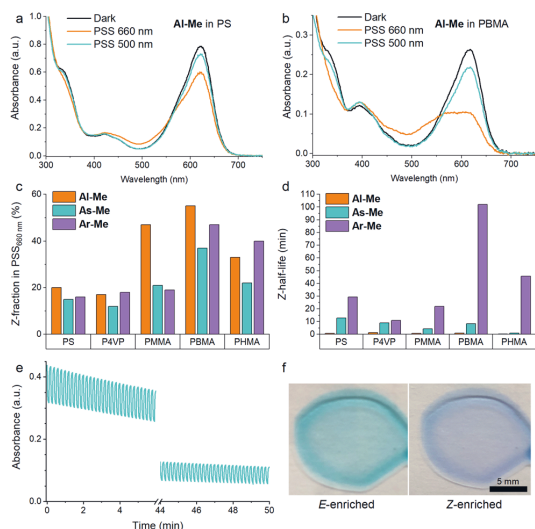


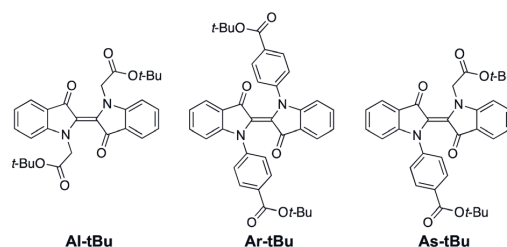
Fig. 2 Absorption spectra of **Al-Me** at room temperature in (a) PS and (b) PBMA, showing the difference between inefficient and efficient switching. (c) Z-Fractions in the photostationary state (illumination with 660 nm light) and (d) Z-half-lives for all indigo-polymer combinations. The half-life of **Ar-Me** in P4VP is calculated with a biexponential fit due to large error margins with the stretched exponential function (see the ESI†). (e) 250 switching cycles for **Al-Me** in PHMA. (f) Photographs of PHMA films with **Ar-Me** upon irradiation with 500 and 660 nm light. Indigo content: 2% (w/w) except 0.5% in (e) and (f). Excitation intensities: 670 mW cm⁻² (660 nm), 220 mW cm⁻² (500 nm).

product. Thus, an additional degradation pathway exists in PBMA and PMMA, which we believe to originate from the end groups or initiator residues present in PMMA and PBMA that were purchased from a different vendor than PHMA. However, the accurate determination of the degradation pathways and how they could be inhibited would require additional experimental and computational studies. The effect of degradation was taken into account when estimating the PSS distributions.

Interestingly, the half-life of the thermal $Z \rightarrow E$ isomerisation remained on the timescale of minutes for both **Al-Me** and **As-Me** in all studied polymers (Fig. 2d, Table S3†), even

though thermal isomerisation of $E \rightarrow Z$ switches is often more than one magnitude faster in solid matrices than in solution.²⁸ The thermal isomerisation of **Ar-Me** was significantly slower in the soft PBMA compared to the more rigid PS, P4VP and PMMA. It is possible that in a rigid matrix the $E \rightarrow Z$ isomerisation induces considerable mechanical strain which relaxes upon $Z \rightarrow E$ isomerisation, speeding up the kinetics compared to a softer environment. Somewhat surprisingly, the Z half-lives were not longest in PHMA, the least rigid polymer. This observation, as well as the slightly diminished PSS distributions (Fig. 2c), can be explained by aggregation that is most pronounced in this matrix (*vide infra*).

Having established that all switches can be successfully isomerised inside a polymer matrix, we investigated the effect of loading by preparing PHMA films with 0.25–10% (w/w) of **Al-Me**. This polymer was chosen as it exhibited the best combination of efficient and clean isomerisation. The isomerisation of azobenzenes in polymeric environments is typically unaffected by the azobenzene concentration, at least up to 10%.⁶⁴ Thus, we were surprised by the drastic effect indigo loading had on the photochemical properties. Absorption spectra were identical up to 2% after which the band broadened and red-shifted (by 10 nm between 2% and 10%), whereas in the fluorescence spectra a shift was visible already between 1% and 2% (Fig. 3a and c). This result indicates the formation of aggregates upon higher loadings. We hypothesized that by increasing the steric bulk of the indigo molecules, their aggregation could be circumvented or at least alleviated, as a similar strategy has been successfully used to minimise diarylethene aggregation in



Scheme 3 Studied *tert*-butyl-substituted indigo derivatives.

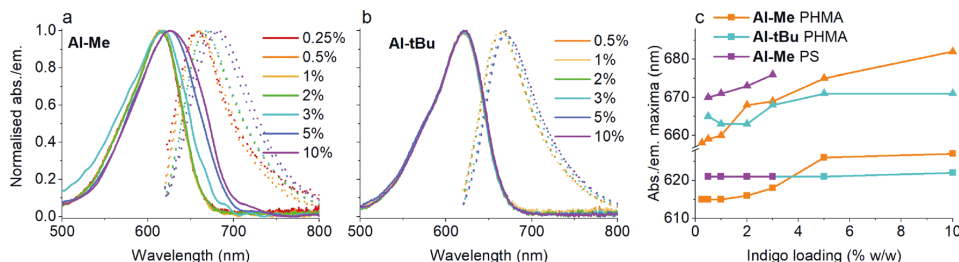


Fig. 3 Absorption and emission spectra of (a) **Al-Me** and (b) **Al-tBu** at different dye loadings in PHMA. (c) Absorption (squares) and emission (triangles) maxima of **Al-Me** and **Al-tBu** in PHMA and **Al-Me** in PS at different dye loadings.

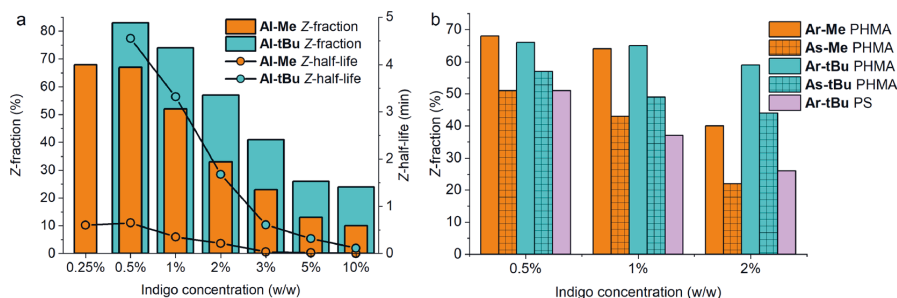


Fig. 4 (a) Z-Fractions upon excitation with 660 nm light and thermal Z half-lives of Al-Me and Al-tBu, and (b) Z-fractions of Ar-Me, As-Me, Ar-tBu and As-tBu at different dye loadings in PHMA and Ar-tBu in PS.

polymer blends of thin film transistors.⁶⁵ To this end, we synthesised **Al-tBu** (Scheme 3) with bulky *tert*-butyl groups to inhibit the aggregation, yet exhibiting similar electronic properties (Fig. S4 and Table S1†). Indeed, the absorption band of **Al-tBu** did not show any bathochromic shift from 0.5 to 10%, although a slight 5 nm shift could still be observed in the fluorescence spectra (Fig. 3b and c). Either some degree of agglomeration takes place even with the new molecular design or the mere changes in the dielectric constant of the surrounding medium are enough to affect the orbital energy levels. Similar trends were also observed in the fluorescence spectra of **As-Me** and **Ar-Me**, but their absorption spectra showed no red-shift, probably because the aryl groups (perpendicular to the indigo core⁴⁴) inhibit aggregation (Fig. S5†). No shifts were observed in the absorption spectra of **Al-Me** in PS (Fig. 3c and S6†) and in PBMA (Fig. S7†), although a shift was visible in the fluorescence spectra. While it is conceivable that the π , π interactions between PS and the indigos could hamper aggregation, the origin of the difference between the spectral changes in PHMA and PBMA is less obvious. One possibility is that the longer alkyl chains in PHMA could lead to lower miscibility of the indigo. Alternatively, the different end groups in PBMA (*vide supra*) may play a role in breaking the aggregation.

Even more importantly, we found that dye concentration plays a major role in determining the photoswitching dynamics of indigos in a solid environment. At an **Al-Me** loading of 10% (in PHMA), the Z-content in PSS₆₆₀ is 10% and the Z half-life only 0.14 seconds. At a loading of 0.5%, the respective values are 67% and 39 s (Fig. 4a). In terms of thermal energy barriers, the difference ($\Delta\Delta G^\ddagger$) is approximately 1.8 kcal mol⁻¹. This could easily be interpreted as a result of aggregation; also the exponential factor *b* in the stretched exponential fit decreased as the dye loading increased, pointing towards reduced homogeneity (Table S3†). However, even though the bulky *tert*-butyl groups prevent or decrease the aggregation of the indigos, the same trend is seen for **Al-tBu**. We note that although these two parameters correlate, there is no causality between them. Apart from perhaps the highest **Al-Me** loadings, thermal isomerisation is not fast enough to affect the PSS distribution with our experimental setup. Most likely the changes in spectra, PSS

distribution, and thermal isomerisation kinetics are caused by additional intermolecular interactions between the switched molecules. Similar dependence between concentration and the isomerisation efficiency was observed for all other indigo-polymer combinations for which concentration series were studied: **Ar-Me** and **As-Me** in PHMA (Fig. 4b) as well as for **Al-Me** in PBMA and PS (Fig. S8†).

Gratifyingly, our strategy to enhance the solid-state switchability by bulking the indigo molecules is effective: **Al-tBu** exhibits generally better PSS distributions and longer Z half-lives than the electronically similar **Al-Me**, reaching a Z-content of 83% in the PSS and a 4.6 min thermal Z half-life at a loading of 0.5% (Fig. 4a). This is logical, as the addition of bulky groups is known to improve the photoswitching parameters of other *E-Z* photoswitches in a constrained environment by increasing the free space these molecules can operate in.^{65,66} Much to our delight, this approach is also applicable to other derivatives. We synthesised **Ar-tBu** and **As-tBu** and studied their isomerisation in PHMA at loadings from 0.5 to 2%, and the Z-fraction in PSS increased for both switches when compared to the respective methyl-capped compounds (Fig. 4b), especially at a loading of 2%. Using this strategy, switching was relatively efficient even in PS, a film containing 0.5% of **Ar-tBu** reaching a PSS with 51% Z. In this case, thermal Z-to-E isomerisation was very slow, exhibiting a half-life of 9.7 hours. This extended stability comes with a markedly greater value than the 26 minutes measured in solution, corresponding to a difference of approximately 1.9 kcal mol⁻¹ in the thermal barrier. For applications operating on the timescale of minutes, the system is virtually bistable (Fig. S9†).

Conclusions

In just one or two synthetic steps, the familiar indigo dye yields photoswitches that operate with red light and exhibit negative photochromism, two key characteristics particularly intriguing for a range of applications from optics to photobiology. Although the synthetic pathways to indigo photoswitches and their photochemistry in solution have been studied in recent years, it has not been established whether their favourable properties can be transferred to solid matrices – which is crucial

for real-world applications. Herein, we have for the first time studied indigo photoswitching in amorphous polymer films made of PS, P4VP, PMMA, PBMA and PHMA. We have doped the polymer matrices with six indigo switches that share favourable photochemical properties but differ in their *N*-substituents and thermal isomerisation dynamics. Every switch is decorated with two ester moieties which, in addition to improving the photochemical properties, serve as synthetic handles for potential further functionalisation. In all of the polymers, the switches can be reversibly isomerised between their *E* and *Z* forms with 660 and 500 nm light, respectively, conserving their spectral qualities with the thermal isomerisation half-lives in the range of minutes. Initial trial showed that the switched percentage is low in rigid environments (PS, P4VP, PMMA), where the *Z*-content remains mainly below 20% under red-light excitation. This inefficiency is presumably due to the constraints applied on the steric switching by the matrix.

We propose that the distribution can be improved by reducing the amount of mechanical strain the *E*-to-*Z* isomerisation creates with one of the two means: (i) choosing a softer polymer matrix such as PBMA or PHMA, or (ii) incorporating bulky *tert*-butyl groups in the molecular design to increase the free volume surrounding the switch. Both strategies are proven effective for all studied indigos, and the switched fractions are greatly improved. Furthermore, as the most intriguing finding, indigo photoswitching is shown to be highly concentration-dependent in a solid environment, even at low loadings (*e.g.*, from 0.5 to 1%): both PSS distribution and the thermal stability of the *Z* isomer increase when indigo concentration is decreased. The behaviour is common for all studied derivatives and can be exploited as a third strategy for enabling efficient solid state photoswitching. When these strategies work in concert (*i.e.*, low loadings of a *tert*-butyl-decorated indigo in a soft polymer), isomerisation in the solid state is as efficient as in solution, reaching up to 83% *Z* for **Al-*t*Bu** in PHMA. Simultaneously, the thermal stability of the *Z* isomer can be improved even beyond the stability in solution. Thus, we conclude that indigo photoswitches show great potential as red-light-responsive molecular tools in material applications. By judicious choice of molecular structures and the solid-state surrounding, photo-isomerisation can occur efficiently in polymer environments. Our current effort is thus focused on translating the indigo photoswitching from the molecular level to the macroscopic level, where the material properties can be modulated by red light.

Data availability

The data are available upon request.

Author contributions

K. K. carried out the synthesis and characterisation of the compounds and preparation and photochemical studies of the polymer films with the help of J. V. and M. V., and wrote the original manuscript. C.-Y. H., S. H. and A. P. initiated and

supervised the work and edited the draft. The final manuscript was written by all authors.

Conflicts of interest

There are no conflicts to declare.

Acknowledgements

K. K. is grateful for the funding from the Tampere University Graduate School. C.-Y. H. is indebted to the financial supports by Institute for Chemical Reaction Design and Discovery (WPI-ICReDD) and Hokkaido University. A. P. acknowledges the financial support of the Academy of Finland (Center of Excellence LIBER, No. 346107, Flagship Programme PREIN, No. 320165). S. H. thanks the German Research Foundation (DFG via SFB 1349, project ID: 387284271) for support. The authors acknowledge Dr Jussi Isokuortti for his help with the fluorescence measurements.

Notes and references

- C. Kaspar, B. J. Ravoo, W. G. van der Wiel, S. V. Wegner and W. H. P. Pernice, *Nature*, 2021, **594**, 345–355.
- A. Walther, *Adv. Mater.*, 2020, **32**, 1905111.
- J. Zhang, Q. Zou and H. Tian, *Adv. Mater.*, 2013, **25**, 378–399.
- A. Goulet-Hanssens, F. Eisenreich and S. Hecht, *Adv. Mater.*, 2020, **32**, 1905966.
- A. Priimagi and A. Shevchenko, *J. Polym. Sci., Part B: Polym. Phys.*, 2014, **52**, 163–182.
- S. L. Oscurato, F. Reda, M. Salvatore, F. Borbone, P. Maddalena and A. Ambrosio, *Laser Photonics Rev.*, 2022, **16**, 2100514.
- X. Huang and T. Li, *J. Mater. Chem. C*, 2020, **8**, 821–848.
- C. Fedele, T.-P. Ruoko, K. Kuntze, M. Virkki and A. Priimagi, *Photochem. Photobiol. Sci.*, 2022, **21**, 1719–1734.
- J. Broichhagen, J. A. Frank and D. Trauner, *Acc. Chem. Res.*, 2015, **48**, 1947–1960.
- K. Hüll, J. Morstein and D. Trauner, *Chem. Rev.*, 2018, **118**, 10710–10747.
- M. J. Fuchter, *J. Med. Chem.*, 2020, **63**, 11436–11447.
- M. M. Lerch, M. J. Hansen, G. M. van Dam, W. Szymanski and B. L. Feringa, *Angew. Chem., Int. Ed.*, 2016, **55**, 10978–10999.
- W. A. Velema, W. Szymanski and B. L. Feringa, *J. Am. Chem. Soc.*, 2014, **136**, 2178–2191.
- Z. Mahimwalla, K. G. Yager, J. Mamiya, A. Shishido, A. Priimagi and C. J. Barrett, *Polym. Bull.*, 2012, **69**, 967–1006.
- Y. Chen, J. Yang, X. Zhang, Y. Feng, H. Zeng, L. Wang and W. Feng, *Mater. Horiz.*, 2021, **8**, 728–757.
- T. Bian, Z. Chu and R. Klajn, *Adv. Mater.*, 2020, **32**, 1905866.
- C. Petermayer and H. Dube, *Acc. Chem. Res.*, 2018, **51**, 1153–1163.
- D. Villarón and S. J. Wezenberg, *Angew. Chem., Int. Ed.*, 2020, **59**, 13192–13202.
- I. Arahamian, *Chem. Commun.*, 2017, **53**, 6674–6684.

- 20 M. W. H. Hoorens, M. Medved', A. D. Laurent, M. Di Donato, S. Fanetti, L. Slappendel, M. Hilbers, B. L. Feringa, W. Jan Buma and W. Szymanski, *Nat. Commun.*, 2019, **10**, 2390.
- 21 S. Crespi, N. A. Simeth, M. Di Donato, S. Doria, C. N. Stindt, M. F. Hilbers, F. L. Kiss, R. Toyoda, S. Wesseling, W. J. Buma, B. L. Feringa and W. Szymański, *Angew. Chem., Int. Ed.*, 2021, **60**, 25290–25295.
- 22 H. M. D. Bandara and S. C. Burdette, *Chem. Soc. Rev.*, 2012, **41**, 1809–1825.
- 23 S. Crespi, N. A. Simeth and B. König, *Nat. Rev. Chem.*, 2019, **3**, 133–146.
- 24 M. Irie, T. Fukaminato, K. Matsuda and S. Kobatake, *Chem. Rev.*, 2014, **114**, 12174–12277.
- 25 S. Helmy, S. Oh, F. A. Leibfarth, C. J. Hawker and J. Read de Alaniz, *J. Org. Chem.*, 2014, **79**, 11316–11329.
- 26 L. Kortekaas and W. R. Browne, *Chem. Soc. Rev.*, 2019, **48**, 3406–3424.
- 27 M. Quant, A. E. Hillers-Bendtsen, S. Ghasemi, M. Erdelyi, Z. Wang, L. M. Muhammad, N. Kann, K. V. Mikkelsen and K. Moth-Poulsen, *Chem. Sci.*, 2022, **13**, 834–841.
- 28 A. Gonzalez, E. S. Kengmana, M. V Fonseca and G. G. D. Han, *Mater. Today Adv.*, 2020, **6**, 100058.
- 29 D. Mutruc, A. Goulet-Hanssens, S. Fairman, S. Wahl, A. Zimathies, C. Knie and S. Hecht, *Angew. Chem., Int. Ed.*, 2019, **58**, 12862–12867.
- 30 J. Boelke and S. Hecht, *Adv. Opt. Mater.*, 2019, **7**, 1900404.
- 31 E. Yousif and R. Haddad, *Springerplus*, 2013, **2**, 398.
- 32 M. M. Becker and Z. Wang, *J. Mol. Biol.*, 1989, **210**, 429–438.
- 33 W. F. Cheong, S. A. Prah and A. J. Welch, *IEEE J. Quantum Electron.*, 1990, **26**, 2166–2185.
- 34 V. J. Pansare, S. Hejazi, W. J. Faenza and R. K. Prud'homme, *Chem. Mater.*, 2012, **24**, 812–827.
- 35 Z. Zhang, W. Wang, M. O'Hagan, J. Dai, J. Zhang and H. Tian, *Angew. Chem., Int. Ed.*, 2022, **61**, e202205758.
- 36 C. Knie, M. Utecht, F. Zhao, H. Kulla, S. Kovalenko, A. M. Brouwer, P. Saalfrank, S. Hecht and D. Bléger, *Chem.–Eur. J.*, 2014, **20**, 16492–16501.
- 37 M. Dong, A. Babalhavaeji, S. Samanta, A. A. Beharry and G. A. Woolley, *Acc. Chem. Res.*, 2015, **48**, 2662–2670.
- 38 L. N. Lameijer, S. Budzak, N. A. Simeth, M. J. Hansen, B. L. Feringa, D. Jacquemin and W. Szymanski, *Angew. Chem., Int. Ed.*, 2020, **59**, 21663–21670.
- 39 D. B. Konrad, G. Savasci, L. Allmendinger, D. Trauner, C. Ochsenfeld and A. M. Ali, *J. Am. Chem. Soc.*, 2020, **142**, 6538–6547.
- 40 K. Kuntze, J. Viljakka, E. Titov, Z. Ahmed, E. Kalenius, P. Saalfrank and A. Priimagi, *Photochem. Photobiol. Sci.*, 2022, **21**, 159–173.
- 41 A. Kerckhoffs, K. E. Christensen and M. J. Langton, *Chem. Sci.*, 2022, **13**, 11551–11559.
- 42 S. Wiedbrauk and H. Dube, *Tetrahedron Lett.*, 2015, **56**, 4266–4274.
- 43 C. Petermayer, S. Thumser, F. Kink, P. Mayer and H. Dube, *J. Am. Chem. Soc.*, 2017, **139**, 15060–15067.
- 44 C.-Y. Huang, A. Bonasera, L. Hristov, Y. Garmshausen, B. M. Schmidt, D. Jacquemin and S. Hecht, *J. Am. Chem. Soc.*, 2017, **139**, 15205–15211.
- 45 A. Goulet-Hanssens, C. Rietze, E. Titov, L. Abdullahu, L. Grubert, P. Saalfrank and S. Hecht, *Chem*, 2018, **4**, 1740–1755.
- 46 J. Isokuortti, K. Kuntze, M. Virkki, Z. Ahmed, E. Vuorimaa-Laukkanen, M. A. Filatov, A. Turshatov, T. Laaksonen, A. Priimagi and N. A. Durandin, *Chem. Sci.*, 2021, **12**, 7504–7509.
- 47 K. Kuntze, J. Isokuortti, A. Siiskonen, N. Durandin, T. Laaksonen and A. Priimagi, *J. Phys. Chem. B*, 2021, **125**, 12568–12573.
- 48 A.-L. Leistner and Z. L. Pianowski, *Eur. J. Org. Chem.*, 2022, **2022**, e202101271.
- 49 J. R. Hemmer, S. O. Poelma, N. Treat, Z. A. Page, N. D. Dolinski, Y. J. Diaz, W. Tomlinson, K. D. Clark, J. P. Hooper, C. Hawker and J. Read de Alaniz, *J. Am. Chem. Soc.*, 2016, **138**, 13960–13966.
- 50 S. Yamazaki, A. L. Sobolewski and W. Domcke, *Phys. Chem. Chem. Phys.*, 2011, **13**, 1618–1628.
- 51 Š. Budzák, J. Jovaišaitė, C.-Y. Huang, P. Baronas, K. Tulaitė, S. Jursėnas, D. Jacquemin and S. Hecht, *Chem.–Eur. J.*, 2022, **28**, e202200496.
- 52 D. Pinheiro, M. Pineiro, A. M. Galvão and J. S. Seixas de Melo, *Chem. Sci.*, 2021, **12**, 303–313.
- 53 D. C. Nobre, C. Cunha, A. Porciello, F. Valentini, A. Marrocchi, L. Vaccaro, A. M. Galvão and J. S. S. de Melo, *Dyes Pigm.*, 2020, **176**, 108197.
- 54 D. Farka, M. Scharber, E. D. Glowacki and N. S. Sariciftci, *J. Phys. Chem. A*, 2015, **119**, 3563–3568.
- 55 S. Ganapathy, R. G. Zimmermann and R. G. Weiss, *J. Org. Chem.*, 1986, **51**, 2529–2535.
- 56 J. H. Porada, J.-M. Neudörfl and D. Blunk, *New J. Chem.*, 2015, **39**, 8291–8301.
- 57 Y. Matsumoto and H. Tanaka, *Heterocycles*, 2003, **60**, 1805–1810.
- 58 M. Poutanen, Z. Ahmed, L. Rautkari, O. Ikkala and A. Priimagi, *ACS Macro Lett.*, 2018, **7**, 381–386.
- 59 S. Hisham, N. Muhammad Sarih, H. A. Tajuddin, Z. H. Zainal Abidin and Z. Abdullah, *RSC Adv.*, 2021, **11**, 15428–15437.
- 60 C. Pakula, C. Hanisch, V. Zaporotchenko, T. Strunskus, C. Bornholdt, D. Zargarani, R. Herges and F. Faupel, *J. Mater. Sci.*, 2011, **46**, 2488–2494.
- 61 G. Clavier, F. Ilhan and V. M. Rotello, *Macromolecules*, 2000, **33**, 9173–9175.
- 62 R. Kohlrausch, *Ann. Phys.*, 1854, **167**, 56–82.
- 63 B. D. Smith, D. E. Alonso, J. T. Bien, E. C. Metzler, M. Shang and J. M. I. I. Roosenberg, *J. Org. Chem.*, 1994, **59**, 8011–8014.
- 64 C. Barrett, A. Natansohn and P. Rochon, *Chem. Mater.*, 1995, **7**, 899–903.
- 65 M. El Gemayel, K. Börjesson, M. Herder, D. T. Duong, J. A. Hutchison, C. Ruzié, G. Schweicher, A. Salleo, Y. Geerts, S. Hecht, E. Orgiu and P. Samori, *Nat. Commun.*, 2015, **6**, 6330.
- 66 E. N. Cho, D. Zhitomirsky, G. G. D. Han, Y. Liu and J. C. Grossman, *ACS Appl. Mater. Interfaces*, 2017, **9**, 8679–8687.

PUBLICATION III

Azobenzene photoswitching with near-infrared light mediated by molecular oxygen

Kuntze, K., Isokuortti, J., Siiskonen, A., Durandin, N. A., Laaksonen, T. & Priimägi, A.

Journal of Physical Chemistry B, vol. 125, p. 12568, 2021

DOI: <https://doi.org/10.1021/acs.jpcb.1c08012>

Publication reprinted with the permission of the copyright holders.

Azobenzene Photoswitching with Near-Infrared Light Mediated by Molecular Oxygen

Kim Kuntze, Jussi Isokuortti, Antti Siiskonen, Nikita Durandin, Timo Laaksonen, and Arri Priimagi*

Cite This: *J. Phys. Chem. B* 2021, 125, 12568–12573

Read Online

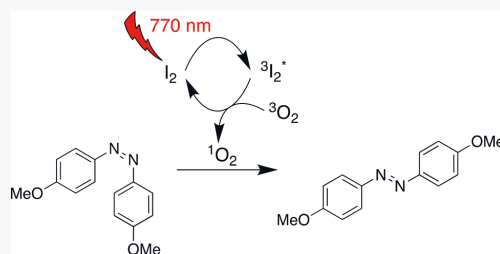
ACCESS |

Metrics & More

Article Recommendations

Supporting Information

ABSTRACT: Efficient photoisomerization between the cis and the trans states of azobenzenes using low-energy light is desirable for a range of applications in, e.g., photobiology yet challenging to accomplish directly with modified azobenzenes. Herein, we utilize molecular iodine as a photocatalyst to induce indirect cis-to-trans isomerization of 4,4'-dimethoxyazobenzene with 770 nm near-infrared light, showing robustness during more than 1000 cycles in ambient conditions. Intriguingly, the catalysis is mediated by molecular oxygen, and we demonstrate that other singlet-oxygen-generating photosensitizers besides iodine, i.e., palladium phthalocyanine, catalyze the isomerization as well. Thus, we envision that the approach can be further improved by employing other catalysts with suitable photoelectrochemical properties. Further studies are needed to explore the applicability of the approach with other azobenzene derivatives.



INTRODUCTION

Molecular iodine is known to catalyze organic reactions when illuminated with visible light. The list of iodine-photocatalyzed reactions includes the oxidation of tertiary amines,¹ allylic and benzylic alcohols,^{2,3} and styrenes⁴ into the respective aldehydes and has recently been extended with the degradation of trichlorophenol⁵ and selected intra- or intermolecular metal-free coupling reactions.^{6–9} In most reactions, the catalytic activity is attributed to iodine radicals formed in the homolysis of the I–I bond, presumably after initial excitation to ³I₂^{*}.^{1–5,8} Also ionic pathways have been reported in which the triplet excited state of iodine functions as a singlet oxygen sensitizer¹⁰ and the singlet oxygen in turn regenerates the iodine at the end of the catalytic cycle.^{6–9} The photochemistry of iodine has been studied over many decades,^{11–19} and it is known that the absorption of molecular iodine in the visible range is attributed to overlapping electronic transitions to three excited states: bound triplet states A and B and an unbound singlet state C (Figure S1).¹⁷ The C ← X and B ← X transitions account for the absorption in most of the visible range, and although the B state is bound, it is crossed by unbound states. This explains the observed dissociation of the iodine molecule when excited with blue or white light.^{11,13,20} However, the A state, reached by irradiation with longer wavelengths (>650 nm), is not crossed by unbound states. Recombination of iodine atoms may result in a slightly lower energy A' state but does not lead to unbound states either.¹⁷ Therefore, excitation at long wavelengths can lead to a fairly stable triplet-excited (A or A' state) iodine molecule which may act as a donor in triplet energy transfer (TET). Even though excitation inside the

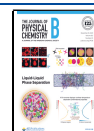
therapeutic optical window (>650 nm) would be greatly beneficial for biological applications, no studies on iodine catalysis using red or near-infrared light excitation have been performed.

An important photochemical reaction that iodine is known to photocatalyze is the cis–trans isomerization of azobenzenes,^{21,22} a photoswitch family utilized in photoresponsive pharmaceuticals,^{23,24} catalysts,²⁵ and materials.^{26–29} These applications benefit from precisely controlled light-driven isomerization, preferably with low-energy (red/near-infrared) light.³⁰ Unfortunately, the lifetime of the metastable cis isomer is typically short for red-light-absorbing azobenzenes, an undesired feature in most applications. This deficiency can be addressed by synthetic modifications, especially ortho substitution with certain moieties^{31–35} that stabilize the cis isomer and in some cases separate the low-energy *n*–*π*^{*} absorption bands of the isomers, allowing selective trans–cis and cis–trans photoisomerization with visible light. These bands are, however, limited to wavelengths below 600 nm with low molar absorptivity in the red end of the visible spectrum. Suitable photocatalysts offer an alternative pathway to control the photoswitching with low-energy irradiation. Azobenzenes

Received: September 10, 2021

Revised: October 25, 2021

Published: November 4, 2021



have a short-living triplet state whose excitation leads mainly to trans-azobenzenes via rapid intersystem crossing.^{22,36–42} Thus, with a suitable triplet sensitizer it is possible to accelerate the cis–trans isomerization using significantly longer wavelengths than those absorbed by the azobenzene.^{39,43} However, isomerization via TET suffers from sensitivity toward oxygen, hampering the functionality of the systems in ambient conditions. If the redox potentials of the *cis*-azobenzene and the sensitizer are matched, photoinduced electron transfer (PET) becomes feasible, and both reductive⁴⁴ and oxidative⁴⁵ PET processes have been used to drive the isomerization with wavelengths as long as 660 nm in the latter case. Despite recent progress in the field, iodine-catalyzed photoisomerization has not been studied since the first reports in the 1960s and 1970s. Therein, either 545 nm green light excitation of iodine or ultraviolet light excitation of a charge transfer complex between iodine and azobenzene was utilized, neglecting the possibility of low-energy-light excitation.^{21,22} Yet iodine would be highly attractive for this purpose because of its low cost, nontoxic nature, environmental friendliness, and, above all, the potential of catalyzing the isomerization in response to NIR light in ambient conditions. In this study, we set out to explore the photocatalytic properties of molecular iodine with the aim of controlling the azobenzene isomerization with low-energy light while also broadening the utility of molecular iodine in other photocatalytic processes.

RESULTS AND DISCUSSION

Initially, we restricted our studies to the moderately electron-rich 4,4'-dimethoxyazobenzene (**1**) that has a relatively stable *cis* isomer (half-life 13 h) and has been found to isomerize efficiently with triplet sensitizers and photoinduced electron transfer agents without considerable fatigue.⁴⁵ Solvents with nucleophilic electron pairs blue shift the absorption spectrum of iodine, so we studied the isomerization in three inert solvents of varying density and polarity: dichloromethane (DCM), carbon tetrachloride (TCM), and *n*-hexane (hexane). First, we recorded and analyzed the absorption spectra of **1** and iodine separately and in one solution (Figure 1). The absorption spectrum of *trans*-**1** is governed by an intense band at ca. 370 nm, corresponding to the π – π^* transition. Upon irradiation with 365 nm light, a photostationary state of >95% *cis*-**1** is acquired. Both *trans*-**1** and *cis*-**1** also exhibit a less intense n – π^* band between 400 and 600 nm, but neither isomer absorbs at >650 nm. The absorption band of iodine, on the other hand, reaches well beyond the visible range: absorption can be observed even at >800 nm with a more concentrated sample (Figure S2). The absorption spectrum of the *cis*-**1** + I_2 mixture is the sum of the spectra of *cis*-**1** and I_2 with no indication of additional absorption bands corresponding to a charge transfer complex.

Having established that in the red/NIR region the only absorbing species is molecular iodine and the excitation should result in $^3I_2^*$ in a nondissociative manner, we proceeded to study the photoisomerization with varying iodine concentrations. This was monitored by recording the absorbance value near the maximum of the π – π^* band of *trans*-**1** (372 nm). Starting from *trans*-**1**, a *cis*-**1**-rich mixture was reached by illuminating the mixture with 365 nm light (Figure 2a), which is seen as a drop in the absorbance. The *cis* fraction in the photostationary state decreased with increasing iodine concentration due to competing absorption by the iodine molecule and subsequent iodine-catalyzed *cis*-to-*trans* isomer-

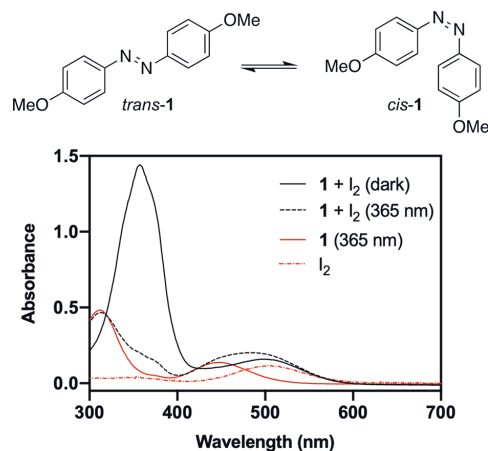


Figure 1. Absorption spectra of **1** (50 μ M) + I_2 (200 μ M) in the dark and upon illumination with UV light as well as pure **1** and iodine in dichloromethane.

ization. When the irradiation was stopped, the absorbance increased slightly, mostly due to diffusion from the unilluminated parts of the solution as thermal isomerization is too slow to be observed in this time scale. Upon illumination with 770 nm near-infrared light, *cis*-to-*trans* isomerization took place rapidly. Initially, we used 1–10 equiv of iodine to ensure fast photoisomerization, as the molar absorptivity of iodine is very low in the NIR region ($\epsilon_{770} = 8.6 \text{ M}^{-1} \text{ cm}^{-1}$). However, the catalysis worked perfectly with only 0.1 equiv of iodine (Figure 2b, Figure S3). In addition to using higher iodine loadings, the rate can be accelerated by a factor of 4.8 using red instead of NIR light ($\epsilon_{660} = 41 \text{ M}^{-1} \text{ cm}^{-1}$), still keeping the excitation wavelength well within the therapeutic optical window. An increase in the rate by approximately this factor (4.4) was indeed observed when switching from 770 to 660 nm excitation (Figure 2b, Table S1), although comparison between different excitation wavelengths is hampered by the differences in the intensities and spectral shapes of the light sources. Furthermore, we would like to highlight the robustness of the system: virtually no photobleaching was observed over the course of 30 switching cycles under ambient conditions (Figure 2c), and the system was fully functional even after 1000 cycles (Figure S4).

Three mechanistic pathways can give rise to the iodine-catalyzed photoswitching: (i) formation of I^* radicals and subsequent radical mechanism,²¹ (ii) triplet energy transfer, and (iii) photoinduced electron transfer. To distinguish between these, we first studied the effect of the solvent. The photocatalyzed reaction proceeded fastest in dichloromethane and slowest in hexane (Figure 3, Table S1). The fact that the catalysis is faster in carbon tetrachloride than that in hexane (by a factor of 3.2) speaks against the I^* mechanism, as the photodissociation rate should be ca. 5 times higher in hexane than that in TCM.²⁰ In addition, the dissociation reaction is unlikely in the NIR region.¹² TET is ruled out by the observation that the rate is 2.2-fold in dichloromethane compared to carbon tetrachloride in which ϵ_{770} is higher (Figure S2) and the triplet state lifetime of iodine is longer, and, thus, TET should be more efficient.¹⁷ This hints toward

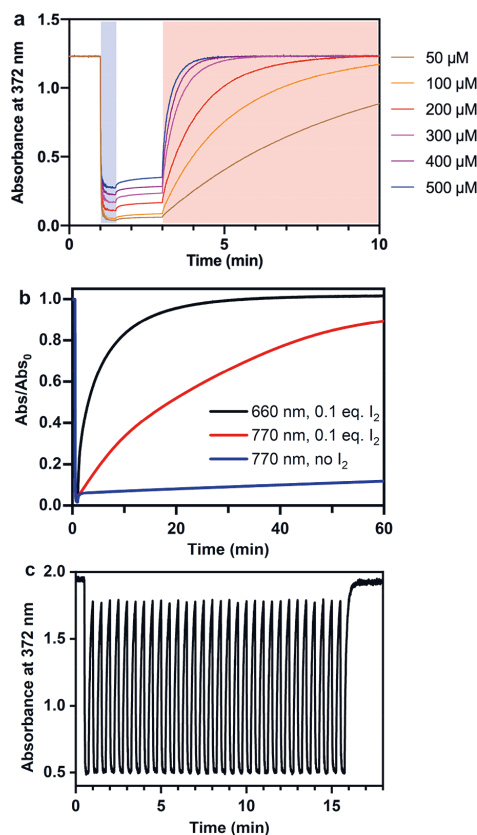


Figure 2. (a) Photoisomerization curves of **1** in DCM with 0–10 equiv of iodine. Illumination with 365 and 770 nm is shown in light purple and red shading, respectively. (b) Photoisomerization curves of **1** in DCM with 0.1 equiv of iodine under illumination with 660 and 770 nm light. (c) Cycles of 365 and 770 nm illumination (~15 s).

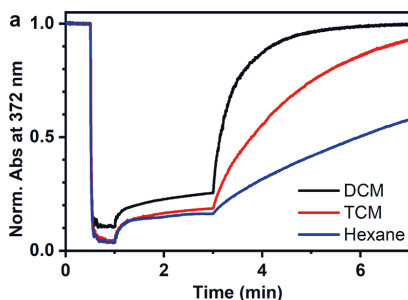


Figure 3. Photoisomerization curves of **1** with 4 equiv of iodine in dichloromethane, carbon tetrachloride, and *n*-hexane. Illumination with 365 nm at 0.5–1.0 min and with 770 nm from 3.0 min onward.

the formation of a charged species during the process. PET seems probable as electron transfer processes are polarity dependent.⁴⁶ We note that the observed solvent effect is not

attributed to the solubility of oxygen, which is highest for *n*-hexane and lowest for dichloromethane.^{47,48}

Both oxidative and reductive PET processes are feasible, but for an electron-rich azobenzene such as **1**, the oxidative pathway is more probable.⁴⁵ We also screened the reaction for three other less electron rich azobenzenes: 4-methoxyazobenzene **2**, unsubstituted azobenzene **3**, and an azobenzene diester **4**. The photocatalysis did not take place for **3** and **4** and was pronouncedly slower for **2** (Figure 4). This is another

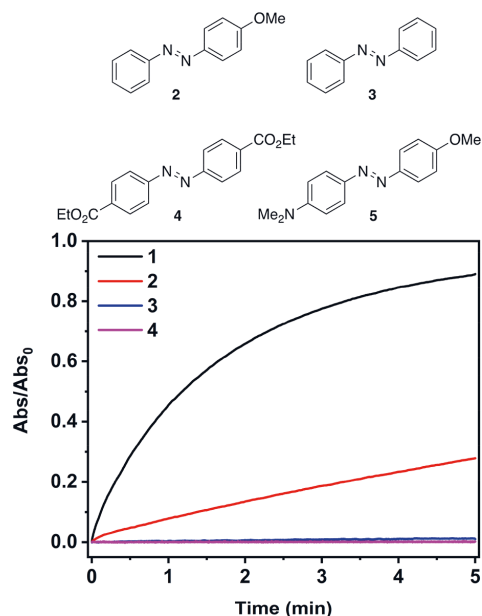


Figure 4. Photoisomerization curves of **1–4** with 4 equiv of iodine in dichloromethane. Illumination with 770 nm starting at 0 min; trans-to-cis isomerization with 365 nm is omitted for clarity. Vertical axis shows the absorbance relative to the initial value, i.e., pure trans isomer.

indication of an oxidative process. We also tried to test the reaction on a more electron-rich azobenzene **5** but were unable to induce the trans-to-cis photoisomerization upon excitation with 405 nm light, probably due to a ground-state interaction between **5** and iodine that blue shifts the absorption spectrum of iodine (Figure S5).

We also carried out the same experiment in nitrogen/argon-purged and freeze–pump–thaw-deaerated solutions, as both PET and TET systems are typically sensitive to oxygen.^{43,45} To our great surprise, photoisomerization was pronouncedly slower in the partly (see SI) deoxygenated solutions than that under ambient conditions (Figure 3, Table S1), contrary to earlier TET and PET studies.^{43,45} This indicates a central role for oxygen in the mechanism. As triplet iodine is capable of sensitizing singlet oxygen,¹⁰ which in turn has been shown to isomerize alkenes,⁴⁹ we investigated the possibility of a singlet-oxygen-mediated route (Figure 5). Our attempts to use oxygen scavengers failed due to ground-state interaction with iodine (Figure S6), and similar results are expected with any scavenger containing nucleophilic electron pairs. Hence, we

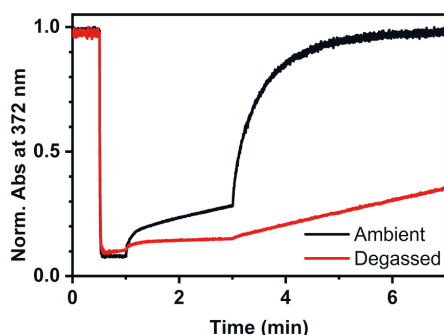
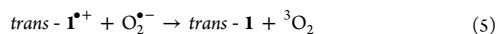
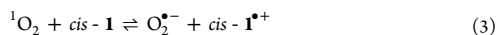
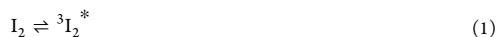


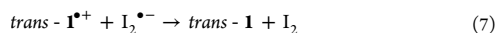
Figure 5. Photoisomerization curves of **1** with 4 equiv of iodine in dichloromethane at ambient conditions and after freeze–pump–thaw deaeration. Illumination with 365 nm at 0.5–1.0 min and with 770 nm from 3.0 min onward.

probed the possibility of a singlet-oxygen-mediated route with palladium octabutoxyphthalocyanine (PdPc), an efficient singlet oxygen sensitizer with a low triplet energy (1.13 eV) and short lifetime (3.5 μ s) and thus low probability of direct TET to **1** to occur.⁵⁰ We first chose the concentration of PdPc (0.36 μ M) so that its optical density at 770 nm was matched with that of a 200 μ M iodine solution. Thus, [$^1\text{O}_2$] should be higher for the PdPc solution as it has a higher quantum yield of singlet oxygen generation.^{10,50} Almost no photocatalyzed isomerization was observed (Figure S7). With an equimolar (50 μ M) concentration of PdPc, however, the *cis*-to-*trans* isomerization was relatively rapid, albeit slower than that for an equivalent amount of iodine (Figure S8). Most importantly, PdPc was also found to function only in the presence of oxygen (Figure S7), ruling out any direct TET or PET processes. These findings reveal that (i) singlet oxygen indeed plays a key role in the mechanism, as this is the only known product of the reaction between excited PdPc and oxygen, and (ii) iodine must have another role besides generating singlet oxygen, since the iodine-catalyzed reaction is faster than the equivalent PdPc-catalyzed reaction even though PdPc undisputedly produces more singlet oxygen to the solution. Thus, the PET most probably takes place between singlet oxygen (a strong oxidant⁵¹) and **1**.

Combining these results, we propose an oxygen-mediated PET mechanism for the catalysis, as illustrated in eqs 1–7. After the initial excitation of I_2 to $^3\text{I}_2^$ (eq 1), the triplet excited species sensitizes the formation of singlet oxygen $^1\text{O}_2$ (eq 2), which then oxidizes **1** (eq 3).⁹ The formed radical cation *cis*- $\text{I}^{\bullet+}$ has an extremely low isomerization energy barrier, rapidly yielding *trans*- $\text{I}^{\bullet+}$ (eq 4).⁴⁵ Electron transfer from $\text{O}_2^{\bullet-}$ to *trans*- $\text{I}^{\bullet+}$ then terminates the cycle (eq 5). All of these reactions are also possible for PdPc.



In the case of iodine, additional steps are possible. The termination step can proceed via electron transfer from $\text{O}_2^{\bullet-}$ to iodine (eq 6)⁵² and then to *trans*- $\text{I}^{\bullet+}$ (eq 7). In addition, it is possible that the oxygen formed when interacting with iodine is singlet excited, further accelerating the reaction.⁵³ These additional routes could explain the markedly higher rate when using iodine as compared to PdPc. We also considered the possibility of iodine dissociation upon interaction with the sensitized singlet oxygen⁵⁴ and subsequent I^{\bullet} radical mechanism but ruled it out as it did not explain the solvent polarity dependence. However, we want to highlight that more mechanistic studies, both experimental and computational, should be carried out for further verification of this plausible mechanism.



CONCLUSIONS

We have shown that singlet oxygen generated upon NIR light excitation of molecular iodine or another sensitizer can be used to induce robust azobenzene photoswitching. In fact, and most interestingly, the catalytic cycle is dependent on molecular oxygen, a feature unknown for any photocatalytic systems operating on photoswitches. Noteworthy, practically no photobleaching was observed after 1000 cycles. This is in stark contrast to our recently published TET-based NIR light catalysis, where molecular oxygen was detrimental for the performance of the azobenzene catalytic system. We envision that our concept can be further developed with other perhaps even more efficient NIR-absorbing singlet oxygen sensitizers with the same or better photoelectrochemical properties than iodine and PdPc. Moreover, our approach provides inspiration for future iodine photocatalysis also outside the field of photoswitch isomerization. Further studies should be carried out to determine what other azobenzene derivatives (and perhaps other photoswitches) the approach can be applied to. Additional experimental and computational studies are also needed to verify the mechanistic pathway of the catalysis.

ASSOCIATED CONTENT

Supporting Information

The Supporting Information is available free of charge at <https://pubs.acs.org/doi/10.1021/acs.jpcb.1c08012>.

Experimental section, synthesis and characterization of the studied materials, deaeration procedures, fitted reaction rates, other supporting results (PDF)

AUTHOR INFORMATION

Corresponding Author

Arri Priimagi – Faculty of Engineering and Natural Sciences, Tampere University, FIN-33101 Tampere, Finland;
 orcid.org/0000-0002-5945-9671; Email: arri.priimagi@tuni.fi

Authors

Kim Kuntze – Faculty of Engineering and Natural Sciences, Tampere University, FIN-33101 Tampere, Finland

Jussi Isokuortti – Faculty of Engineering and Natural Sciences, Tampere University, FIN-33101 Tampere, Finland

Antti Siiskonen – Faculty of Engineering and Natural Sciences, Tampere University, FIN-33101 Tampere, Finland
Nikita Durandin – Faculty of Engineering and Natural Sciences, Tampere University, FIN-33101 Tampere, Finland; orcid.org/0000-0002-5734-7377

Timo Laaksonen – Faculty of Engineering and Natural Sciences, Tampere University, FIN-33101 Tampere, Finland

Complete contact information is available at:
<https://pubs.acs.org/10.1021/acs.jpcb.1c08012>

Author Contributions

The manuscript was written through contributions of all authors.

Notes

The authors declare no competing financial interest.

ACKNOWLEDGMENTS

This research was supported by the Academy of Finland (Decision nos. 311142 and 326416). K.K. is grateful for the financial support from the Tampere University Graduate School. The authors acknowledge Dr. Zafar Ahmed and Dr. Matti Virkki for their help on this work.

REFERENCES

- (1) Gangloff, A. R.; Judge, T. M.; Helquist, P. Light-Induced, Iodine-Catalyzed Aerobic Oxidation of Unsaturated Tertiary Amines. *J. Org. Chem.* **1990**, *55* (11), 3679–3682.
- (2) Itoh, A.; Kodama, T.; Masaki, Y. New Synthetic Method of Benzaldehydes and α,β -Unsaturated Aldehydes with I₂ under Photoirradiation. *Chem. Lett.* **2001**, *30* (7), 686–687.
- (3) Farhadi, S.; Zabardasti, A.; Babazadeh, Z. Aerobic Photocatalytic Oxidation of Activated Benzylic and Allylic Alcohols to Carbonyl Compounds Catalyzed by Molecular Iodine. *Tetrahedron Lett.* **2006**, *47* (50), 8953–8957.
- (4) Itoh, A.; Kodama, T.; Masaki, Y.; Inagaki, S. Oxidative Cleavage of the Double Bonds of Styrenes with a Combination of Mesoporous Silica FSM-16 and I₂ under Photoirradiation. *Synlett* **2002**, *2002* (03), 0522–0524.
- (5) Hu, M.; Wang, Y.; Xiong, Z.; Bi, D.; Zhang, Y.; Xu, Y. Iodine-Sensitized Degradation of 2,4,6-Trichlorophenol under Visible Light. *Environ. Sci. Technol.* **2012**, *46* (16), 9005–9011.
- (6) Becker, P.; Duhamel, T.; Stein, C. J.; Reiher, M.; Muñoz, K. Cooperative Light-Activated Iodine and Photoredox Catalysis for the Amination of Csp³-H Bonds. *Angew. Chem., Int. Ed.* **2017**, *56* (27), 8004–8008.
- (7) Liu, Y.; Wang, B.; Qiao, X.; Tung, C. H.; Wang, Y. Iodine/Visible Light Photocatalysis for Activation of Alkynes for Electrophilic Cyclization Reactions. *ACS Catal.* **2017**, *7* (6), 4093–4099.
- (8) Sudo, Y.; Yamaguchi, E.; Itoh, A. Photo-Oxidative Cross-Dehydrogenative Coupling-Type Reaction of Thiophenes with α -Position of Carbonyls Using a Catalytic Amount of Molecular Iodine. *Org. Lett.* **2017**, *19* (7), 1610–1613.
- (9) Krumb, M.; Lucas, T.; Opatz, T. Visible Light Enables Aerobic Iodine Catalyzed Glycosylation. *Eur. J. Org. Chem.* **2019**, *2019* (28), 4517–4521.
- (10) Olmsted, J.; Karal, G. Iodine-Sensitized Photoformation of Singlet Oxygen. *J. Am. Chem. Soc.* **1972**, *94* (10), 3305–3310.
- (11) Strong, R. L.; Willard, J. E. Primary Quantum Yield for the Dissociation of Iodine Molecules in Carbon Tetrachloride Solution and the Rate Constant for the Recombination Reaction. *J. Am. Chem. Soc.* **1957**, *79* (9), 2098–2102.
- (12) Meadows, L. F.; Noyes, R. M. The Dependence on Wave Length of Quantum Yields for Iodine Dissociation. *J. Am. Chem. Soc.* **1960**, *82* (8), 1872–1876.
- (13) Booth, D.; Noyes, R. M. The Effect of Viscosity on the Quantum Yield for Iodine Dissociation. *J. Am. Chem. Soc.* **1960**, *82* (8), 1868–1872.
- (14) Voigt, E. M. Absorption Maxima of the Visible Band of Iodine in Different Groups of Solvents. *J. Phys. Chem.* **1968**, *72* (9), 3300–3305.
- (15) Tellinghuisen, J.; Whyte, A. R.; Phillips, L. F. Kinetics of Molecular Iodine Following Argon Fluoride (ArF) Laser Excitation: Thermal Dissociation of the A'(2u) State. *J. Phys. Chem.* **1984**, *88* (25), 6084–6087.
- (16) Berg, M.; Harris, A. L.; Harris, C. B. Rapid Solvent-Induced Recombination and Slow Energy Relaxation in a Simple Chemical Reaction: Picosecond Studies of Iodine Photodissociation in CCl₄. *Phys. Rev. Lett.* **1985**, *54* (9), 951–954.
- (17) Harris, A. L.; Berg, M.; Harris, C. B. Studies of Chemical Reactivity in the Condensed Phase. I. The Dynamics of Iodine Photodissociation and Recombination on a Picosecond Time Scale and Comparison to Theories for Chemical Reactions in Solution. *J. Chem. Phys.* **1986**, *84* (2), 788–806.
- (18) Abul-Haj, N. A.; Kelley, D. F. Reactions of Electronically Excited Iodine: Quenching of the A' State. *J. Phys. Chem.* **1987**, *91* (23), 5903–5905.
- (19) Ooe, H.; Kimura, Y.; Terazima, M.; Hirota, N. Photodissociation Quantum Yield of Iodine in the Low-, Medium-, and High-Density Fluids Studied by the Transient Grating Method. *J. Phys. Chem. A* **1999**, *103* (38), 7730–7741.
- (20) Lampe, F. W.; Noyes, R. M. Absolute Quantum Yields for Dissociation of Iodine in Inert Solvents. *J. Am. Chem. Soc.* **1954**, *76* (8), 2140–2144.
- (21) Yamashita, S.; Cosgrave, D. P.; Ono, H.; Toyama, O. The Photoisomerization of Cis-Azobenzene in the Presence of Iodine. *Bull. Chem. Soc. Jpn.* **1963**, *36* (6), 688–692.
- (22) Arnaud, R.; Lemaire, J. Isomerisation Cis-Trans de l'azobenzene Catalysée Par l'Iode. III. *Can. J. Chem.* **1974**, *52*, 1868–1871.
- (23) Lerch, M. M.; Hansen, M. J.; van Dam, G. M.; Szymanski, W.; Feringa, B. L. Emerging Targets in Photopharmacology. *Angew. Chem., Int. Ed.* **2016**, *55* (37), 10978–10999.
- (24) Hüll, K.; Morstein, J.; Trauner, D. In Vivo Photopharmacology. *Chem. Rev.* **2018**, *118* (21), 10710–10747.
- (25) Neilson, B. M.; Bielawski, C. W. Illuminating Photoswitchable Catalysis. *ACS Catal.* **2013**, *3* (8), 1874–1885.
- (26) Zhang, J.; Zou, Q.; Tian, H. Photochromic Materials: More than Meets the Eye. *Adv. Mater.* **2013**, *25* (3), 378–399.
- (27) Goulet-Hanssens, A.; Eisenreich, F.; Hecht, S. Enlightening Materials with Photoswitches. *Adv. Mater.* **2020**, *32* (20), 1905966.
- (28) Dong, L.; Feng, Y.; Wang, L.; Feng, W. Azobenzene-Based Solar Thermal Fuels: Design, Properties, and Applications. *Chem. Soc. Rev.* **2018**, *47* (19), 7339–7368.
- (29) Lancia, F.; Ryabchun, A.; Katsonis, N. Life-like Motion Driven by Artificial Molecular Machines. *Nat. Rev. Chem.* **2019**, *3* (9), 536–551.
- (30) Dong, M.; Babalhavaeji, A.; Samanta, S.; Beharry, A. A.; Woolley, G. A. Red-Shifting Azobenzene Photoswitches for in Vivo Use. *Acc. Chem. Res.* **2015**, *48* (10), 2662–2670.
- (31) Knie, C.; Utecht, M.; Zhao, F.; Kulla, H.; Kovalenko, S.; Brouwer, A. M.; Saalfrank, P.; Hecht, S.; Bléger, D. Ortho-Fluoroazobenzenes: Visible Light Switches with Very Long-Lived Z Isomers. *Chem. - Eur. J.* **2014**, *20* (50), 16492–16501.
- (32) Ahmed, Z.; Siiskonen, A.; Virkki, M.; Priimagi, A. Controlling Azobenzene Photoswitching through Combined: Ortho-Fluorination and -Amination. *Chem. Commun.* **2017**, *53* (93), 12520–12523.
- (33) Lameijer, L. N.; Budzak, S.; Simeth, N. A.; Hansen, M. J.; Feringa, B. L.; Jacquemin, D.; Szymanski, W. General Principles for the Design of Visible-Light-Responsive Photoswitches: Tetra- Ortho-Chloro-Azobenzenes. *Angew. Chem.* **2020**, *132* 21847.
- (34) Konrad, D. B.; Savasci, G.; Allmendinger, L.; Trauner, D.; Ochsenfeld, C.; Ali, A. M. Computational Design and Synthesis of a

Deeply Red-Shifted and Bistable Azobenzene. *J. Am. Chem. Soc.* **2020**, *142* (14), 6538–6547.

(35) Kuntze, K.; Viljakka, J.; Titov, E.; Ahmed, Z.; Kalenius, E.; Saalfrank, P.; Priimagi, A. Towards Low-Energy-Light-Driven Bistable Photoswitches: Ortho-Fluoroazobenzenes. Submitted for publication. *Res. Square* **2021** DOI: 10.21203/rs.3.rs-608595/v1

(36) Jones, L. B.; Hammond, G. S. Mechanisms of Photochemical Reactions in Solution. XXX.1 Photosensitized Isomerization of Azobenzene. *J. Am. Chem. Soc.* **1965**, *87* (18), 4219–4220.

(37) Fischer, E. Photosensitized Isomerization of Azobenzene. *J. Am. Chem. Soc.* **1968**, *90* (3), 796–797.

(38) Ronayette, J.; Arnaud, R.; Lebourgeois, P.; Lemaire, J. Isomérisation Photochimique de l'azobenzène En Solution. I. *Can. J. Chem.* **1974**, *52* (6), 1848–1857.

(39) Ronayette, J.; Arnaud, R.; Lemaire, J. Isomérisation Photosensibilisée Par Des Colorants et Photoréduction de l'azobenzène En Solution. II. *Can. J. Chem.* **1974**, *52*, 1858–1867.

(40) Bortolus, P.; Monti, S. Cis-Trans Photoisomerization of Azobenzene. Solvent and Triplet Donors Effects. *J. Phys. Chem.* **1979**, *83* (6), 648–652.

(41) Monti, S.; Gardini, E.; Bortolus, P.; Amouyal, E. The Triplet State of Azobenzene. *Chem. Phys. Lett.* **1981**, *77* (1), 115–119.

(42) Monti, S.; Dellonte, S.; Bortolus, P. The Lowest Triplet State of Substituted Azobenzenes: An Energy Transfer Investigation. *J. Photochem.* **1983**, *23* (2), 249–256.

(43) Isokuortti, J.; Kuntze, K.; Virkki, M.; Ahmed, Z.; Vuorimaa-Laukkanen, E.; Filatov, M. A.; Turshatov, A.; Laaksonen, T.; Priimagi, A.; Durandin, N. A. Expanding Excitation Wavelengths for Azobenzene Photoswitching into the Near-Infrared Range via Endothermic Triplet Energy Transfer. *Chem. Sci.* **2021**, *12* (21), 7504–7509.

(44) Goulet-Hanssens, A.; Utecht, M.; Mutruc, D.; Titov, E.; Schwarz, J.; Grubert, L.; Bléger, D.; Saalfrank, P.; Hecht, S. Electrocatalytic Z → E Isomerization of Azobenzenes. *J. Am. Chem. Soc.* **2017**, *139* (1), 335–341.

(45) Goulet-Hanssens, A.; Rietze, C.; Titov, E.; Abdullahi, L.; Grubert, L.; Saalfrank, P.; Hecht, S. Hole Catalysis as a General Mechanism for Efficient and Wavelength-Independent Z → E Azobenzene Isomerization. *Chem.* **2018**, *4* (7), 1740–1755.

(46) Berberich, M.; Krause, A.-M.; Orlandi, M.; Scandola, F.; Würthner, F. Toward Fluorescent Memories with Nondestructive Readout: Photoswitching of Fluorescence by Intramolecular Electron Transfer in a Diaryl Ethene-Perylene Bisimide Photochromic System. *Angew. Chem., Int. Ed.* **2008**, *47* (35), 6616–6619.

(47) Bakalyar, S. R.; Bradley, M. P. T.; Honganen, R. The Role of Dissolved Gases in High-Performance Liquid Chromatography. *J. Chromatogr. A* **1978**, *158*, 277–293.

(48) Sato, T.; Hamada, Y.; Sumikawa, M.; Araki, S.; Yamamoto, H. Solubility of Oxygen in Organic Solvents and Calculation of the Hansen Solubility Parameters of Oxygen. *Ind. Eng. Chem. Res.* **2014**, *53* (49), 19331–19337.

(49) Turque, O.; Greer, A.; Wauchope, O. R. Synthetic Feasibility of Oxygen-Driven Photoisomerizations of Alkenes and Polyenes. *Org. Biomol. Chem.* **2020**, *18* (45), 9181–9190.

(50) Rihter, B. D.; Kenney, M. E.; Ford, W. E.; Rodgers, M. A. J. Synthesis and Photoproperties of Diamagnetic Octabutoxyphthalocyanines with Deep Red Optical Absorbance. *J. Am. Chem. Soc.* **1990**, *112* (22), 8064–8070.

(51) Krumova, K.; Cosa, G. Chapter 1 Overview of Reactive Oxygen Species. In *Singlet Oxygen: Applications in Biosciences and Nanosciences*, Vol. 1; The Royal Society of Chemistry: London, 2016; Vol. 1, pp 1–21. DOI: 10.1039/9781782622208-00001.

(52) Schwarz, H. A.; Bielski, B. H. J. Reactions of HO₂ and O₂- with Iodine and Bromine and the I₂- and I Atom Reduction Potentials. *J. Phys. Chem.* **1986**, *90* (7), 1445–1448.

(53) Scully, F. E. J. Generation and Subsequent Quenching of Singlet Oxygen in the Reaction of Potassium Superoxide with Iodine. In *Biochemical and clinical aspects of oxygen*; Caughey, W. S., Ed. Academic Press, 1979; pp 627–634.

(54) Van Benthem, M. H.; Davis, S. J. Detection of Vibrationally Excited Molecular Iodine in the Dissociation Region of Chemical Oxygen-Iodine Lasers. *J. Phys. Chem.* **1986**, *90* (5), 902–905.

PUBLICATION IV

A visible-light-driven molecular motor based on barbituric acid

Kuntze, K.,[†] Pooler, D. R. S.,[†] Di Donato, M., Hilbers, M. F., van der Meulen, P.,
Buma, W. J., Priimägi, A., Feringa, B. L. & Crespi, S.

Chemical Science, 2023

DOI: <https://doi.org/10.1039/D3SC03090C>

[†] Equal contribution.

Publication reprinted with the permission of the copyright holders.



Cite this: DOI: 10.1039/d3sc03090c

All publication charges for this article have been paid for by the Royal Society of Chemistry

A visible-light-driven molecular motor based on barbituric acid†

Kim Kuntze,^{‡ab} Daisy R. S. Pooler,^{‡a} Mariangela Di Donato,^{‡cd} Michiel F. Hilbers,^e Pieter van der Meulen,^a Wybren Jan Buma,^{‡ef} Arri Priimagi,^{‡b} Ben L. Feringa^{‡*a} and Stefano Crespi^{‡*ag}

We present a class of visible-light-driven molecular motors based on barbituric acid. Due to a serendipitous reactivity we observed during their synthesis, these motors possess a tertiary stereogenic centre on the upper half, characterised by a hydroxy group. Using a combination of femto- and nanosecond transient absorption spectroscopy, molecular dynamics simulations and low-temperature ¹H NMR experiments we found that these motors operate similarly to push–pull second-generation overcrowded alkene-based molecular motors. Interestingly, the hydroxy group at the stereocentre enables a hydrogen bond with the carbonyl groups of the barbituric acid lower half, which drives a sub-picosecond excited-state isomerisation, as observed spectroscopically. Computational simulations predict an excited state “lasso” mechanism where the intramolecular hydrogen bond pulls the molecule towards the formation of the metastable state, with a high predicted quantum yield of isomerisation (68%) in gas phase.

Received 16th June 2023

Accepted 20th July 2023

DOI: 10.1039/d3sc03090c

rsc.li/chemical-science

Introduction

The fast (<200 fs)¹ and efficient (quantum yield, $\phi = 67\%$)² light-triggered nanoscale motion of the protonated Schiff base of 11-*cis*-retinal (PSBR) represents a continuous inspiration for chemists developing photoactive molecules based on *E*–*Z* isomerisation which can harvest light as effectively as the ones designed by Nature.^{3–6} Among these, light-driven rotary molecular motors have been developed (Fig. 1A), which absorb photons to fuel the unidirectional rotation of a rotator moiety about a stator moiety through successive photochemical *E*–*Z* isomerisations and thermal ratcheting steps.^{7,8} These motors can undergo repetitive, unidirectional rotary motion,^{8–13} can be integrated into larger artificial molecular machines,^{14,15} and are

the key components to drive complex systems out of equilibrium.^{16–18} Their ability to control dynamic movement at the molecular level is a marvellous prospect, with potential applications ranging from biotechnology^{19–21} to materials science.^{22–24} Further adaptation of these molecular motors towards structures similar to PSBR stimulated the development of an oxindole-based molecular motor (Fig. 1A), exploiting an engineered electronic charge-transfer effect which drives the decay from the excited state in a similar manner to PSBR.²⁵

Taking direct inspiration from the molecular structure of a natural product and translating it into a synthetic molecule is a powerful biomimetic strategy, which has been employed successfully by Olivucci and co-workers with respect to PSBR, giving rise to the positively charged *N*-alkylated indanylidene-pyrrolinium (NAIP) photoswitches that demonstrate similar photoreaction dynamics to PSBR.^{26–29} As another example, the biomimetic strategy has also been applied to the chromophore of the Green Fluorescent Protein (GFP), another natural product with impressive photoactivity,³⁰ to synthesise *p*-hydroxydimethylindanylidene-oxopyrrolone (*p*-HDIOP) anionic photoswitches.³¹ In both NAIP and *p*-HDIOP photoswitches, the *E*–*Z* isomerisation is driven by biomimetic charge-transfer character in *S*₁, a result echoed in the aforementioned oxindole-based molecular motor (Fig. 1A).²⁵

Barbituric acid is a readily available chemical building block with a strongly electron-withdrawing core. For this reason, it has remarkably acidic methylene protons ($pK_a \approx 4$) enabling Knoevenagel condensations with various electrophiles under mild conditions.³² Its electron-withdrawing nature has also been exploited in the design of dyes and photoswitches with

^aStratingh Institute for Chemistry, University of Groningen, Nijenborgh 4, 9746 AG Groningen, The Netherlands. E-mail: b.lferinga@rug.nl; stefano.crespi@kemi.uu.se

^bFaculty of Engineering and Natural Sciences, Tampere University, FI-33101 Tampere, Finland

^cEuropean Laboratory for Non Linear Spectroscopy (LENs), via N. Carrara 1, 50019 Sesto Fiorentino, Italy

^dICCOM-CNR, via Madonna del Piano 10, 50019 Sesto Fiorentino, FI, Italy

^eVan't Hoff Institute for Molecular Sciences, University of Amsterdam, Science Park 904, 1098 XH, Amsterdam, The Netherlands

^fInstitute for Molecules and Materials, FELIX Laboratory, Radboud University, Toernooiveld 7c, 6525 ED, Nijmegen, The Netherlands

^gDepartment of Chemistry, Ångström Laboratory, Uppsala University, Box 523, 751 20 Uppsala, Sweden

† Electronic supplementary information (ESI) available. CCDC 2269893. For ESI and crystallographic data in CIF or other electronic format see DOI: <https://doi.org/10.1039/d3sc03090c>

‡ These authors contributed equally.

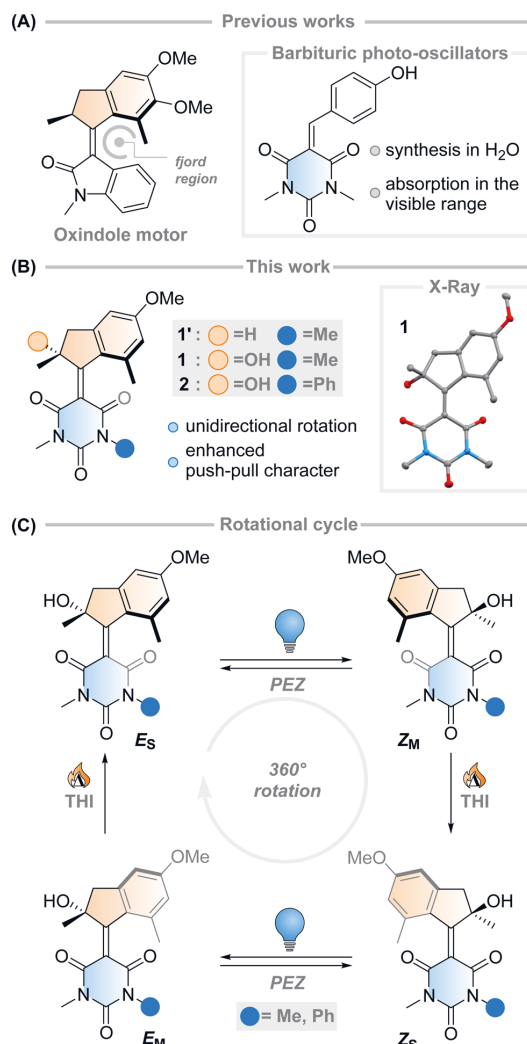


Fig. 1 (A) Previous literature examples that led to the Feringa-type light-driven molecular motor presented in this work. The molecule is based on a charge-transfer oxindole structure and barbituric acid-based photo-oscillators. (B) This work, an investigation of barbituric acid-based molecular motors **1** and **2** (X-ray structure of **1**: non-H atoms represented as 50% probability ellipsoids, H-bond evidenced for clarity). (C) Proposed rotational cycle of motors **1** and **2**.

push-pull character, most notably donor-acceptor Stenhouse adducts.³³ Recently, a family of photo-oscillators based on barbituric acid were introduced, featuring high molar absorptivity between 350–400 nm and ultrafast photodynamics (Fig. 1A).³⁴ They can be readily obtained in high yields by an easily accessible synthetic route *via* a Knoevenagel condensation in water. However, the possibility of utilising barbituric acid derivatives in photoswitches or molecular motors has not been explored yet.

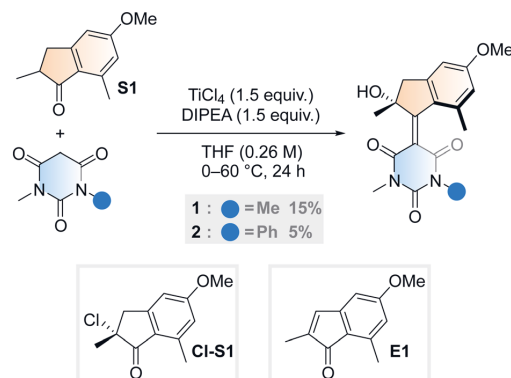
Intrigued by this work, we envisioned that an overcrowded alkene-based design featuring barbituric acid in the lower half could operate as a second-generation Feringa-type molecular motor with high visible light absorptivity (**1'**, Fig. 1B). Surprisingly, when attempting to synthesise motor **1'** we consistently obtained motor **1**, with a stereocentre featuring a tertiary alcohol. Mechanistic experiments support the presence of a peroxide as an intermediate in the formation of the motor and quantum chemical calculations show that **1** is 2.4 kcal mol^{−1} more stable than its hydrogenated counterpart **1'** (see ESI† for further details). These results hint towards the formation of a thermodynamically favoured product in the dynamic covalent chemistry of barbituric acid condensation.³²

Inspired by this serendipitous discovery, we report the detailed investigation of the photochemical *E*–*Z* (PEZ) steps that convert the stable states (E_S or Z_S) into the respective isomerised metastable states (Z_S or E_M), and thermal helix inversion (THI) steps of the novel motor **1** (Fig. 1C).²⁵ We show that the OH group present in **1** plays a crucial role in the S_1 photoisomerisation step: as the lower half rotates, the OH group forms hydrogen bonds with the carbonyl groups on the barbituric acid half, actively pulling the rotation forwards. The absence of a strong solvent effect and computational insights suggest that **1** may act as a motor in apolar solvents, with its unidirectional efficiency decreasing in more polar ones.³⁵

Results and discussion

Synthesis

Aiming to further expand the scope of motors operating continuously at room temperature,^{36–38} we reacted the barbituric acid moiety with an upper half featuring a five-membered ring because the combination of the latter with six-membered lower halves typically provides motors with low THI barriers.⁴ The ketone precursor is synthesised in one step from 3-methylanisole and methacrylic acid in a Friedel–Crafts acylation followed by a Nazarov cyclisation, facilitated by polyphosphoric acid (PPA). To attain our motor design, we tested typical



Scheme 1 Synthetic procedure for motor **1** and **2**, initially hypothesised alpha-chlorinated intermediate **Cl-S1** and elimination side product, **E1**.

Knoevenagel conditions reported for barbituric acid condensations with ketones.³⁹ Contrary to previously published reactions involving less hindered ketones or aldehydes,³⁴ we only observed reactivity when both a Lewis acid (TiCl_4) and a non-nucleophilic base (diisopropylethylamine, DIPEA) were used⁴⁰ (Scheme 1). Even though barbituric acid is more enolisable than oxindole,^{25,40} the reaction was markedly slower than in our previous studies on oxindole-based motors: after 24 hours at 60 °C, 65% of the ketone precursor was recovered. Most surprisingly, instead of the typical tertiary stereogenic centre at the allylic position of overcrowded alkene-based motors (**1'**, Fig. 1B), we isolated exclusively compound **1**, featuring a stereocentre with a hydroxy group at the tertiary carbon (Scheme 1). To the best of our knowledge, this alpha-hydroxylation during a Knoevenagel condensation is unprecedented in the literature. In addition to **1** and recovered starting materials, the reaction yielded varying amounts of an elimination product **E1** (see Scheme 1) as well as side products originating from the reaction between TiCl_4 and tetrahydrofuran.⁴¹

To gain insight into the mechanism of the unexpected reaction, we explored how various parameters affected its outcome. The product composition was unaffected by ambient light, residual moisture, atmospheric oxygen and whether the reaction was quenched with water, deuterium oxide or methanol (see ESI, Table S1†). Our initial hypothesis of an alpha-chlorinated intermediate was refuted when no product was acquired starting from the alpha-chloroketone **Cl-S1** (Scheme 1). We also ran the reaction with an ^{18}O -labelled **S1**, yielding **1** in an identical yield to a control reaction run in parallel, and with no trace of ^{18}O in the structure (see ESI, Fig. S1†). Thus, we concluded that the unexpected oxygen originates from outside the starting materials and not from a rearrangement reaction. Probing the reaction mixture directly to record any reactive intermediates was attempted by running the reaction in THF-d_8 , but NMR on the unquenched reaction mixture could not be measured possibly due to paramagnetic species forming during the reaction.

However, some hints to the mechanism were obtained by studying the reaction mixture with UPLC-MS immediately after quenching. Interestingly, instead of the expected $[\text{M} + \text{H}]^+$ and $[\text{M} + \text{Na}]^+$ signals for **1**, we observed for each m/z values 16 mass units larger. After full work-up, the expected signals for **1** were observed. This result might suggest that the reaction proceeds through the addition of an O_2 molecule forming a peroxide intermediate, and that the O–O bond is broken during the work-up. However, such a mechanism seems to be at odds with the observation that the reaction appears to proceed similarly under ambient conditions and in carefully degassed solutions under an argon atmosphere.

Single crystals of **1** suitable for X-ray diffraction were grown from a saturated solution of the compound in an EtOAc/pentane mixture (see Fig. 1 and ESI†). Compound **1** crystallised with two molecules of **1** in the unit cell, both possessing the same chirality at the methyl stereocentre. The molecules have a $\text{C}=\text{C}$ bond length of 1.38 Å, a value which is relatively elongated compared to typical overcrowded alkenes (~ 1.35 Å).^{40,42} This result may allude to a higher degree of single-bond

character in the central alkene bond, possibly due to push–pull nature arising from the highly electron-withdrawing barbituric acid lower half and the electron-donating OMe group on the upper half. The dihedral angles (angle $\text{C}_\text{A}\text{C}_\text{B}\text{C}_\text{C}\text{C}_\text{D}$, see Scheme 1 for labelling) of both motors in the unit cell were 27.35° and 29.70° respectively, consequently showing helical chirality, a key requisite for unidirectional molecular motors.⁴ Additionally, due to the hydroxy group at the stereocentre, compound **1** undergoes hydrogen bonding in the solid state. The preferred intramolecular interaction is reflected in the length of the H-bond between the OH and the $\text{C}=\text{O}$ group on the barbituric acid moiety, which is either 2.61 or 2.65 Å, while the intermolecular H-bonding between the OH group and the OMe group on a neighbouring molecule is considerably longer (3.03 Å, see Fig. 1 and S7†).

Desymmetrised motor **2** was synthesised using the same method as motor **1** but with 1-methyl-3-phenylbarbituric acid as the lower half reactant. The asymmetric barbituric acid lower half was prepared in two steps from methylamine, phenyl isocyanate and malonic acid. The Knoevenagel step was slower and lower-yielding than for **1**, but the same stereocentre bearing an OH group was formed. The product was isolated as a 1 : 1 mixture of the *E* and *Z* isomers. They were separated by supercritical fluid chromatography (SFC, see ESI†) and subsequently concentrated by freeze-drying in the dark, to mitigate unwanted thermal and photochemical isomerisation processes. After purification, the 1 : 1 mixture could be enriched to contain a 73 : 27 ratio of both stable isomers (**2a** : **2c**). Unfortunately, the exact stereochemistry of these isomers could not be determined, due to fast thermal and photochemical isomerisation at ambient conditions.

Photochemical isomerisation

Motor **1** shows an absorption maximum between approximately 420–445 nm in multiple solvents (Fig. 2A and Table 1) with a solvatochromic effect, reflecting the push–pull nature of the molecule. The molar absorption coefficients reflect the $\pi\pi^*$ nature of the first absorption band. Since **1** has an asymmetric centre alpha to the central alkene axle, the structure presents strong similarities with typical molecular motors.⁴³ Due to the symmetrical nature of the lower half, we predict that **1** will act similarly to a second-generation motor with only two isomers: a stable isomer, **1_S** and a metastable isomer, **1_M**. By extension, the asymmetric structure **2** will operate in a 4-step process, as described by Fig. 1C.

We studied the ultrafast excited state behaviour of compounds **1** and **2** by measuring their transient absorption spectra upon excitation at 400 nm in multiple solvents. The ultrafast behaviour of the two compounds is similar, so we will describe the behaviour of compound **1** and refer the reader to the ESI† for compound **2**.

Fig. 3 displays a selection of transient absorption spectra recorded upon 400 nm excitation of solution of **1** in MeOH. As noticed by looking at the time/wavelength map (Fig. 3A), an intense negative band peaking at ~ 430 nm appears immediately after excitation. Considering the steady-state absorption of

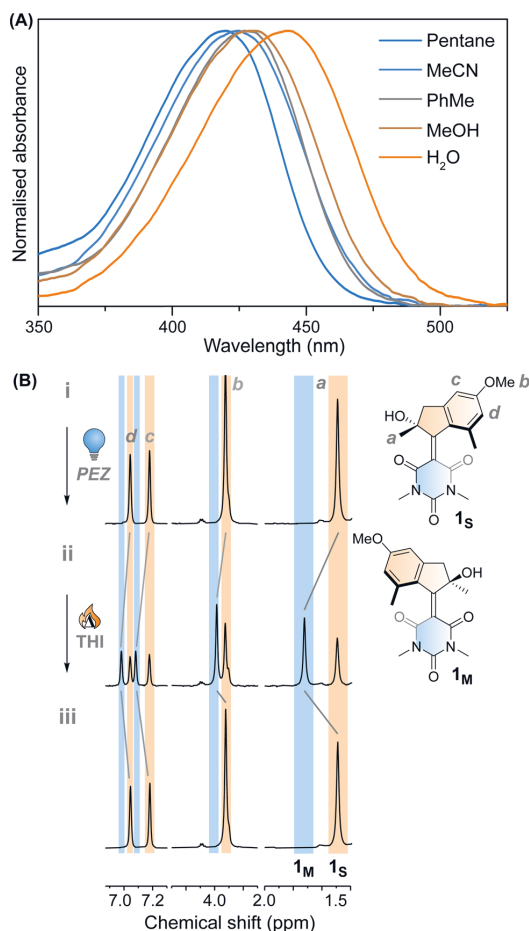


Fig. 2 (A) Normalised UV-vis absorption spectra of **1_S** in different solvents. (B) ¹H NMR irradiation studies of **1_S** in CD₃OD (*c* = 1 × 10^{−5} M) at −90 °C. (i) **1_S** before irradiation; (ii) PSS₄₂₀, 63 : 37 (**1_M** : **1_S**); (iii) THI, −45 °C, 15 min.

the samples, this band is attributed to ground state bleaching. A very broad and less intense negative signal is also noticed, extending up to 650 nm, associated with a very weak stimulated emission (see ESI†). This transient signal is a fingerprint of the emissive Franck-Condon state in molecular motors.^{25,44} In less than 1 ps, the ground state bleaching signal recovers significantly and a red-shifted positive band develops, which we assign to the absorption of the photoisomerisation product. This band indicates that once excited, the sample rapidly reaches a conical intersection (CInt)⁴⁵ and subsequently returns to the ground state, S₀. The excited sub-ps dynamics is similar to the one observed in the barbituric acid photo-oscillators.³⁴ During the ensuing evolution occurring on the picosecond time scale, the intensity of the differential signal decreases without a significant change of the bandshape.

We attribute these dynamics to vibrational and solvent-induced relaxation of the photoproduct in the ground state.

We assign the final signal to the metastable state (**1_M**), which is characterised by a red-shifted absorption band for molecular motors.^{25,44}

This assignment is also confirmed by ¹H NMR at −90 °C in CD₃OD. A new set of signals were formed upon *in situ* irradiation with 420 nm light, which we ascribe to **1_M**, giving a photo-stationary distribution (PSD) of 63 : 37 **1_M** : **1_S** (Fig. 2B). The isomerisation can be clearly followed by the substantial shift of the stereogenic group protons, H_a, from 1.51 ppm to 1.62 ppm. Under these conditions, no photodegradation was observed, proving motor **1** to be photochemically robust. Furthermore, we analysed the solvent dependence of the actinic process by measuring the transient absorption spectra of the compounds in a variety of solvents of different polarity/polarisability. As noticed by the comparison of the kinetic traces recorded at the maximum of the bleaching signal (Fig. 3B), the dynamics of the excited state evolution is almost independent from the solvent properties. Comparing the kinetic traces recorded on the product band, we instead notice a higher solvent dependence (Fig. 3C).

This effect is attributed to the different solvent-induced relaxation dynamics of the **1_M** that reaches the ground state on a sub-ps scale, in a vibrationally hot state. It appears that the relaxation process is slightly faster in polar solvents, such as DMSO, than in non-polar ones, like hexane, but this may also be attributed to viscosity⁴⁶ and the possibility to interact with the hydroxy group of the upper half. The relaxation dynamics of compound **2** is slightly more sensitive to the solvent nature as compared to compound **1** (see ESI, Fig. S9†).

We performed an excited state molecular dynamics simulation of **1_S** at the OM2/MRCI level of theory^{47–49} to obtain a more qualitative understanding of the excited state dynamics. Out of the initial 400 initial conditions obtained from a Wigner sampling, 332 were successfully propagated for 2 ps using an NVT ensemble with a Nosé-Hoover thermostat after initial excitation to the S₁ state. The simulation predicted an excited-state lifetime of 0.53 ps in the gas phase, which is in excellent agreement with the experimental value of 0.5 ps obtained from the femtosecond spectroscopy experiments in hexane (see Table 1 and ESI† for details on data analysis). In our simulation, the ensemble proceeds following a rotational movement of the double bond towards a perpendicular configuration of the upper and lower halves. In this region, characterised by a dihedral angle of rotation about the double bond of 90°, the molecule funnels to the ground state *via* a CInt, populating either the metastable **1_M** or leading unproductively back to **1_S**.

Interestingly, we predicted the excited state of the molecule to be diradical in nature along the entire isomerisation path, explaining the limited effect that the solvent has on the actinic process. The simulation conducted in the gas phase led to a predicted quantum yield of 68% (see Fig. 4A), a high value in which the hydroxy group and the absence of explicit solvents interacting with it could play a crucial role. Indeed, after excitation the hydrogen bond between the OH group and the C=O in its immediate proximity is lost, with the concomitant rotation of the lower half about the double bond. Immediately after the molecule reaches the perpendicular orientation of the CInt

Table 1 Photophysical parameters of motor **1** in different solvents, excited state lifetimes of **1_s** and thermal lifetimes of **1_m** as measured by laser flash photolysis. The solvents are ordered according to increasing polarity

	λ_{max} (nm)	ϵ (M ⁻¹ cm ⁻¹)	τ_1 1_s * (ps)	τ_2 1_s * (ps)	τ_3 1_s * (ps)	τ 1_m → 1_s (10 ⁻² s)
Pentane	425	19 200				1.23
Hexane			0.5	10.5		
1,4-Dioxane	421	18 900				1.97
Toluene	441	18 500	0.6	8.5	38.2	2.88
DCM	432	20 400	0.7	6.6	30.3	7.47
THF	428	18 300				1.17
Decanol	433	18 100				1.46
<i>i</i> PrOH	435	19 100				0.588
EtOH	428	20 100				0.181
MeOH	432	19 100	0.7	3.3	44.4	0.134
MeCN	424	18 600	0.6	1.5	13.7	3.42
Glycerol	430	15 300				0.181
DMSO	432	14 400	0.7	6.8	170.9	7.55
H ₂ O	444	12 800				7.87 × 10 ⁻⁴

and funnels through it to the ground state, the OH starts to interact with the second C=O, leading to a “lasso” effect that pulls the geometry towards the formation of the metastable state (see Fig. 4B). This behaviour is similar to the one predicted by García-Iriepa and coworkers, who designed computationally a retinal-based motor with high rotational speed and absence of thermal steps, thanks to the formation of hydrogen bonds imparting directionality to the motion.⁵⁰ We also underline that the diradical nature of the excited state could be crucial in the sub-ps dynamics observed.²⁵ Indeed, the limited pyramidalization at the computed conical intersection geometry could allow a fast rotational movement at the excited state, as hypothesized by Olivucci and Filatov.⁵ It is worth mentioning that the high quantum yield values could be a reflection of the absence of medium in the molecular dynamics simulation. Indeed there are different reports that confirm the fundamental contribution of explicitly treated solvent molecules in lowering the predicted efficiency of the photochemical step.³⁶ This observation is further explored in a recent preprint of Olivucci *et al.* focusing on the explicit cavity effect on the computed quantum yields of Rhodopsin and the biomimetic molecular rotor *para*-methoxy *N*-methyl indanylidene-pyrrolinium.⁵¹

Thermal isomerisation steps

The thermal pathway of isomerisation of **1** was studied using nanosecond transient spectroscopy. After the pump pulse, we were able to observe the formation of a transient signal red-shifted compared to the ground state bleach (see ESI†), which we assigned to the absorption of the metastable state **1_m** in accordance with the femtosecond transient spectroscopy data (*vide supra*). In most of the solvent analysed, we noted only a minimal effect of the solvent polarity on the recovery of the metastable state (see Table 1). This finding is expected for the THI process,⁵² and is supported by our calculations at the DSD-BLYP-D3BJ/def2-QZVP//r²SCAN-3c level (see Fig. 4D), which predict the THI step to be considerably lower in energy than the transition step associated with the thermal *E*-*Z* isomerisation (TEZI). We found two pathways for the THI with barriers of 19

and 14 kcal mol⁻¹ when considering the presence (or absence, respectively) of hydrogen bonding between the OH and the neighbouring C=O group of the lower half.

These values equate to lifetimes of milliseconds at room temperature, well in line with our experimental results (Table 1). However, when attempting to measure exchange spectroscopy (EXSY) in a D₂O : DMSO-*d*₆ (9 : 1) mixture, we observed gradual bleaching of the solution and the disappearance of the signals for **1**. Hence, it is not possible to clearly assign the process observed in water, due to a competing decomposition pathway (see Fig. S5†).

The different solvent polarisability could have a more peculiar effect. We computed the barriers for TEZI and THI using both gas and water as implicit solvent at the CPCM level.⁵³ We observed that the barrier for TEZI is higher in gas phase than THI (21 kcal mol⁻¹ vs. 14 kcal mol⁻¹), but this is inverted in a highly polar medium, *viz.* water (14 kcal mol⁻¹ vs. 16 kcal mol⁻¹).

This finding is supported by the OM2/MRCI computations which predict a zwitterionic, closed-shell nature for the TEZI transition state, explaining the stabilisation of the thermal C=C bond breaking pathway. Nevertheless, we predict this molecule to be a motor at room temperature in all solvents of different polarisability (although with different degrees of efficiency). Indeed, due to the relatively similar energy barriers between TEZI and THI, in water the thermal *E*-*Z* isomerisation remains a competing event which can be compared to the metastable to stable photochemical back isomerisation competing with the formation of **1_m**. Indeed, upon photochemical population of the metastable state, **1_m** can revert back to **1_s** via TEZI which is slightly more favoured than the THI. However, considering the low values of both barriers (see Fig. 4B, blue lines), also the THI transition state will be accessible. Hence, the ratcheting step of the THI at room temperature will lead to an overall continuous unidirectional motion. Moreover, the similar values of the predicted thermal barriers explain the minimal difference observed with nanosecond transient spectroscopy when evaluating the metastable to stable thermal recovery. In addition, the presence of a solvent that

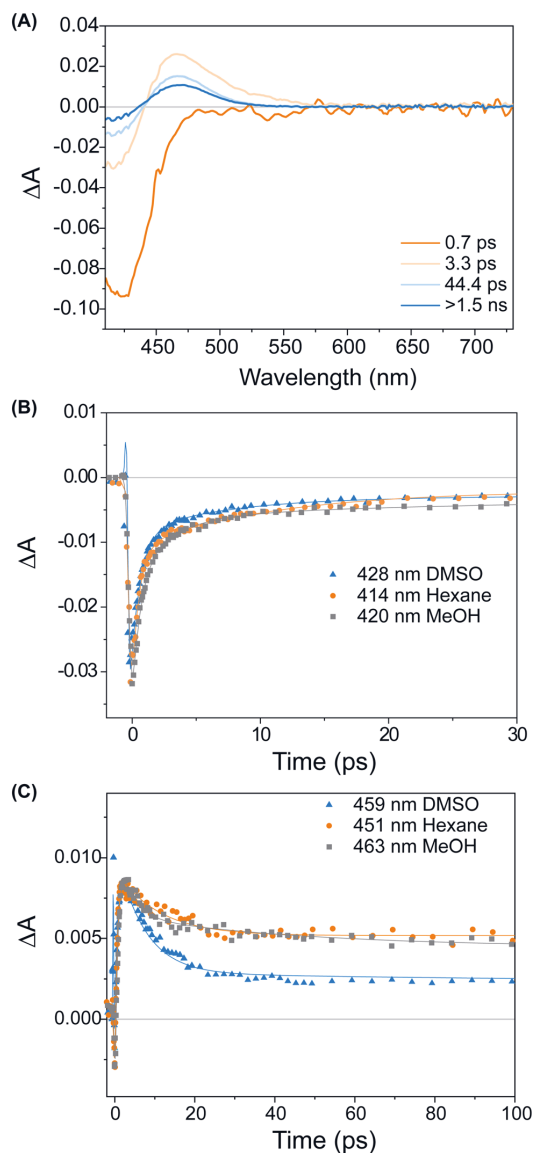


Fig. 3 (A) Evolution Associated Difference Spectra (EADS) obtained from global analysis of the transient absorption data of compound **1** recorded in MeOH. (B) Comparison of kinetic traces recorded on the ground state bleach band of compound **1** in various solvents. (C) Comparison of kinetic traces recorded on the product absorption band of compound **1** in various solvents. The solid lines represent the global fit of the signals.

weakens the intramolecular hydrogen bond lowers the barriers (Fig. S25[†]), but provides qualitative trends similar to the ones predicted in Fig. 4B.

To prove these hypotheses experimentally, photochemical switching of compound **2** was carried out in ^1H NMR at -90°C in CD_3OD , in an effort to see sequential population of all four

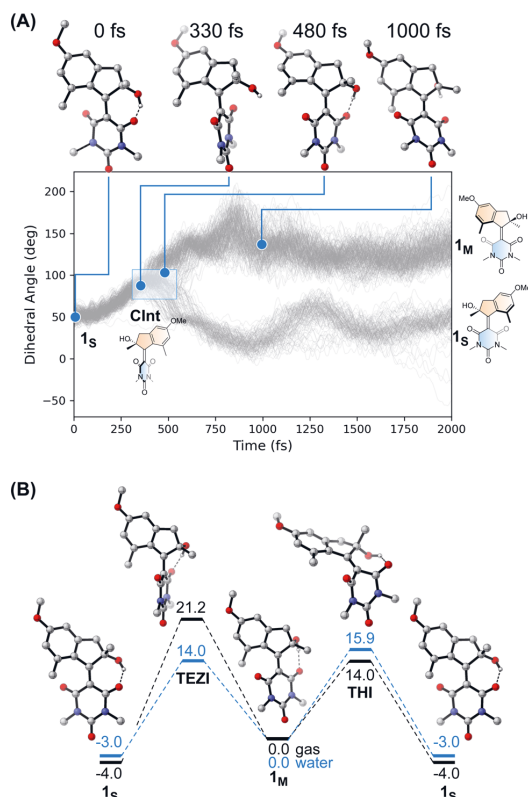


Fig. 4 (A) Evolution of the dihedral angle associated with the rotation about the central $\text{C}=\text{C}$ bond over time obtained at the OM2/MRCI level. It is possible to appreciate the different distribution of **1_M** and **1_s** after reaching the Cint region (highlighted in the figure). Top: Snapshots of the isomerisation of **1** selected from a productive MD simulation that led to the formation of **1_M** underlining the hydrogen bond "lasso" effect. (B) Gibbs free energies (DSD-BLYP-D3BJ/def2-QZVP//r²SCAN-3c level, in kcal mol^{-1}) for the thermal processes of motor **1** on the ground state surface. The black surface depicts the energies of the structures computed in the gas phase. The blue surface, in contrast, represents the energies of the structures computed using water as implicit solvent (CPCM).

isomers in the rotation cycle (see ESI[†]). Upon irradiation of the enriched mixture of the diastereomeric stable isomers (**77** : **23**, **2a** : **2c** after SFC separation, dubbed as such due to the nontrivial assignment of the *E/Z* configuration to a specific set of NMR signals) with a 420 nm LED, two new sets of signals appeared, which we assign to the metastable isomers **2b** and **2d**. The PSS ratio at 420 nm was found to be 12 : 19 : 9 : 61 (**2a** : **2b** : **2c** : **2d**) (Fig. S3[†]). The THI process was monitored at -90°C in the NMR, and both metastable states fully converted back to their corresponding stable states after 70 min in the dark (Fig. S4[†]) to a new population of 73 : 27, **2a** : **2c**. From this data, it can be determined that both processes are unimolecular, that **2d** converts thermally into **2a**, and that **2b** converts thermally into **2c**. While the directionality of rotation cannot be univocally

proven with this data, the variation of the distribution of the stable diastereomers hints towards a motor function.

Conclusions

In summary, we present a novel light-driven rotary molecular motor with a lower half based on barbituric acid. The motor could be obtained in modest yields in a simple synthetic route, the key step being a Knoevenagel condensation. Surprisingly, a hydroxy unit is installed in the stereogenic centre during the condensation. Many modifications of the original synthetic strategy were ventured, however we cannot yet be sure of the mechanistic steps towards motor **1**. Due to this unexpected reaction, the stereogenic centre on the upper half becomes a tertiary alcohol. We investigated the photochemical and thermal isomerisation steps with femtosecond- and nanosecond-scale transient absorption spectroscopy and low-temperature NMR spectroscopy. Motor **1** functions as a second-generation Feringa-type molecular motor, exhibiting sub-picosecond *E*–*Z* isomerisation dynamics under visible-light excitation and ultrafast thermal barriers for helix inversion. Compared to typical second-generation motors, **1** has high isomerisation quantum yields (68% estimated computationally), which is attributed to two factors: (i) the strongly electron-withdrawing nature of the barbituric acid lower half leads to efficient axial rotation, and (ii) hydrogen bonding between the fortuitous hydroxy group and the carbonyl groups of the lower half actively promotes the isomerisation.

Data availability

The datasets supporting this article have been uploaded as part of the ESI.† All cartesian coordinates for all the compounds considered are provided as a separate additional file in a figshare repository with the following DOI: https://figshare.com/articles/dataset/dx_doi_org_10_6084_m9_figshare_6025748/6025748.

Author contributions

K. K. and D. R. S. P. contributed equally to this work. D. R. S. P. and S. C. conceived the project and designed the molecules. K. K. synthesised all molecules and carried out all synthetic troubleshooting. D. R. S. P. and K. K. carried out NMR experiments and steady state UV-vis experiments. D. R. S. P. measured X-ray diffraction and carried out preparative SFC. S. C. performed computational calculations. M. D. D. and D. R. S. P. carried out femtosecond TA experiments. M. H., S. C. and W. J. B. performed nanosecond TA experiments. K. K., D. R. S. P. and S. C. wrote the manuscript. B. L. F., S. C., M. D. D., A. P. and W. J. B. supervised the work. All authors discussed and commented on the manuscript. S. C., A. P., and B. L. F. acquired funding.

Conflicts of interest

There are no conflicts to declare.

Acknowledgements

K. K. and D. R. S. P. thank Pieter van der Meulen and Dr Johan Kemmink for guidance with low temperature NMR measurements, Renze Sneepe for guidance with preparative SFC, and Jacob Baas for guidance in measuring XRD. D. R. S. P. and M. D. D. thank Laura Bussotti, Sandra Doria and Alessandro Iagatti for supporting the femtosecond transient absorption spectroscopy measurements. We thank the Centre for Information Technology of the University of Groningen for their support and for providing access to the Peregrine high performance computing cluster. Financial support from the Horizon 2020 Framework Programme (ERC Advanced Investigator Grant No. 694345 to B. L. F., ERC Consolidator Grant No. 101045223 for A. P.), the Netherlands Ministry of Education, Culture and Science (Gravitation Programme 024.001.035 to B. L. F.), the Marie Skłodowska-Curie Action (Individual Fellowship No. 838280 to S. C.) and the Swedish Vetenskapsrådet (for the Starting Grant 2021-05414 to S. C.). The Tampere University Graduate School (K. K.), Finnish Cultural Foundation (K. K.), and Tampere Science Fund (K. K.) are gratefully acknowledged. This project has received funding from the European Union's Horizon 2020 Research and Innovation Programme (Laserlab-Europe No. 871124 to M. D. D. and D. R. S. P.) and Academy of Finland Center of Excellence "Life-Inspired Hybrid Materials Research" (LIBER, No. 346107). We thank the Swedish National Infrastructure for Computations (SNIC) for a Small Compute Grant (SNIC 2022/22-525).

Notes and references

- 1 R. Schoenlein, L. Peteanu, R. Mathies and C. Shank, *Science*, 1991, **254**, 412–415.
- 2 H. J. A. Dartnall, *Vision Res.*, 1968, **8**, 339–358.
- 3 *Molecular Switches*, ed. B. L. Feringa and W. R. Browne, Wiley-VCH Verlag GmbH & Co. KGaA, Weinheim, Germany, 2011.
- 4 D. R. S. Pooler, A. S. Lubbe, S. Crespi and B. L. Feringa, *Chem. Sci.*, 2021, **12**, 14964–14986.
- 5 M. Filatov and M. Olivucci, *J. Org. Chem.*, 2014, **79**, 3587–3600.
- 6 *Molecular Photoswitches*, ed. Z. L. Pianowski, Wiley, 2022.
- 7 S. Corra, M. Curcio and A. Credi, *JACS Au*, 2023, **3**(5), 1301–1313.
- 8 N. Koumura, R. W. J. Zijlstra, R. A. van Delden, N. Harada and B. L. Feringa, *Nature*, 1999, **401**, 152–155.
- 9 N. Koumura, E. M. Geertsema, A. Meetsma and B. L. Feringa, *J. Am. Chem. Soc.*, 2000, **122**, 12005–12006.
- 10 J. C. M. Kistemaker, P. Štacko, J. Visser and B. L. Feringa, *Nat. Chem.*, 2015, **7**, 890–896.
- 11 L. Greb and J. M. Lehn, *J. Am. Chem. Soc.*, 2014, **136**, 13114–13117.
- 12 M. Guentner, M. Schildhauer, S. Thumser, P. Mayer, D. Stephenson, P. J. Mayer and H. Dube, *Nat. Commun.*, 2015, **6**, 8406.
- 13 A. Gerwien, M. Schildhauer, S. Thumser, P. Mayer and H. Dube, *Nat. Commun.*, 2018, **9**, 1–9.

- 14 S. Krause and B. L. Feringa, *Nat. Rev. Chem.*, 2020, **4**, 550–562.
- 15 Q. Zhang, D. H. Qu, H. Tian and B. L. Feringa, *Matter*, 2020, **3**, 355–370.
- 16 M. Kathan, S. Crespi, N. O. Thiel, D. L. Stares, D. Morsa, J. de Boer, G. Pacella, T. van den Enk, P. Kobauri, G. Portale, C. A. Schalley and B. L. Feringa, *Nat. Nanotechnol.*, 2022, **17**, 159–165.
- 17 Q. Li, G. Fuks, E. Moulin, M. Maaloum, M. Rawiso, I. Kulic, J. T. Foy and N. Giuseppone, *Nat. Nanotechnol.*, 2015, **10**, 161–165.
- 18 N. Giuseppone and A. Walther, *Out-of-Equilibrium (Supra) molecular Systems and Materials*, Hoboken, NJ, 1st edn, 2021.
- 19 A. S. Lubbe, Q. Liu, S. J. Smith, J. W. De Vries, J. C. M. Kistemaker, A. H. De Vries, I. Faustino, Z. Meng, W. Szymanski, A. Herrmann and B. L. Feringa, *J. Am. Chem. Soc.*, 2018, **140**, 5069–5076.
- 20 Q. Zhou, J. Chen, Y. Luan, P. A. Vainikka, S. Thallmair, S. J. Marrink, B. L. Feringa and P. van Rijn, *Sci. Adv.*, 2020, **6**, eaay2756.
- 21 V. García-López, F. Chen, L. G. Nilewski, G. Duret, A. Aliyan, A. B. Kolomeisky, J. T. Robinson, G. Wang, R. Pal and J. M. Tour, *Nature*, 2017, **548**, 567–572.
- 22 C. Stähler, L. Grunenberg, M. W. Terban, W. R. Browne, D. Doellerer, M. Kathan, M. Etter, B. V. Lotsch, B. L. Feringa and S. Krause, *Chem. Sci.*, 2022, **13**, 8253–8264.
- 23 W. Danowski, T. van Leeuwen, S. Abdolazadeh, D. Roke, W. R. Browne, S. J. Wezenberg and B. L. Feringa, *Nat. Nanotechnol.*, 2019, **14**, 488–494.
- 24 Z. T. Shi, Y. X. Hu, Z. Hu, Q. Zhang, S. Y. Chen, M. Chen, J. J. Yu, G. Q. Yin, H. Sun, L. Xu, X. Li, B. L. Feringa, H. B. Yang, H. Tian and D. H. Qu, *J. Am. Chem. Soc.*, 2021, **143**, 442–452.
- 25 D. R. S. Pooler, R. Pierron, S. Crespi, R. Costil, L. Pfeifer, J. Léonard, M. Olivucci and B. L. Feringa, *Chem. Sci.*, 2021, **12**, 7486–7497.
- 26 A. Sinicropi, E. Martin, M. Ryazantsev, J. Helbing, J. Briand, D. Sharma, J. Léonard, S. Haacke, A. Cannizzo, M. Chergui, V. Zanirato, S. Fusi, F. Santoro, R. Basosi, N. Ferré and M. Olivucci, *Proc. Natl. Acad. Sci. U. S. A.*, 2008, **105**, 17642–17647.
- 27 A. Strambi, B. Durbeej, N. Ferré and M. Olivucci, *Proc. Natl. Acad. Sci. U. S. A.*, 2010, **107**, 21322–21326.
- 28 A. D. Dunkelberger, R. D. Kieda, J. Y. Shin, R. R. Paccani, S. Fusi, M. Olivucci and F. F. Crim, *J. Phys. Chem. A*, 2012, **116**, 3527–3533.
- 29 M. Gueye, M. Manathunga, D. Agathangelou, Y. Orozco, M. Paolino, S. Fusi, S. Haacke, M. Olivucci and J. Léonard, *Nat. Commun.*, 2018, **9**, 313.
- 30 M. Zimmer, *Chem. Rev.*, 2002, **102**, 759–781.
- 31 M. Paolino, M. Gueye, E. Pieri, M. Manathunga, S. Fusi, A. Cappelli, L. Latterini, D. Pannacci, M. Filatov, J. Léonard and M. Olivucci, *J. Am. Chem. Soc.*, 2016, **138**, 9807–9825.
- 32 S. Kulchat, K. Meguellati and J. M. Lehn, *Helv. Chim. Acta*, 2014, **97**, 1219–1236.
- 33 M. M. Lerch, W. Szymański and B. L. Feringa, *Chem. Soc. Rev.*, 2018, **47**, 1910–1937.
- 34 T. T. Abiola, B. Rioux, J. M. Toldo, J. Alarcán, J. M. Woolley, M. A. P. Turner, D. J. L. Coxon, M. Telles do Casal, C. Peyrot, M. M. Mention, W. J. Buma, M. N. R. Ashfold, A. Braeuning, M. Barbatti, V. G. Stavros and F. Allais, *Chem. Sci.*, 2021, **12**, 15239–15252.
- 35 L. Pfeifer, S. Crespi, P. van der Meulen, J. Kemmink, R. M. Scheek, M. F. Hilbers, W. J. Buma and B. L. Feringa, *Nat. Commun.*, 2022, **13**, 2124.
- 36 M. Filatov, M. Paolino, R. Pierron, A. Cappelli, G. Giorgi, J. Léonard, M. Huix-Rotllant, N. Ferré, X. Yang, D. Kaliakin, A. Blanco-González and M. Olivucci, *Nat. Commun.*, 2022, **13**, 6433.
- 37 M. Paolino, T. Giovannini, M. Manathunga, L. Latterini, G. Zampini, R. Pierron, J. Léonard, S. Fusi, G. Giorgi, G. Giuliani, A. Cappelli, C. Cappelli and M. Olivucci, *J. Phys. Chem. Lett.*, 2021, 3875–3884.
- 38 I. Schapiro, M. Gueye, M. Paolino, S. Fusi, G. Marchand, S. Haacke, M. E. Martin, M. Huntress, V. P. Vysotskiy, V. Veryazov, J. Léonard and M. Olivucci, *Photochem. Photobiol. Sci.*, 2019, **18**, 2259–2269.
- 39 A. Pałasz and T. Pałasz, *Tetrahedron*, 2011, **67**, 1422–1431.
- 40 D. R. S. Pooler, D. Doellerer, S. Crespi and B. L. Feringa, *Org. Chem. Front.*, 2022, **9**, 2084–2092.
- 41 P. A. Delaney, R. A. W. Johnstone and I. D. Entwistle, *J. Chem. Soc. Perkin Trans.*, 1986, **1**, 1855.
- 42 C. Stähler, D. R. S. Pooler, R. Costil, D. Sudan, P. van der Meulen, R. Toyoda and B. L. Feringa, *J. Org. Chem.*, DOI: [10.1021/acs.joc.2c01830](https://doi.org/10.1021/acs.joc.2c01830).
- 43 P. Štacko, J. C. M. Kistemaker and B. L. Feringa, *Chem. – Eur. J.*, 2017, **23**, 6643–6653.
- 44 J. Conyard, K. Addison, I. A. Heisler, A. Cnossen, W. R. Browne, B. L. Feringa and S. R. Meech, *Nat. Chem.*, 2012, **4**, 547–551.
- 45 Y. Boeije and M. Olivucci, *Chem. Soc. Rev.*, 2023, **52**, 2643–2687.
- 46 A. S. Sardjan, P. Roy, W. Danowski, G. Bressan, L. Nunes dos Santos Comprido, W. R. Browne, B. L. Feringa and S. R. Meech, *ChemPhysChem*, 2020, **21**(7), 594–599.
- 47 A. Kazaryan, Z. Lan, L. V. Schäfer, W. Thiel and M. Filatov, *J. Chem. Theory Comput.*, 2011, **7**, 2189–2199.
- 48 W. Thiel, *Wiley Interdiscip. Rev.: Comput. Mol. Sci.*, 2014, **4**, 145–157.
- 49 S. Crespi, N. A. Simeth, M. Di Donato, S. Doria, C. N. Stindt, M. F. Hilbers, F. L. Kiss, R. Toyoda, S. Wesseling, W. J. Buma, B. L. Feringa and W. Szymański, *Angew. Chem., Int. Ed.*, 2021, **60**, 25290–25295.
- 50 C. García-Iriepa, M. Marazzi, F. Zapata, A. Valentini, D. Sampedro and L. M. Frutos, *J. Phys. Chem. Lett.*, 2013, **4**, 1389–1396.
- 51 A. Blanco-Gonzalez, M. Manathunga, Y. Xuchun and M. Olivucci, *ChemRxiv*, preprint, DOI: [10.26434/chemrxiv-2023-mncbr](https://doi.org/10.26434/chemrxiv-2023-mncbr).
- 52 A. S. Lubbe, J. C. M. Kistemaker, E. J. Smits and B. L. Feringa, *Phys. Chem. Chem. Phys.*, 2016, **18**, 26725–26735.
- 53 V. Barone and M. Cossi, *J. Phys. Chem. A*, 1998, **102**, 1995–2001.

